2011

Optimization of a Tri-layered Vascular Graft: The Influence of Cellular and Mechanical Properties

Michael McClure
Virginia Commonwealth University

OPTIMIZATION OF A TRI-LAYERED VASCULAR GRAFT: THE INFLUENCE OF MECHANICAL AND CELLULAR PROPERTIES

A dissertation submitted in partial fulfillment of the requirements for the degree of Doctor of Philosophy in Biomedical Engineering at Virginia Commonwealth University.

by

Michael James McClure
Bachelor of Engineering, Vanderbilt University, 2005
Master of Science, Virginia Commonwealth University, 2007

Director: Dr. Gary L. Bowlin
Professor, Biomedical Engineering

Virginia Commonwealth University
Richmond, Virginia
June, 2011

TABLE OF CONTENTS

Page

Acknowledgement

I would like to thank everyone in the lab for being someone to bounce ideas off of, to just chat with about things other than science, or having fun at conferences; in particular, Scott Sell, Patricia Wolfe, Jennifer McCool, Isaac Rodriguez, and Koyal Garg. It has also been fun getting to know Yang and Yali, the new additions to the lab. I would also like to thank Dr. Gary Bowlin and Dr. David Simpson for their guidance as I progressed through my research.

I would to thank all my family for their support and encouragement in my science endeavors: Mom, Dad, Chris, Nancy, Kay, Daniel, Liam, Ray, Jennifer, Kahtra, Jack, Ben, Ellie, Kate, Alex, Kerry, Colyn, and Chase. Everyone in the family is always an inspiration and having a great support system like this keeps the wheels continuously moving. Lastly, I would like to thank my wife Erin (and Bambino) who has been especially supportive, listening to how my days went whether I came back excited because something worked or disappointed because nothing worked. She always has a smiley face ☺ to give. I'm looking forward to continuing research in the future and working towards helping people.

List of Tables

List of Figures

Figure Page

List of Abbreviations

ANSI– American National Standards Institute
BMC– Bone Marrow Cell
BSA– Bovine Serum Albumin
COL– Collagen
CWS– Circumferential Wall Stress
CVD– Cardiovascular Disease
DAPI– 4'-6-diamidino-2-phenylinole
DMEM– Dulbeco's Modified Eagle Medium
EC– Endothelial Cell
eNOS– Endothelial Nitric Oxide Synthase
EPC– Endothelial Progenitor Cell
EBP– Elastin Binding Protein
EDC– 1-ethyl-3-(dimethylaminopropyl)-carbodiimide
EGDE– Ethylene Glycol Diglycidylether
ELAS– Soluble Elastin
ePTFE– expanded Polytetrafluoroethylene
FB– Fibroblast Cell
aFGF– acidic Fibroblast Growth Factor
bFGF– basic Fibroblast Growth Factor
FN– Fibronectin
Gel/NMCS– Gelatin/N-Maleic Acyl-Chitosan
GEN– Genipin
GLUT– Glutaraldehyde
GAG– Glycosaminoglycan
GAPDH– Glyceraldehyde 3-Phosphate Dehydrogenase
HUVEC– Human Umbilical Vein Endothelial Cell
HGF– Hepatocyte Growth Factor
HDF– Human Dermal Fibroblast Cell
HFP– 1,1,1,3,3,3 hexafluoro-2-propanol
hAEC– Human Aortic Endothelial Cell
hUASMC– Human Umbilical Smooth Muscle Cell
ID– Inner Diameter
myoFB– Myofibroblast Cell
NHS– N-hydroxysuccinimide
nvPFA– Non Viable Pig Femoral Artery
NT– No Treatment
PLA– Poly(lactic acid)
PGA– Poly(glycolic acid)
PDO– Poly(dioxanone)
PCL– Poly(caprolactone)
PLCL– Poly(D,L-lactide-co-ε-caprolactone)

PEUU– Poly(ester urethane urea)
PLLA– Poly(-L-lactic acid)
PMAA– Poly(methacrylic acid)
PGI– Prostacylin
PEO– Poly(ethylene oxide)
PDGF– Platelet Derived Growth Factor
PVA– Poly(vinyl alcohol)
PEG– Poly(ethylene glycol)
PRP– Platelet Rich Plasma
PBS– Phosphate Buffered Saline
PQQ– Pyrroloquinoline Quinone
pCol– PureCol Collagen
RT– Room Temperature
RGD– Arginine-Glycine-Aspartic Acid
SMC– Smooth Muscle Cell
SIS– Small Intesting Submucosa
SDF-1α– Stromal Cell-Derived Factor-1α
SEM– Scanning Electron Microscope
SF– Silk Fibroin
TGF-β1– Transforming Growth Factor-β1
TIPS– Thermally Induced Phase Separation
TNBS– 2,4,6 – trinitrobenzenesulfonic acid
vWF– von Willebrand Factor
VEGF– Vascular Endothelial Growth Factor
VGVAPG– Valine-Glycine-Valine-Alanine-Proline-Glycine

Abstract

OPTIMIZATION OF A TRI-LAYERED VASCULAR GRAFT: THE INFLUENCE OF MECHANICAL AND CELLULAR PROPERTIES

By Michael James McClure, M.S.

A dissertation submitted in partial fulfillment of the requirements for the degree of Doctor of Philosophy in Biomedical Engineering at Virginia Commonwealth University.

Virginia Commonwealth University, 2011

Major Director: Dr. Gary L. Bowlin
Professor, Biomedical Engineering

Electrospinning is a polymer processing technique which allows for the production of nano to micro size fibers and scaffolds which can be composed of numerous synthetic biodegradable materials and natural biopolymers. Natively, elastin and collagen are the main components of vascular tissue. Arranged in a tri-layered structure, they create a specific mechanical environment that can withstand the rigors of circulation. The goal of this study was to develop a mechanically 'biomimicking' vascular graft composed of three distinct layers through the process of electrospinning. We hypothesize that the use of bioactive agents such as elastin, collagen, and silk to supplement poly(caprolactone) at specified ratios for each layer would provide a finely tuned vascular replacement. This was accomplished by establishing cross-linking parameters for the biopolymer materials and then assessing the mechanical properties of individual materials and eventually a whole tri-layered graft. Additionally, while mechanical testing can lead to a good graft, a replacement graft requires excellent cellular properties as well to promote cell infiltration,

proliferation, and migration. Therefore, the conclusion of this study examines the integrin binding characteristics of the electrospun biopolymers.

First, the results from the preliminary cross-linking study examined the dissipation of soluble elastin when uncross-linked v. cross-linked. It was determined through this initial study that synthetic scaffolds blended with soluble proteins such as elastin require a fixation in order to retain their protein mass within the scaffold. Retaining this mass, incrementally changed the material properties of the blended scaffolds. This initial study was then carried further to establish optimal cross-linking parameters using two different types of reagents: carbodiimide and genipin. It was found that lower cross-linking molarities produced excellent results based on assays performed to assess cross-linking percentages and rate of reaction. Some differences in mechanical properties were seen, but they did not constitute a choice of one cross-linker over the other. The next portion of this study aimed to design a tri-layered graft. This was performed with the aid of mathematical analysis to observe circumferential wall stresses based on simple tensile properties. A series of tri-layered grafts were electrospun using poly(caprolactone), elastin, and collagen. The medial layers of these grafts were changed while the intima and adventitia remained constant. Differences were demonstrated as the elastin content of the medial layer decreased, proving that each layer had an affect on the overall graft properties and that it was possible to tune graft mechanics. A larger tri-layered study looked to evaluate changes in the adventitial and medial layers while keeping the intimal layer constant using poly(caprolactone), elastin, collagen, and silk fibroin. In this study, differences were exhibited under compliance and burst strength testing, narrowing the scope of material

choices. Results from a 4 week degradation study with the best tri-layered grafts revealed no evidence of degradation, but did generate some positive compliance results for two of the grafts. Finally, integrin binding and protein analysis portrayed results that were indicative of the existence of ligand binding sites for collagen scaffolds and the possibility of a small amount of ligand sites on silk. Elastin, however, displayed low to non-existent adhesion. These studies produced results that allowed us to continuously narrow the scope of materials as the experiment progressed towards an optimized tri-layered vascular graft.

CHAPTER 1: Vascular Structure and Graft Development

Preface: The following manuscript is currently published in the Journal of Drug Delivery Science and Technology. The work reviews a large range of vascular grafts for tissue engineering from the use of acellular biodegradable polymers to autologous cell lines without the use of a scaffold material.

Bioengineered Vascular Grafts: Improving Vascular Tissue Engineering Through Scaffold Design

Michael J. McClure, Patricia S. Wolfe, Isaac A. Rodriguez, and Gary L. Bowlin
Department of Biomedical Engineering, Virginia Commonwealth University, Richmond, Virginia 23284

Abstract

Arteriosclerosis has accounted for three quarters of the deaths related to cardiovascular disease (CVD). Arteriosclerosis is a vascular disease that is characterized by a thickening of the arterial wall and subsequent decrease in the arterial lumen, eventually causing loss of circulation distal to the site of disease. Small diameter arteries (< 6 mm) are affected the most by CVD due to their already decreased blood flow. The increasing populations of people who are obese, diabetic, or aging supplement a strong need for the production of a commercially available small diameter vascular graft. Tissue engineering has become a promising approach for generating a biocompatible vessel with the potential to regenerate new tissue. Multiple factors have to be accounted for when designing a vascular graft that has the ability to self-repair and self-remodel such as the choice of polymer, choice of cell type, and choice of growth conditions. To date, historical landmarks such as the initial research of Weinberg and Bell have led researchers closer and closer to a functional end product.

Keywords: Tissue Engineering, Vascular Grafts, Biodegradable, Collagen, Elastin

Introduction

CVD, specifically coronary heart disease resulting from arteriosclerosis, remains the leading cause of death in the United States and has been so virtually every year since

1900 [1]. Once blood flow in the coronary artery is compromised, vascular bypass is an option to restore blood flow to tissues distal to the restriction or blockage [2]. In 2005 there were 469,000 bypass procedures performed due to CHD [1], which typically involve the replacement of a coronary artery with a patients own saphenous vein or internal mammary artery. Biological grafts are a formidable option since they already retain the natural architecture that arteries require. When these grafts are used as replacements, they begin to adapt to their new environment, altering their structure to match the mechanical requirements of the tissue.

While these autologous replacements have an acceptable patency rate, they are not always a viable option as the patient may also suffer from peripheral vascular disease; affecting upwards of 8 million Americans and up to 20% of those 65 years of age or older [1]. Further complicating the use of autologous vessels is the fact that they are limited in number and a previous bypass operation may have already required the vessel's use [3]. Currently available commercial alternatives to the autologous vessel gold standard are limited to synthetic vessels made of ePTFE and woven or knitted Dacron®. These materials have been used with moderate success as medium and large diameter prosthetics, but their efficacy is severely limited when used as small diameter vessels. Larger diameter vessels experience higher flows and less resistance than small diameter vessels, such as the popliteal or coronary arteries, where low blood flow and high shear makes the synthetic graft more prone to thrombus formation and intimal hyperplasia [2-13]. Dacron® and ePTFE grafts are non-degradable and lack the ability to promote native tissue regeneration, making them a permanent fixture in the body. As a permanent fixture, the graft is

constantly threatened with attack from the patient's own foreign body response as well as bacterial graft infection [10, 12, 14]. To this extent, a vascular replacement that matches the body's mechanical and cellular requirements is highly necessary in the field of vascular tissue engineering, requiring "ideal" characteristics.

A tissue engineered vascular graft needs to meet several criteria to be considered ideal:

1. Easy for surgeons to handle with excellent suture retention and resistance to kinking while remaining flexible.

2. Grafts need to be biocompatible and retain non-toxic, non-thrombogenic, and infection resistant characteristics. All of which are associated with a confluent, quiescent, nonactivated endothelium.

3. They must induce an appropriate healing response that does not result in inflammation, hyperplasia, or fibrous capsule formation.

4. It is necessary for the grafts to be leak resistant yet have sufficient porosity to allow for the ingrowth of autologous tissue, leading to tissue that is indistinguishable from the native vessel.

5. Mechanical strength is a paramount concern where grafts must retain a compliance, the ability to withstand long-term hemodynamic stress without failure, similar to that of native artery to prevent intimal hyperplasia while;

6. Resisting creep and permanent deformation leading to aneurysm formation.

7. Grafts should express physiological properties such as vasoconstriction and relaxation.

8. Finally, they should be easy to manufacture, produce, sterilize, and store, as well as be economical and available off-the-shelf in a variety of sizes [10, 15].

Vascular tissue, more specifically arterial tissue, is subdivided into two separate categories: elastic (> 6 mm inner diameter (ID)) and muscular (< 6 mm ID). The architecture of both elastic and muscular arteries is composed of three separate layers: intima, media, and adventitia, which vary in thickness and composition as a function of anatomic location. The intima is the innermost layer of all blood vessels and is composed of a single layer of ECs lining the vascular wall, a thin basal lamina, and a subendothelial layer containing collagenous bundles, elastic fibrils, smooth muscle cells (SMCs), and some fibroblasts (FBs). The media, the thickest of the three layers, is made up of SMCs, a various number of laminae depending on location, bundles of collagenous fibrils, and a network of elastin fibrils. The adventitia is the outermost layer of the vessel wall and like the media, its thickness varies as a function of anatomic location, consisting of dense fibroelastic connective tissue containing FBs [16, 17]. Incorporated with these three layers, is the vasa vasorum, a network of blood vessels which innervate both the media and adventitial layers to supply oxygen and nutrients to the cells in those regions.

As arteries move away from the heart and towards the periphery, their diameter decreases. This decrease in diameter coincides with changes in the architectural makeup. Structurally, the intima is similar in both elastic and muscular arteries and therefore does not affect the overall properties when comparing the two. Instead, both the medial and adventitial layers change in thickness and composition as arteries move away from the heart and toward the periphery. Those arteries with larger diameters, such as the aorta or carotid, contain a medial layer with SMCs and numerous elastic laminae. Muscular

arteries, such as the femoral, retain the three layered structure yet their medial layer contains a higher density of SMCs and a lower number of elastic laminae. As for the adventitia, elastic arteries contain a relatively thin outer layer that constitutes only 10% of the vascular wall whereas in muscular arteries the adventitia often occupies 50% of the vascular wall. Functionally, for the media, this design change is due to a smaller circumferential stress in the wall of the muscular artery, decreasing the overall demand for elastic recoil and energy dissipation [18], while increases in nerve innervations account for the increased adventitial thickness [16].

Blood vessels are continuously subjected to stress and strain in the circumferential and longitudinal directions. In the circumferential direction, the pulsatile nature of blood pressure induces a cyclic stretch on the arterial wall. Each layer in the wall plays a significant mechanical role to its proper functionality. *In vivo* studies and clinical observations have shown that decreased values of tensile and shear stress in surgically injured vessels are correlated with activation of cell proliferation and extracellular matrix (ECM) production, leading to vessel occlusion [19]. A decrease in tensile properties is not just a change in the circumferential direction, but a multi-directional change. As a consequence, compliance, hoop stress, and overall hysteretic properties can be affected. These changes can affect cell and fiber orientation.

In addition to circumferential and longitudinal stress, one of the most important stresses exerted on the inner lumen of arterial tissue is shear stress. Arteriosclerosis tends to develop in regions of the circulation where flow is either low or turbulent, such as regions where arteries bifurcate [20-22]. ECs respond to increased blood flow by causing

the relaxation of the surrounding smooth muscle through nitric oxide. Conversely, decreased flow induces vessel narrowing that is also mediated by signals from the endothelium, and in severe cases low flow leads to vessel regression and apoptosis of ECs [23].

Besides the ultimate importance of shear stress, circumferential stress due to cyclic loading also mediates proper functionality of the arterial wall, preventing arteriosclerosis. Vascular ECs sense and respond to cyclic strain both morphologically and phenotypically. The influence of cyclic strain on ECs is visually apparent as early as 15 minutes after strain with the formation of actin stress fibers and morphological alignment of cells perpendicular to the force vector [22]. However, if hypertension occurs in a blood vessel, ECs, in addition to SMCs, are highly affected. Accumulating evidence demonstrates that high cyclic strain affects ECs, whereby in one study Reape *et al.* found that monocyte chemotactic protein-1 is synthesized when ECs are subjected to high mechanical deformation [24], while other studies have found that mechanical strain in hypertensive models influences atherosclerotic plaque development through increased expression of adhesion molecules [25-27]. SMCs are mostly affected by increases or decreases in blood pressure. Normal blood pressure and flow allows both SMCs and ECs to cross-talk and maintain the integrity of the vascular wall over time. If blood pressure rises over a long period of time, signal transduction pathways begin to break down the ECM and remodel the arterial wall, resulting in vascular hypertrophy [28]. If the pathophysiology involved in vascular disease was better understood, then this knowledge may produce vascular graft designs that approach what would be considered ideal.

Historical Vascular Replacements

Vascular grafts have been in the process of development since the late 19th century when Eck attempted the first delineation of a basic technique for vascular suture, performing a lateral anastomosis of the portal vein to the inferior vena cava [29]. However, it was not until the early 20th century when Alexis Carrel explored the basic patterns of healing of arteries and veins, the reactions to different types of sutures, and the possibility of organ transplantation, winning him the Nobel Prize for Physiology or Medicine in 1912 [30].

There were many ventures into bridging the gap of a particular blood vessel. In World War I, German surgeons treated aneurysms by bridging the defect with pieces of the patient's vein [30]. A femoro-popliteal bypass with a reversed saphenous vein graft was first performed by Kunlin in 1948. During the same period, fresh arterial allografts were beginning to be used in human vascular reconstructive surgery. In 1952, Blakemore and Voorhees developed one of the first synthetic vascular prostheses, Vinyon-N cloth, which was used to bridge arterial defects in dogs [31]. Although early clinical results were promising, Vinyon-N did not display sufficient long-term stability, nor did it provide an appropriate scaffold for tissue in-growth. These historical experimentations paved the way towards tissue engineered vascular grafts, and set into motion the quest for the ideal vascular replacement.

Endothelial Cell Seeding

This quest began by modifying materials that were already approved for vascular replacement surgeries, ePTFE and Dacron. In 1978, Herring *et al.* introduced a single-

stage technique whereby venous ECs were seeded onto Dacron grafts with enhanced patency in canine models [32]. Since this point, numerous methodologies have been used to gain a confluent monolayer of ECs: gravitational, hydrostatic, and electrostatic. The most basic and extensively studied of these is gravitational EC seeding. Coating the graft surface prior to this method of seeding has been performed in many cases. For instance, Zilla and associates have looked into multiple ways in which to increase EC attachment onto ePTFE grafts through lining the graft with fibronectin [33] and fibrin glue [34]. However, outcomes from these studies demonstrated insufficient cell density, poor adhesion under flow conditions, and failure to achieve confluence. Another major disadvantage of this technique is any surface that is not covered by ECs becomes highly thrombogenic. Poor adhesion of cells under flow conditions was due to a number of factors, one of which being cell seeding duration was too short (<2 hours) [35]. This was leading to a significant loss of cells upon implantation. Therefore, studies such as Shindo *et al.* and Prendiville *et al.* were performed to increase maturation time [36, 37]. Biological glues and adhesive proteins such as fibronectin, collagen, laminin, fibrin, FB matrix, and plasma have been extensively studied as further means to adhere ECs to the inner lumen surface of a vascular graft [38-44]. The necessity for an incubation period to allow for significant adhesion and maturation of ECs is related to the basic nature of the electrostatic interactions between the polymeric graft materials and the cells. Clinically successful vascular prosthetics such as ePTFE are highly negatively charged, which can repel cells. Several *in vitro* studies have been performed utilizing the electrostatic seeding technique. Bowlin *et al.* found that when umbilical vein ECs were seeded onto ePTFE

through electrostatics, complete nodal area coverage of morphologically mature ECs was obtained within 16 minutes [45]. Using this same technique under flow conditions with a wall shear stress of 15 dynes/cm^2 for up to 120 minutes revealed no significant loss of ECs [46]. However, problems associated with permanent synthetic graft material still pose major hurdles. Therefore, bioresorbable vascular grafts became of interest since they deviate from the permanent scaffolding and resorb *in situ* while autologous tissue remodels the graft.

Scaffold-Based Approaches to Improve Vascular Grafts

Bioresorbable grafts are advantageous due to the fact that a resorbable vascular prosthetic with adequate mechanical properties can be implanted and degraded gradually over a period of time, leaving behind no permanent synthetic materials to initiate a chronic foreign-body reaction [12]. Through the years, there have been many different approaches. Wesolowski *et al.* first introduced the concept of a bioresorbable vascular prosthetic in the early 1960s. These first bioresorbable incarnations were composed of a variety of Dacron® yarns, COL coatings, and COL fibers. The permanent Dacron® provided mechanical stability, while the COL added bioactivity to the structure and promoted the ingrowth of native tissue as it was degraded and remodeled [47, 48]. The 1970s and '80s saw the advent of a number of different aliphatic polyesters (poly(lactic acid) (PLA), poly(glycolic acid) (PGA), polydioxanone (PDO), etc.). These polymers breakdown through hydrolysis in the body, and can have their rate of degradation tailored by altering their structures [12, 49-53]. While this preliminary work failed to result in a successful commercially available graft, it laid the foundation for current research in bioresorbable prosthetics and

demonstrated the possibilities of *in situ* tissue engineering. Despite the ability of bioresorbable grafts to have products added to or subtracted from the created matrix to aid the body in regeneration, other approaches find that the body alone is not sufficient enough to sustain a fully regenerative capacity, and that much of that work should be done *in vitro*. This type of tissue engineering approach can be accomplished with the combination of cells and specific scaffold materials. Regardless of approach, the way in which a scaffold material is designed is equally as important as the source of the cells that utilized in the experimental procedures.

The ideal cell source should be non-immunogenic, functional and easy to achieve and expand in culture. Cells are arguably the most important element in any tissue engineering model. For an arterial replacement, a functional graft cannot be achieved without an endothelium-like interface to the circulating blood and vasoactive SMCs within the wall [54]. Autologous ECs and SMCs isolated from patients themselves are usually the first choice. However, this procedure is quite limited in the number of cells that are able to come from a single biopsy punch of an autologous vascular tissue. Therefore, stem and progenitor cells become a more viable option as they have a higher capacity to expand in culture. Endothelial progenitor cells (EPCs) typically circulate throughout the bloodstream and can be isolated using techniques such as those done by Asahara *et al.*[55, 56], where magnetic beads coated with antibodies such as CD34, AC133, or markers common to both early and more differentiated progenitors were used to capture EPCs. Autologous bone marrow sources have also shown promise through studies that have been done by Shin'oka *et al.*[57], seeding the cells onto a PLCL copolymer and then implanting in humans.

Campbell *et al.* have shown that the cells located in the peritoneal cavity will display promise, where silicone tubing was implanted into the peritoneal and pleural cavities of dogs for 2-3 weeks, and cells from those cavities migrated onto the tubing, subsequently forming a biological graft material [58, 59]. Nieponice *et al.* has shown how muscle-derived stem cells are also a plausible autologous source for vascular tissue engineering, combining these cells with PEUU scaffolds through a vacuum seeding procedure and implanting them as an aortic interposition bypass graft [60]. Non-autologous cell sources also include those of embryonic stem cells, which have the capability to differentiate into several different cell types including those of the vasculature.

The combination of specific cell types and biomaterials to create a structure which mimics both mechanically and architecturally the native tissue is at the heart of the tissue engineering field. Vascular tissue engineering has looked at a myriad of scaffold based approaches involving the use of pure polymer, polymer blends, and manufacturing co-polymers to achieve its ideal goal.

Poly(glycolic acid), Poly(lactic acid), and Copolymer Blends

PGA is a biodegradable aliphatic polyester with a glass transition temperature between35-40°C, melting point between 225-230°C, and acrystallinefraction of 45-55% (Table I). Within the field of vascular surgery, PGA was first used as a biomaterial for sutures in the 1970s [61, 62]. In 1983, Lauritzen was the first to conduct preliminary studies on PGA tubes as vessel grafts. This experiment suggested PGA tubes as a promising construct for instant and absorbable microvascular grafts [63]. Since then, various approaches to improving PGA grafts have been developed and extensively studied.

Niklason *et al.* fabricated tubular PGA scaffolds with a chemically modified surface (NaOH) and seeded grafts with bovine SMCs exposed to pulsatile flow conditions for 8 weeks. After 8 weeks of culture, the gross appearance of the scaffolds was similar to native arteries with histology showing migration of SMCs forming a smooth luminal surface for EC seeding. After 4 weeks implantation in pigs, scaffolds showed 100% patency [64]. In order to minimize residual polymer fragments after culture, Prabhakar *et al.* treated PGA mesh tubes by exposing them to heat, 1.0M NaOH, and γ-irradiation to hasten degradation. Porcine carotid SMCs were cultured on treated PGA scaffolds under pulsatile conditions. After 8 weeks of culture, treatment with NaOH increased polymer degradation rate under hydrated conditions and NaOH and γ-modified scaffolds showed native vessel morphology, a more even distribution of SMCs, and fewer polymer residual fragments. It was also noted that the COL content of some scaffolds were approximately similar to that of native vessels, however, the mechanical integrity of the engineered scaffolds was less than native [65]. Boland *et al.* were the first to publish results on electrospun PGA as a tissue engineering scaffold comprised of submicron fiber diameters. In this study, HCl pretreated PGA scaffolds were incorporated into the surrounding tissue and showed increased cell proliferation rates when implanted in rats [66]. The above studies have demonstrated that independent of scaffold fabrication technique, PGA grafts with a chemically modified surface can serve as potential vascular grafts. More recently, Iwasaki *et al.* bioengineered a three-layered tubular scaffold where PGA, PCL, and PGA layered sheets were seeded with three types of vascular cells under pulsatile conditions to mimic artery structure, integrity, and blood flow. Results from this study demonstrated that the

engineered vessels produced sufficient amounts of COL and elastin (ELAS) and exhibited similar appearance, elasticity, and ultimate strength as native arteries [67].

Table 1. PGA, PLA, and Copolymer Blends

Biodegradable Polymer	Manufacturing Method	Improvement	Cell Seeded	Culture Condition	Ref
PGA					
Nikalson *et al.*	Chemically modified w/ NaOH	Cell attachment and proliferation	SMCs	Pulsatile and Pig Implant	64
Prabhakar *et al.*	Mesh tube w/ NaOH, γ-irradiation	Cell attachment and proliferation	SMCs	Pulsatile	65
Boland *et al.*	Chemically modified electrospun PGA w/ HCL	Cell proliferation	—	Rat Implant	66
Iwasaki *et al.*	PGA, PCL, PGA layered sheets	Cell attachment, proliferation, collagen, and elastin content	EC, SMC, FB	Pulsatile	67
PLA/PLLA					
Stitzel *et al.*	Electrospun PLA w/ wound collagen	Cell attachment and orientation	SMC	Static	73
Wang *et al.*	Electrospun PLA and silk-gelatin	Mechanical strength	—	—	74
Zhu *et al.*	Surface modified w/ gelatin/N-Maleic acyl-chitosan	Cell attachment, proliferation, and high expression of CD31 and vWF	hUVEC	Static	75
PGA-PLA					
Hibino *et al.*	PGA and PCL/PLLA woven fabric	No evidence of rupture, infection, calcification, or aneurysm	—	Human Implant	76
Mooney *et al.*	PGA mesh coated w/ PLGA	Mechanical properties and cell proliferation	SMC and EC	Static and Rat Implant	77
Wen *et al.*	70:30 PLGA sponge	Cell attachment and proliferation	SMC and EC	Static	83
Izhar *et al.*	PELA coated filament-wound Lycra	Enhanced healing and mechanical properties	—	Dog Implant	85
Roh *et al.*	PGA mesh coated w/ P(CL/LLA)	Pre-seeding led to no calcification, a neo-intima, and neo-tissue formation	BMC	Static and Lamb Implant	84

PLA is a biodegradable aliphatic polyester with a glass transition temperature between 60-65°C, melting temperature between 173-178°C, and crystallinity of approximately 37%. PLA can exist in several distinct isoforms, most commonly as poly-L-lactic acid (PLLA). In the 1980s the first studies were conducted exploring the possibilities

of PLA as a vascular graft coating [68] and PLLA as a microporous, compliant, biodegradable vascular graft [69-72]. In 2001 Stitzel *et al.* developed a tubular scaffold comprised of a helical wind of COL fibers encompassed by a layer of electrospun PLA fibers. After 10 days incubation, SMCs formed a 100% confluent monolayer on the tubular scaffold oriented along the principle stress lines [73]. Within the past few years electrospun PLA and PLLA have been extensively studied and are considered an ideal biomaterial candidate for tissue engineering blood vessels. Wang *et al.* electrospun a tubular graft composed of PLA (outside layer) and silk fibroin-gelatin (inner layer) with a porosity of 82 ± 2%, breaking strength (2.2 MPa), pliability (60.6%), suture retention strength (4.6 N), and a burst pressure strength of 1596 mmHg [74]. Whereas many PGA studies use surface modifications to achieve desired results, PLA can be more readily used "as is" to produce vascular engineered scaffolds. However, there are certain advantages to chemically modifying PLA surfaces. To improve EC biocompatibility, Zhu *et al.* grafted a gelatin/*N*-Maleic acyl-chitosan (gel/NMCS) complex on the surface of PLA films. This study concluded that gel/NMCS modified PLA enhanced human umbilical vein EC proliferation and expressed a higher structured CD31 and vonWillebrand Factor (vWF), ultimately suggesting photo-initiated grafting of gel/NMCS complexes as an effective method for modifying the surfaces of vascular grafts [75].

PGA and PLA have also been combined to create novel biodegradable vascular tissue engineering scaffolds. Most recently in 2010, Hibino *et al.* developed a tubular woven fabric vascular scaffold composed of PGA and poly(caprolactone) (PCL)/PLLA which was implanted in 25 human patients as a extracardiac cavopulmonary conduit. After

a mean follow up of 5.8 years, scaffolds showed no evidence of rupture, infection, ectopic calcification, aneurysm formation, or scaffold related mortality. One patient had partial thrombosis and four patients had scaffold stenosis but all were successfully treated [76].

PGA and PLA have been combined with each other as well as other polymers to form new copolymers: PLGA, poly(ethylene glycol/lactic acid) (PELA), and PLLA-PCL to name a few. PLGA was first used in vascular tissue engineering in 1996 when Mooney *et al.* coated PGA mesh tubes with PLGA (50:50) [77]. Since then many have focused on prolonged sustained release of drugs and growth factors [78-82]. Wen *et al.* developed vascular scaffold segments by coculturing human vascular SMCs and ECs on a PLGA (70:30) sponge and concluded that cells could successfully be grown on the scaffold and after 2 months complete cell layers similar to native artery were formed [83]. Roh *et al.* implanted vascular scaffolds comprised of PGA mesh tubes coated with a copolymer of P(CL/LLA) pre-seeded with bone marrow derived vascular cells in juvenile lambs and assessed patency for up to 30 days. All scaffolds were patent without signs of thrombosis or calcification, exhibited neo-endotheliaization, and the neo-tissue formed was composed of ECM, mesenchymal stem cells, and residual polymer matrix [84]. A PELA coated filament-wound Lycra graft was developed by Izhar *et al.*, which compared to ePTFE graft controls, showed enhanced healing and improved mechanical properties when implanted in mongrel dogs for up to 12 weeks [85]. Shum-Tim *et al.* demonstrated 100% patency at 5 months of a copolymer scaffold (PGA and polyhydroxyalkanoate) seeded with cells from lamb carotid arteries and implanted into lamb aorta [86]. Overall, the versatility of PGA and PLA fuels the use of these polymers as practical materials for fabricating vascular

grafts. Although, both these synthetic polymers have demonstrated promising results there are several drawbacks to using such materials. Both PLA and PGA are stiff and significantly different from native artery, which could lead to hyperplasia at the site of anastomosis. Additionally, PGA's quick degradation characteristics make it desirable for designing a functional artery and dangerous as an implant which could lead to aneurysm or rupture.

Poly(caprolactone) and Copolymer Blends

PCL is a semicrystalline, non-toxic, tissue compatible biomaterial with a degradation rate of around 12 months (Table II). Mechanically, PCL displays highly desirable characteristics for vascular grafts, mostly high strength and excellent compliance. Surface properties of biomaterials, such as surface roughness, affect cell behavior and may induce thrombotic clots in some cases. Researchers have found that rough and smooth surfaces will encourage different types of cell adhesion [87]. Some groups have attempted to modify the hydrophobic surface of PCL to provide more hydrophilic groups. Zhu *et al.* first looked to modify PCL's surface chemistry with poly(methacrylic acid) (PMAA) [88]. This was accomplished by immersing a PCL membrane in a quartz tube with 30% hydrogen peroxide, and subsequently exposing the tube to UV light. The photo-oxidized membrane was then placed in a copolymerization tube containing 4% PMAA and irradiated with UV, leading to a higher EC attachment when compared to non-modified grafts.

Table 2. PCL and Copolymer Blends

Biodegradable Polymer	Manufacturing Method	Improvement	Cell Seeded	Culture Condition	Ref
PCL					
Zhu *et al.*	Surface modified PCL film w/ PMMA	Cell attachment	EC	Static	88
Serrano *et al.*	Surface modified PCL film w/ NaOH	Increased hydrophilicity and cell attachment	EC and SMC	Static	89
Ma *et al.*	Surface modified electrospun PCL w/ carboxyl groups	Increased hydrophilicity and cell attachment	EC	Static	91
Duling *et al.*	Electrospun PCL	Mechanical properties	—	—	92
Pektok *et al.*	Electrospun PCL	*In situ* degradation	—	Rat Implant	93
Drilling *et al.*	Different concentrations of electrospun PCL	Optimized burst pressure	—	—	96
Lee *et al.*	Thermal treatment of electrospun PCL	Suture retention, burst pressure	—	—	97
Vaz *et al.*	Electrospun PCL and PLA	Cell attachment and mechanical properties	FB and myoFB	Static	98
Hanson *et al.*	Dip casted PCL and PLA	Mechanical properties	—	Canine	100
Watanabe *et al.*	50:50 P(CL/LA) poured into PGA mesh	Mechanical properties and cell attachment	Mixed population from femoral vein	Canine	101

Serrano *et al.* used a NaOH treatment of the PCL grafts to provide better adherence of vascular ECs and SMCs through increased hydrophilicity [89]. In this study, PCL films were prepared by hot pressing and then submerged in a solution of 2 N NaOH for two hours. Scanning electron microscopy (SEM) analysis of cell morphology showed both cell types growing properly on NaOH treated films, but untreated films did not seem appropriate substrates to support cell growth by causing cytoplasmic retraction. Serrano *et al.* then followed this preliminary study up 3 years later, evaluating EPC adherence proliferation to NaOH treated films, and the effect of PCL on nitric oxide content [90]. EC derived cells from EPCs were first characterized using classical markers CD31, von Willebrand factor, and endothelial nitric oxide synthase (eNOS) using flow cytometry, where CD31 is a clear marker of EC maturation. After 4 days, it was found that PCL-NaOH films contained large numbers of cells on their surface, however, PCL films had

significantly lower numbers, further demonstrating the benefits of NaOH treatment. Furthermore, Ma *et al.* improved the surface chemistry of PCL through modification of electrospun fibers with air plasma treatment, introducing carboxyl groups on PCL nanofiber surfaces. These carboxyl groups were then used to bind gelatin to the surface, increasing hydrophilicity and increasing EC proliferation when compared to no treatment [91]. Surface modification of PCL films to increase hydrophilicity, definitively improved scaffold materials for enhanced cellular attachment. However, an implanted vascular graft will not respond well to a tubular film, leading to encapsulation with no cellular infiltration of the scaffold material. For this reason, porous scaffolds have been manufactured through the process of electrospinning.

Mechanically, PCL is a highly desirable material for vascular tissue engineering in addition to other soft tissue applications. Several studies have set out to characterize the mechanical behavior of PCL. Duling *et al.* punched out "dogbone" shapes from electrospun nanofibers to test for stress relaxation, loading response, tensile failure testing, and cyclic stress relaxation, comparing these results using Fung's quasilinear viscoelastic theory [92]. Others have looked at the degradation characteristics both in a rat descending aorta for 24 weeks (Pektok *et al.*) [93], and *in vitro* in Ringer solution stirred gently for 6 months (Bolgen *et al.*) [94]. Pektok *et al.* found that after 24 weeks molecular weight decreased by 20%, while Bolgen found that molecular weight decreased by only 5%, indicating that *in situ* degradation occurs faster. In these cases if degradation occurs too fast or too slow, then the vascular graft will either become too weak and develop an aneurysm or not dissolve out quickly enough causing other downstream affects.

Therefore, optimization of graft mechanical and cellular parameters is necessary. Nottelet *et al.* demonstrated an optimal design for electrospun PCL grafts in a rat model by electrospinning several combinations of solvent/polymer concentrations [95]. Drilling *et al.* optimized burst pressure results of electrospun PCL grafts through analyzing several different solvent/polymer concentrations, resulting in 5 mm diameter grafts that could withstand in excess of 2000 mmHg [96]. Lee *et al.* demonstrated increased mechanical properties through thermal treatment of electrospun PCL grafts, which resulted in increased suture retention and burst pressure, without much change in compliance [97]. While there are many studies surrounding the sole use of PCL as the vascular graft material, other studies have combined PCL and other synthetics by copolymerizing the two structures together or separately manufacturing them.

Vaz *et al.* selected two different polymers to be electrospun together, PCL and PLA, in a multilayered approach, characterizing their properties through uniaxial tensile testing, 3T3 mouse FBs, and human venous myofibroblasts (myoFBs) [98]. While this study produced good results, the addition of a stiff material such as PLA could significantly reduce compliance and increase the downstream affects of compliance mismatch. Williamson *et al.* created a more compliant structure from a PCL-polyurethane (PU) composite vascular graft using gravity spun PCL fibers out of acetone while PU fibers electropun directly on top of the PCL to create a bi-layered graft [99]. In 1988, Hanson *et al.* looked into the mechanical properties of selected copolymers, PLA and PCL [100]. These vascular grafts were dip casted using three different kinds of copolymers to produce single layer and bi-layered grafts. These grafts were then tested for compliance,

tensile strength, and kink resistance. Mechanical results looked promising except for compliance, which was significantly lower than a canine femoral artery, where this once again demonstrates the stiffness of PLA. Watanabe *et al.* synthesized a P(CL/LA) copolymer in a 50:50 combination to be poured into a PGA nonwoven fabric and subsequently freeze dried. Mechanical testing, cell seeding, and implantation of the vascular scaffold into the inferior vena cava of a canine were performed with promising results as an "ideal" venous scaffold with antithrombogenic activity [101]. However, a venous graft is not subjected to the same circumferential and shear stresses that occur in the arterial network. Several other poly(D,L-lactide-*co*-ε-caprolactone) (PLCL) copolymers have been used for vascular tissue engineering applications demonstrating the possible use of bone marrow cells (BMCs) seeded onto scaffolds and implanted into a non-human model [102, 103], and evaluating electrospun PLCL scaffolds with SEM, porosimetry, tensile testing, and cell culture analysis using human umbilical ECs [104].

Poly(dioxanone)

PDO is a colorless, crystalline, bioabsorable polymer that was developed specificially for wound closure sutures. PDO exhibits a crystalline fraction of 55% and a glass transition temperature between -10°C and 0°C (Table III). Greisler *et al.* were the first to have published several results on PDO absorbable vascular prosthetics using a mesh tube with 250 micron fiber diameter and 400 micron pore size. Evaluations of these first took place in a rabbit aorta [53] at 2 weeks up to 12 months, displaying myoFB migration occurring in parallel to the macrophage-mediated degradation of the PDO structure. This study was followed with the aorta-iliac canine model using 70% PDO and 30%

polypropylene. Results from the study of up to a 1 year implantation demonstrated 86% patency rates compared to Dacron® and ePTFE which had a rate of 68% and 54%, respectively. An additional study examined prostacylin (PGI_2) and thromboxane A_2 production from the endothelium. The rationale for this was based on the importance of these components with the endothelium non-thrombogenic properties. This is attributed to a balance between PGI_2 and TxA_2 (or the PGI_2/TxA_2 ratio), where it is more desirable to have a higher PGI_2 levels than TxA_2 in native vessels. The results of Greisler's study demonstrated that the explanted PDO graft had the highest ratio of PGI_2/TxA_2 versus PGA and almost equal to native aorta control [105].

Since Dr. Greisler's extensive research using animal models, PDO has only been used in a handful of studies. Teebken *et al.* performed a comparison study between EC seeded decellularized carotid arteries and woven 4 mm diameter PDO prostheses, concluding that decellularized vascular tissue had higher patency rates than that of PDO prostheses [106]. A few years later, Boland *et al.* produced a study on electrospinning PDO into non-woven nanofibers examining the effects of polymer concentration on fiber diameter, pore area, and mechanical properties [107]. This led to several studies out of the same lab to test PDO in combination with biopolymers such as ELAS [108-111], COL [111, 112], and silk [113] to determine both cellular and mechanical behavior. Sell *et al.* developed PDO-ELAS vascular conduits using a range of polymer-ELAS blends and characterized them utilizing compliance, suture retention, uniaxial tensile testing, and cellular seeding with human dermal FBs. Since compliance mismatch between the graft and native artery is one of the major causes of graft failure, the authors of this manuscript

have tested several combinations of PDO and ELAS in order to determine its mechanical behavior *in vitro* [109]. A difference in this study, compared to other publications of vascular graft compliance, was that compliance was determined under dynamic conditions mimicking physiological parameters, therefore providing a lucid interpretation as to how the graft should perform in the body. In this study, it was determined that certain PDO/ELAS blends closely matched those of native artery.

Mechanical properties, specifically compliance, are of utmost importance in order to prevent a mismatch and ultimately intimal hyperplasia at the site of anastomosis; however, chemical properties of the vascular materials once implanted inside the body must also be evaluated so as to determine the material's response to monocytes and macrophages *in vivo*. Garg *et al.* aimed to evaluate the angiogenic potential of PDO-ELAS vascular grafts to promote *in situ* arterial tissue regeneration by measuring the amount of vascular endothelial growth factor (VEGF), acidic fibroblast growth factor (aFGF), basic fibroblast growth factor (bFGF), and transforming growth factor beta-1 (TGF-β1) released upon interaction between the macrophages and the polymer-ELAS blend [114]. Results demonstrated that macrophages remained on the surface of high ELAS content PDO-ELAS blends, but penetrated both low ELAS content blends and pure PDO grafts. As a consequence, at day 28 VEGF was high for all grafts, aFGF was found to remain largely independent of graft material, and TGF-β1 was gradually decreased from day 7 to day 21. Another study done by Wolfe *et al.* observed the thrombogenic potential of PDO materials through acute monocyte tissue factor expression [115]. In this study, PDO concentrations of 60, 80, 120, and 160 mg/ml were electrospun and seeded with human peripheral blood

monocytes. The results from the study revealed that PDO grafts did not result in levels of tissue factor expression capable of a higher risk than that of the current standard, ePTFE. Through these studies, PDO has proven itself to retain low thrombogenicity and excellent mechanical properties by itself and when blended with other biopolymers. However, more information still needs to be examined in regards to cellularization of the scaffold materials and degradation characterization.

Polyester Urethane Urea

For engineering soft tissues such as the vascular system, elastic scaffolds are highly desirable since they are amenable to mechanical conditioning regimens that might be desirable to tissue development [116]. Martz *et al.* developed one of the first small diameter vascular graft from Mitrathane, a polyether urethane urea [117]. However, after a subsequent study in a canine carotid artery, all grafts were occluded after 4 to 6 months [118]. Since then, polyurethanes have been redeveloped by Wagner and associates (Table III) through synthesis of two kinds of biodegradable poly(urethane ureas), namely poly(ester urethane) urea (PEUU) and poly(ether ester urethane) urea (PEEUU) from PCL, poly(caprolactone)-b-poly(ethylene glycol)-b-poly(caprolactone), 1,4-diisocyanatobutane and putrescine. Grafts were fabricated by thermally induced phase separation and subsequent solvent extraction. Hydrolytic degradation of the grafts demonstrated a clear loss in scaffold weight after 56 days. Grafts were also conducive to SMC attachment and growth after 7 days in culture [116]. This sparked the use of PEUU by both the Wagner and Vorp labs using several different scenarios: electrospinning to form a whole tube [119], electrospinning on top of a porcine internal jugular vein as a reinforcement for

venous graft replacements [120], thermally induced phase separation (TIPS) to create a tubular scaffold for cell seeding with muscle derived stem cells [121], a TIPS tubular scaffold with an additional electrospun PEUU layer on top [122], and a blended electrospun scaffold using PEUU and poly(2-methacryloyloxyethyl phosphorylcholine-co-methacryloyloxyethyl butylurethane) [123]. These studies have had excellent results in terms of mechanical properties associated with their application and cellular seeding and proliferation *in vitro* and *in situ*. However, one of the possible disadvantages of using PEUU, especially in human implantation models, is its cytotoxicity due to the urethane component as the scaffold material degrades.

Table 3. PDO and PEUU

Biodegradable Polymer	Manufacturing Method	Improvement	Cell Seeded	Culture Condition	Ref
PDO					
Greisler *et al.*	70:30 PDO:Polypropylene Mesh Tube	Lower thrombogenic properties compared to PGA	—	Rabbit Aorta	105
Boland *et al.*	Electrospun PDO	Mechanical properties	—	—	107
Sell *et al.*	Electrospun PDO and elastin	Mechanical properties and compliance	FB	Static	109
Garg *et al.*	Electrospun PDO and elastin	Cell penetration of low elastin content	Macrophage	Static	114
Wolfe *et al.*	Electrospun PDO	Low thrombogenic potential	Monocyte	Static	115
PEUU					
Wagner, Vorp, *et al.*	Thermally induced phase separation and electrospun PEUU	Cell attachment, proliferation, and mechanical properties	SMC and Pericytes	Static and Vacuum Seeding	116, 119-123

Collagen

COL is the most abundant protein in the human body, a key element of the ECM, and imparts structural integrity and tensile strength to tissues. Tissue disruption following injury requires COL for the repair and restoration of structure and function. Excessive COL deposition at a wound site results in loss of anatomical structure, function and

fibrosis. Conversely, if insufficient amounts of COL are deposited, the wound is weak and may rupture [124]. This confers directly towards vascular tissue engineering; a vascular graft can be initially strong due to a synthetic polymer, however, once degradation occurs to a point where that strength is lost, there must be something to take over the mechanical requirements. In this case, not enough COL remodeling will cause the graft to develop an aneurysm and rupture.

COL has been used in a variety of tissue engineering applications because of its predominance in the ECM, non-immunogenicity and available methods of isolation from a variety of sources (Table IV). However, the typical procedures used to isolate and reprocess this natural scaffolding into an engineered material may compromise many of its biological and structural properties [125]. COL fibers also possess some unique structural properties important for tissue engineering: they transmit forces, dissipate energy, prevent premature mechanical failure and provide biological signals to adjacent cells that regulate functional responses. Additionally, COL is resorbable, has high water affinity, low antigenicity, very good cell compatibility and ability to promote tissue regeneration [126]. These factors combine to make COL one of the most ideal biopolymers available for tissue engineering applications.

In vascular tissue engineering, COL alone has been used in a number of applications. In 1986, Weinberg and Bell were the first to pioneer the idea of living blood vessels produced *in vitro* using cell seeded COL gel tubes [127]. The Weinberg and Bell arterial graft consisted of an adventitia of bovine FBs embedded in a COL gel; a media of gelled COL and bovine SMCs, and a lumen lined by ECs. One of the main limitations of

this approach was the lack of mechanical strength, demonstrating a burst pressure of only 90 mmHg. Investigators thereafter have attempted a number of other strategies to increase burst pressure strength, and maintain the biological aspect using ECs and SMCs. Berglund *et al.* mixed COL and human dermal fibrolasts together in the form of gels, which were subsequently crosslinked under different conditions to impart higher mechanical strength, resulting in a burst pressure over 600 mmHg [128]. Cummings *et al.* performed a similar experiment using the same manufacturing protocol, but with higher concentrations of COL and no cross-linking [129]. Matthews *et al.* forewent the COL gel construct and used electrospinning. Cells were well incorporated into cylindrical COL constructs placed in a 55 mL bioreactor with aortic SMCs [130]. COL by itself provides a construct that is advantageous for cellular seeding, but comes with drawbacks mechanically. Therefore, synthetic biodegradables are highly desired to provide mechanical stability for COL based grafts. PCL and COL constructs have been studied extensively and have been produced mostly through the form of electrospinning [131-133]. Each of the studies found that when PCL and COL were combined, COL provided increased cellular attachment and proliferation for FBs, ECs, and SMCs. Additionally, Ju *et al.* found that fiber diameter highly affected SMC penetration of the PCL/COL scaffolds under static culture. Other synthetics that have been investigated include electrospun PDO/COL [112], surface modified electrospun PLLA-co-CL with an air plasma coating of COL [134], a porous COL mold with electrospun PLGA [135], and a combined COL gel/particulate leached PLCL graft [136], where each study has clearly shown the cellular benefits associated with the addition of COL. COL is a very attractive protein to add to vascular grafts, increasing

adhesive properties and cellular infiltration and penetration. However, mechanically it can add significant stiffness to the material, therefore the proper amounts of COL need to be paid special attention when utilizing it.

Elastin

In vivo, ELAS is a chemically inert, highly insoluble polymer composed of covalently cross-linked molecules of its precursor, tropoelastin, a soluble, non-glycosylated and highly hydrophobic protein. Tropoelastin expression and subsequent ELAS synthesis typically occurs in FBs, vascular SMCs, ECs, and chondrocytes [137]. During the process of elastogenesis, tropoelastin is synthesized, preventing its premature intracellular aggregation and protecting it from proteolytic degradation by binding a 67 kDa galactoectin (elastin binding protein, EBP). This association lasts until the complex is excreted into the extracellular space. EBP then interacts with galactosugars of the microfibrils, dramatically decreasing its own affinity for tropoelastin. In order for proper elastogenesis to occur, the interaction of the N-terminal part of the microfibrillar-associated glycoprotein with the C-terminal end of tropoelastin is required. Once aligned, lysyl oxidase deaminates and oxidizes the lysyl residues to allysine following the action of Cu^{2+}. Cross-links are then formed by the reaction of the allysines with themselves or with an unmodified lysine [137-139].

As a biomaterial, ELAS is becoming more and more popular for tissue engineering applications as one of the main structural components of the vascular ECM (Table IV). The incorporation of ELAS into biomaterials has been used in several different forms, including insoluble ELAS occurring in autografts, allografts, xenografts, decellularized

ECM, and in purified ELAS preparations where the insoluble ELAS is hydrolyzed to a soluble form of α, β, and κ ELAS [140]. Although insoluble ELAS in its different graft forms could be considered a more "natural state," there is an advantage to its solubility which makes handling and analysis of the material more straightforward. Additionally, ELAS peptides influence signaling, chemotaxis, proliferation, and protease release via the ELAS receptor [141]. Daamen *et al.* not only found that solubilized ELAS induced angiogenesis, but also increased elastic fiber synthesis and displayed no signs of calcification when compared to grafts containing its insoluble form [142]. Leach *et al.* created α-ELAS discs using a diepoxy crosslinker, finding that vascular SMCs adhered well to the substrates [143]. This is one of many studies that have proven soluble ELAS to be an advantageous biopolymer.

As stated previously, tropoELAS provides the necessary building blocks to form native ELAS *in vivo*. Li *et al.* demonstrated that recombinant human tropoelastin could be electrospun to form both nanofibers and microfibers, depending on the delivery rate [144]. In their study, both tropoelastin and solubilized α-elastin were electrospun. The parameters were optimized and the final products were compared through microscopy, mechanical tensile moduli, and cellular activity with human embryonic palatal mesenchymal cells. Welsh *et al.* manufactured crosslinked ELAS-like polypeptide films, and performed tensile testing where stress-strain curves produced the low stress toe region of native tissue J-curves [145]. Again, like COL, ELAS by itself will fail to perform properly under the physiological stresses imposed by the vasculature. Investigators have looked into the combination of ELAS and synthetic materials. As mentioned previously,

PDO/ELAS grafts were electrospun and tested mechanically to find that certain blends emerged as comparable to native artery [109]. This study subsequently led to another blending PDO and ELAS in a layered fashion with PDO sutures as reinforcement between each layer [108]. ELAS-like polypeptide has also been implemented into vascular tissue engineering. Nicol and Urry explored the possibility of incorporating cell recognition peptide sequences into ELPs in order to promote EC adhesion, finding that too small an amount of RGD sequence significantly decreased cellular attachment [146]. More recently, tropoelastin was combined with PCL to form a bi-layered vascular scaffold with pure electrospun tropoelastin on the inner layer and combined PCL/tropoelastin on the outer layer [147]. Results displayed enhanced EC interaction, improved blood compatibility, excellent mechanical properties, and full cell penetration of the scaffold structure when implanted *in situ*. While ELAS is known as an essential, key factor in vascular arteries, its addition to scaffold materials comes with both advantages and disadvantages. Mechanically, ELAS enhances compliance and distensibility of scaffold material. From the cellular perspective, it has come with mixed results where specific types of ELAS are conducive to cellular attachment and others are not. These factors must be considered when working with ELAS as a biomaterial.

Combined Elastin and Collagen

As COL and ELAS are two of the most prevalent protein constituents in native vessel, it is only logical that they are often used in concert as tissue engineering scaffolds for vascular applications (Table IV). Berglund *et al.* looked to take their previous COL gel study and enhance its biomechanical properties through the incorporation of organized

intact ELAS to form hybrid constructs [148]. Histological staining from the study revealed that both the COL gel control and the COL/ELAS hybrid exhibited dense layers of cells along their outer walls. Additionally, ELAS incorporation increased mechanical properties by 11 fold. Boland *et al.*[2], in an attempt to create a biomimicking layered vascular structure, first electrospun an 80/20 COL type I/ELAS tube on a 4 mm diameter mandrel. This tube was subsequently seeded with both FBs and SMCs. Another tubular scaffold of 30/70 COL type I/ELAS was electrospun on a 2 mm diameter mandrel. This electrospun scaffold was then inserted into the 4 mm diameter scaffold and the lumen was filled with a SMC suspension. After 3 days in culture, a suspension of human umbilical vein endothelial cells (HUVECs) was injected into the lumen, and the entire construct was cultured for 2 more days. Histological examination revealed complete cellular infiltration into the three-layered construct after 21 days. The artificial intima was covered by morphologically mature ECs and SMCs were present throughout the media, and had begun to align circumferentially around the axis of the scaffold. The FBs and SMCs in the adventitia created a dense population throughout the outermost wall. This study proved that an electrospun scaffold that mimics the native ECM is highly beneficial in the field of vascular tissue engineering. However, the lack of synthetic polymers in the tubular structures did not allow for sustained mechanical viability.

In a study by Buttafoco *et al.*[149], soluble COL type I from calf skin and soluble ELAS from bovine neck ligament were electrospun from aqueous acidic solutions in order to avoid the use of organic solvents. To ensure continuous and homogenous fibers, poly(ethylene oxide) (PEO) and sodium chloride (NaCl) was added. Meshes composed of

fibers with diameters ranging from 220 to 600 nm were obtained by spinning the COL/ELAS solutions. Scaffolds completely devoid of PEO and NaCl were obtained by cross-linking with EDC and N-hydroxysuccinimide (NHS). SMCs were successfully cultured on cross-linked scaffolds and a confluent layer of cells was observed after 14 days on the surface of the different scaffolds.

Combinations of COL and ELAS with synthetic polymers have also been used in order to create scaffold and graft materials with desirable mechanical properties, bioactivity, and sustained mechanical integrity. Nanofiber grafts were fabricated using a mixture of 40% COL type I, 15% ELAS and 45% PLGA by weight electrospun onto a 4.75 mm diameter cylindrical mandrel. Compliance testing results showed that the diameter change was approximately 9% for native vessels and 12–14% for electrospun grafts under a physiologic pressure range. *In vitro* cell proliferation of SMCs and ECs showed an average of 82% of SMCs and 72% of ECs survived on the grafts [150].

In a similar study, an array of synthetic materials with 45% COL, 15 % ELAS, and 40% biodegradable synthetic (PLGA, poly(L-lactide) (PLLA), PCL, and poly(D,L-lactide-*co*-ε-caprolactone) (PLCL)) were electrospun. Tubular grafts were characterized through SEM, uniaxial tensile testing, and biocompatibility. Once again it was demonstrated that graft mechanical properties were improved with the addition of synthetic polymers. This study also demonstrated that in order for a graft to remain patent when using biopolymers such as COL and ELAS, the addition of a synthetic is necessary for sustained stability [151]. Recently studies have come out that have looked to mimic the natural architecture of blood vessels with the use of synthetic polymers, COL, and ELAS. McClure *et al.* used

electrospun PCL, ELAS, and COL in different ratios to develop a cross-linked mechanically tunable vascular graft characterized by compliance, tensile properties, suture retention, and burst pressure strength [152]. Thomas *et al.* performed a similar study with the use of an uncross-linked, electrospun polyglyconate, ELAS, and gelatin, demonstrating a distinctive tri-layered design [153]. Working with the natural polymers and architecture that are provided by Mother Nature could prove to be an advantageous method for vascular tissue engineering.

Table 4. Collagen, Elastin, and Collagen/Elastin Blends

Biopolymer	Manufacturing Method	Improvement	Cell Seeded	Culture Condition	Ref
Collagen					
Weinberg and Bell	Collagen gel	Cell proliferation	SMC, FB, and EC	Static	127
Berglund *et al.*	Crosslinked collagen gel	Mechanical strength	FB	Static	128
Cummings *et al.*	High concentration collagen gel	Mechanical strength	SMC	Cyclic mechanical stimulation	129
Matthews *et al.*	Electrospun collagen	Collagen nanofibers for cell attachment and proliferation	SMC	Rotary Bioreactor	130
Elastin					
Leach *et al.*	Crosslinked elastin discs	Cell attachment	SMC	Static	143
Li *et al.*	Electrospun tropoelastin	Mechanical elasticity and cell attachment	Meschymal Stem Cell	Static	144
Welsh *et al.*	Elastin-like polypeptide film	Stress-strain curve	—	—	145
Collagen and Elastin					
Berglund *et al.*	Collagen and elastin gel	Mechanical properties and cell proliferation	FB	Static	148
Boland *et al.*	Electrospun collagen and elastin in three layers	Cell proliferation and native arterial architecture	FB, SMC, EC	Rotary Bioreactor	149
Buttafoco *et al.*	Electrospun collagen and elastin with PEO and NaCl additives	Cell attachment and proliferation	SMC	Static	150
McClure *et al.*	Crosslinked electrospun PCL, collagen, and elastin	Mechanical compliance and burst pressure with tunable properties	—	—	152
Thomas *et al.*	Uncrosslinked electrospun elastin, gelatin, polyglyconate	Tunable properties	—	—	153

Decellularized Vessels

One obvious choice for vascular tissue engineering is finding a hollow tissue with the appropriate extracellular matrix components and removing cells from the construct (Table V). Several types of decellularized tissues have already been developed including human veins [154], bovine ureters [155], canine arteries [156], and small intestine submuscosa (SIS) [157]. Results found varying signs of proximal and distal hyperplasia with a varying patency rate between 40 and 100%. Lantz *et al.* grafted dog jejunal submucosa as an autologous vascular graft and found that after 28 days the graft was histologically similar to native vessel [158]. More recently, Gui *et al.* developed a decellularized human umbilical artery with a compliance of 4.3% / 100 mmHg and a maximum burst pressure of 970 mmHg [159]. As most of the aforementioned decellularized matrices were COL-based, there are some groups who have looked into ELAS-based products. Lu *et al.* utilized the Rasmussen protocol [160] on aorta samples to obtain an ELAS network [161]. The advantages of ELAS-based scaffolds is their distensibility, which, according to the experiment, remained the same as native aorta and significantly higher than COL-based aorta tested under the same conditions; however, tensile strength was severely decreased. Additionally, hDF studies revealed that ELAS based scaffolds had a higher degree of cellular infiltration after 28 days in rotary culture. Berglund *et al.* used the Starcher and Galione extraction method [162] with carotid arteries [148]. These ELAS grafts were repopulated using cells encapsulated in a COL gel, cultured, and then tested mechanically. Positive aspects of decellularized tissues include a more "off the shelf" type graft with no maturation time. However, despite a readily

available supply of artificial arteries is attractive, drawbacks include the inability to tailor the matrix content and architecture.

Fully Biological Grafts

The concept of a completely biological living graft implies the ability to remodel, grow, self-repair and respond to the immediate environment (Table V). The graft would also contain enough COL and ELAS proteins to display desirable viscoelastic properties, and would lack any synthetic foreign material that would initiate chronic inflammatory responses or be susceptible to infection [31]. L'Heureux developed an approach to biological scaffolds using human FBs and vascular SMCs in sheet form, which were subsequently wrapped around a PTFE coated mandrel [163]. The assembled constructs required an 8 week maturation period and were then seeded with human ECs, resulting in burst pressures able to withstand 2000 mmHg. Recently, L'Heureux and associates have performed a human trial using rolled cell sheets for radial artery, A-V shunts, and lower limb indications. This study demonstrated grafts that were able to withstand burst pressures in excess of 3000 mmHg while retaining an average compliance of 8.8%/100 mmHg after 6 months implantation [164]. Campbell *et al.* produced another graft through an inflammatory reaction, where a silastic tube was placed in the peritoneal cavity of rats and rabbits for 2 weeks and was covered in a layered fashion with myoFBs, COL matrix, and a single layer of mesothelium [58]. Lengths of myoFB-rich tubes were then grafted by end-to-end anastomoses into the carotid artery of a rabbit and the abdominal aorta of a rat. *In situ*, cells responded to local environmental cues, remodeled, and produced structures similar to those of native vessel. More recently, Stickler *et al.* aimed to assess the

possibility to strengthen these peritoneal cavity grafts, shortening the time for development [165]. This was achieved through the use of an implantable device which consisted of an inner stretchable tub, a perforated external tube and a transabdominal tube. So, as tissue grew onto the device, it was subjected to cyclic stretch to enhance growth. Mechanically, pulsed tubes displayed a significantly higher failure strength and failure strain compared to unpulsed tissue. This was most likely attributed to the higher organization of COL in the circumferential direction. While work in the area of fully biological grafts has demonstrated promise in vascular tissue engineering, there are still some drawbacks to the process, including culture time, risk of infection during the culture period, and a prolonged maturation time that takes away from "off the shelf" capabilities.

Table 5. Decellularized and Fully Biological Grafts

Biopolymer	Manufacturing Method	Improvement	Cell Seeded	Culture Condition	Ref
Decellularized					
Lantz *et al.*	Jejunal submucosa	Histologically similar	—	Canine implant	158
Gui *et al.*	Umbilical artery	Compliance and burst pressure	—	—	159
Lu *et al.*	Aorta with elastin network	Higher cell penetration	FB	Rotary Bioreactor	161
Berglund *et al.*	Carotid artery with collagen gel	Mechanical properties	FB	Static	148
Fully Biological Graft					
L'Heureux *et al.*	Rolled SMC sheets	Mechanical properties and autologous cell use	SMC	Static	163
Campbell *et al.*	Silastic tube in peritoneal cavity	Structure similar to native vessel	—	Rat Implant	58
Stickler *et al.*	Silastic tube in peritoneal cavity with cylic strain	Mechanical properties	—	—	165

Drug Delivery for Improved Vascular Grafts

Delivery of growth factors from scaffolds has been gaining interest as a therapy for a variety of tissue engineering applications, including vascular graft regeneration (Table VI). Growth factors play a critical role in the communication and information transfer

between cells and their environment by binding to specific receptors on cell surfaces. They modulate a variety of cell activities, including proliferation, differentiation, migration, adhesion, and gene expression. Due to their ability to play such a key role in cell activity, cell fate, tissue development, and repair, especially in the vascular system, it is no surprise that their use in therapies has been proposed. However, their success in clinical applications has been limited. The delivery of one, or several, factors in therapies is complicated, as there is limited knowledge behind the signaling and release of growth factors physiologically. In addition, there are several parameters that must be considered, including the delivery vehicle, the quantity/concentration of factor to deliver, the duration of the delivery, and the ability to control the release both temporally and spatially [166-170]. Furthermore, the route of travel by the growth factor(s)/drug(s) once it is delivered is also an important parameter, particularly if there could be a potential detrimental effect downstream.

Growth factors that play key roles in the angiogenic process necessary for vascular graft regeneration include VEGF, FGF, platelet derived growth factor-bb (PDGF-bb), stromal cell-derived factor-1α (SDF-1α), TGF-β, and angiopoietins-1 and 2 (Ang-1 and 2). VEGF and bFGF are heparin-binding growth factors involved in the initiation of the process, promoting EC proliferation and migration. PDGF-bb recruits SMCs and pericytes which, along with TGF-β, promote ECM deposition to stabilize neovessels [167]. SDF-1α plays an important role in angiogenesis as well by recruiting EPCs from the bone marrow [171]. For vascular applications, numerous studies have been performed on the delivery of

these growth factors, either alone, or in concert with one or two others, with the use of different delivery vehicles, as well as different delivery methods.

Table 6. Biopolymers and Synthetic Polymers for Drug Delivery

Drug Delivery	Drug Additive	Improvement	Cell Seeded	Culture Condition	Ref
Biopolymers					
Pang *et al.*	R136K to bind to collagen scaffolds	Lower thrombogenic properties	—	—	189
Wissink *et al.*	Immobilized heparin onto collagen scaffolds	Increased amounts of bFGF to material and cell proliferation	EC	Static	192
Synthetic Polymers					
Thevenot *et al.*	PLGA salt-leached scaffold injected with SDF-1α	Cell proliferation, angiogenesis, lower inflammatory response	EPC and MSC	Mouse Implant	203
Mooney *et al.*	VEGF and PDGF-bb released from PLGA scaffolds	Increased angiogenesis and maturation	—	Hindlimb Ischemia Model	204
Saif *et al.*	VEGF, HGF, Ang-1 released form PLGA scaffolds	Increased angiogenesis and maturation	EPC	Hindlimb Ischemia Model	206

Delivery methods and vehicles

Traditionally, growth factors are administered systemically (transdermal), orally, or intravenously. However, these methods of delivery are likely to be ineffective due to the short half-lives of the growth factors, their relatively large size, slow tissue penetration, and their potential toxicity at high systemic levels [167, 168]. For these reasons, polymeric materials, both natural and synthetic, are frequently used as delivery vehicles. Using polymers for this application allows for a more timely and spatially controlled delivery. Biomaterials used for this function must be nonimmunogenic, have degradation products that are soluble and nontoxic, and must be able to be produced sterile and free of infectious pathogens [169]. While natural polymers are beneficial due to their bioactive factor for cell recognition and degradation, synthetic polymers have very controlled and reproducible

chemical and physical properties. Another attractive feature of natural polymers are that some have specific binding sequences for and intermolecular interactions with many angiogenic growth factors [172].

Natural derived polymers

Natural polymers that have been previously used for delivery vehicles include alginate [173-175], agarose [176], chitosan [177, 178], gelatin [179, 180], fibrin [181], and COL [182-185]. They are often formed as a gel, or as microspheres, and are usually processed by freeze-drying or cross-linking in an aqueous solution [186].

Often, fibrin glue, which is a mixture of fibrinogen and thrombin, is used therapeutically, as it serves as a temporary platform for the gradual development of granulation tissue. Clinical application of fibrin glue has been studied as a deliverer of angiogenic growth factors to create a confluent endothelium on the luminal surface of synthetic vascular grafts [181, 187]. After coating e-PTFE grafts with fibrin glue and FGF-1, it was found to produce better EC retention and expansion after seeding, eliminating graft thrombogenicity and improving graft patency [188]. Recently, Pang *et al.* studied the affinity and distribution of a fusion protein consisting of R136K, a relatively thrombin-resistant mutant derivative of FGF-1, and a COL-binding domain, to 3-D COL scaffolds [189]. They found that R136K-COL binding domain had a greater affinity for COL scaffolds than either R136K or FGF-1, demonstrating a 1.7 fold lower release rate.

To suppress initial burst release often seen in hydrogel-type delivery systems, and still permit longer retention in the delivery carrier, heparinization has been proposed, either by covalent conjugation of heparin molecules, or the encapsulation of growth factor

together with heparin-binding material within the delivery vehicle. Modifying the network structure, such as cross-linking with glutaraldehyde, has also been done, so as to couple the rate of release to the rate of matrix degradation [190, 191]. Other studies have used *N*-(30 dimethylaminopropyl)-*N'*-ethylcarbodiimide (EDC) and NHS to cross-link COL and heparin, or COL and heparin sulfate, enhancing growth factor capture within the hydrogel, enhancing HUVEC expansion onto the graft [192], and producing a strong and stable vascularization throughout the hydrogel in a subcutaneous implant [193].

Synthetic derived polymers

Synthetic matrices that studies have reported on have been composed of poly(vinyl alcohol) (PVA), poly(alpha-hydroxyester)s including poly(ethylene glycol) (PEG) [194], PLGA [195-200], PLLA, or PCL [201], polyanhydrides, and polyorthoesters [180, 202]. They are typically processed into porous grafts that provide mechanical support for cells or microspheres for injection and are fabricated by techniques such as solvent casting, gas foaming, particulate leaching, double emulsion, electrospinning, and rapid prototyping [186]. Synthetic matrices for this application must completely degrade and be resorbed into the body, and must temporarily act as mechanical support to allow cells to infiltrate and produce native ECM.

A PLGA salt-leached scaffold injected with SDF-1α was implanted subcutaneously into mice to determine the ability of the scaffold to promote stem cell recruitment, reduce inflammatory response and fibrosis, and enhance angiogenic processes [203]. MSC migration and EPC engraftment near the SDF-1α incorporated scaffold were found to be enhanced after 7 days over a PLGA control scaffold. In addition, there was decreased

inflammatory cell recruitment, with reduced fibrotic capsule formation and proinflammatory cytokines around the scaffold. Histological analysis illustrated improved angiogenesis by EPCs throughout the SDF-1α incorporated scaffold over a PLGA control scaffold, with vessel-like formations occurring at the interface of the scaffold. The results from this study demonstrate the potential for these SDF-1α incorporated scaffolds to be used in vascular graft applications, as they elicit improved tissue response and regeneration.

Angiogenesis and tissue survival after implantation is essential for the survival of any implant, including tissue engineered vascular grafts. Dual growth factor delivery from synthetic grafts was first reported by Mooney's group, where both VEGF and PDGF-bb were released with distinct kinetics from grafts of PLGA fabricated by a high-pressure carbon dioxide process [204]. In looking at blood vessel size and distribution in a hindlimb ischemia model, relative to either growth factor delivered individually, both vessel size and distribution were improved when the delivery of the two growth factors were together. This demonstrates that therapies involving growth factor delivery for angiogenesis would benefit from the actions of multiple growth factors over just a single delivery. For this study, VEGF was responsible for the increase in blood vessel density, whereas PDGF contributed to the maturation and size of the blood vessels. Another study fabricated PLGA grafts from gas foaming and particulate leaching with VEGF and PDGF incorporated into different layers of the graft [205]. This layered graft system allowed compartmentalization of VEGF and PDGF and controlled spatial and temporal presentation of the growth factors.

Saif *et al.* took it a step further and incorporated three growth factors into a scaffold for delivery. In a murine hindlimb ischemia model, PLGA microparticles were fabricated containing VEGF, hepatocyte growth factor (HGF), and Ang-1 using a double emulsion technique [206]. These microparticles, along with cord blood-derived vascular progenitor cells, were coadministered into the hindlimb of a mouse. This resulted in a robust enhancement of vascularization, superior to any single growth factor administered. Including increased muscular capillary density and enhanced number of conductant vessels, with sufficient vessel stabilization and maturation.

In the presence of TGF-β1, SMCs cultured on adhesive ligand-modified glass surfaces, specifically RGDS-modified surfaces, increased matrix production. In addition, tethering TGF-β1 to PEG diacrylate hydrogel with RGDS resulted in a significant increase in matrix production over the same amount of soluble, unmodified TGF-β1 incorporated into scaffolds, most likely due to the diffusion of the soluble growth factor into the culture medium [194].

The authors of this paper have successfully electrospun lyophilized platelet rich plasma (PRP) with PCL to form nanofibrous grafts [207]. As PRP contains various supraphysiologic, autologous growth factors and cytokines that enhance healing, its addition to a synthetic construct has the potential to increase the bioactivity of the graft and enhance regeneration through the release of growth factors contained within the PRP. Results from a protein assay have demonstrated successful release from the electrospun grafts for 35 days, as well as quantifiable release of PDGF-bb over 14 days. The PRP containing grafts were also chemotactic towards macrophages, and significantly enhanced

proliferation of adipose derived stem cells over synthetic grafts. These results are promising for the use of electrospun grafts incorporated with PRP as an improved therapeutic strategy for tissue engineering applications such as vascular grafts.

Other growth factors/drugs used to improve scaffolds for vascular graft applications include heparin [208], a known anticoagulant, insulin [209], nitric oxide [210, 211], a known vasodilator and mediator of EC growth and function, cyclosporine [212], a potent immunosuppressive that inhibits SMC proliferation and intimal hyperplasia, and other antibiotics. A study by Javerliat *et al.* implanted vascular grafts preloaded with antibiotics, rifampin and tobramycin, into the infrarenal aortas of dogs [213]. The grafts implanted were: gelatin-sealed knitted polyester grafts used as controls, and antiobiotic-bonded gelatin-sealed knitted polyester grafts loaded with rifampin and tobramycin at normal doses, and twice the normal doses. After 21 days, histological analysis of the grafts revealed complete patency of all grafts, with no signs of local toxic response to the antiobiotics. Healing of the preloaded grafts, whether at standard or twice standard loading of antibiotics, was always similar to that of the conventional gelatin-sealed grafts, with no signs of poor healing. These results are encouraging, seeing as how vascular prosthetic infections still remain a serious complication of vascular surgery.

Conclusion

Despite the many obstacles to overcome in the creation of a successful vascular graft, research from the last 10 years has exponentially increased our knowledge and understanding of what is required of a vascular substitute. Biohybrid and tissue engineered vascular grafts have been investigated using material properties, complex tissue culture,

and cell seeding techniques. Investigators have looked at several approaches to the issues that still prevent an ideal graft from being designed. At the present time, both *in vivo* and *ex vivo* solutions have significant drawbacks; however, through the combination of bioresorbables, biopolymers, drug delivery, and cells, we can surmount the setbacks and ameliorate these problems.

Overview of the Current Study

As mentioned previously, arteries are designed in a tri-layered fashion represented by the intima, media, and adventitia. Each of these layers imparts its own composition of cells and ECM depending on its anatomical location and has an affect on the overall mechanical properties. Mechanically, if we are able to mimic this tri-layered arterial structure, then this could potentially make large strides towards a graft which would adequately replace the diseased tissue for a significant period of time. Three layers provides us with a multitude of options where microscopic and macroscopic properties can be fine tuned through a series of tests with different synthetic biodegradable polymers and biopolymers. At the microscopic end, graft properties such as fiber diameter, the addition of proteins, and eventually drug delivery techniques can be employed to enhance both mechanical and cellular properties. Macroscopically, we can derive polymer blends to mimic native tissue through a series of tests so that compliance mismatch and aneurysmal formations present less limitations. Additionally, biodegradable polymers can be tailored to degrade different layers at different time points to potentially time the degradation of the material and to match that of cellular occupation. These potential benefits due to a tri-layered structure could lead us to a better vascular graft.

The search for the ideal vascular graft has been defined by some as the search for the "Holy Grail." [214] It is a daunting task that many have investigated. Multi-layer electrospinning was first attempted by Kidoaki *et al.* [215] using type I COL, gelatin, segmented polyurethane, and PEO. Since then multi-layer electrospinning has been studied using PCL, PLA, PDO, Poly(glycolide-co-trimethylene carbonate), gelatin, and ELAS [98, 108, 153, 216]. These studies employed different uses of multilayered techniques. Smith *et al.* [108] electrospun PDO-ELAS bilayered constructs with a suture wound in the center for reinforcement. Vaz *et al.* [98] electrospun a bilayered tube structure made of PCL and PLA, varying the anisotropy of the layers, but not including natural polymers. Yang *et al.* [216] performed a layer-by-layer approach electrospinning PCL and COL together, seeding HDFs, and then repeating the PCL/COL and HDF layers. These cellularized constructs were done is sheet form and not with tubes. Thomas *et al.* [153] utilized PGA, ELAS, and gelatin in a tri-layered form. However, the use of PGA and gelatin would not be conducive to an arterial graft as gelatin, *in vivo*, has been shown to display a large cytotoxic response [217] and PGA is a fast degrading polymer.

Vascular graft development has currently produced cellular and acellular products. Cellularized grafts have made headway for many such as the completely autologous vascular graft developed by Nicolas L'Heureux [163]. However, a cellularized structure introduces an extremely high level of complexity, cost, and risk. Harvesting a patience own cells, growing them in culture, and then coming out with a final product can take in excess of 6 months. Additionally, during the culture process, the graft is prone to infection. Within this time frame, the patient could die before receiving a fully developed

cellularized vascular graft. This study, however, uses an acellular vascular graft providing an off-the-shelf product that can be implanted immediately, and using the body as its own natural bioreactor to regenerate and develop the native arterial tissue.

The materials chosen for this experiment were PCL, ELAS, COL, and silk fibroin (SF). PCL is a semicrystalline, non-toxic, and tissue compatible biomaterial with a degradation rate of around 12 months. Mechanically, PCL displays highly desirable characteristics for vascular grafts, mostly high strength and good compliance. For this study, PCL was utilized as the main vascular graft material, providing the mechanical backbone for the biopolymers which are integrated into the scaffolding in different quantities. ELAS is one of the main structural components of the vascular ECM, imparting distensibility and elastic recoil. Daamen *et al.* not only found that solubilized ELAS induced angiogenesis, but also increased elastic fiber synthesis and displayed no signs of calcification when compared to grafts containing its insoluble form [142]. This is one of many studies that have proven soluble ELAS to be an advantageous biopolymer. COL is one of the most plentiful proteins found in native blood vessel, conferring circumferential strength to the vessel wall. COL fibers also possess some unique structural properties important for tissue engineering: they transmit forces, dissipate energy, prevent premature mechanical failure and provide biological signals to adjacent cells that regulate functional responses. Additionally, COL is resorbable, has high water affinity, low antigenicity, very good cell compatibility and ability to promote tissue regeneration [126]. These factors combine to make COL one of the most ideal biopolymers available for tissue engineering applications. Silk exhibits excellent biocompatibility with a foreign body

response comparable to other degradable sutures, hemocompatibility, and oxygen and water permeability. Silk also possesses remarkable mechanical properties not seen in other naturally occurring proteins [218-220]. In this study, we observed the affect that each polymer exhibited on one another through a series of mechanical and cellular tests.

CHAPTER 2: Preliminary Investigation of Chemical Crosslinking

Preface: The following manuscript is currently published in the Journal of Electrospun Fibers and Fabrics. This work investigates two goals to be achieved through this experiment: 1. To determine the maximum amount of elastin that could be retained within an uncrosslinked electrospun mat of soluble elastin and polydioxanone (PDO), and 2. To investigate several different ways the soluble elastin can be cross-linked and the resulting mechanical properties of those scaffolds.

Cross-linking Electrospun Polydioxanone-Soluble Elastin Blends: Material Characterization

Michael J. McClure, Scott A. Sell, Catherine P. Barnes, Whitney C. Bowen, and Gary L. Bowlin
Department of Biomedical Engineering, Virginia Commonwealth University, Richmond, Virginia 23284

Abstract

The purpose of this study was to establish whether material properties of ELAS co-electrospun with PDO would change over time in both the uncross-linked state and the cross-linked state. First, uncross-linked scaffolds were placed in phosphate buffered saline (PBS) for three separate time periods: 15 minutes, 1 hour, and 24 hours, and subsequently tested using uniaxial materials testing. Several cross-linking reagents were then investigated to verify their ability to crosslink ELAS: EDC, ethylene glycol diglycidyl ether (EGDE), and genipin. Uniaxial tensile testing was performed on scaffolds cross-linked with EDC and genipin, yielding results that warranted further investigation for PDO-ELAS blends. Material properties of the cross-linked scaffolds were then found within range of both pig femoral artery and human femoral artery. These results demonstrate PDO-ELAS blends could potentially be favorable as vascular grafts, thus warranting future *in vitro* and *in vivo* studies.

Key Words: electrospinning, vascular graft, elastin, polydioxanone, cross-linking

Introduction

For over a hundred years, CVD has remained the number one cause of death in the United States. In 2003, preliminary mortality data showed CVD accounted for 37.3% of

all deaths (16.7% of those people were under the age of 65). Atherosclerosis accounted for three quarters of deaths related to CVD. This thickening of arterial wall due to disrupted blood flow can lead to a myriad of complications [221, 222]. In an attempt to treat patients with this disease, an estimated 467,000 bypass surgeries occurred in 2003 [221].

Currently, for small diameter (< 6mm) vascular grafts, autologous blood vessels, such as the saphenous vein, are the standard. However, many patients do not have a suitable vessel for use because of peripheral vascular disease, amputation, or prior harvest [29, 30, 223]. If autologous blood vessels are unavailable, then the replacement must be prosthetic. Several options are available when choosing among the number of grafts currently on the market. The most common options are ePTFE and Dacron®. However, at the small diameter level, the properties of these materials have generally proved inadequate due to acute thrombogenicity of the graft, anastomotic intimal hyperplasia, aneurysm formation, infection, and progression of atherosclerotic disease [223]. Therefore, new design criteria must be implemented. Qualities of an ideal design would include the ability to be nonthrombogenic, nonimmunogenic, infection resistant, capable of inducing an appropriate healing response, flexibile, kink resistant, easily manufactured, affordable, easily stored, available in a variety of sizes (lengths and diameters), and mechanically compliant [222-225].

Arteries require a complex design in order to withstand high flow rates and high pressures at pulsatile intervals. The vessels themselves can be considered as viscoelastic tubes, where their diameter is maintained by the balance between elasticity and strength imparted by the different components of the wall and the applied transmural pressure [226-

228]. These tubes experience two primary hemodynamic forces: the circumferential force resulting from the wall tension due to blood pressure, and the frictional force or shear stress resulting from blood flow along the vessel wall. The relationship between shear stress, vascular restructuring, and growth has led to speculation of an association between shear stress and the formation of atherosclerotic lesions [229]. Therefore, in low flow environments, such as small diameter blood vessels, it is essential to match the mechanical forces of a vascular graft with the native artery for proper graft functionality.

To elicit these specific properties, the proper choice of polymers and fabrication must be made. While other scaffold fabrication techniques exist for vascular conduits, electrospinning has emerged as one of the leading techniques for generating biomimetic scaffolds made of synthetic and natural polymers. Electrospinning uses an electric field to control the formation and deposition of polymer fibers and is remarkably efficient, rapid, and inexpensive [230]. Using this technique, a number of biomaterial constructs have been fabricated [150], including constructs that hold potential for blood vessel engineering [231]. Previous research has shown COL types I and III, ELAS, and PDO to be readily spinnable into submicron scale fibrous scaffolds [144, 222, 232-235]. Therefore, creating a scaffold that combines the mechanical strength of a biodegradable polymer with the bioactive properties of the ECM could prove to be a beneficial design in the quest for a bioresorbable vascular grafts [236]. Ideally, once these scaffolds are processed and implanted *in situ*, cells will recognize the surface, adhere, migrate, and proliferate.

In vivo ELAS [137-139] strongly differs from its soluble form [140], α-ELAS and β-ELAS, which is commonly used in vascular engineering scaffold fabrication. Previous

experiments have blended COL and ELAS scaffolds [222, 232], leading to the instantaneous dissolution of the electrospun fibers in water as demonstrated by Buttafoco *et al.* However, the characteristics of ELAS dissipation, when co-electrospun with PDO, are unknown. Therefore, cross-linking the scaffolds may be a necessity. The most common crosslinker, glutaraldehyde, has been used with numerous types of electrospun scaffolds [222, 233, 237-240], but with cytotoxic drawbacks [241]. EDC and genipin, on the other hand, have exhibited lower cytotoxicity [241-243], making them better suited for implantation.

This study focused on the 50:50, 60:40, 70:30, 80:20, 90:10, and 100:0 PDO:α,β–ELAS blend ratios, and their behavior as an uncross-linked scaffold when immersed in PBS solution for three separate time periods: 15 minutes, 1 hour, and 24 hours. All scaffolds were tested for dry weight loss and material properties. Cross-linked scaffolds were subsequently investigated to determine if any material property changes occurred over time.

Materials and Methods

Electrospinning

The following were blended in ratios of 100:0, 90:10, 80:20, 70:30, 60:40, 50:50, and 0:100 (250 mg/ml for electrospinning pure ELAS fibers) by volume (PDO:ELAS) and dissolved in 1,1,1,3,3,3 hexafluoro-2-propanol (HFP, Sigma Aldrich Co.): PDO (Ethicon, Inc.) with a concentration of 100 mg/mL and ELAS concentration from bovine neck ligament, α-ELAS and β-ELAS, (Elastin Products Co., Inc.) of 200 mg/mL. These solutions were then inserted into a plastic 5 ml Becton Dickinson syringe with a blunt tip

18 gauge Becton Dickinson PrecisionGlide® needle. The syringe and needle were placed in a KD Scientific syringe pump to be dispensed at a rate specific to the PDO:ELAS blend (between 4 and 8 ml/hr). The solutions were electrospun onto a flat rotating mandrel (2.5 cm wide x 10.2 cm long x 0.3 cm thick) to produce a flat sheet with random fiber orientation for weight testing and uniaxial tensile testing. Each sample was electrospun with an applied voltage of 22 kV at a distance of 10-13 cm from the needle tip to the mandrel and a rotational speed of 500 revolutions per minute (rpm).

Weight Loss After Hydration

Scaffolds were cut randomly into rectangular shapes (approximately 1.5cm x 1cm) from the electrospun sheet, weighed, and randomly placed into a specific time group (15 minutes, 60 minutes, or 24 hours) based on ELAS's instantaneous dissolution in PBS. The scaffold was placed in a 35x10mm Petri dish with 3mL of PBS for the specified time. The scaffolds were then extracted and washed 3 times with 3 mL of deionized water. The scaffolds were placed in a desiccation chamber for 24 hours to dry. Each sample was then weighed to determine any weight loss (percent remaining)

$$\%\ Remaining = \frac{Weight_{Time}}{Weight_{Initial}} \times 100 \qquad (1)$$

where $Weight_{Time}$ was specified as the weight remaining after being soaked in PBS and dried, and $Weight_{Initial}$ was specified as the initial dry weight of the sample prior to its PBS soak.

Dry Scaffold Characterization

Scaffold characterization was performed using scanning electron microscopy on small pieces cut from the electrospun mats (SEM, JEOL JSM-820 JE Electron Microscope). SEM images were digitized with a Hewlett-Packard Scanjet 5550c flatbed scanner and analyzed with ImageTool 3.0 software (Shareware provided by UTHSCSA). Characterization included determining the average fiber diameter for the electrospun structure by taking the average of 60 measurements chosen randomly from across the image. For all of the measurements made from the SEM images, calibration of the ImageTool software was done with the scale bar on each image. The sample size for each measurement was n = 60.

Uniaxial Tensile Testing

Uniaxial tensile testing was performed on dry and hydrated samples at each time point. Uniaxial tensile testing was also performed on ePTFE, 100% electrospun ELAS, and decellularized pig femoral artery. "Dog-bone" shaped samples were punched from the electrospun mat (2.75 mm wide at their narrowest point with a gage length of 7.5 mm) and tested on a MTS Bionix 200 testing system with a 50 N load cell (MTS Systems Corp.) and an extension rate of 10.0 mm/min. Tangential modulus, peak stress, and strain at break were calculated using Test Works version 4. The sample size for each specimen was n = 6.

Cross-linking

Scaffolds were cross-linked using EDC (Fluka Biochemika), genipin (Wako Pure Chemical Industries, Ltd.), and ethylene glycol diglycidyl ether (EGDE, Sigma Aldrich, Inc.).

Cross-linking with EDC

For EDC crosslinking a 50x molarity solution (166.5 mM) was prepared in accordance with Barnes *et al.* [244] in ethyl alcohol (Fisher Scientific). Scaffolds were placed in the EDC solution, and allowed to cross-link for 18 hours followed by a 0.1M Na_2HPO_4 rinse for 1 hour and a PBS rinse for 1 hour.

Cross-linking with Genipin

A 30mM solution of genipin dissolved in ethyl alcohol was used to cross-link ELAS scaffolds. Scaffolds were electrospun and placed in the cross-linking solution for a period of 72 hours [245], followed by a PBS rinse for 2 hours.

Cross-linking with EGDE

Based on the work performed by Leach *et al.* [143], ELAS scaffolds were cross-linked using 50% EGDE. At room temperature electrospun ELAS scaffolds were placed in a Petri dish with EGDE and allowed to crosslink for 24 hours followed by a PBS rinse for 2 hours.

Visual Inspection of Cross-linked Scaffolds

Cross-linked scaffolds were initially placed in PBS for a 24 hour period to determine structural stability. Observations were recorded at time intervals of 0 minutes,

15 minutes, 1 hour, and 24 hours and scaffolds were subsequently measured for free amine groups.

Determination of Free Amino Groups

The concentration of free primary amine groups present in cross-linked electrospun ELAS was determined using 2,4,6-trinitrobenzenesulfonic acid (TNBS, Research Organics) [244]. Scaffold samples were electrospun, punched into "dog bone" shapes, massed and cross-linked using the procedures listed above. Samples were placed in 15mL Fisherbrand® centrifuge tubes. $NaHCO_3$ (1.0 mL 4% w/v) and TNBS (1.0 mL 0.5% w/v) were added and placed in an incubator at 40°C for 2 hr. 3.0 mL of 6M HCL was then added to the solution, which was placed in an oven at 60°C for 2 hr. The samples were diluted with 9 mL of PBS, cooled to room temperature. The absorbance at 345 nm was measured using a SPECTRAmax® PLUS^{384} microplate spectrophotometer. Measured absorbance values were then placed into a percent cross-linking equation

$$\%Cross-linked = 1 - \left[\frac{Abs_c / Mass_c}{Abs_{nc} / Mass_{nc}} \right] \quad (2)$$

where Abs_c is the measured absorbance of the cross-linked solution, Abs_{nc} is the measured absorbance of the non-cross-linked solution, $Mass_c$ is the dry mass of the cross-linked scaffold, and $Mass_{nc}$ is the dry mass of the non-cross-linked scaffold. The sample size for each measured absorbance group was n = 9.

Statistical Analysis

Anaylsis of variance (ANOVA) was performed in NCSS® 2004 statistical software (NCSS, USA) using a Kruskal-Wallis test (p <0.01) to determine if at least two medians were different, and a Tukey-Kramer pair wise multiple-comparison test (p < 0.01) to ultimately determine significant differences between groups.

Results and Discussion

Weight Loss After Hydration

Soluble ELAS is known to immediately dissociate into aqueous solutions. PDO and ELAS were electrospun together in order to demonstrate the possibility of PDO retaining the ELAS fibers. Thus, PDO could prevent ELAS dissociation in PBS without a cross-linking agent.

The total weight of each electrospun scaffold illustrated the relationship between the different blends of PDO and ELAS; as the amount of ELAS increased, the weight of the dry scaffold increased as well. Once hydrated, the results indicated that as the amount of ELAS was increased, the faster the scaffold degraded or dissociated. PDO:ELAS blends of 50:50 experienced a 50.4% reduction in the weight of the scaffold in the first 15 minutes alone. After 24 hours an additional 10.1% reduction in weight occurred, creating an almost exponential decrease. As the initial amount of ELAS in the scaffolds was reduced, weight loss over time tended to become more linear (Figure 1, Table 7).

Table 7.Average Remaining Dry Weight

Graft Material	Remaining 15 minutes (%)	Remaining 60 minutes (%)	Remaining 24 hours (%)
50:50	50 ± 12	41 ± 7.5	39 ± 5.9
60:40	71 ± 17	64 ± 11	58 ± 2.7
70:30	94 ± 2.5	77 ± 3.9	67 ± 5.2
80:20	96 ± 3.3	91 ± 7.4	85 ± 2.1
90:10	106 ± 5.8	107 ± 7.0	99 ± 3.6
100:0	100 ± 2.9	100 ± 3.8	102 ± 2.0

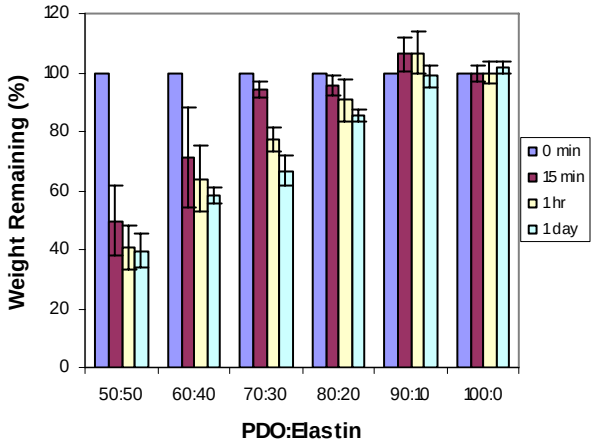

Figure 1. Percent of scaffold weight remaining after t = 0 minutes, 15 minutes, 60 minutes, and 24 hours, respectively in PBS.

The initial weight was significantly different from 15 minutes, 60 minutes, and 24 hours for both blends of 50:50 and 60:40; however, the 15 minutes, 60 minutes, and 24 hours blends were not different from each other. Therefore, the two blends lost most of their weight in the first 15 to 60 minutes, leading to a slowed rate of loss as time progressed. Significant differences existed among the three timed groups for 70:30, but not between the initial weight and 15 minute batch time. Differences existed between the initial weight, 60 minutes, and 24 hours batch times for 80:20. However, initial weight and

15 minutes did not exhibit any differences for 80:20. This result indicates the scaffolds were retaining their weight in the first 15 minutes in PBS, but as time progressed there was a significant drop in scaffold weight. 90:10 and 100:0 results demonstrated no significant differences.

As there was no change in PDO content of the scaffolds over such a short exposure to an aqueous environment, all weight loss is attributed to the dissolution of ELAS. Results indicate as the ELAS content decreased, it took longer for the ELAS to dissipate out of the scaffold. This can be clearly observed in the 80:20, 70:30, 60:40, and 50:50 scaffolds, where a logarithmic relationship exists between time and weight percent (Figure 2).

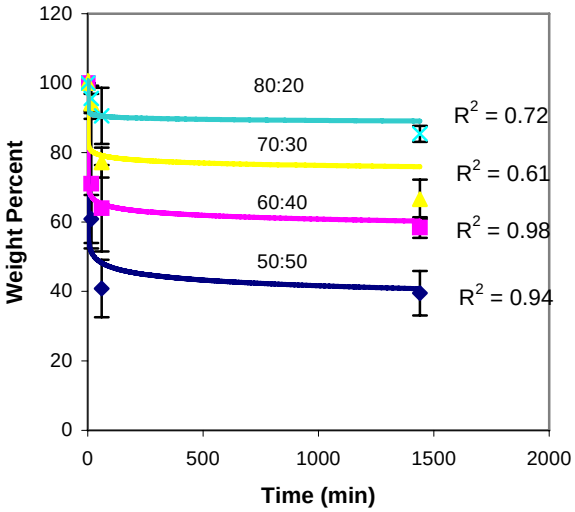

Figure 2. Weight percent of PDO:ELAS blends 50:50, 60:40, 70:30, and 80:20 vs. time (0, 15, 60, and 1440 minutes). The data is fit to a logarithmic curve where R^2 values display the degree of association between weight percent and time.

So, as ELAS content increased its ability to dissipate in a shorter period of time also increased with a high degree of association for 50:50 and 60:40 (R^2 values). 90:10

and 100:0 demonstrated no ELAS loss over time. The lack of ELAS loss could indicate that with minimum ELAS content PDO may have successfully retained the ELAS fibers, or it could indicate PDO is slightly hydrophobic and does not allow an aqueous solution to fully dissociate the electrospun ELAS. Therefore, it was determined that electrospun soluble ELAS was not able to be retained in scaffolds containing high percentages of ELAS when co-electrospun with PDO. However, as the ELAS decreases and PDO increases, there is evidence that the dissipation of ELAS from the scaffold is slowed, or possibly stopped.

Dry Scaffold Characterization

Scanning electron microscopy demonstrated that PDO and ELAS were successfully electrospun into a random non-woven mat Figure 3. This is demonstrated by the thin, flat, ribbon-like fibers which represent ELAS compared to the more rounded fibers which represents PDO. Mean fiber diameter and pore area were calculated for all scaffold types, where mean fiber diameter ranged from 0.88 – 0.56 μm and mean pore area ranged from 4.7 – 1.5 μm^2.

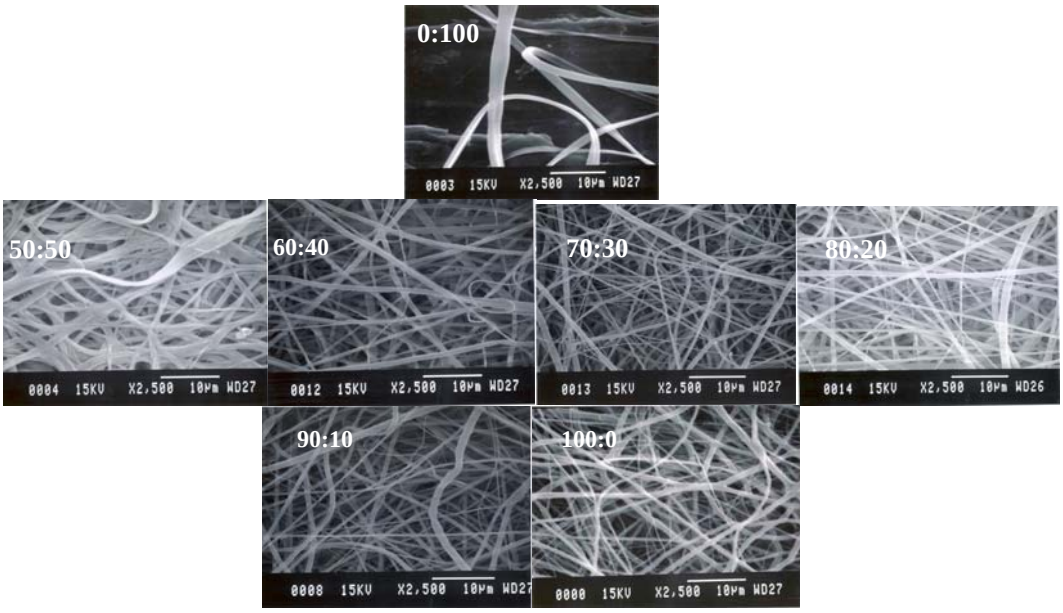

Figure 3. Scanning electron micrograph of electrospun PDO:ELAS. All micrographs are taken at 2500x magnification and the scale bar is equivalent to 10 microns.

Uncross-linked PDO:ELAS Uniaxial Tensile Testing

As weight sampling indicates, ELAS dissociation definitely occurs in some blends over time. Consequently, scaffold mechanical properties could also change with time. Results of uniaxial tensile testing are displayed in Figure 4 and Table 8 with peak stress, tangential modulus, and strain at break.

The scaffolds were tested dry as well as at timed hydrations of 15 minutes, 60 minutes, and 24 hours. Timed hydration results for peak stress indicated there were no differences among the 50:50 scaffolds. Samples at 24 hours were different from both 15 minutes and 60 minutes among the 60:40 scaffolds. Among the 70:30 scaffolds, times of 15 minutes, 60 minutes, and 24 hours were different from each other. There were no significant differences among the 80:20 scaffolds. 90:10 scaffolds showed significant differences between 24 hours and both 15 minutes and 60 minutes. The group timed at 15

minutes was different from those timed at 60 minutes in the pure PDO scaffold. One possible difference that could account for the differences seen in 90:10 and pure PDO scaffolds are batch to batch differences in PDO or ELAS that occur during the electrospinning process for use in the 24 hours hydration. Due to the preliminary nature of this study, further investigation is required.

Table 8. Material Properties of Uncross-linked PDO:Elastin at Times of 15 minutes, 1 hour, and 24 hours.

Graft Material	Peak Stress (MPa)	Modulus (MPa)	Strain at Break (mm/mm)
50:50 15 minutes	2.7 ± 0.2	6.1 ± 0.9	0.8 ± 0.04
50:50 60 minutes	2.7 ± 0.5	6.0 ± 0.9	0.8 ± 0.1
50:50 24 hours	2.3 ± 0.4	6.5 ± 1.0	0.9 ± 0.1
60:40 15 minutes	5.1 ± 0.4	8.1 ± 1.2	0.9 ± 0.1
60:40 60 minutes	4.7 ± 0.7	7.3 ± 1.5	0.9 ± 0.03
60:40 24 hours	3.0 ± 0.8	6.0 ± 1.9	0.7 ± 0.1
70:30 15 minutes	7.3 ± 0.4	6.2 ± 0.1	1.4 ± 0.1
70:30 60 minutes	6.2 ± 0.3	6.0 ± 0.8	1.4 ± 0.2
70:30 24 hours	3.4 ± 0.4	4.1 ± 0.7	1.1 ± 0.1
80:20 15 minutes	5.9 ± 0.6	4.3 ± 0.4	1.7 ± 0.1
80:20 60 minutes	6.3 ± 0.3	4.9 ± 0.2	1.6 ± 0.1
80:20 24 hours	5.3 ± 0.8	5.7 ± 0.8	1.3 ± 0.2
90:10 15 minutes	10 ± 0.6	13 ± 1.0	1.5 ± 0.1
90:10 60 minutes	12 ± 2.4	16 ± 4.7	1.3 ± 0.2
90:10 24 hours	5.1 ± 0.3	5.2 ± 0.4	1.4 ± 0.1
100:0 15 minutes	6.3 ± 0.4	6.6 ± 0.5	2.8 ± 0.4
100:0 60 minutes	4.9 ± 0.7	7.5 ± 0.7	2.0 ± 0.3
100:0 24 hours	5.6 ± 0.7	20 ± 0.7	2.1 ± 0.4

Trends of the tangential modulus results closely resembled those of peak stress for the 50:50, 60:40, and 70:30 samples. Among the 80:20 scaffolds, the batch timed at 15 minutes was different from the batch timed at 24 hours. This discrepancy was also true for the 90:10 and 100:0 blends, where times of 15 minutes and 60 minutes were different from

24 hours in the 90:10 and pure PDO scaffolds. 90:10 actually increased in stiffness from 15 minutes to 60 minutes, but dropped dramatically after 24 hours. Results for 80:20 and 90:10 could once again be due to batch differences in ELAS or PDO; however, further investigation is required to determine this.

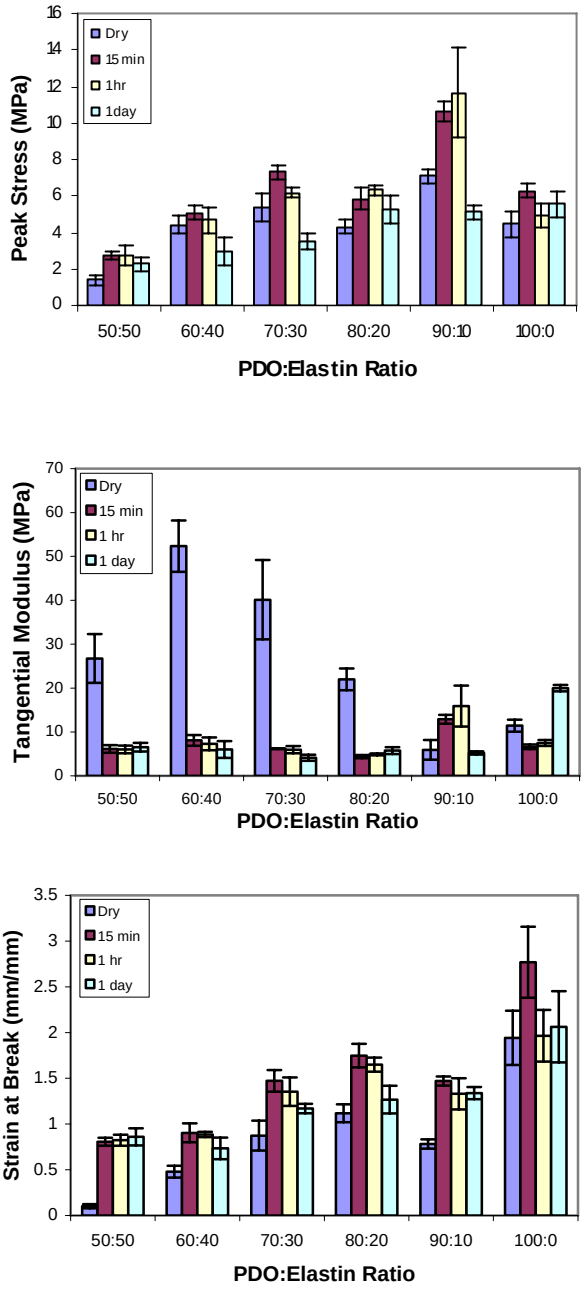

Figure 4. Comparison of uniaxial tensile test values for peak stress, modulus, and strain at break, for uncross-linked PDO:ELAS blends.

No significant differences existed among the 50:50, 60:40, and 90:10 scaffolds for strain at break. Among the 70:30 scaffolds, the batch time of 15 minutes is different from

24 hours, and 15 minutes and 60 minutes are different from 24 hours among the 80:20 scaffolds, indicating a change has occurred over a 24 hour period. In addition, the batch timed at 15 minutes is different from 60 minutes in pure PDO scaffolds.

Material properties of the uncross-linked PDO:ELAS blends demonstrated overall changes in the scaffolds over a time period of 24 hours. No differences were visible in the 50:50 and 60:40 scaffolds, indicating ELAS had dissociated too quickly in the 50:50 and 60:40 scaffolds for any noticeable change to be seen. However, 70:30 scaffolds, demonstrated an overall change from 15 minutes to 24 hours for all material properties, whereby the material became less stiff, peak stress decreased, and strain at break decreased. 80:20 and 90:10 scaffolds showed changes over time as well, but not for all properties. Therefore, the material properties change over a period of one day when the scaffolds are uncross-linked, providing evidence suggesting PDO does not adequately retain the soluble ELAS in the scaffolds, making cross-linking a necessity.

Cross-linking Elastin

The cross-linked results for electrospun ELAS scaffolds are illustrated in Figure 5, where 166.5 mM EDC had a percent cross-link average of 45.1%, while genipin had an average of 23.3%. EGDE was not calculated because the scaffolds dissociated immediately in $NaHCO_3$ solution prior to incubation, indicating minimal to no cross-linking. Statistical differences existed between the 166.5 mM EDC and 30mM genipin, demonstrating 166.5 mM EDC had the maximum cross-linking among the groups.

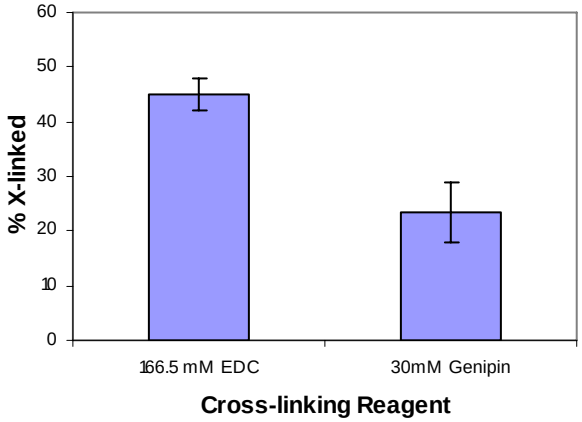

Figure 5. Percent cross-linkage of EDC and genipin for electrospun ELAS scaffolds.

Cross-linking PDO:Elastin

Figure 6 shows the results of a weight loss study, clearly demonstrating ELAS retention after cross-linking in a 50:50 PDO:ELAS scaffold after soaking in PBS for 24 hours. There is no statistical difference between the scaffold cross-linked with EDC and the initial weight. However, there is a statistical difference between the initial weight of the uncross-linked scaffold and its final weight after one day.

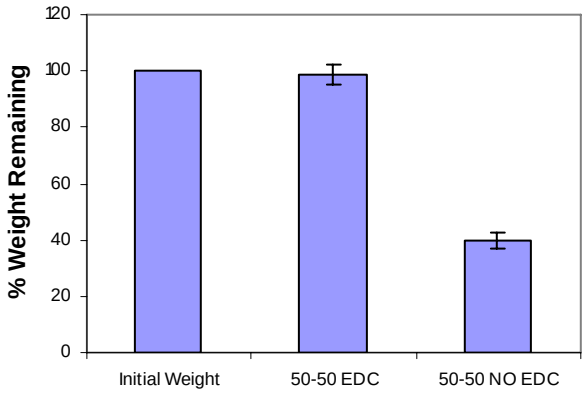

Figure 6. Percent of weight remaining of EDC cross-linked 50:50 PDO:ELAS scaffolds and uncross-linked 50:50 PDO:ELAS scaffolds after being soaked in PBS for 24 hours.

Cross-linked PDO:Elastin Uniaxial Tensile Testing

Since EDC had the highest degree of cross-linking, materials cross-linked by this method were the focus of uniaxial tensile testing. The results obtained were compared to ePTFE and pig artery. Peak stress, tangential modulus, and strain at break for particular EDC scaffolds are contained in Table 9.

Table 9. Material Properties of EDC Cross-linked and Uncross-linked Electrospun Scaffolds Compared to Human Femoral Artery [246, 247], ePTFE, and Decellularized Pig Artery.

Graft Material	Peak Stress (MPa)	Modulus (MPa)	Strain at Break (mm/mm)
Femoral Artery	1.5 ± 0.5	11 ± 1.5	0.7 ± 0.1
Pig Artery	3.4 ± 1.6	2.7 ± 1.3	3.0 ± 0.8
ePTFE	5.8 ± 0.2	9.5 ± 0.6	10 ± 0.6
50:50	2.3 ± 0.5	6.5 ± 0.9	0.9 ± 0.1
50:50 EDC	1.4 ± 0.2	5.3 ± 0.6	0.7 ± 0.1
50:50 Gen	0.9 ± 0.1	3.1 ± 0.3	0.8 ± 0.1
70:30	3.5 ± 0.4	4.1 ± 0.7	1.2 ± 0.1
70:30 EDC	2.4 ± 0.2	6.3 ± 0.6	1.1 ± 0.2
70:30 Gen	3.8 ± 0.5	6.3 ± 0.5	1.0 ± 0.1
PDO	5.6 ± 0.7	30 ± 3.8	0.6 ± 0.1

In Figure 7, there was a noticeable gradual increase in average peak stress of EDC cross-linked PDO:ELAS ranges from 0:100-100:0. Similar to the uncross-linked scaffolds, higher PDO content correlates to a higher peak stress value. Modulus results demonstrated similar values over the PDO:ELAS ranges, 50:50-80:20. However, as PDO content increased after this range, the modulus dramatically increased, which is also consistent with the uncross-linked data. Strain at break results demonstrated increases as the PDO content increased up to the 70:30 blend. However, at this strain at break point it began to fall as it reached 100:0. Therefore, an unknown factor in the cross-linking process may

affect the amount the graft is allowed to strain as PDO content increases, or there could have been some batch differences as the scaffolds were electrospun.

Overall, peak stress demonstrated EDC cross-linked pure ELAS was statistically different from all tested materials. 50:50 PDO:ELAS was statistically different from the 80:20-100:0 PDO:ELAS blends, pig artery, and ePTFE. 60:40 was statistically different from PDO:ELAS ranges of 70:30-100:0, ePTFE, and pig artery. 70:30 was statistically different from all materials except 50:50. 80:20-100:0 and ePTFE were statistically different from all materials, and pig artery was statistically different from all materials except 80:20.

In terms of modulus, EDC cross-linked pure ELAS was significantly different from all materials except pig artery. 50:50 and 80:20 were significantly different from ePTFE, 90:10, and 100:0. 60:40 and 70:30 were both significantly different from 90:10 and 100:0 PDO:ELAS blends, as well as the pure ELAS. However, 60:40 was also significantly different from the pig artery. 90:10 is significantly different from all materials except ePTFE, and 100:0 was significantly different from all materials. ePTFE was significantly different from 50:50, 80:20, 90:10, pure ELAS, and pig artery.

Strain at break consisted of a fairly smooth distribution when considering PDO:ELAS ranges of 50:50-100:0. Pure ELAS was significantly different from both pig artery and ePTFE. Pig artery and ePTFE were significantly different from the full range of PDO:ELAS blends. Interestingly, the pure ELAS scaffolds cross-linked with EDC had higher strain at break values than the 50:50 scaffolds. This result indicates higher ELAS content alone was not the foremost cause of lower strain at break values. Therefore, the

blending of PDO and ELAS as well as the properties provided to the scaffold result in lower strain at break values.

Pig artery was used as a comparison tool for a native extracellular matrix (ECM) containing COL, ELAS, and proteoglycans. The peak stress and tangential modulus of PDO:ELAS blends were all within the range of the pig artery; however, strain at break was not. In native artery, ELAS generally takes the majority of the initial load, while COL stretches from its crimped position. Once the COL is fully stretched, stress increases dramatically, even though the artery has already stretched a significant amount prior to fracture. While this behavior was observed in the pig artery, the PDO:ELAS scaffolds, on the other hand, do not contain this crimped structure. Thus, PDO and ELAS worked together as the scaffold was stretched and subsequently fractured at a lower strain.

Pig artery demonstrated an average tangential modulus of 2.7 MPa, which is significantly less than all tested materials with the exception of the EDC pure ELAS scaffolds. This result illustrated a need for a decrease in the amount of synthetic polymer blended into scaffolds, but at the cost of possible graft failure due to rupture or aneurysmal formation. Therefore, a significant amount of materials testing outside of uniaxial tensile testing is required, including compliance and burst strength, which involve biaxial stretch.

The importance of peak stress, tangential modulus, and strain at break for vascular graft material properties are to give a preliminary understanding of material behavior if implanted *in situ*. Peak stress is a good indicator for burst strength properties and prevention of aneurysmal formation. Values obtained through tangential modulus are related to the overall stiffness of the material and are indicative of the material compliance.

Strain at break is another indicator for compliance and distensibililty. Individually, these properties only provide small details of the overall picture, but, when combined with a description of the stress-strain curves and more advanced testing, these material properties become more valuable at predicting the mechanical properties of a combination of materials.

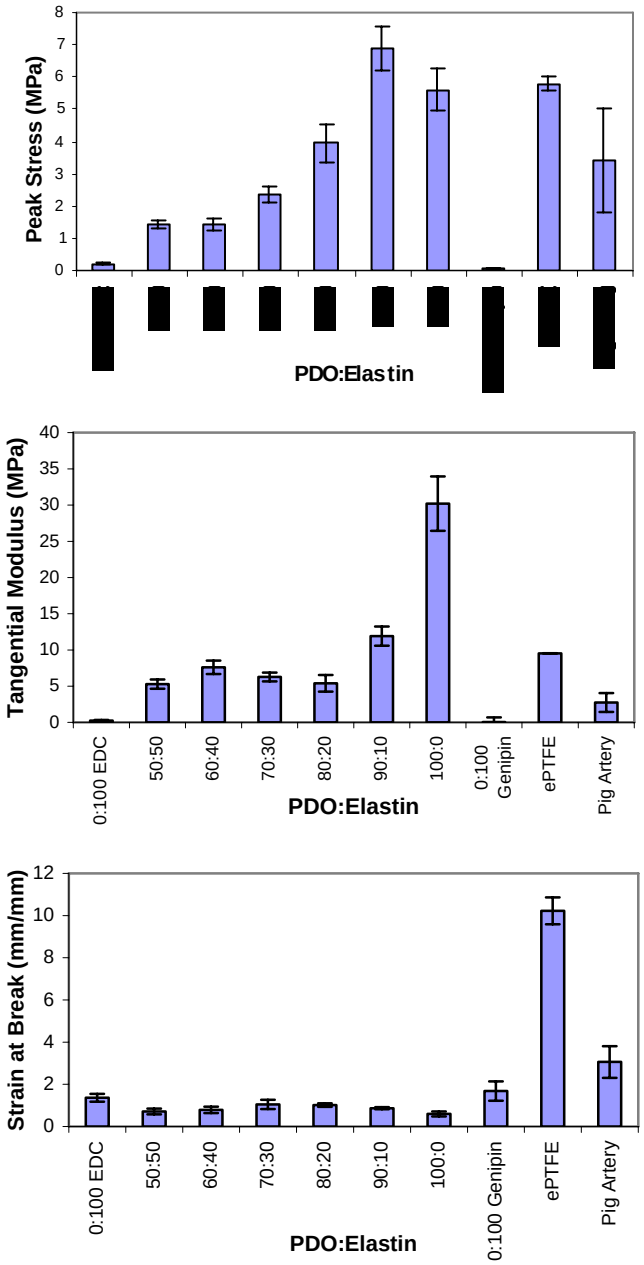

Figure 7. Uniaxial tensile test values for peak stress, modulus, and strain at break for EDC cross-linked PDO:ELAS blends, genipin, ePTFE, and pig artery.

Since genipin's cytotoxic properties are considered to be conducive to the body, PDO:ELAS blends of 50:50 and 70:30 cross-linked with genipin were examined through uniaxial tensile testing in a side-by-side comparison with EDC cross-linked scaffolds and

pig artery (Figure 8). Results revealed no statistical differences between the 50:50 scaffolds, but a difference existed between the 70:30 scaffolds. Additionally, the 70:30 scaffold cross-linked with genipin was not different from the pig artery. Tangential modulus illustrated a difference between the 50:50 scaffolds, but not the 70:30 scaffolds. No difference existed between the pig artery and 50:50 genipin scaffold. Finally, strain at break did not show differences among the individual scaffolds, which had different strain at break compared to pig artery. Therefore, cross-linking with genipin demonstrates a decrease in the stiffness of the material compared to EDC when enough ELAS is added to the scaffold. The same could be true for peak stress since the average peak stress decreases for the 50:50. However, 70:30 demonstrates an increase in peak stress when cross-linked with genipin. Thus, this inconsistency could be due to the cross-linker used or to batch differences with higher PDO content compared to the scaffold cross-linked with EDC.

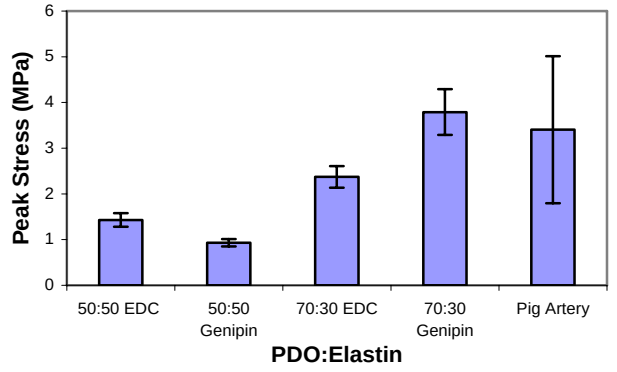

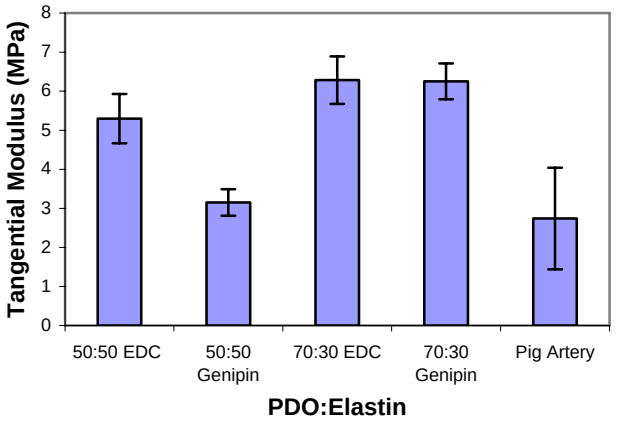

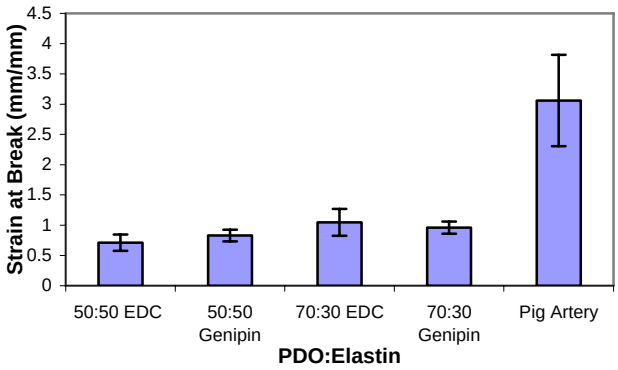

Figure 8. Uniaxial tensile test values for peak stress, modulus, and strain at break, for EDC and genipin cross-linked PDO:ELAS blends of 50:50, 70:30, and pig artery.

Conclusion

The given results have shown that electrospun PDO-soluble ELAS blends demonstrate changes in material properties over a period of one day when uncross-linked,

leading to the conclusion that cross-linking is a necessity for ELAS containing scaffolds. Several cross-linkers were investigated for this study, but only EDC and genipin were considered for additional testing based on percent cross-linking and documented cytotoxic properties. Mechanically, the addition of ELAS creates scaffolds that exhibited ranges of properties resembling that of both pig artery and native human artery. Previous data indicated uncross-linked PDO-ELAS cell culture with blends of 70:30 and 90:10 demonstrated excellent migration into the uncross-linked scaffolds [248]. Future studies will investigate mechanical properties based on uniaxial hysteretic testing, compliance testing, and the possible inclusion of COL.

CHAPTER 3: Preliminary Methods Towards a Tri-Layered Design

Preface: The following manuscript is currently published in Acta Biomaterialia. This work investigates the feasibility of designing and testing a tri-layered vascular graft composed of PCL, elastin, and COL. Through the use of a tri-layered design, it is possible to change material properties of individual layers, causing changes in the material properties of the whole graft.

A Three Layered Electrospun Matrix to Mimic Native Arterial Architecture Using Polycaprolactone, Elastin, and Collagen: A Preliminary Study

Michael J. McClure [1], Scott A. Sell [1], David G. Simpson [2], Beat H. Walpoth[3], and Gary L. Bowlin [1]

[1]Department of Biomedical Engineering, Virginia Commonwealth University, Richmond, Virginia 23284-3067

[2]Department of Anatomy and Neurobiology, Virginia Commonwealth University, Richmond, Virginia 23298-0709

[3]Department of Cardiovascular Surgery, University Hospital of Geneva, Geneva 14,Switzerland.

Abstract

Throughout native artery, collagen and ELAS play an important role, providing a mechanical backbone, preventing vessel rupture, and promoting recovery under pulsatile deformations. The goal of this study was to mimic the structure of native artery by fabricating a multi-layered electrospun conduit composed of PCL with the addition of ELAS and COLwith blends of 45-45-10, 55-35-10, and 65-25-10 PCL-ELAS-COL to demonstrate mechanical properties indicative of native arterial tissue, while remaining conducive to tissue regeneration. Whole grafts and individual layers were analyzed using uniaxial tensile testing, dynamic compliance, suture retention, and burst strength. Compliance results revealed that changes to the middle/medial layer changed overall graft behavior with whole graft compliance values ranging from 0.8 - 2.8 % / 100 mmHg, while uniaxial results demonstrated an average modulus range of 2.0 - 11.8 MPa. Both modulus and compliance data displayed values within the range of native artery. Mathematical modeling was implemented to show how changes in layer stiffness affect the overall circumferential wall stress, and as a design aid to achieve the best mechanical combination of materials. Overall, the results indicated that a graft can be designed to mimic a tri-layered structure by altering layer properties.

Keywords: Electrospinning;Vascular Graft; Multilayer; Polycaprolactone; ELAS

Introduction

Although there is a strong patient demand for small diameter (< 6 mm) vascular bypass grafts every year, the development of an ideal replacement has been a daunting task with minimal success. All arteries are subjected to multiple stresses including circumferential, longitudinal, torsional, and shear. These combined stresses account for an artery's unique arrangement as a tissue with three concentric layers: intima, media, and adventitia. Each layer displays its own unique characteristics based on its location *in vivo*. For example, larger arteries like the aorta, which experience high shear rates, and high blood velocity have increased ELAS content compared to muscular arteries such as the coronary or popliteal which experience lower shear and blood flow velocity. As blood flow transitions from the large diameter arteries to small diameter arteries, the potential for complications increase dramatically as there is more time for blood-borne components to interact with the inner surface of the artery, posing problems for smaller diameter vascular graft replacements.

Currently used bypass grafts such as Dacron® and ePTFE work well for larger diameters but fail for small diameters due to acute thrombogenicity of the graft, anastomotic intimal hyperplasia, aneurysm formation, infection, and progression of atherosclerotic disease [223]. Therefore, efforts have been made to create a successful bypass graft using biodegradable materials such as PGA [103, 249], PLA [250-252], PDO [107-110], PCL [93, 99, 132, 253, 254], and several co-polymer blends [151, 255]. Nevertheless, most of these materials by themselves have had limited success. PGA is a

rapidly degrading polymer which ultimately leads to failure of the graft material under physiological pressures. Additionally, PGA has the potential to produce insults at the site of the graft or downstream due to its rapid degradation and subsequent decreased pH levels from glycolic acids. Although PLA is slower degrading than PGA, its stiffness makes it to be less desirable when designing a vascular graft. PDO has been investigated by our lab and has shown promise *in vitro*, but, when tested *in situ* in a rat model, degradation of the PDO structure without enough cellular infiltration led to aneurismal formations (unpublished data). PCL has been investigated and reported by many groups. Its long degradation time, documented bioactivity for ECs and SMCs [256, 257], and innate compliance makes it a suitable candidate for vascular graft material. Biodegradable materials provide a key advantage. As the material degrades hydrolytically over time, cells continuously infiltrate the matrix, producing COL, ELAS, and proteoglycans to replace the degrading material. Eventually, a fully functional artery is created composed of autologous smooth muscle and ECs. If PCL is utilized as the main vascular graft material, providing the mechanical backbone, then its degradation should be slow enough for cells to infiltrate and slowly take over mechanical function.

This concept, however, involves a critical time table. Biodegradable materials lose their mechanical integrity over time, and regeneration of the vascular wall must take place simultaneously as the material degrades. If regeneration time does not match degradation time, then the implanted graft runs the risk of aneurysm or rupture. In order to attract cells into the graft material, natural polymers such as COL and ELAS can be included in the matrix. The native extracellular matrix (ECM) of the vasculature is composed mostly of

COL and ELAS. These ECM components are constantly synthesized, secreted, oriented, and modified by the cellular components that they support. Classically, the function of native ECM was only believed to be as a structural framework for tissues. However the ECM, through interaction with receptors on the surfaces of cells, directly takes part in promoting cell adhesion, migration, growth, differentiation, and apoptosis. The ECM also plays a role in cytokine activity and intracellular signaling, both of which serve numerous functions in cell regulation and activation [258]. Extensive research has been performed incorporating electrospun COL, gelatin, and ELAS [132, 232, 233, 259, 260] into vascular conduit materials; however, no one has attempted to manufacture a multilayered electrospun vascular tube with a profuse amount of native COL and ELAS. To date, high natural polymer content decreases peak stress and modulus while increasing the risk of aneurysm or rupture of the graft material. Nonetheless, if support is provided for the graft material through multilayered electrospinning and/or chemical cross-linking, then high natural polymer content becomes a viable option again.

The purpose of this study was to examine the concept of utilizing a three-layered graft structure, mimicking the natural architecture of an artery while providing tunable material properties for each layer. PCL, COL, and soluble ELAS were electrospun sequentially at different polymer ratios in order to produce an inner (intima), intermediate (media), and outer (adventitia) layer each with a unique polymer blend. PCL was chosen as a synthetic polymer based on promising results from *in vivo* rat studies that have been conducted by Pektok *et al.*, whereby histological analysis revealed rapid enthothelialization of the inner lumen of the graft and becoming confluent at 12 weeks

[93]. Vascular tissue contains between 25-30 % COL and 40-50 % ELAS. Therefore, ratios were chosen for each of the three layers based on native extracellular matrix design while keeping mechanical integrity throughout the graft structure. The intimal layer (98-2-0 PCL-ELAS-COL) providing initial stiffness with a compact PCL dominated structure to allow for the attachment of ECs while disallowing cellular infiltration, the medial layer (45-45-10, 55-35-10, or 65-25-10 PCL-ELAS-COL) containing a high amount of ELAS to decrease stiffness and a small portion of COL to attract cells into the layer, and the adventitial layer (70-0-30 PCL-ELAS-COL) to prevent rupture and to attract cells from outside the graft and into the matrix.

As described earlier, artery is subjected to circumferential, longitudinal, torsional, and shear stress. Although important to the study of coronary arteries, torsion and shear stresses do not ultimately dictate the mechanical behavior of an artery when considering blood pressure supplying a force to the arterial wall *in vivo*. Therefore, mathematical modeling was implemented to help describe circumferential wall stress (CWS) of the individual layers and their mechanical effects on surrounding layers using the equations developed by Vorp *et al.* [120, 261]. These results would aid in future design work, providing valuable information regarding layered behavior which has yet to be tested *in vitro*.

Materials and Methods

Collagen Extraction

COL type I was extracted from 6 month bovine corium through an acetic acid based process previously described [262]. Briefly, tissue is homogenized, suspended in

acetic acid, and subsequently purified via a series of dissolutions, precipitations, and dialyses [263]. Following the final dialysis, COL solutions were frozen and lyophilized.

Electrospinning

Concentrations of 100 mg/ml of PCL (MW: 65,000, Sigma Aldrich), 200 mg/ml of soluble ELAS from bovine neck ligament (Elastin Products Co. Inc.), and 70 mg/ml of COL I (6 month bovine corium) were dissolved in HFP (TCI America) and blended in ratios of 98-2-0 PCL-ELAS-COL (intima), 45-45-10, 55-35-10, and 65-25-10 PCL-ELAS-COL (media), and 70-0-30 PCL-ELAS-COL (adventitia).

To create vascular tubes, each polymer mixture was then loaded into a 3 ml plastic Becton Dickinson syringe with an 18 gage blunt tip needle. Insulated Tygon tubing was then run from the needle tip to a 3-1 (input-output) nozzle charged to 25 kV at an air gap distance of 20 cm. The solutions were sequentially electrospun onto a 2 mm diameter cylindrical mandrel rotating at 500 RPM with a translational speed of 6 cm/s over a distance of 12 cm. Flow rates and volumes were as such: the intima was electrospun at a rate of 4 ml/hr and a volume of 0.5 ml followed by a transition combining both intimal and medial syringes for 0.2 ml at 2 ml/hr each. The intimal syringe was then shut off and the medial layer was allowed to spin for 0.6 ml at 4 ml/hr followed by a transition between the media and adventitia for 0.2 ml of polymer solution at 2 ml/hr each. Finally, the media was stopped and the adventitia was allowed to spin for 0.4 ml at 4 ml/hr.

Each individual layer, 98-2-0, 45-45-10, 55-35-10, 65-25-10, and 70-0-30 PCL-ELAS-COL was electrospun onto a 2 mm diameter mandrel to observe the effect of dynamic compliance on each layer. However, since the 2 mm diameter grafts were too

small to use "dog bone" punches, rectangular mandrels were chosen for uniaxial tensile testing. Blended ratios of 98-2-0 PCL-ELAS-COL (intima), 45-45-10, 55-35-10, and 65-25-10 PCL-ELAS-COL (media), and 70-0-30 PCL-ELAS-COL (adventitia) were electrospun separately onto a flat, rectangular mandrel at a rate of 4 ml/hr, 25kV, and an air gap distance of 20 cm (2.5 cm wide x 10.2 cm long x 0.3 cm thick) at 500 RPM with a translational speed of 6 cm/s over a distance of 12 cm to create separate layers for uniaxial testing, utilizing the modulus for mathematical modeling.

All tubes and rectangular samples were cross-linked using a 50 mM solution of EDC (Pierce) and 70 % ethanol (Sigma Aldrich) using a previously described method [110].

Nonviable Pig Femoral Artery

Porcine femoral arteries were frozen in PBS, and subsequently washed 5 times for 30 minutes each in PBS. Artery was immediately tested thereafter. For uniaxial tensile testing, samples were prepared by slicing the artery in the longitudinal direction, creating a zero stress state. "Dog bone" shaped samples were then punched for testing. For dynamic compliance, nonviable porcine femoral arteries were tested under the same simulated physiological conditions.

Scaffold Characterization

Scaffold characterization was performed using scanning electron microscopy on the electrospun mats (SEM, Zeiss EV050). SEM images were analyzed with ImageTool 3.0 software (Shareware provided by UTHSCSA). Multilayer electrospun vascular grafts were dissected by cutting the graft in half in the longitudinal direction. Forceps were then used to carefully peel apart the intimal, medial, and adventitial layers. These layers were then

imaged on both sides and analyzed. Characterization included determining the average fiber diameter and average pore area for the electrospun structure by taking the average of 60 measurements chosen randomly from across the image. Measurements for pore area were defined as such: the space created by multiple fibers at a depth of only two fibers; no fibers beyond the superficial surface were considered for pore area measurements. For all of the measurements made from the SEM images, calibration of the ImageTool software was done with the scale bar on each image.

Material Properties of Individual Layers

Uniaxial tensile testing was performed on six samples (n = 6) from one electrospun sheet hydrated in PBS for 24 hours. "Dog-bone" shaped samples were punched from electrospun mats (2.75 mm wide at their narrowest point with a gage length of 7.5 mm) and tested on a MTS Bionix 200 testing system with a 100 N load cell (MTS Systems Corp.) and an extension rate of 10.0 mm/min. Peak stress, modulus, and strain at break were calculated using TestWorks version 4.

Mathematical Modeling

The constitutive equations developed by Vorp *et al.* [120, 261] are based on the principle of the Lamé equations. Following similar assumptions as previously described [261], a three-layered model (Figure 9) was used, describing CWS, at any radius, *r*, of the three layers.

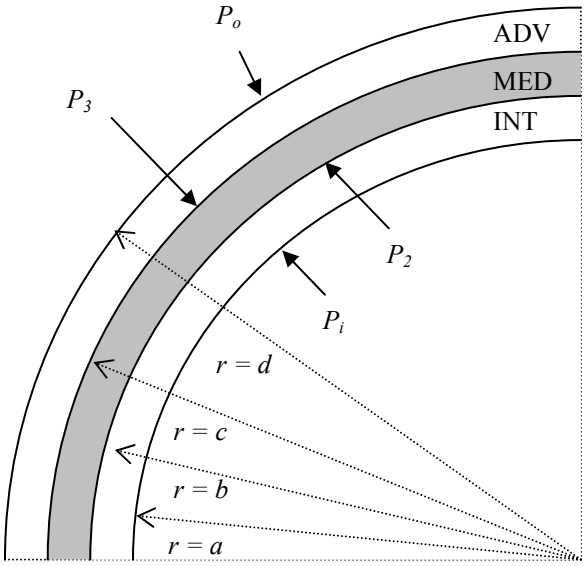

Figure 9. Schematic adopted from [25, 26] showing cross-sectional view of the three-layered model. ADV (adventitia), MED (media), INT (intima).

Through this we come up with:

$$CWS = \frac{R_I^2 P_I - R_O^2 P_O}{R_O^2 - R_I^2} + \frac{(P_I - P_O) R_I^2 R_O^2}{(R_O^2 - R_I^2) r^2} \quad \text{for } R_I \leq r \leq R_O \tag{3}$$

Where R_I is the inner radius of a particular layer, R_O is the outer radius of a particular layer, P_I is the inner pressure of a particular layer, and P_O is the outer pressure of a particular layer.

$$P_2 = P_i \frac{2a^2 b}{(b^2 - a^2) E_{INT}} \left[\frac{(c^2 - b^2)^2 E_{MED} k_2}{(c^2 - b^2)^2 E_{MED}^2 k_2 k_1 - 4b^3 c^3} \right] \tag{4}$$

$$P_3 = P_i \frac{2a^2 b}{(b^2 - a^2) E_{INT}} \left[\frac{2(c^2 - b^2) E_{MED} b^2 c}{(c^2 - b^2)^2 E_{MED}^2 k_2 k_1 - 4b^3 c^3} \right] \tag{5}$$

$$k_1 = \frac{b^3 (1 - \upsilon_{INT}) + a^2 b (1 + \upsilon_{INT})}{(b^2 - a^2) E_{INT}} + \frac{b^3 (1 - \upsilon_{MED}) + b^2 c (1 + \upsilon_{MED})}{(c^2 - b^2) E_{MED}} \tag{6}$$

$$k_2 = \frac{c^3(1-\upsilon_{MED}) + b^2c(1+\upsilon_{MED})}{(c^2-b^2)E_{MED}} + \frac{c^3(1-\upsilon_{ADV}) + d^2c(1+\upsilon_{ADV})}{(d^2-c^2)E_{ADV}} \quad (7)$$

Where k_1 and k_2 are constants, E_{INT}, E_{MED}, and E_{ADV} represent the moduli for the intimal, medial, and adventitial layers, respectively, υ_{INT}, υ_{MED}, and υ_{ADV} represent Poisson's ratio for the intimal, medial, and adventitial layers respectively, and a, b, and c are the inner radii for the intimal, medial, and adventitial layers, respectively, and d is the outer radii of the adventitial layer (equations are adopted from [120, 260]).

Suture Retention

Suture retention testing was performed on six 2 mm inner diameter tubular specimens (n = 6) from six different electrospun grafts, soaked in PBS for 24 hours at 37°C, on a MTS Bionix 200 testing system with a 50 N load cell (MTS Systems Corp.) and an extension rate of 150.0 mm/min in accordance with the straight across procedure described in section 8.8 of the American National Standards Institute (ANSI)/Association for the Advancement of Medical Instrumentation (AAMI) ANSI/AAMI VP20:1994 entitled "Cardiovascular Implants – Vascular Graft Prostheses" [264]. 5-0 commercial PDS™ II violet monofilament suture (Ethicon, Inc.) was placed 2 mm from the end of the sample and extended until the suture had pulled through the graft. Peak load was recorded in grams-force using TestWorks version 4.

Burst Pressure

Burst strength testing on six samples (n = 6) from six different electrospun grafts was completed using a device designed in accordance with section 8.3.3.3 of ANSI/AAMI VP20:1994 [264]. Tubes, 2–3 cm in length, were hydrated in PBS, fitted over 1.5 mm

diameter nipples attached to the device, and secured with 2-0 SF suture. Air was introduced into the system, increasing the pressure at a rate of 5 mmHg/s until the tubes burst. Results are reported as the pressure in mmHg at which tubes ruptured.

Dynamic Compliance

Dynamic compliance was determined for six 2 mm inner diameter tubular grafts (n = 6) taken from six different electrospun grafts at a length of 3 cm under simulated physiological conditions in accordance with section 8.10 of ANSI/AAMI VP20:1994 [264]. Both individual layers and multi-layered tubular constructs were electrospun and tested under the same conditions. The specimens were tested in an Intelligent Tissue Engineering via Mechanical Stimulation (ITEMS™) Bioreactor developed by Tissue Growth Technologies (Minnetonka, MN) filled with PBS at 37°C. The bioreactor provided a cyclic (1 Hz, representing 60 beats per minute) pressure change to the inside of the graft; three different pressure levels (90/50, 120/80, and 150/110 mmHg systolic/diastolic) were investigated. Briefly, specimens were secured at either end to a nipple with 2-0 SF suture and placed in the bioreactor chamber. PBS then filled the chamber and was run continuously on the outside of the graft to maintain a temperature of 37^{o}C and a pressure of 0 mmHg. Simultaneously, PBS was pumped through the inside of the graft and an actuator in the bioreactor created the difference in pressure. Prior to compliance measurements for each pressure level, all grafts were allowed to stress relax for 30 minutes or 1800 cycles.

Internal pressure was measured with a pressure transducer capable of measuring dynamic pressure up to 200 ± 2 mmHg, while the external diameter was recorded with a

laser micrometer system with an accuracy of ±0.001 mm. Prior to insertion into the bioreactor, the grafts were soaked in PBS at 37°C for 24 hours, after which time their average wall thickness was measured. From this, the internal radii of the graft was determined and used in the following equation to calculate compliance for each specimen:

$$\%\ Compliance = \frac{(R_{P2} - R_{P1})/R_{P1}}{(P_2 - P_1)} \times 10^4 \quad (8)$$

Where R is the internal radius, P_1 is the lower internal pressure, and P_2 is the higher internal pressure [29]. Grafts were tested with individual layers electrospun at a wall thickness of 200 μm, and with whole graft samples with an overall wall thickness of 500 μm.

Statistical Analysis

Unless otherwise stated, all statistical analysis was based on a Kruskal-Wallis one way analysis of variance on ranks and a Tukey-Kramer pair-wise multiple comparison procedure ($\alpha = 0.05$) performed with the JMP®IN 4.0.3 statistical software package (SAS Institute, Inc).

Results

Scaffold Characterization

SEM images in Appendix A depict the apparent differences between the inner and outer surfaces of each layer. This demonstrates the differences in electrospun fibers when transitioning from one polymer blend to the next. From the first layer, the intimal layer, the two surfaces are fairly similar in appearance; however, differences arise when the inner and outer surfaces of the medial and adventitial layers are considered, particularly at the

transition from the medial to the adventitial layer. This transition produces very large fibers that are most likely the result of wet electrospinning and fiber welding caused by the blending of the two polymers and their subsequent electrical characteristics. While most SEM images tended to contain a high packing density especially on the intimal and adventitial layers, a wide range of fiber diameters were present. Cellular infiltration can be inhibited by the packed fibers of the intimal layer containing lower amounts of natural protein. However, where natural protein, such as COL, is more prevalent, infiltration and migration may be more probable regardless of packing density. Here natural proteins can attract cells inside the scaffold while larger fibers give way to large pores for migration. As mentioned earlier, both COL and ELAS can provide the necessary recognizable protein sequences to promote cellular interaction. A study by Barnes *et al.* demonstrated that electrospun COL fibers promoted the infiltration of human FB [112]. Additionally, ELAS peptides can influence signaling, chemotaxis, proliferation, and protease release via the ELAS receptor [142].

After determining the feasibility of electrospinning three different polymeric blends of both synthetic and natural polymers, the effect each individual layer posed on its neighboring layers needed to be determined initially from the microscopic level. Therefore, the medial layer was subjected to incremental increases in synthetic polymer, PCL at 10 % each interval, and incremental decreases in natural polymer, ELAS at 10 % each interval, resulting in medial blends of 45-45-10, 55-35-10, and 65-25-10 PCL-ELAS-COL. At the macroscopic level, Figure 10 displays a dissected view of a three layered

graft with a 45-45-10 PCL-ELAS-COL medial layer to provide a cross-sectional view and the graft and demonstrate the relation of one layer to another.

Figure 10. Dissected view of a 45-45-10 three layered graft.

SEM images were taken of both the inner and outer surface, and average fiber diameter was determined for each surface. Figure 11 displays the results of the inside and outside fiber diameters of the intimal, medial and adventitial surfaces. Average fiber diameter of each blend remained unchanged for the inner and outer surfaces of the intimal layers. Medial surfaces, however, displayed a gradual decrease in average fiber diameter for the outer surface, where 45-45-10 was significantly different ($p< 0.05$) from 65-25-10. The inner surface remained unchanged with no significant differences. Adventitial layers of all three blends demonstrated a gradual decrease in fiber diameter for the inner surface with significant differences between 45-45-10 and 65-25-10, while the outer surface remained unchanged.

A

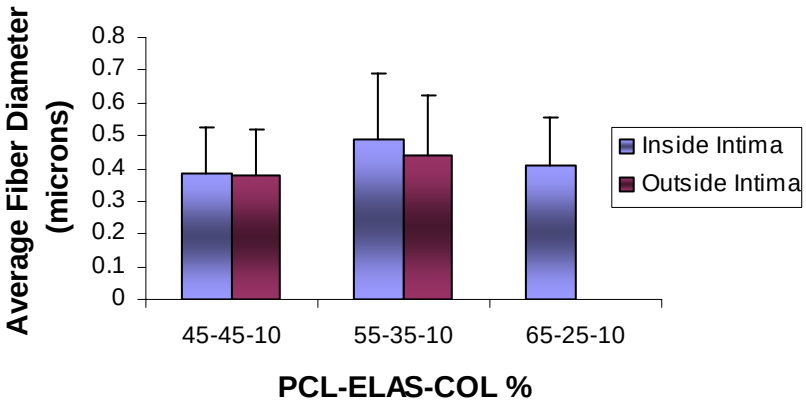

B

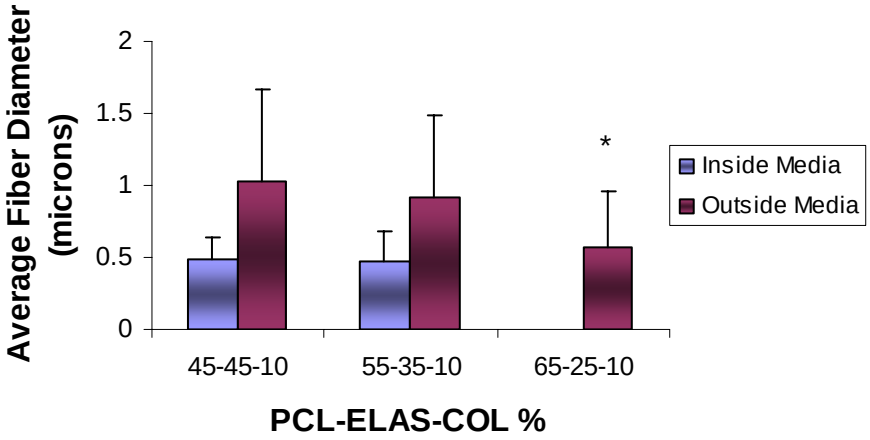

C

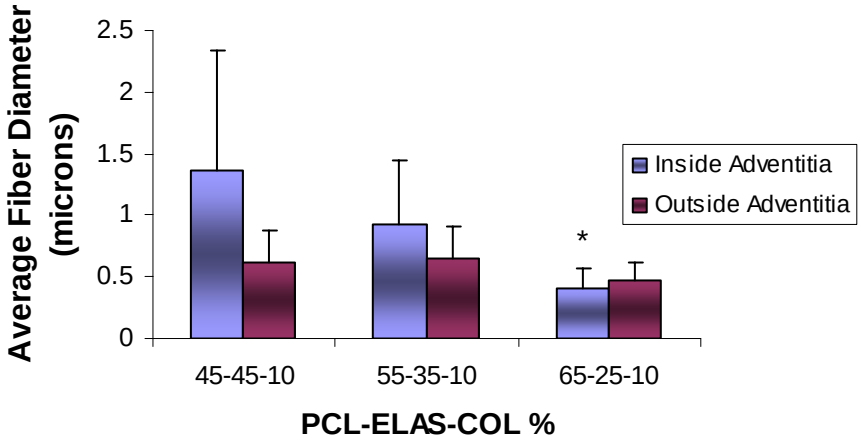

Figure 11. Average fiber diameter measurements taken from SEM images of the inside and outside intimal (A), medial (B), and adventitial (C) layers of a 45-45-10, 55-35-10, and 65-25-10 PCL-ELAS-COL layer. * indicates significant differences between 45-45-10 and 65-25-10 ($p< 0.05$).

Figure 12 displays the average pore area for the intimal, medial, and adventitial layers. According to the results, like the average fiber diameter measurements in Figure 11, there was no change amongst the inner and outer surfaces of the intimal layers. Similarities between Figure 11 and Figure 12 also existed for the medial surface and adventitial surface where the average pore area values of the outer medial surface and inner adventitial surface gradually decreased. This demonstrates a relationship between fiber diameter and pore area, where larger fiber diameters can confer larger pores. Again significant differences ($p< 0.05$) occurred between 45-45-10 and 65-25-10 for the outer medial surface and inner adventitial surfaces. However, significant differences ($p< 0.05$) also occurred between the 45-45-10 and 65-25-10 outer adventitial surfaces and between the 45-45-10 and 55-35-10 outer medial surfaces.

A

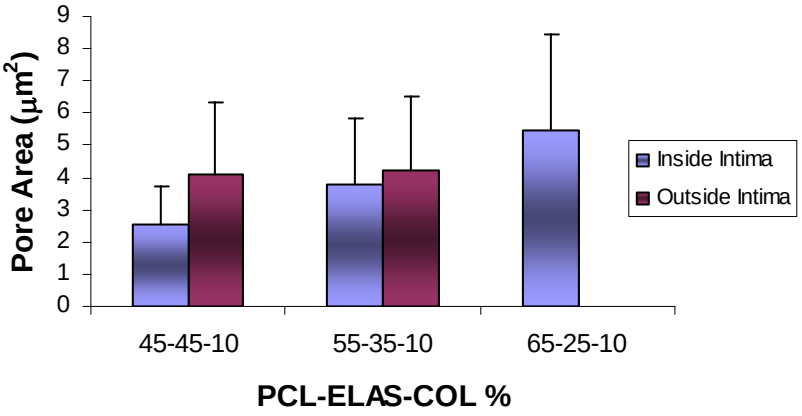

B

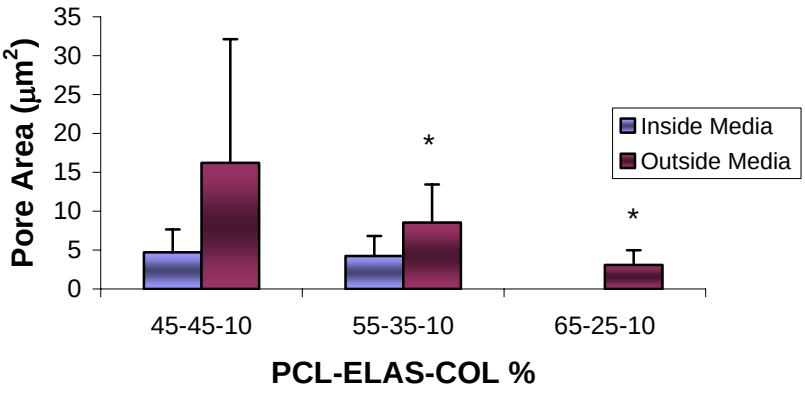

C

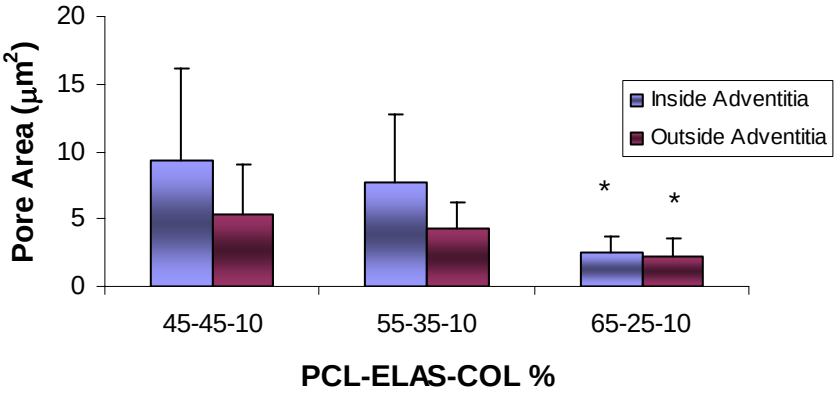

Figure 12. Average pore area measurements taken from SEM images of the inside and outside intimal (A), medial (B), and adventitial (C) layers of a 45-45-10, 55-35-10, and 65-25-10 PCL-ELAS-COL layer. * indicates a significant difference from 45-45-10 ($p< 0.05$).

Uniaxial Tensile Testing of Individual Layers

Figure 13 displays the tensile properties of each layer electrospun individually onto a flat mandrel. These properties provide further insight into how the materials will behave when combined into one cohesive vascular graft. Initially, the medial layers, 45-45-10, 55-35-10, and 65-25-10, display trends of increasing peak stress and tangential modulus with increases in PCL content, while strain to break decreases. Average values for medial layers gradually increased from 1.1 to 1.5 MPa for peak stress, 2.0 to 3.7 MPa for tangential modulus, and gradually decreased from 0.9 to 0.7 mm/mm for strain to break. Statistical differences for these medial layers existed only for strain to break values, where 45-45-10 was different from 55-35-10 and 45-45-10 was different from 65-25-10 ($p< 0.05$). Although medial layers revealed no differences for peak stress and modulus, differences did exist for peak stress and modulus between all medial values and their intimal (98-2-0) and adventitial values (70-0-30).

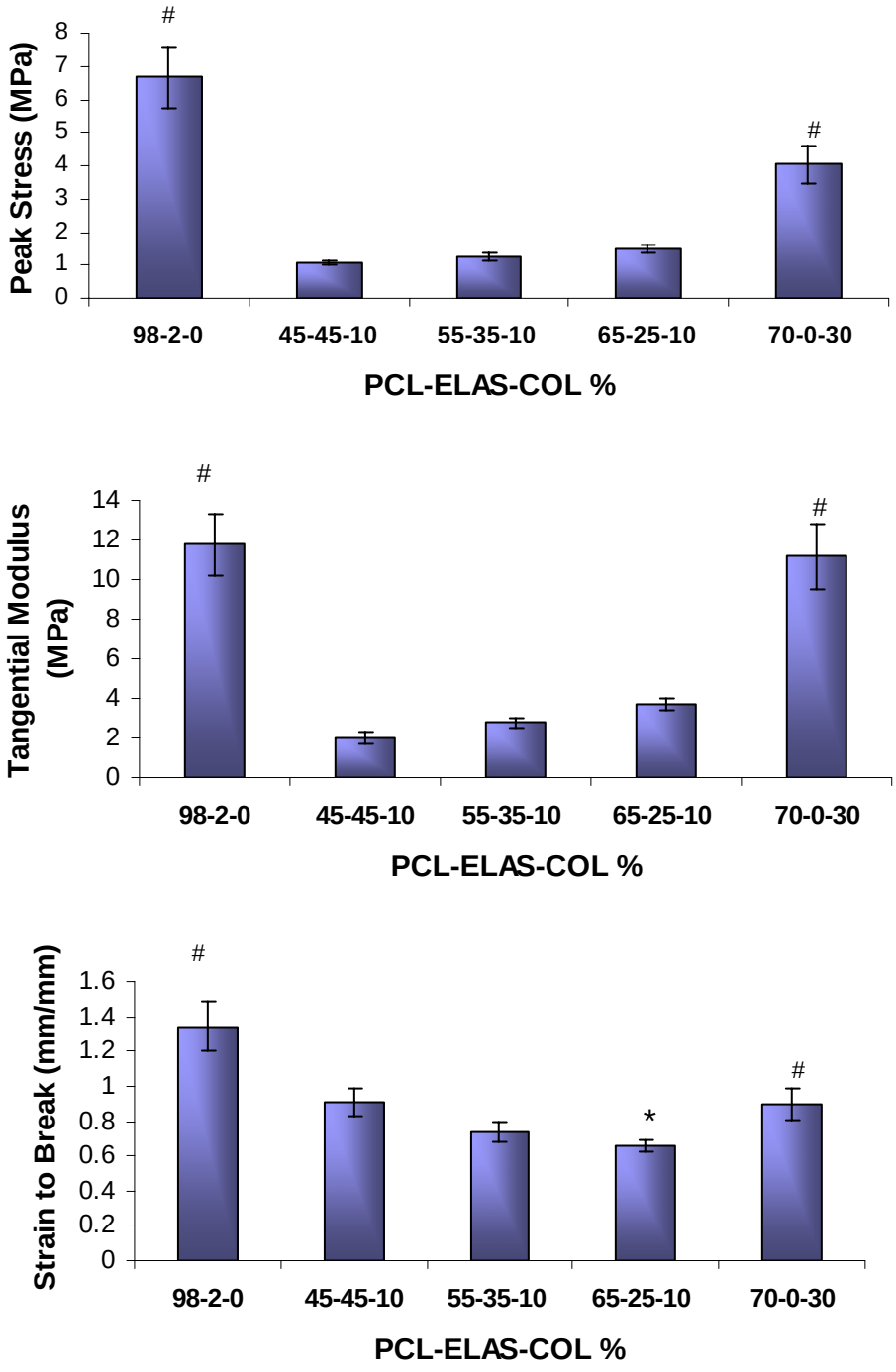

Figure 13. Uniaxial tensile test values for peak stress, tangential modulus, and strain to break for individual intimal, medial, and adventitial layers containing specific PCL-ELAS-COL blends. * indicates significant differences between 55-35-10 and 65-25-10 while # indicates a significant difference from 45-45-10, 55-35-10, and 65-25-10 ($p< 0.05$).

Mathematical Modeling

Mathematical modeling was implemented in order to determine where we could effect a change in graft behavior by altering individual layer moduli. Utilizing the previously described equations, Figure 14A demonstrates that as stiffness increases for the medial layer, there is both a subsequent decrease in CWS seen by the intimal layer and an increase in CWS seen by the medial layer. So, when an increase in medial stiffness occurs, it takes on more circumferential stress and decreases the amount of initial stress imposed on the whole arterial wall. This could be beneficial for endothelial cell attachment and proliferation. There is only a slight decrease in CWS for the adventitial layer.

Figure 14B displays an increase in the intimal modulus and how it affects the other two layers. As modulus increases, the intimal layer is able to accept more stress and relieve stress from the medial and adventitial layers, but only slightly. If the modulus is increased in the adventitial layer, Figure 14C, then that layer is able to allow more stress while it relieves a significant amount of stress from the intimal layer, and slightly increases the amount of stress seen by the medial layer.

Finally, Figure 14D displays a comparison of the moduli values obtained from two studies performed on human coronary arteries in comparison to the three-layered graft. Values obtained from Lu *et al.* [265] are based on the assumption of a bi-layered scaffold consisting of an intima-media and an adventitia, where moduli were 299 kPa and 132 kPa, respectively. Additionally, values from Holzapfel *et al.* [266] considered a three-layered structure, separating the intima, media, and adventitia for testing. The results for the moduli were 7.56 kPa, 1.27 kPa, and 27.9 kPa for the intima, media, and adventitia,

respectively. Figure 14D displays similar trends between Holzapfel values and the three-layered graft with the 45-45-10 PCL-ELAS-COL layer. Both decrease CWS from the intimal to the medial layers, and both increase CWS transitioning from the medial to the adventitial layer. This increase is more pronounced in the native artery since the adventitial modulus is 22x larger than the medial modulus, whereas the adventitial layer in the three-layered graft is only 5.6x larger. The adventitial layer in the Holzapfel study is also responsible for the smaller decrease in CWS from the intima to the media, where both the intimal moduli of the 45-45-10 and Holzapfel are 5.9x larger than the medial moduli.

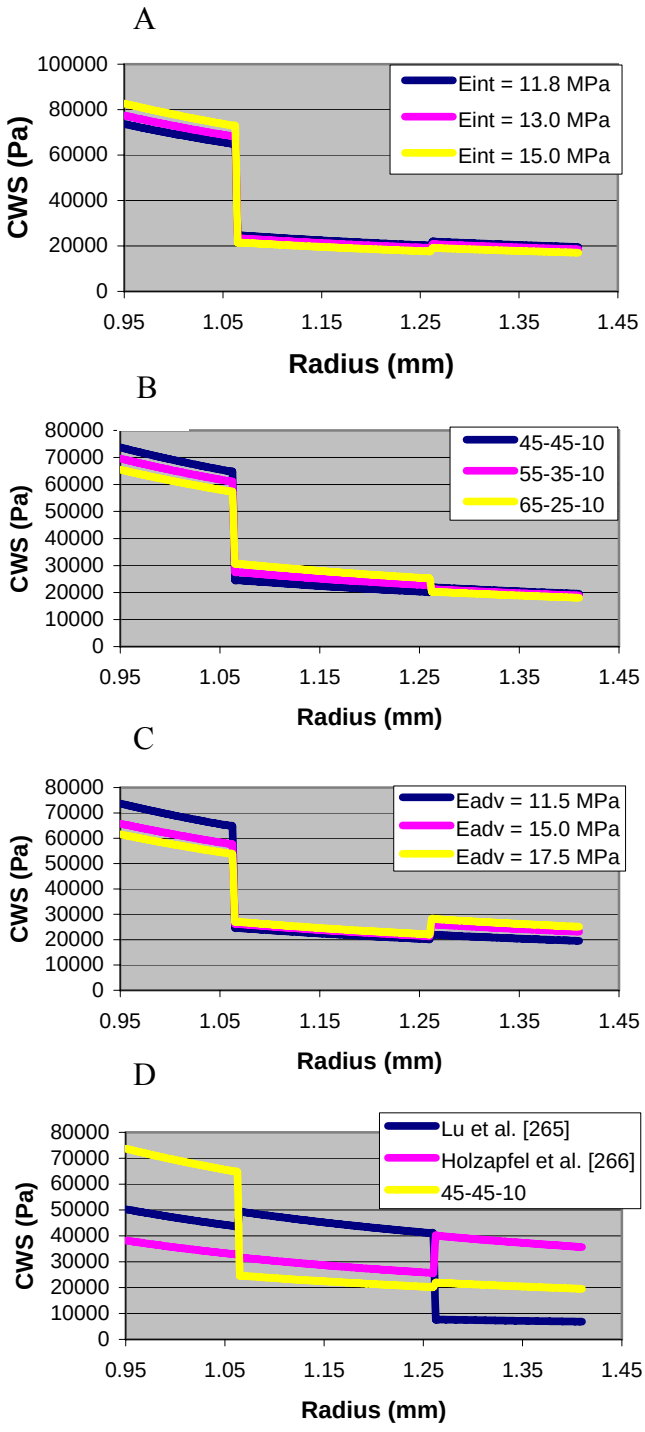

Figure 14. Mathematical modeling using equations 1-5 to determine CWS on increased medial stiffness, increased intimal stiffness, increased adventitial stiffness, and a comparison of the moduli found in [265] and [266] to the 45-45-10 medial layer graft.

Suture Retention: Whole Graft

In Figure 15 suture retention results demonstrated that as PCL content in the medial layer is increased and ELAS is decreased, an increase in force is required to pull the suture through the graft. Average values ranged from 91-189 grams-force with significant differences ($p< 0.05$) between 45-45-10 and 65-25-10 PCL-ELAS-COL. A nonviable porcine femoral artery (nvPFA) and ePTFE were both used as comparison tools for the three different grafts. nvPFA displayed a range of 235 - 358 gf while ePTFE ranged from 500 – 680 gf. This placed the 65-25-10 medial layer graft just within the range of nvPFA with a peak value of 236 gf while peak values of 45-45-10 and 55-35-10 were lower. ePTFE had the highest of all the values.

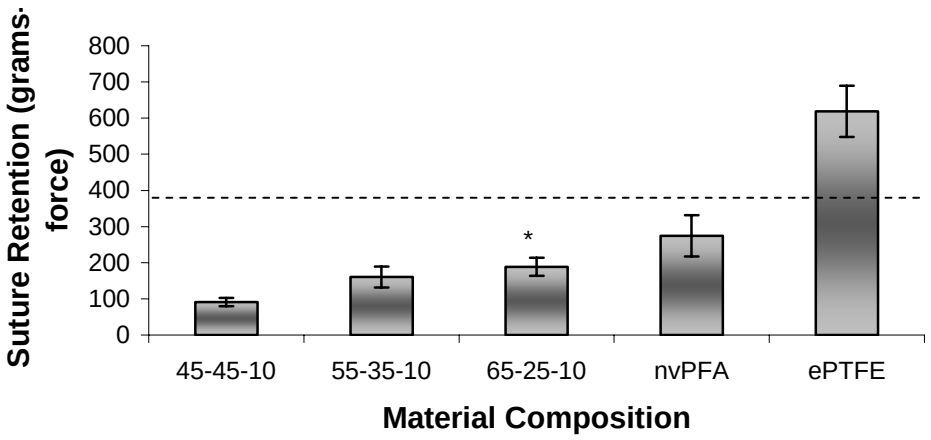

Figure 15. Suture retention with 5-0 PDS II suture for three-layered graft compositions containing medial layers of 45-45-10, 55-35-10, and 65-25-10 PCL-ELAS-COL %. nvPFA and ePTFE were tested as comparisons and the dashed line represents saphenous vein [35]. * indicates significant differences between 45-45-10 and 65-25-10 ($p< 0.05$).

Burst Strength

Figure17 displays the burst pressure results of whole graft specimens for medial layers 45-45-10, 55-35-10, and 65-25-10. Graft 45-45-10 PCL-ELAS-COL burst at an

average pressure of 2387 mmHg whereas both 55-35-10 and 65-25-10 exceeded a pressure limit of 3000 mmHg on the pressure regulator being used to supply the burst system.

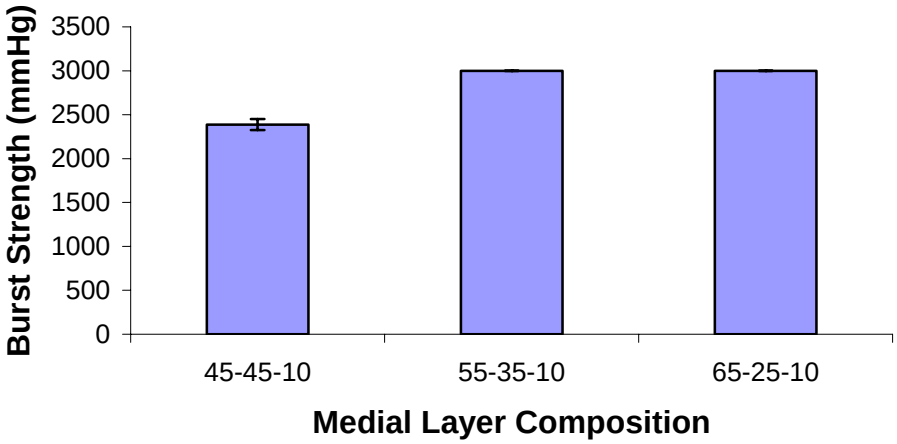

Figure 16. Burst pressure results for whole graft specimens with medial layers of 45-45-10, 55-35-10, and 65-25-10 PCL-ELAS-COL.

Dynamic Compliance: Individual and Whole Graft

Dynamic compliance measurements made with single layered graft specimens and three-layered graft specimens provides an encompassing picture. Figure 17 displays the compliance of individual layers at three different pressure readings. Calculated values show that at lower pressures, the grafts displayed a larger standard deviation, indicating a less stable reading. As pressure was increased these deviations decreased and better measurements were obtained. At pressures of 120/80 mmHg, significant differences for the medial layers included differences between 45-45-10 and 65-25-10 ($p< 0.05$), and between 55-35-10 and 65-25-10 ($p< 0.05$). There was no difference between the 45-45-10 and 55-35-10 layers. This was also the case for pressures at 150/110 mmHg. 98-2-0 was different from 70-0-30 for pressures of 120/80 and 150/110 ($p< 0.05$).

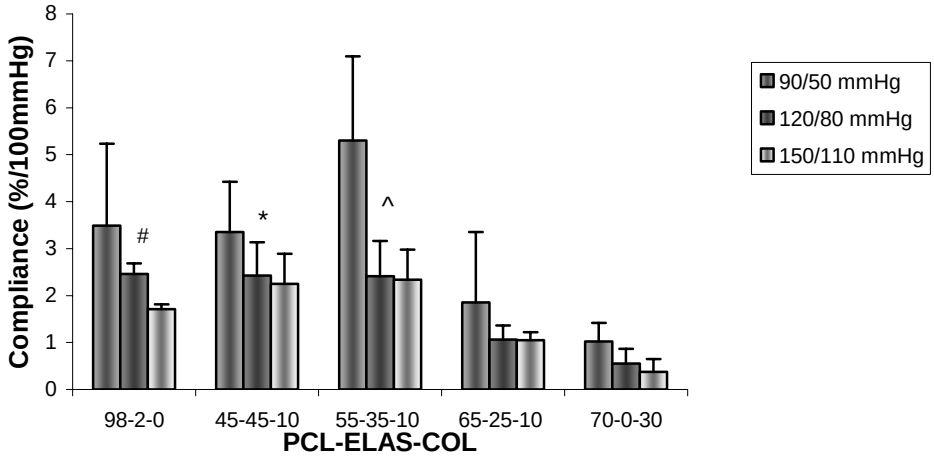

Figure 17. Compliance determined from internal radii at three different mean arterial pressures (90/50, 120/80, and 150/110 mmHg). *, ^, and # indicate significant differences between 45-45-10 and 65-25-10, 55-35-10 and 65-25-10, and 98-2-0 and 70-0-30, respectively ($p< 0.05$).

At 120/80 mmHg for Figure 17, average values were highest for the 98-2-0 layer at 2.45 % / 100 mmHg followed closely by 45-45-10 at 2.42 % / 100 mmHg and 55-35-10 at 2.41 % / 100 mmHg, sharing similar compliance values. 65-25-10 clearly demonstrates a drop in compliance with an average value of 1.06 % / 100 mmHg, indicating a stiffer material than the other two. This is confirmed by the tangential modulus results. 70-0-30 demonstrated the overall lowest compliance, 0.55 % / 100 mmHg, of all the grafts.

Figure 18 displays compliance values for whole graft combinations using the materials tested in the individual layer compliance. Average values for these different combinations ranged from 2.83 – 0.77 % / 100 mmHg at 120 mmHg with a gradual decrease in compliance as PCL content in the medial layer was increased and ELAS content was decreased. 45-45-10 was significantly different ($p< 0.05$) from both 55-35-10 and 65-25-10 for 90/50 mmHg, 120/80 mmHg, and 150/110 mmHg. Additionally, nvPFA

and ePTFE were used as comparison tools. nvPFA was significantly different ($p< 0.05$) from 55-35-10, 65-25-10, and ePTFE at a pressure of 120/80 mmHg, while 45-45-10 was comparable to nvPFA. ePTFE was significantly different ($p< 0.05$) from all other materials tested.

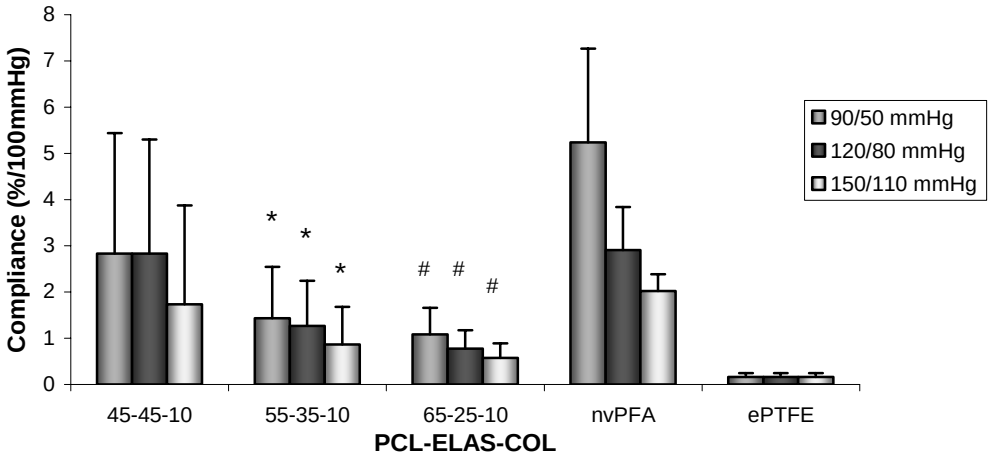

Figure 18. Compliance determined from internal radii at three different mean arterial pressures (90/50, 120/80, and 150/110 mmHg). *, # indicates significant differences between 45-45-10 and 55-35-10, and 45-45-10 and 65-25-10, respectively ($p< 0.05$).

Discussion

Scaffold Characterization

Characterization and fiber measurements are important and help describe surface morphology based on the electrospinning parameters used. This provides vital information regarding potential cellular interaction with the surface and scaffold optimization at the microscopic level. In this study, each individual layer needed to be examined for structural analysis to provide key insights into future optimization strategies for a three layered structure. This was accomplished by carefully separating the individual layers after a complete multi-layered graft had been electrospun. Although the fibers between the layers

may have been slightly affected by pulling, stretching, and breaking, this method was determined to be the best way in which to view between the layers.

Controlling the fiber diameter and tuning it to specific requirements can lead to subsequent control over porosity and cellular behavior. This parameter is then adjustable for each individual layer. To test the tunability of PCL, ELAS, and COL, SEM images were taken of both the inner and outer surface of the media. These results showed that fiber diameter gradually decreased on the outer surface and the inner surface of the media and adventitia, respectively. Clearly, this demonstrates that as the blends decrease in ELAS content and gain PCL there is a subsequent decrease in fiber diameter. This could indicate two possibilities based on electrohydrodynamics: 1) fiber welding, displayed in Figure 12 for both the medial and adventitial surfaces, decreases with the addition of PCL and subtraction of ELAS, or 2) ELAS inherently has larger fiber diameters when electrospun under these conditions; so, as ELAS content decreases, there is a direct decrease in average fiber diameter as well. Three separate studies performed by our lab have revealed that higher ELAS content conveys larger average fiber diameters [109, 110, 267]. One study demonstrated values at 0.8 μm for 50-50 PDO-ELAS blends and 0.4 μm for 80-20 PDO-ELAS blends [109].

To demonstrate the further tunability of scaffold morphology, average pore area measurements were also done. These measurements demonstrated that as fiber diameters increased in size, pore area subsequently increased as well. From a structural perspective, larger pores will allow for the dynamic movement of fibers as a scaffold is being subjected to loads. Conversely, smaller pores restrict the fibers to a limited space and can cause the

scaffold to become stiffer without a change in polymer type or crystallinity, adversely affecting the scaffolds mechanical properties. Cell-scaffold interactions are also changed with a decrease or increase in pore area. A structure containing smaller pores will disallow the movement of cells through the scaffold, causing them to attach and proliferate only on the surface. Whereas, a structure that contains larger pores can permit the passage of cells throughout the scaffold. These cell-scaffold characteristics also have the ability to change the mechanical properties as tissue is formed and polymer degrades. Additionally, a larger pore structure has a higher diffusivity and degraded polymer by-products can easily be removed, changing the degradation rate. Therefore, scaffold optimization is of high importance, especially when multiple polymers are chosen to create multiple scaffold morphologies.

Uniaxial Tensile Testing of Individual Layers

Although spinning onto a flat mandrel may create slight alterations in the electrostatic field in comparison to a cylindrical mandrel, the cylindrical mandrel for this study was too small to perform mechanical testing in the circumferential direction. The properties of individual layers provide some clues as to how a multi-layered vascular graft should perform under physiological conditions when these results are used in conjunction with a mathematical model. Firstly, peak stress indicates how much stress or pressure can be applied to the structure prior to rupturing. If the desired medial layer is one that is fairly weak with stress values around 1 MPa, its surrounding layers need to be able to take the majority of the imposed stress. Secondly, modulus indicates how stiff the layer is going to be, which will contribute to the overall compliance of the graft.

Results from Figure 13 display a weaker medial layer surrounded by a strong intima and adventitia, regardless of medial layer content. This is reflected in both peak stress and tangential modulus graphs. Although the results are based on six samples punched from a single electrospun sheet, similarities in uniaxial tensile values should be seen if electrospun conditions remain the same. Electrospinning can be influenced by several different factors, such as voltage, flow rate, concentration, solvent volatility, temperature, and humidity, directly influencing fiber size and cellular interaction. In this particular study, the authors made extensive efforts to keep all aspects of electrospinning the same for consistent results.

Generally, native artery displays characteristics where the media bears the majority of tension under *in vivo* conditions while the adventitia serves to protect the vessel from overstretch. Lu *et al.* validated this notion by using an incremental model based on the strain energy function, finding that in the circumferential direction the media and adventitial layers of coronary artery bear 62 $\pm$ 13 % and 38 $\pm$ 13 % of tension, respectively [265]. A separate study, Holzapfel *et al.*, examined the individual layer-specific properties of human coronary arteries and found their experimental data to indicate that the media seemed to be the softest layer over the whole deformation domain, and intima and adventitia exhibited considerable stiffness in the high loading domain [266]. Additionally, ultimate tensile stress data indicated that the adventitia changes to a stiff "jacketlike" tube, preventing the artery from overstretch or rupture.

Therefore, for the purpose of the theory behind this study, the intimal and adventitial layers should be relatively stiff, while the medial layer is softer in comparison,

but still able to take on a large amount of circumferential stress. So, the original concept of the design is confirmed and can be applied to a whole graft scenario with the intimal layer (98-2-0) providing initial stiffness with a compact PCL dominated structure to allow for the attachment of ECs, the medial layer (45-45-10, 55-35-10, or 65-25-10) containing a high amount of ELAS to decrease stiffness and a small portion of COL to attract cells into the layer, and the adventitial layer (70-0-30) to prevent rupture and to attract cells from outside the graft and into the matrix, producing three significantly different graft layers.

Mathematical Modeling

We wanted to observe the CWS at physiological pressures for changes in the tangential modulus of medial layers 45-45-10, 55-35-10, and 65-25-10. Additionally, if the material properties were to be fine tuned for the intimal and adventitial layers, then we wanted to observe how these changes would affect the other layers. Finally, a comparison of human coronary moduli (Figure 14D) [265, 266] was made with the 45-45-10 medial layer graft to help further evaluate native arterial behavior in comparison to future graft designs.

According to Figure 14A, 14B, and 14C, changes in layer stiffness can attribute large or small changes in overall graft behavior. The most highly affected layer under all three conditional changes is the intimal layer, relieving CWS or increasing CWS depending on the layer that is changed. The medial layer is only affected through a direct increase or decrease in layer modulus. Indirectly, it appears that it does not provide a significant change to the whole graft. Current studies are being done to determine the

validity of this hypothesis. Lastly, an indirect change in adventitia does not largely affect graft mechanics, but a direct change causes major differences.

This model provides a picture as to how the graft will behave mechanically when subjected to physiological pressures. Under these pressures, each layer is affected differently as the stress travels through the wall of the graft. Vorp *et al.* [261] first developed this model to predict how an implanted bioresorbable graft would behave *in situ* by modeling a single layered graft encapsulated by tissue on either side of the graft. As the graft degraded and the tissue grew, there would be changes to the moduli of both the graft and tissue over time until the graft had fully resorbed, displaying again how critical the time of graft degradation and tissue in-growth can be. Comparing the results of Vorp *et al.* to this study, the three-layered behavior shows similarities when the inside and outside layers increase in stiffness and the middle layer decreases in stiffness. This confirms that the equations were properly interpreted for this study. From the standpoint of our design implanted *in situ,* the transmural stress distribution will have to be modeled using a five layered design to initially account for tissue growth on the inner and outer surfaces prior to any type of cell migration.

The mechanical properties of human coronary artery from two separate studies were compared to the multilayered graft with a medial layer of 45-45-10 PCL-ELAS-COL. The moduli from each paper, Holzapfel *et al.* and Lu *et al.*, were imported into equations 2 – 5 to calculate under the same assumed physiological pressure conditions as all other specimens. Characteristics of graph shape were analyzed and it was shown that Holzapfel's intimal, medial, and adventitial moduli were similar to the shape of the 45-45-

10 graph. While the 65-25-10 and 55-35-10 all have a drop in CWS from the intimal layers to the medial layers, there is a slight drop in CWS transitioning from the medial layer to the adventitial layer. Although it is not clearly evident, Figure 14D demonstrates a slight drop in CWS from the intimal layer to the medial layer of Holzapfel *et al.* with a large rise from the medial layer to the adventitial layer. The graph of Lu *et al.* demonstrates instead a rise in CWS when transitioning from the intimal layer to the medial layer with a large drop from the medial layer to the adventitial layer. This difference is directly attributable to the testing conditions of those particular studies. Holzapfel separated the three layers of an aged human coronary artery using a scalpel. Strips of the separated tissue were then tested under uniaxial conditions. Lu *et al.* dissected an intact coronary artery with the aid of a stereomicroscope. The intima-media was left intact and tested under biaxial conditions with a circulative pump. The same was done with the adventitia. Therefore, the results obtained from Lu *et al.*'s study were not as directly related to our testing conditions and may have caused the difference seen in Figure 14D. Additionally, the intima and media were left intact which provides a thicker wall and can contribute to the larger stiffness seen in the medial layer compared to its adventitial layer, 299 kPa and 132 kPa respectively. Nonetheless, Holzapfel's study is more closely related to our testing conditions and should therefore be of main use for future mathematical calculations.

Furthermore, Holzapfel's study can be used as a tool to finely tune the electrospinning parameters of each layer. The 45-45-10 graph shows similar trends, yet it does not match the Holzapfel graph. In order to make the trends in either case equivalent,

several options must be considered: 1) decreasing the stiffness in the intimal layer, 2) increasing the stiffness of the medial layer, and 3) increasing the stiffness of the adventitial layer. Relative to one another, the 45-45-10 graft contains a higher intimal stiffness and lower medial and adventitial stiffness than Holzapfel. As Figure 14B demonstrated earlier, a decrease in intimal stiffness will cause both the stress distribution of the medial and adventitial layers to shift upward, taking on more stress. At the same time, an increase in medial stiffness (Figure 14A) will cause the intimal layer to shift further downward, decreasing the amount of stress imposed on it, while the medial layer shifts upward taking on more stress. Finally, an increase in adventitial stiffness will once again create a downward shift in the transmural stress distribution of the intimal layer with a slight upward shift in the medial layer, while the adventitial layer has a significant upward shift. These actions (decreasing the intimal stiffness, and increasing the medial and adventitial stiffness) would have a pronounced effect on overall graft behavior and could match the stress distribution seen with Holzapfel.

From an electrospinning standpoint, a full range of polymers blends would need to be created. As we have shown, an increase in ELAS content will decrease the stiffness of a material. Therefore, the addition of ELAS to the intimal layer would be a primary starting point. Moreover, a higher ratio of PCL in the medial layer would cause an increase in stiffness; however, the addition of PCL to the adventitial layer is questionable. Here an increase in stiffness becomes a challenge since increasing the medial stiffness creates a negative effect on the adventitial stress distribution. Therefore, a range of

polymers with an increase in COL content and an increase in PCL content would be required to determine the best course of action.

Suture Retention

In order for the implantation of a vascular graft to be successful a sufficient amount of suture retention strength is needed. Although a graft may possess adequate strength that will initially suffice, biodegradation of a vascular graft should be taken into consideration as well. If a vascular graft is a rapidly degradable material, then the cyclic loads imposed at the site of anastomosis could potentially fail. The "gold standard" for vascular bypass is the saphenous vein. Ideally, suture retention results should fall within this range, a value that averages 380 gf [268]. From our study, nvPFA is slightly below this average, and the three-layered grafts tested in this study are also well below that of saphenous vein, while ePTFE is significantly higher than saphenous vein and all grafting materials tested. Nevertheless, it is encouraging that nvPFA displays values that are close to the grafts manufactured for this study. Lastly, 45-45-10 and 65-25-10 were significantly different from each other ($p< 0.05$), showing that a significant change in the medial layer provides a significant change for the whole graft. Although biodegradation of PCL would be slow enough to allow cellular infiltration and tissue development to occur, the results indicate that further optimization of the graft design is needed.

Burst Strength

Burst strength of the three grafts demonstrated ample ability to withstand pressure. The bursting properties also showed how changing the medial layer of the graft material influenced its final burst pressure, proving that as the medial stiffness is increased the

stresses imposed on both the intimal and adventitial layers are reduced and allowing the graft to take on more pressure prior to bursting. Additionally, a separate test was performed to test the influence of the "jacketlike" properties of the adventitial layer. After the 55-35-10 and 65-25-10 grafts exceeded the pressure regulator, the adventitial layer was slowly rubbed, causing a thin spot in the material. At this spot, an aneurysm formed followed by graft bursting.

Dynamic Compliance: Individual and Whole Graft

The intimal layer, 98-2-0, had a surprisingly higher compliance value than originally anticipated compared to the medial layer results. According to the modeling results, there will not be a significant change in CWS seen by the medial layer and adventitial layer with a slight increase or decrease in intimal stiffness, but a higher compliance value could allow for a higher CWS in the medial layer than predicted, which would result in an increased distension of the graft wall.

When enough PCL was added to the medial layer, the compliance dropped a significant amount. Combinations of PCL and COL, though, clearly have a large impact on scaffold compliance looking at the differences between 98-2-0, 65-25-10, and 70-0-30. 98-2-0, containing almost pure PCL, has a higher compliance than either of the other two layers, but no COL is present. At the other side of the spectrum, 70 % PCL and 30 % COL in the adventitial layer with 0 % ELAS has the lowest compliance of all the grafts. The medial layer has a slight amount of COL present at 10 % and provides a similar compliance value to 98-2-0 at significantly lower PCL percentages. COL's impact is somewhat contradictory to other studies which have shown that higher COL content

dictates a higher compliance [257]. This could be explained by the extraction processes undertaken between the two studies and the possible age difference in the skin used.

When these three layers are superposed in a whole graft, their individual compliance results should be additive, contributing to the combined behavior of the three layers. Medial layer differences were tested to see if a higher stiffness would significantly alter the compliance of the whole graft. This was confirmed with the results. The highest average compliance was demonstrated by the 45-45-10 PCL-ELAS-COL followed by 55-35-10 and 65-25-10. This showed that when all of the layers worked together a lower compliance value was achieved with decreases in ELAS and increases in PCL content in the medial layer. Referring back to the individual compliance results of the three medial layers tested, this is surprising considering that 45-45-10 and 55-35-10 were similar at 120/80 mmHg. The significant decrease in compliance found in the 55-35-10 graft ($p< 0.05$), which was found to be similar to 45-45-10 in Figure 17, could be different due to a combination of a slight increase in stiffness and the outer 70-0-30 layer. As the medial layer stiffness increases the adventitial layer is able to perform a better "jacket-like" duty and prevent the graft from distending too far. This is confirmed by modeling where an increase in medial stiffness provides an increase in the amount of CWS taken by it and a decrease in the amount of CWS taken by the adventitial layer.

nvPFA demonstrated that ranges of both 45-45-10 and 55-35-10 PCL-ELAS-COL fell within its range at 120/80 mmHg. Additionallly, these values also fell within the initial compliance range of L'Heureux *et al.* tissue engineered blood vessel, an average of 3.4 % / 100 mmHg [164]. In the L'Heureux study, the graft was explanted after 6 months and

demonstrated a remarkably higher average compliance value of 8.8 % / 100 mmHg which was comparable to that of internal mammary artery. This is encouraging for this study, indicating that the initial compliance does not have to exactly match native arterial compliance values. Although mismatch can lead to intimal hyperplasia and graft failure, a complete match of graft and arterial compliance properties may end up in graft failure as well since the construct may be too weak. *In vivo*, mechanical properties can change drastically when using a bioresorbable scaffold. Theoretically, compliance could increase significantly as the synthetic polymer structures degrade. Therefore, an identical starting compliance could lead to aneurysm due to polymer degradation, while an initially lower compliance could end up an identical match long before intimal hyperplasia.As an alternative approach to vascular design, compliance values could actually be slightly lower than native tissue so as to allow for future increased compliance upon scaffold degradation and remodeling.

General Discussion

Multi-layer electrospinning was first attempted by Kidoaki *et al.* [215] using COL, gelatin, segmented polyurethane, and PEO. Since then multi-layer electrospinning has been studied using PCL, PLA, PDO, Poly(glycolide-co-trimethylene carbonate), gelatin, and ELAS [98, 108, 153, 216]. These studies employed different uses of multilayered techniques. Smith *et al.* [108] electrospun PDO-ELAS bilayered constructs with a suture wound in the center for reinforcement. Vaz *et al.* [98] electrospun a bilayered tube structure made of PCL and PLA, varying the anisotropy of the layers, but not including natural polymers. Yang *et al.* [216] performed a layer-by-layer approach electrospinning

PCL and COL together, seeding human dermal fibroblasts (HDF), and then repeating the PCL/COL and HDF layers. These cellularized constructs were done is sheet form and not with tubes. Thomas *et al.* [153] utilized PGA, ELAS, and gelatin in a 3 layered form. However, the use of PGA and gelatin would not be conducive to an arterial graft as gelatin, *in vivo*, has been shown to display a large cytotoxic response [217] and PGA is a fast degrading polymer. Additionally, only one study used a cross-linker to stabilize the natural polymer, Smith *et al.* The use of PCL, ELAS, and COL in tubular form with unique combinations for each layer, taking a closer look at how electrospun constructs containing different polymer blends in different layers had yet to be done until now. This technique allows one to control the parameters of each layer, tuning it to the specific desired outcome. Native tissue has been studied relentlessly, using mechanical properties and mathematical modeling of coronary intima, media, and adventitia to gain information that explains how the arterial wall reacts under physiological conditions [120, 265, 266, 269-273]. Ultimately, each layer in an artery has a specific function to allow the vessel to continue transporting blood and nutrients. A vascular graft must provide this same function over an extended period of time, avoiding aneurysm formation, graft rupture, and intimal hyperplasia.

Using a multi-layered technique, grafts can be tailored to exact specifications and optimized thereafter. Aneurysms and graft rupture could be avoided through the use of a "jacketlike" outer layer that would prevent the graft from overextending itself. The middle layer can be tailored to have the lowest modulus, providing the distension required for proper compliance and blood flow, similar to native artery. The inner most layer can be

manufactured so that ECs will attach and proliferate, creating a confluent, non-thrombogenic surface, preventing or significantly decreasing intimal hyperplasia.

Conclusion

In conclusion, we were able to produce nano- to micro-fibrous three-layered small diameter vascular grafts with distinct material properties for each layer. These layers proved to change the overall graft properties in regards to fiber diameter, suture retention, and compliance, containing values that were within the range of native artery. Individual layer evaluation and mathematical modeling proved to be beneficial in the overall analysis of graft behavior, and can be used in the future to help predict how certain material combinations will act. This prediction will allow for future graft optimization, electrospinning multiple combinations of polymers in order to develop the highest quality vascular replacement. Additionally, future work will investigate possible limitations such as delamination of the layers while the scaffold undergoes degradation in addition to adequate pore size for cellular infiltration. To test this, both acellular and cellular *in vitro* degradation studies will be performed under static and dynamic culture. These tests will determine both the migratory capabilities of the scaffolds and how they will effectively degrade under physiological conditions.

CHAPTER 4: Investigating Crosslinking Parameters for Polycaprolactone, Elastin, Collagen, and Silk Blended Scaffolds

Abstract

The purpose of this study was to evaluate the affect of two different cross-linking reagents: EDC and genipin. These two cross-linkers had undergone preliminary investigation by our lab, however, we aimed to elucidate any microscopic or macroscopic differences using three different biopolymers, ELAS, COL, and SF, blended with a biodegradable polymer, PCL. Results from the study determined through a TNBS assay that percent cross-linking increased as higher molarities of reagents were used. Additionally, BCA protein assays indicated that higher concentrations of cross-linking molarity also tended to cross-link scaffolds at a faster rate than lower concentrations. Fiber diameter measurements displayed differences as ELAS protein content was increased in addition to an increase in diameter due to genipin cross-linking. Tensile strength testing, on the other hand, did not produce significant changes in material properties between the two cross-linkers. This study provided insight into the reaction rates, degree of cross-linking, and macroscopic properties of EDC and genipin.

Introduction

Electrospinning can be used to process native, synthetic or blended polymers into fibrous mats that show considerable promise as tissue engineering scaffolds [274]. Both scaffold and fiber-level properties can be adjusted at several stages in the electrospinning process. Fiber composition and diameter can be tailored based upon polymer/solvent concentrations and polymer identity. Once completed, the material properties of a protein-

based scaffold can be further modified through various cross-linking protocols [275]. Each of these variables can be manipulated and tuned to produce a scaffold that meets two basic criteria. First, the macroscale material properties and architectural features of the electrospun scaffold must be consistent and mimic the profile of the native tissue of interest. Second, the local microscale environment must provide physiologically relevant binding sites to anchor cells to the surrounding scaffold [274]. *In vivo*, COL possesses a specific amino acid sequence, Arginine-Glycine-Aspartic acid (RGD), which provides a specific site for cell-integrin attachment. Although ELAS does not contain these RGD peptides, it possesses a Valine-Glycine-Valine-Alanine-Proline-Glycine (VGVAPG) peptide sequence which is conducive to cellular attachment at the ELAS receptor or through the $\alpha_v\beta_3$ integrin protein [137].

The native ECM of the vasculature is composed mostly of COL and ELAS. These ECM components are constantly synthesized, secreted, oriented, and modified by the cellular components that they support. Classically, the function of native ECM was only believed to be as a structural framework for tissues. However the ECM, through interaction with receptors on the surfaces of cells, directly takes part in promoting cell adhesion, migration, growth, differentiation, and apoptosis. The ECM also plays a role in cytokine activity and intracellular signaling, both of which serve numerous functions in cell regulation and activation [258]. COL is the most abundant protein in the human body, a key element of the ECM, and imparts structural integrity and tensile strength to tissues. Within the native architecture of an artery, particularly the adventitia, collagens type I and III prevent aneurysmal formations under high physiological pressures by providing a

"jacket-like" structure. ELAS is one of the main structural components of the vascular ECM. Its principal role is to provide elastic recoil properties and resilience to proper function of tissues that are subject to repetitive distension and physical stress. Natively both COL and ELAS are insoluble proteins containing isodesomosine and desmosine crosslinks [139, 142, 276]. However, when these proteins are extracted for biomedical use, they become soluble structures, leaving them readily dissolvable by aqueous environments.

In addition to native proteins, other proteins have been gaining some momentum for biomaterials research. SF is an intriguing natural protein, used for centuries as a medical grade suture, which is gaining momentum as a tissue engineering scaffold due to its unique blend of material characteristics and bioactivity. SF exhibits excellent biocompatibility with a foreign body response comparable to other degradable sutures, hemocompatibility, and oxygen and water permeability. SF also possesses remarkable mechanical properties not seen in other naturally occurring proteins [218-220]. SF has also been recently utilized in the creation of electrospun bioresorbable vascular grafts with promising results. Zhang *et al.* successfully seeded electrospun SF with both human aortic endothelial cells (hAEC) and human coronary artery smooth muscle cells (hCASMC) [277]. Both hAECs and hCASMCs demonstrated an affinity for the electrospun SF.

In order to successfully create a three dimensional scaffold structure containing COL and ELAS, fixation techniques must be investigated to fine tune both macroscopic and microscopic properties. By themselves, COL and ELAS are unable to support their own structure without fixation. Several studies have demonstrated this, where both

proteins immediately dissolve upon immersion in an aqueous solution [110, 278]. Stable proteins that have the potential to improve cell adhesion and infiltration of the scaffolds alongside an improved mechanical performance would be essential to a tissue engineered vascular replacement. The most common crosslinker, glutaraldehyde, has been used with numerous types of electrospun scaffolds [222, 233, 237-240], but with cytotoxic drawbacks [241]. EDC and genipin (GEN), on the other hand, have exhibited lower cytotoxicity [241-243], making them better suited for implantation. While COL and ELAS require the use of a chemical crosslinker, SF has been shown to form β-sheet crosslink formations when SF scaffolds were dipped in either ethanol or methanol for 30 minutes [279]. Therefore, this study aimed to determine suitable cross-linking conditions using both EDC and GEN dissolved in ethanol for blended electrospun scaffolds composed of ELAS, COL, and SF blended with a synthetic biodegradable material, PCL.

Materials and Methods

Protein Extraction

SF was extracted from the cocoons of *Bombyx mori* silk worms (The Yarn Tree) through an established protocol [280]. Briefly, the cocoons are cut into pieces and boiled in a 0.02 M Na_2CO_3 (Sigma Aldrich) solution for 30 minutes to remove the sericin gum, followed by thorough rinsing in de-ionized water (DI), and drying in a fume hood. The SF is then dissolved in a LiBr (Fisher Scientific) solution at 60°C for 4 hours. This solution is then dialyzed against deionized water for 3 days using 3500 MWCO dialysis tubing (Fisher Scientific). The SF solution is then frozen and lyophilized to provide a pure SF for electrospinning.

COL type I was extracted from 6 month bovine corium through an acetic acid based process previously described [262]. Briefly, tissue is homogenized, suspended in acetic acid, and subsequently purified via a series of dissolutions, precipitations (using NaCl (Fisher Scientific) and Tris (Fisher Scientific)), and dialyses [263]. Following the final dialysis, COL solutions are frozen and lyophilized.

Electrospinning

The electrospinning setup consisted of a syringe pump (KD Scientific), a high voltage power supply (Spellman CZE1000R, Spellman High Voltage Electronics Corp.), a plastic Becton Dickinson syringe used as the polymer reservoir, attached to an 18-gauge blunt-tip needle. Concentrations of 150 mg/ml of PCL (MW: 125,000, Lakeshore Biomaterials), 200 mg/ml of soluble ELAS from bovine neck ligament (Elastin Products Co. Inc.), 70 mg/ml of COL I (6 month bovine corium), and 80 mg/ml of SF were dissolved in HFP (TCI America). These were then blended in ratios of 50-50 PCL-ELAS, PCL-COL, and PCL-SF. Additionally, scaffold materials were blended in ratios of 45-45-10, 55-35-10, 65-25-10, 45-10-45, 55-10-35, and 65-10-25 PCL-ELAS-COL and PCL-ELAS-SF. To evaluate both cross-linking and material properties, blended scaffolds were electrospun onto rectangular mandrels measuring 2.5 cm wide x 10.2 cm long x 0.3 cm thick. The parameters for electrospinning were kept constant with an applied voltage of 25 kV, air gap distance (distance between the needle and rotating drum) of 15 cm, and solution dispensing rate of 4 ml/hr

Cross-linking

Scaffolds were cross-linked using EDC (FlukaBiochemika), genipin (GEN, Wako Pure Chemical Industries, Ltd.). In order to determine optimal cross-linking parameters, a range of concentrations, solvent additives, and time points were used to crosslink ELAS, COL, and SF blended scaffolds. Using EDC, a 5 and 50 mM cross-linking solution was prepared in 90 % ethanol (Fisher Scientific) with a 0, 5, and 10% addition of PBS to the ethanol mixture. EDC has been previously shown to cross-link PCL-COL scaffolds at a concentration of 5 mM [281]. Therefore, 50 mM was chosen as a significantly higher concentration. The addition of an aqueous solution, PBS, to the ethanol was used to determine the extent of cross-linking that would occur prior to protein dissipation. In this way, we wanted to optimize cross-linking parameters and determine if the addition of PBS would affect the cross-link ability of the scaffolds. Scaffolds for TNBS Assay (Research Organics) were placed in the EDC solution, and allowed to cross-link for 18 hours [275] followed by a 0.1M Na_2HPO_4 rinse for 1 hour and a PBS rinse for 1 hour.

Using GEN, a 10 and 30 mM cross-linking solution was prepared in 90 % ethanol (Fisher Scientific) with a 0, 5, and 10% addition of PBS to the ethanol mixture. In the case for GEN, 30 mM has been previously shown to fully cross-link collagen samples over a period of 72 hours at room temperature [245]. Therefore, a lower concentration was also chosen for GEN, 10 mM, however, based on the length of time it takes for GEN to chemically cross-link protein structures we did not choose a 10x lower concentration. Like the EDC cross-linked scaffolds, we again wanted to determine the cross-linking parameters due to the addition of PBS in the ethanol mixture. Scaffolds for TNBS were electrospun

and placed in the cross-linking solution for a period of 72 hours [245], followed by a PBS rinse for 2 hours.

TNBS Assay

The concentration of free primary amine groups present in cross-linked electrospun protein scaffolds (ELAS, COL, and SF) was determined using a TNBS Assay (Research Organics) [244]. Scaffold samples were electrospun, punched using a 12 mm biopsy punch, massed and cross-linked using the procedures listed above. Samples were placed in 15mL Fisherbrand® centrifuge tubes. $NaHCO_3$ (1.0 mL 4% w/v) and TNBS (1.0 mL 0.5% w/v) were added and placed in an incubator at 40°C for 2 hr. 3.0 mL of 6M HCL was then added to the solution, which was placed in an oven at 60°C for 2 hr. The samples were diluted with 9 mL of PBS, cooled to room temperature. The absorbance at 345 nm was measured using a SPECTRAmax® PLUS^{384}microplate spectrophotometer. Measured absorbance values were then placed into a percent cross-linking equation

$$\%Cross-linked = 1 - \left[\frac{Abs_c / Mass_c}{Abs_{nc} / Mass_{nc}} \right]$$

WhereAbs_c is the measured absorbance of the cross-linked solution, Abs_{nc} is the measured absorbance of the non-cross-linked solution, $Mass_c$ is the dry mass of the cross-linked scaffold, and $Mass_{nc}$ is the dry mass of the non-cross-linked scaffold. The sample size for each measured absorbance group was n = 3, and each sample was run in triplicate.

Protein Assay

In order to determine time dependence of cross-linking at room temperature, scaffolds were cross-linked using EDC protocols at times of 0, 10, 30, 60, 180, and 1080

minutes, and using GEN protocols at times of 0, 6, 24, 48, and 72 hours. Following the specified cross-linking time periods, the EDC or GEN mixture was immediately removed and scaffolds were washed in 2 ml of 90 % ethanol 4 times. These cross-linked scaffolds were then placed in a 48 well plate and filled with 500 µl of PBS. The scaffolds were allowed to incubate overnight at room temperature and their protein release was measured using a Pierce BCA Protein Assay Kit (Thermo Scientific) with a working range of 20 – 2000 µg/ml. Briefly, 25 µl of each standard and unknown were pipetted into a 96 well plate. 200 µl of the working reagent was then mixed with the standard and unknowns, and subsequently incubated at 37^{o}C for 30 minutes. After incubation, the samples were measured at an absorbance wavelength of 562 nm. The sample size for each measured absorbance group was n = 3, and each sample was run in triplicate.

Scaffold Characterization

Scaffold characterization was performed using scanning electron microscopy on the electrospun mats (SEM, Zeiss EV050). SEM images were analyzed with ImageTool 3.0 software (Shareware provided by UTHSCSA). Measurements for fiber diameter were defined such that no fibers beyond the superficial surface were considered for measurement. For each SEM image, sixty random fibers were measured. Additionally, calibration of the ImageTool software was done with the scale bar on each image for all measurements.

Uniaxial Tensile Testing

Uniaxial tensile testing was performed on six samples (n = 6) from one cross-linked electrospun sheet hydrated in PBS for 24 hours. "Dog-bone" shaped samples were

punched from electrospun mats (2.75 mm wide at their narrowest point with a gage length of 7.5 mm) and tested on a MTS Bionix 200 testing system with a 100 N load cell (MTS Systems Corp.) and an extension rate of 10.0 mm/min. Peak stress, modulus, and strain at break were calculated using TestWorks version 4.

Results

% Cross-linked

The aim of this portion of the experiment was to test samples for their optimal cross-linking conditions. This was done through the use of two different molarities, two different crosslinkers, and three sets of PBS additions. The hypothesis behind the experiment was that higher molarities of cross-linking solution would have more available moieties to form cross-linked structures, further stabilizing the materials to produce a higher percent cross-linked value. The different crosslinkers, EDC and GEN, were chosen because of their aforementioned low cytotoxicity and biocompatibility. Finally, 0, 5 and 10% PBS additions to the ethanol/crosslinker solutions were chosen to determine how PBS would affect the percentage of cross-linking. It was hypothesized that if a higher amount of PBS was added to the solution then a larger portion of protein would dissipate out of the scaffold prior to the TNBS assay, leaving a lower number of free amine groups left in solution and thereby possessing a lower absorbance value.

According to the results displayed in Figure 19, absorbance values using the EDC crosslinker displayed a clear upward trend for both ELAS and COL samples, where both COL and ELAS cross-linked absorbance values were significantly different ($p < 0.05$) from their no treatment (NT) values. Specifically for ELAS, 0% PBS for 50mM concentrations was different ($p < 0.05$) from both 5 and 10% PBS additions to the cross-

linking solution. This would indicate that both 5 and 10% successfully dissipated free amine groups prior to TNBS treatment. For COL, 10% PBS for a concentration of 5 mM was different ($p < 0.05$) from 5% PBS, while 10% PBS for a concentration of 50 mM was different ($p < 0.05$) from both 0 and 5%. PBS additions to the COL solutions did not exhibit the same trends as ELAS. Instead, the addition of water appears to not have dissipated the free amine groups prior to TNBS treatment, but it seems to have made them more readily available to dissociate during TNBS treatment, decreasing cross-linking. Both ELAS and COL results aim to confirm that a larger number of free amine groups exist in solutions of uncross-linked materials while less free amine groups existed in cross-linked materials with the use of EDC. For SF, NT absorbance values were not different from any of the 5 mM concentrations nor were any of the 5mM concentrations different from each other, however, the SF 50 mM concentrations were different ($p < 0.05$) from NT values, indicating that there may have been some carboxyl groups available on SF for EDC cross-linking but that a higher concentration of crosslinker was needed to successfully create an amide bond.

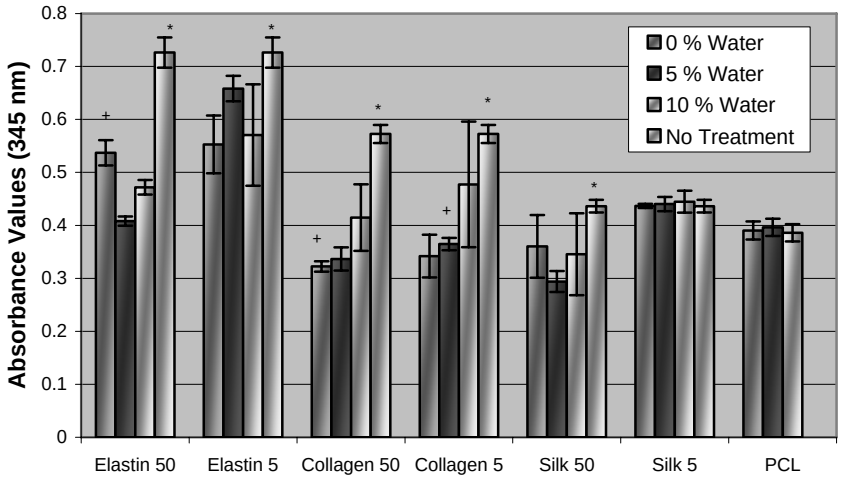

Figure 19. Absorbance values at 342 nm for TNBS assays with EDC cross-linking for 50-50 PCL-ELAS, PCL-COL, and PCL-SF.* indicates that 0, 5, and 10 % PBS were significantly different from NT. + indicates either 0 or 5 % PBS significantly different from 10 % PBS.

Results displayed in Figure 20 demonstrate similar trends for ELAS cross-linked samples; ELAS NT samples are significantly different ($p < 0.05$) from both 10 and 30 mM GEN concentrations. Additionally, 10% PBS is different ($p < 0.05$) from 0% PBS for both 10 and 30 mM concentrations, where higher absorbance values were seen in the 0% PBS samples. This would again indicate that free amine groups were dissipated from the scaffold during the cross-linking process, producing smaller absorbance values. Similar trends are seen in 30 mM COL samples, however, NT COL samples possess lower absorbance values than any of the 10 or 30mM concentrations. This possibly indicates an interference from the GEN cross-linking given that GEN turns a green-blue color during the cross-linking process and the absorbance values are measured at 345 nm, a wavelength within the range of green. This interference can be seen again in the SF samples, which also possess higher absorbance values than their NT samples.

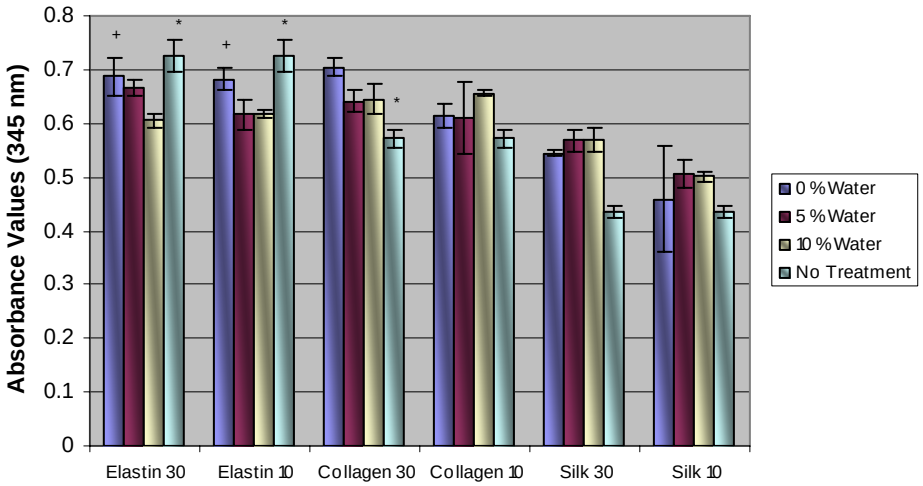

Figure 20. Absorbance values at 342 nm for TNBS assays with GEN cross-linking for 50-50 PCL-ELAS, PCL-COL, and PCL-SF. * indicates that 0, 5, and 10 % PBS were significantly different from NT. + indicates either 0 or 5 % PBS significantly different from 10 % PBS.

Figure 21 demonstrates the percent cross-linked values for all EDC samples. Averages suggested an upward trend as EDC concentration increases with 21.8% for 0% 5 mM ELAS and 33.1% for 0% 50 mM ELAS and values of 8.0% for 0% 5 mM COL and 20.4% for 0% 50 mM COL. However, no differences between EDC concentrations occur for ELAS, and only one difference for COL exists between 5% 50 mM and 0% 5 mM. Although closely clustered together, results from Figure 19 would suggest that a lower absorbance value would have created a lower percent cross-linked value. However, original weight values were used in the calculation of these percentages, which would skew the results of absorbance values and appear as a higher percentage of cross-linking than in actuality. The way in which weight values skew the results for percent cross-linking can be most readily seen in the SF samples where values contain extremely large

standard deviations and averages around 25% which would be expected to be more near 0%.

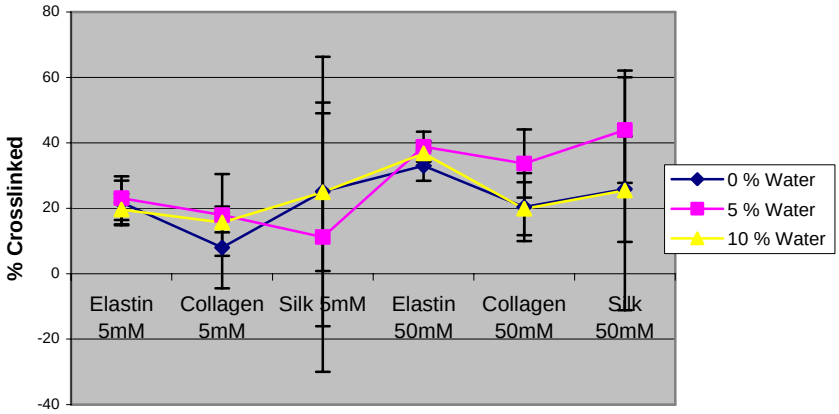

Figure 21. Percent cross-linking based on absorbance values obtained from Figure 19 and dry mass values for 50-50 PCL-ELAS, PCL-COL, and PCL-SF cross-linked with EDC.

Observing Figure 22, again similar trends to EDC concentrations are displayed with ELAS samples increasing in percent cross-linking as GEN concentrations increase from 22.7% to 33.4% cross-linking for 10 and 30mM concentrations, respectively. However, COL samples display a wide range of negative values further exacerbating the affect of the green-blue color due to the GEN crosslinker. Meanwhile, SF samples again display similar results as with Figure 21, containing high standard deviations and no significant differences. The results from the GEN TNBS assay demonstrated that a significant amount of protein needed to be present within the scaffold in order to create a successful experiment, as with the ELAS samples, without the negative effects of the GEN crosslinker interference.

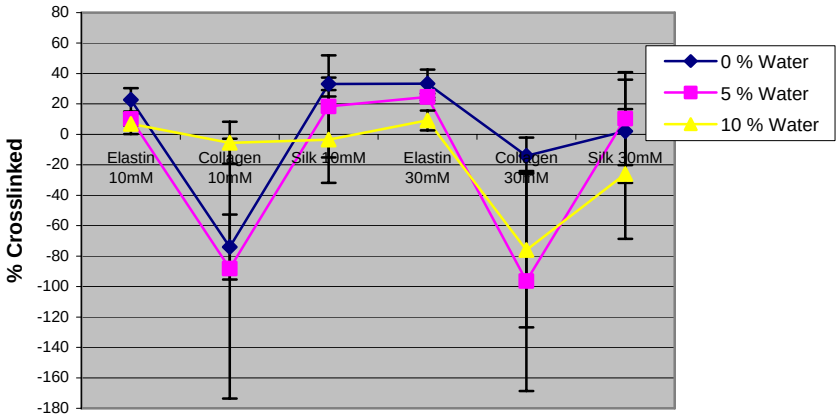

Figure 22. Percent cross-linking based on absorbance values obtained from Figure 20 and dry mass values for 50-50 PCL-ELAS, PCL-COL, and PCL-SF cross-linked with GEN.

Cross-linking Kinetics

In order to further determine the characteristics of cross-linking with regards to time dependency, a protein assay was used to measure protein release from the scaffold materials pre- and post-cross-linking. These results demonstrated the kinetics of the reactions that occur within the scaffolds and the differences between either COL or ELAS blended structures. Figure 23 displays the reaction of GEN at concentrations of 10 and 30 mM. These results showed similar reaction rates regardless of the protein being cross-linked. Figure 23 (top) demonstrated a quicker rate of reaction time with COL structures and a slower reaction time with ELAS, dropping from an intial protein concentration of 4.1 and 4.6 mg/ml to a protein concentration of 0.9 and 2.9 mg/ml for COL and ELAS blended samples, respectively, within the first 6 hours. Figure 23 (bottom) displays similar reaction rates with a higher cross-linking molarity dropping from 4.5 and 5.6 mg/ml to 0.8 and 2.4 mg/ml for COL and ELAS, respectively, within the first 6 hours. These reactions begin to slow down, but continually decrease their protein release from the scaffold materials until times of 48 and 72 hours. These results may have been influenced by the green-blue color

that bleeds from the genipin cross-linked scaffolds, interfering with the absorbance output at a wavelength of 562 nm.

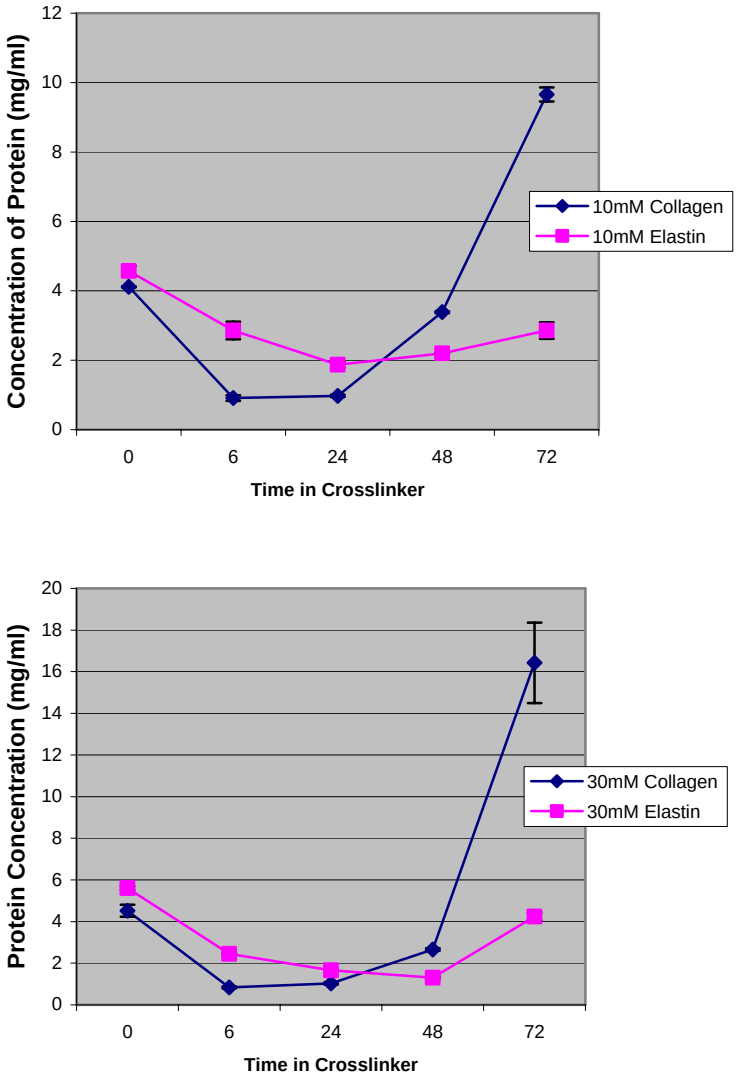

Figure 23. Results from BCA protein assay measuring protein concentration as a function of time. (Top) Represents time dependency with 10mM GEN cross-linking. (Bottom) Represents time dependency with 30mM GEN cross-linking.

While results from GEN displayed interference with the protein assay, results from the EDC cross-linked scaffolds showed slower reactions rates with COL blended scaffolds when cross-linking molarity was decreased to 5 mM. This is evident in Figure 24 (top)

where the protein concentration of the COL blended scaffolds decreases from 0.44 to 0.42 mg/ml after a period of ten minutes; however, 50 mM EDC, in Figure 24 (bottom), cross-linked the COL scaffolds at a much higher rate decreasing from 4.1 to 0.6 mg/ml. ELAS blended scaffolds were almost fully cross-linked after 10 minutes decreasing protein release concentrations from 3.5 to 1.1 mg/ml for 5mM EDC and 4.6 to 1.4 mg/ml for 50mM EDC. For both COL and ELAS blended scaffolds, cross-linking is still occurring after 10 minutes with significant differences between 10 and 30 minute samples. However, it is clearly evident that cross-linking occurs faster in ELAS blended scaffolds than it does for COL blended scaffolds, where no significant differences are present after 30 minutes of cross-linking time in ELAS samples. Nevertheless, differences are present between 30 and 180 minutes for 50mM cross-linked COL samples, and 30, 60, and 180 minutes are all different from each other with 5mM samples. These results prove that EDC reacts faster in ELAS samples and that crosslinker molarity plays a vital role in reaction rates, providing more available chemical to produce crosslinks with carboxyl groups.

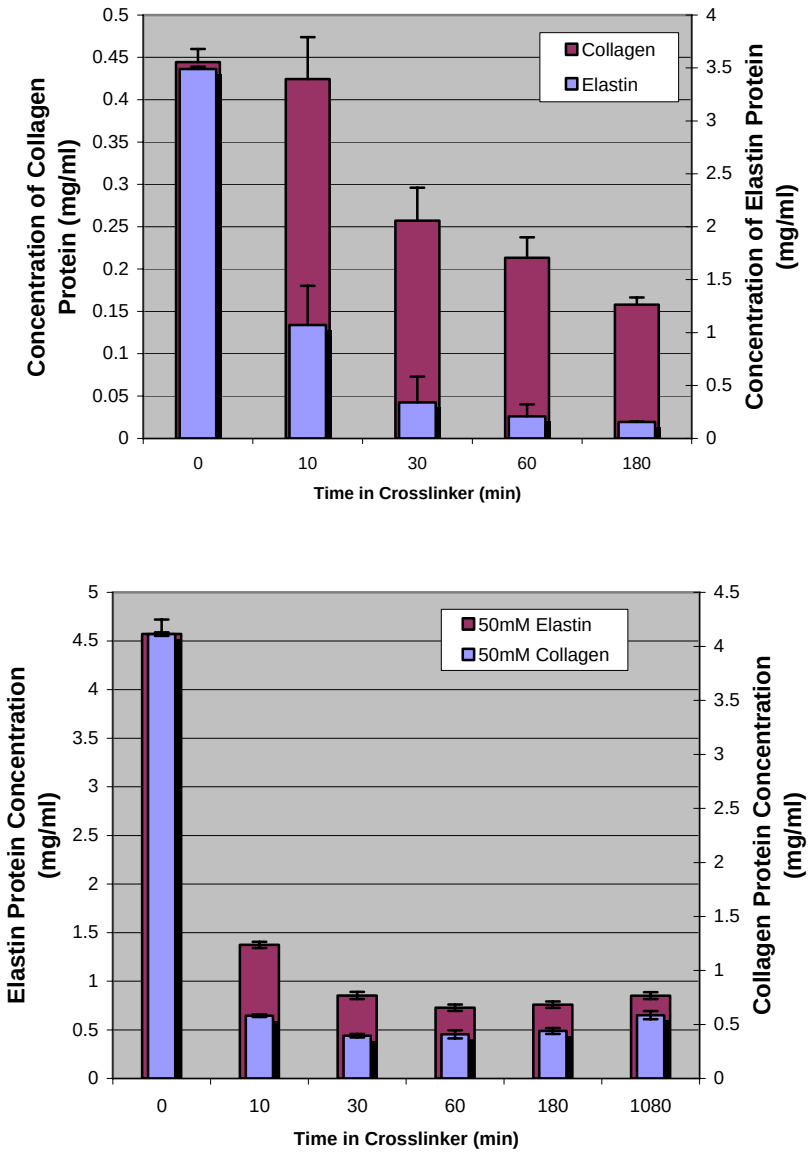

Figure 24. Results from BCA protein assay measuring protein concentration as a function of time. (Top) Represents time dependency with 5mM EDC cross-linking. (Bottom) Represents time dependency with 50mM EDC cross-linking.

Fiber Diameter

Fiber diameter results were measured to determine whether or not chemical cross-linking with either EDC or GEN would result in an increase, decrease, or no change in fiber diameter. Observing the general trends in fiber diameter from Figure 25 (top), ELAS

has an evident affect on the PCL-ELAS-COL blended scaffolds, where as ELAS content is increased the overall average fiber diameter increases as well. This is apparent with uncross-linked scaffold averages ranging from 1.1 – 2.3 μm. Interestingly, cross-linking significantly increases average fiber diameter. This is especially apparent in 45-45-10 scaffolds where the average fiber size is 3.1 and 3.9 μm for EDC and GEN, respectively. Additionally, these 45-45-10 samples were all significantly different from each other. 55-35-10 samples also displayed significant differences, where GEN cross-linked scaffolds were different from both EDC and uncross-linked (No Xlink) scaffolds. Both trends in 45-45-10 and 55-35-10 scaffolds with GEN cross-linking displayed increased fiber diameters when compared to either EDC or No Xlink. Significant differences were present in 65-25-10 scaffolds where GEN was different from both EDC and No Xlink, however, the average fiber diameter for the GEN cross-linked scaffolds of 65-25-10 were lower than both EDC and No Xlink, indicating the existence of a threshold for the relationship between fiber diameter increase with GEN and ELAS concentration in the electrospun solution. When the solution ratios were reversed and higher quantities of COL were added to the electrospun solution, there were very few trends and cross-linking did not seem to affect fiber diameter as pronounced as when higher quantities of ELAS were added to the solutions. No differences existed for either 45-10-45 or 65-10-25, however, differences were present for 55-10-35 where No Xlink was different from both GEN and EDC cross-linked scaffolds.

In Figure 25 (bottom), it is evident that higher quantities of ELAS did not affect the fiber diameter size when COL was replaced by SF in the electrospun solution. This was

shown through the lack of significant differences amongst the cross-linked and uncross-linked samples. For 45-45-10 there were no differences, and for both 55-35-10 and 65-25-10 differences were between No Xlink and both EDC and GEN cross-linked scaffolds. Additionally, as less ELAS was added to the polymer solution, average fiber diameter increased amongst No Xlink scaffolds. When the SF and ELAS ratios were reversed, fiber diameter increased appreciably. Trends demonstrated that as SF quantities incrementally decreased from 45 to 65 fiber diameter also decreased. This was present regardless of crosslinker type. Differences amongst the groups were as such: 45-10-45 No Xlink was different from both EDC and GEN, 55-10-35 were all different from each other, and 65-10-25 GEN cross-linked scaffolds were different from both EDC and No Xlink. None of the significant differences present amongst the groups displayed any similar characteristics, except that No Xlink scaffolds had a higher average fiber diameter than either cross-linked group.

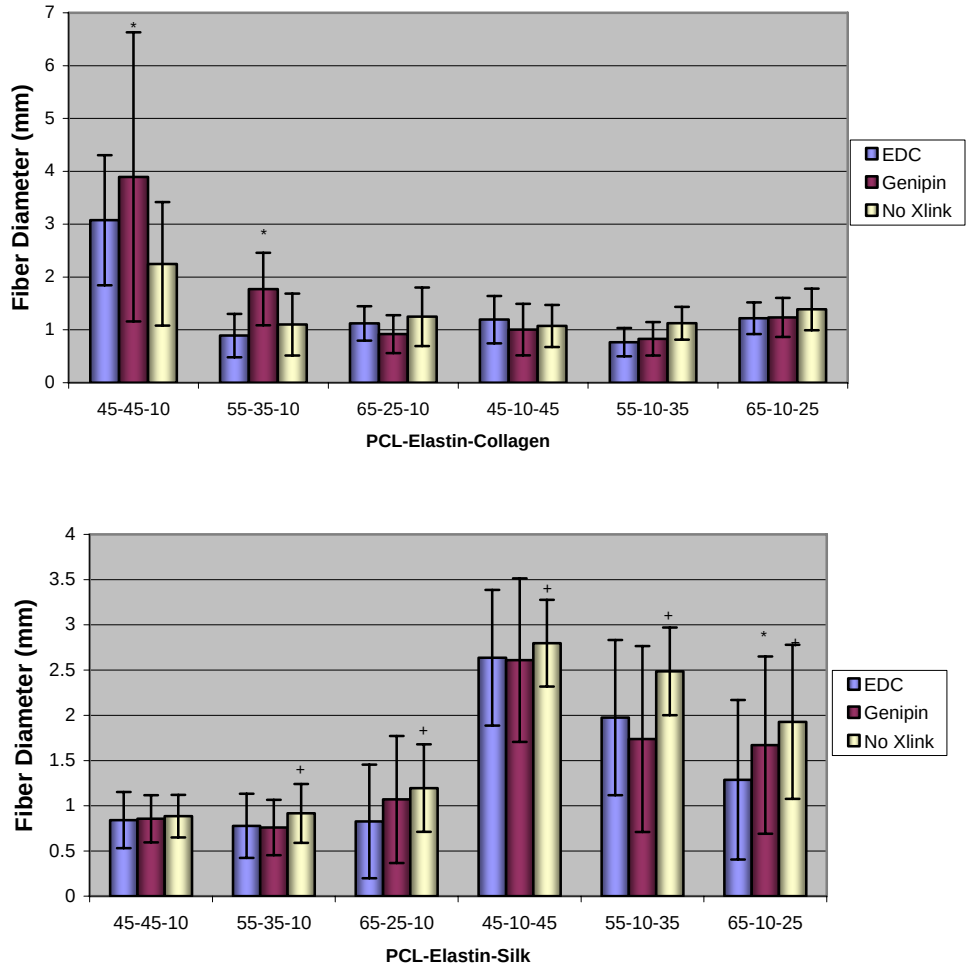

Figure 25. Results from fiber diameter measurements to determine differences between cross-linkers. (Top) Represents fiber diameters with PCL-ELAS-COL blended scaffolds (Bottom) Represents fiber diameter measurements with PCL-ELAS-SF blended scaffolds. * represents a significant difference between EDC and GEN. + represents a significant difference between No Xlink and both EDC and GEN.

Figure 26 portrayed both fiber diameter and % cross-linked to determine whether or not a correlation existed between the two for blended scaffolds with PCL, ELAS, COL, and SF. These scaffolds exhibited an incremental increase in fiber diameter of 0.64, 0.60, 1.4, and 2.8 μm with the addition of COL, ELAS, and SF cross-linked with 10mM GEN, respectively. These results also confirmed the fiber diameter results from Figure 25, where

GEN caused an increase in fiber diameter for ELAS blended scaffolds when compared to EDC, but no difference was seen in either SF or COL blended samples. % cross-linked displayed incremental increases in cross-linking percentage as fiber diameter increased as well. However, as mentioned previously, the standard deviations of SF still make its TNBS results suspect. Therefore, according to the data in Figure 26, it appears that as fiber diameter increases, an increase in % cross-linking can be seen as well. Nonetheless, further testing would have to be done to determine if this was correct.

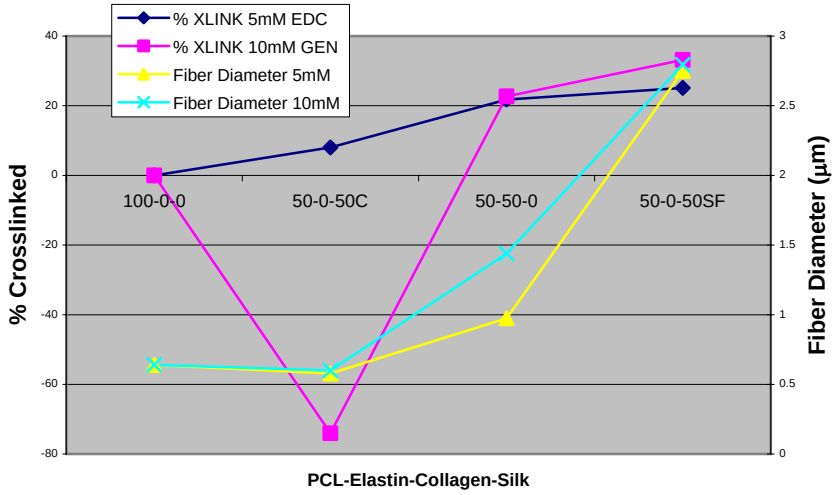

Figure 26. Comparing percent cross-linked and fiber diameter to determine correlations.

Material Properties

Uniaxial tensile testing was performed on 50-50 samples of PCL-COL, PCL-ELAS, and PCL-SF to determine if differences between GEN and EDC occurred. Results from Figure 27 presented a decrease in average peak stress and modulus when any protein was added to the electrospun polymer solution, where PCL-ELAS scaffolds displayed the lowest peak stress values and PCL-SF scaffolds displayed the lowest modulus values. This is consistent with previous research [113, 152]. One of the main questions was whether or

not different chemical fixations would impact the material properties of the scaffolds. For both peak stress and modulus values, no differences were seen between EDC and GEN cross-linked groups. A difference was seen between EDC and GEN with PCL-COL for strain to break values. This could be indicative that the molecular length of the crosslinker could impact the strain values, although since this is the only case it is unlikely. Despite no significant differences, it is worth noting that average moduli values for COL, ELAS, and SF decreased when cross-linked with GEN, where PCL-COL decreased from 6.8 to 5.8 MPa, PCL-ELAS decreased from 4.5 to 3.5 MPa, and PCL-SF decreased from 3.5 to 2.7 MPa.

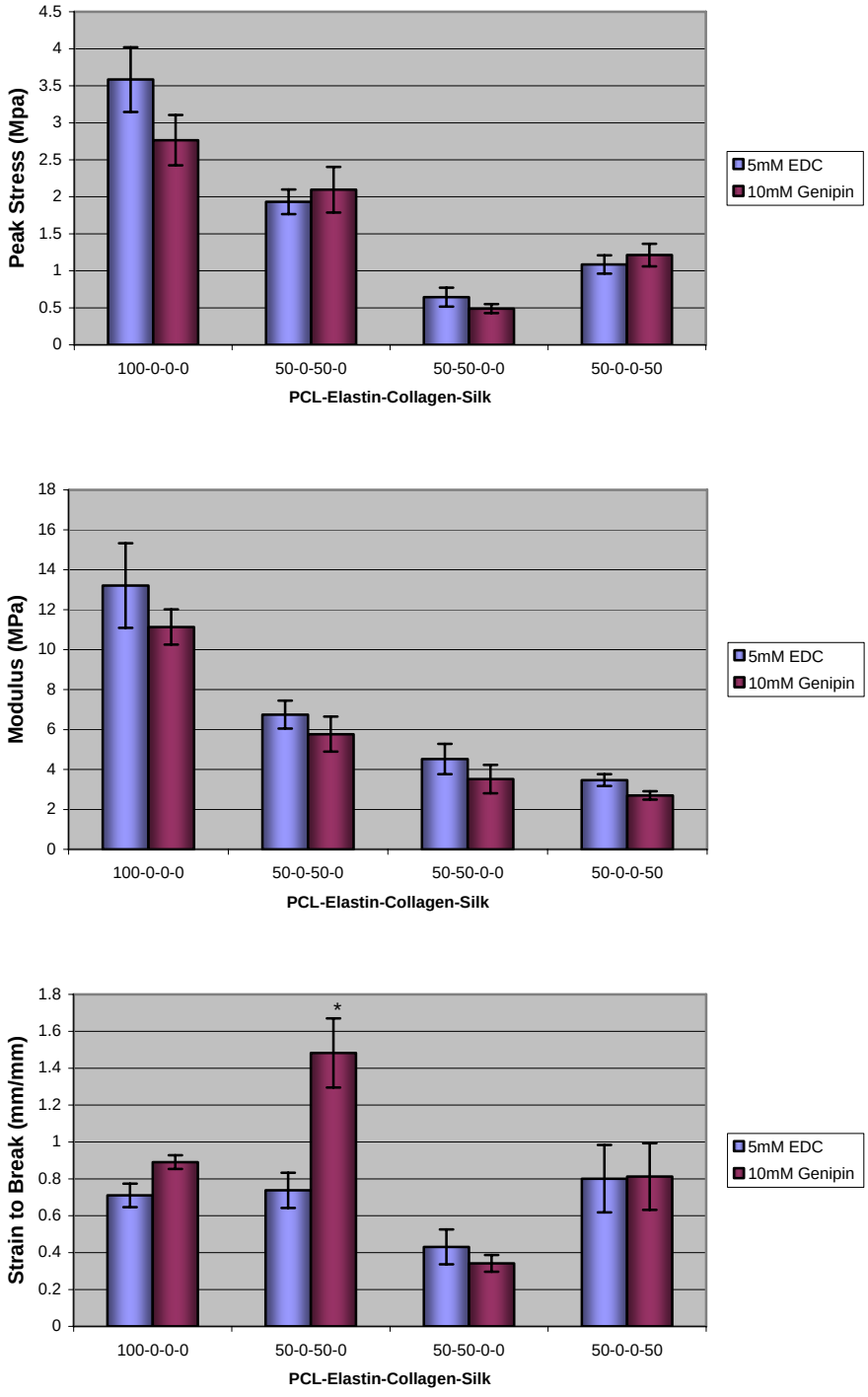

Figure 27. Uniaxial tensile test values for peak stress, tangential modulus, and strain to break for PCL, 50-50 PCL-COL, 50-50 PCL-ELAS, and 50-50 PCL-SF. * indicates a difference between EDC and GEN.

Discussion

The aim of this study was to further elucidate the affect of two different crosslinkers, EDC and GEN, on scaffold properties composed of different combinations of PCL, COL, ELAS, and SF. EDC and GEN crosslink proteins through two different methods. EDC involves the activation of carboxylic acid groups of glutamic and aspartic acid residues present in the polypeptide chains to give O-acylisourea groups. Zero length cross links are formed after nucleophilic attack by free amine groups of lysine or hydoxylysine residues found on other polypeptide chains [282]. GEN, on the other hand, is not as well understood and is still being investigated by other groups to determine the exact cross-linking mechanism. As of now, the first step is the nucleophilic attack of the GEN C3 carbon atom from a primary amine group to form an intermediate aldehyde group. The just formed secondary amine reacts with the aldehyde group to from a heterocyclic compound. The following step is a nucleophilic substitution reaction that involves the replacement of the ester group on the G molecule by a secondary amide linkage. The reaction is complicated by the oxygen radical-induced polymerization of GEN that occurs once the heterocyclic compound has formed, giving the scaffold a blue color [283, 284].

The primary goal of this experiment was to optimize the parameters of the solution concentrations for EDC and GEN. One of the key elements of this study was to determine whether the molecular length of the crosslinker changed the microscopic and macroscopic properties of the scaffolds. Other studies have shown mechanical properties to change with different types of crosslinkers used alongside purely COL-based scaffolds [283]. Although a synthetic polymer would be used in addition to proteins for this study, it was

thought that the differences in cross-linked protein structure would be great enough to provide differences in scaffold properties. From the microscopic perspective, the concentration of free amine groups and the concentration of free proteins were investigated by setting up two different cross-linking assays. A TNBS assay was chosen to measure percentage of cross-linked material, as it has been used in several different experiments. This assay is one that measures the number of free amine groups available in the solution into which the protein-based scaffold has dissolved, reacting readily with primary amino groups. In order to determine the most optimal percentage of cross-linking that occurs for both EDC and GEN, the TNBS assay was carried out at different molarities with the addition of different percentages of PBS. A method used to partially dissipate proteins from the scaffold and determine its affect on the process of cross-linking.

Both Figures 20 and 21 portrayed the raw TNBS absorbance data for the two crosslinkers. In Figure 19, EDC cross-linked scaffolds with ELAS demonstrated a dissipation of free amine groups during the cross-linking process with the addition of both 5 and 10% PBS for 50mM concentrations. However, COL did not display dissipation during the cross-linking process. Instead, its average absorbance values were higher for 5 and 10%, indicating that the COL dissipated during the TNBS assay, which would further indicate that the COL proteins may have made them more readily available to dissociate during TNBS treatment, decreasing cross-linking and causing them to not form stable bonds and eventually dissipate. SF only seems to have been affected by the 50mM concentration of EDC, which may signify that some carboxyl groups are available for cross-linking. Figure 20 also displayed the raw absorbance data for GEN cross-linked

scaffolds. These values displayed similar trends to EDC for ELAS blended scaffolds, where 5 and 10% PBS decreased the absorbance values when compared to 0% PBS. This indicated that free amine groups had dissipated during the cross-linking process. However, the results were slightly skewed due to the interference of the green-blue color of GEN after dissolution during the TNBS assay. This is very evident in the COL scaffolds where the absorbance values are higher for the GEN treated scaffolds than they are for the NT scaffolds. Although these scaffolds turned a green-blue color prior to the assay, which would indicate that they were cross-linked, the absorbance values determined that there was negative cross-linking.

Figures 22 and 23 demonstrated the percentage of cross-linking for all three protein-based scaffold types. Figure 21 shows that for EDC the cross-linking percentage was slightly increased with an augment in EDC molarity. However, this increase was not pronounced enough to determine significant differences, and, therefore, did not indicate any benefit to using an increased molarity with either COL or ELAS scaffolds. Figure 22 also displayed similar finding where ELAS-based scaffolds increased in cross-linking percentage, yet they failed to produce any significant differences. Based on the TNBS assay and percent cross-linked data there were only slight differences with the addition of PBS to the cross-linking solution. However, this may have been a result of the loss of free amine groups during the cross-linking process, subsequently skewing the data to have a larger cross-linking percentage than in actuality.

Although the results from the TNBS assay had some variability, the raw absorbance data did demonstrate that ELAS and COL proteins seemed to behave

differently in terms of reaction rates when PBS was added to the solution. Therefore, the second protein assay was conducted so as to determine the time dependence of cross-linking and further elucidate optimal conditions. Since it was assumed that GEN scaffolds cross-linked at a slower rate than EDC scaffolds, based on the accepted time frame of 3 days for GEN and 18 hours for EDC, time periods were chosen as such: 0, 10, 30, 60, 180, and 1080 minutes for EDC scaffolds and 0, 6, 24, 48, and 72 hours for GEN scaffolds. For GEN scaffolds, a 6 hour period was enough time to begin the cross-linking process and decrease the protein released from the scaffolds. Surprisingly, these reactions occurred faster in COL than ELAS. This could be explained by the larger amount of ELAS protein available in the scaffold due to the electrospinning conditions with ELAS's 200 mg/ml compared to COL's 70 mg/ml. This could have allowed more protein to be released into solution. For both ELAS and COL scaffolds, it appears that with either 10mM or 30mM concentrations of GEN the reaction rates are similar and that most of the cross-linking occurs within the first 24 hours. Looking at Figure 24 (top) and (bottom) for EDC scaffolds, a difference between molarities was observed where 5mM tended to react slower than 50mM, especially with the COL-based scaffolds. With either ELAS or COL added to the electrospun polymer solution, it appears that the majority of cross-linking occurred within the first 30 minutes and only slightly changed thereafter.

Based on the results from both the TNBS assay and the protein release assay, a decision point had to be made so as to narrow down the cross-linking parameters and carry out the study further. Therefore, it was determined that 5mM and 10mM EDC and GEN, respectively, without the addition of PBS would provide optimal cross-linking parameters.

Additionally, it was theorized that a lower molarity could be more conducive to cellular attachment and proliferation. These molarities were then used to determine fiber diameter characteristics and material properties. According to the fiber diameter results, ELAS plays a major role when combined with COL. However, it does not have as pronounced of an impact when it is combined with SF. Conventionally, fiber diameter is affected by an increased polymer concentration, which subsequently increases the number of chain entanglements and the density of these entanglements [285]. Shenoy *et al.* explains this phenomenon as such: "Chain entanglements are essentially the physical interlocking of polymer chains, which is a direct consequence of chain overlap. In a polymer solution, chain overlap, and hence the number of entanglements, increases with polymer chain length or molecular weight…It is worth noting that physical chain entanglements behave in a similar manner as chemical cross-links, although the chains can slide past one another affecting viscoelastic behavior." Therefore, the molecular weight and concentration have a large effect on fiber diameter. PCL has a molecular weight of 125 kDa, COL has proteins within the molecular weight range of 120-220 kDa (based on SDS-PAGE), ELAS has molecular weight of 60 kDa, and SF has a molecular weight of 188 kDa [286].

By itself and when mixed with a synthetic polymer, ELAS has proven to possess large fiber diameters [109, 110, 152]. Observing Figure 26, COL did not affect the overall fiber diameter with an average of 0.6 μm. However, both ELAS and SF do affect fiber diameter with average values of 1.4 and 2.8 μm, respectively. The lower molecular weight of ELAS could explain the lower average fiber diameter values compared to SF, if the concentration of the two proteins is just above the critical value of chain entanglements.

When Figures 26 (top) and (bottom) are examined, SF tends to bring the average values of the higher ELAS content scaffolds down whereas COL, which has a similar average molecular weight to SF, tends to keep fiber diameter values high. Therefore, both the structure of these proteins and their chain entanglement densities are interacting with one another to produce different results. These combinations could be leading to a doping or "poisoning" of the each different polymer in solution, changing their electrospun properties and parameters.

Several studies have investigated the ideal fiber diameter size for tissue engineered scaffolds. This ideal electrospun fiber size would then dictate the pore diameter as well, allowing for adequate cellular infiltration. A study performed by Ju *et al*. determined that PCL-COL blended scaffolds with an average fiber diameter size of 2.39 μm had the best cellular infiltration under static cell seeding conditions at four weeks. Additionally, in this same study, average fiber diameters between 0.27 and 1.00 μm, demonstrated low cellular infiltration after four weeks with cells mainly concentrating on the surface of the scaffolds [133]. In this study we found that fibers diameters ranged from 1.1 – 2.3 μm in uncross-linked scaffolds while cross-linked scaffolds demonstrated a range from 0.8 – 3.9 μm. While the low end of the values could inihibit cellular infiltration, the higher numbers from 2.0 up to 3.9 μm could prove to be extremely beneficial. This demonstrates that future studies need to investigate the limitations of certain scaffold blends based on both fiber size and protein composition.

Chemical cross-linking could also attribute some of the changes seen in fiber diameter results, especially GEN. When GEN cross-links, it produces a large molecular

structure that retains the ability to create cross-links within the electrospun fibers. This has the potential to lead to fiber swelling, or to create cross-links between electrospun fibers, which could lead to fiber welding. Additionally, ELAS is electrospun at a high concentration which would produce a large number of sites for cross-linking. Each of these different scenarios explains the larger fiber diameter results with higher ELAS content when combined with COL. When higher ELAS concentrations are combined with SF, however, there is a marked decrease in fiber diameter values with no affect due to GEN cross-linking. This could be due to the interaction of SF with the ELAS proteins. For SF, cross-linking occurred at a minimum due to GEN or EDC. Instead, cross-linking was due to the ethanol, as it is well known that SF materials can be converted into a more stable crystalline β-sheet structure through the use of alcohols [279, 287]. The β-sheet formation could attribute some initial encapsulation of ELAS proteins, preventing inter-fiber cross-links with the use of GEN. Finally, higher SF scaffolds displayed larger fiber diameters, consistent with the 50-50 PCL-SF results.

Uniaxial tensile testing is an excellent method to determine the macroscopic material properties of a tissue engineering scaffold. Studies have shown that different types of fixation and the amount of fixation can affect the overall material properties for the same initial untreated scaffold [274, 282, 283, 288]. Therefore, this study aimed to determine whether differences would existed between EDC and GEN cross-linked scaffolds. As it turns out, there were no significant differences. This could be due to PCL dominating the mechanical properties, where only infinitesimal changes in material properties would be seen owing to the chemical cross-linking of the electrospun proteins.

Despite no significant differences, the average moduli values for COL, ELAS, and SF decreased when cross-linked with GEN. This was consistent with some of our previous findings with the use of EDC and GEN on pure ELAS constructs [110]. This could point toward the long molecular chain of GEN. A longer cross-linked molecular structure could produce a scaffold with a decreased stiffness due to its ability to slide further than a zero length molecular bond. This is evident in PCL-COL GEN cross-linked scaffolds, but is not consistent over the course of all materials and would, consequently, require future testing to fully investigate.

Conclusion

In conclusion, we were able to successfully crosslink PCL, COL, ELAS, and SF blended scaffolds using either EDC or GEN. These cross-linked scaffolds were assessed for % cross-linking and reaction rate using two different protein assays. The results from these assays allowed the study to be narrowed to the optimal cross-linking parameters, which wre found to be the lower cross-linking molarities of 5 mM EDC and 10 mM GEN. From that point on the remainder of the study was performed under those conditions. Results from fiber diameter and material properties demonstrated changes in the scaffolds when cross-linked with GEN, a longer molecule, and demonstrated little to no changes with EDC, a zero length crosslink. However, these results did not transfer over to material properties, where no significant changes were found between the two crosslinkers. Since the degree of cross-linking demonstrated large amounts of variability for certain polymer blends, other quantification techniques should be investigated in future studies. One type of investigatory method is the degree of swelling that a substrate has once cross-linked.

This method is standard and can be correlated with the degree of cross-linking [289, 290]. Additionally, the shrinkage of a cross-linked scaffold due to increased temperature can also be correlated to the degree of cross-linking. This is also a standard method and has been used previously to demonstrate how increases in degree of cross-linking also increase the temperature required to shrink the scaffold [282]. Once the swelling and shrinkage studies have been performed, future studies will investigate the use of these optimal cross-linking conditions for vascular graft design.

Chapter 5: Tri-layered Vascular Grafts Composed of Polycaprolactone, Elastin, Collagen, and Silk: Optimization of Graft Properties

Abstract

The purpose of this study was to create seamless, acellular, small diameter bioresorbable arterial grafts that attempt to mimic the extracellular matrix and mechanical properties of native artery using synthetic and natural polymers. SF, COL, ELAS, and PCL were electrospun to create a tri-layered structure for evaluation. Dynamic compliance testing of the electrospun grafts ranged from 0.4–2.5 %/100 mmHg, where saphenous vein (1.5 %/100 mmHg) falls within this range. Increasing PCL content caused a gradual decrease in medial layer compliance, while changes in PCL, ELAS, and SF content in the adventitial layer had varying affects. Mathematical modeling was used to further characterize these results. Burst strength results ranged from 1614–3500 mmHg, where some exceeded the capacity of the pressure regulator. Four week degradation studies demonstrated no significant changes in compliance or burst strength, indicating that these grafts could withstand the initial physiological conditions without risk of degradation. Overall, we were able to manufacture a multi-layered graft that architecturally mimics the native vascular wall and mechanically matches the gold standard of vessel replacement, saphenous vein.

Introduction

Native artery is an extremely complex multi-layered tissue composed of a number of different proteins and cell types, which each plays an integral role in the mechanical behavior of the structure. In order to withstand the high flow rate, high pressure, and pulsatile nature of blood flow, an artery is comprised of three distinct layers: intima, media, and adventitia. Each of these layers has a different composition and plays a different physiological role. The intimal layer is the innermost layer of the vessel wall and is made up of a single layer of ECs on a thin basal lamina and a subendothelial layer made of COL type IV and ELAS. This layer contacts the bloodstream and therefore provides a critical barrier to platelet activation. The thick medial layer is composed of several layers of SMCs in a matrix of COL types I and III, ELAS, and proteoglycans. The outermost adventitial layer is made of FBs and randomly arranged COL type I [2, 291, 292]. The major protein components of native artery, COL and ELAS, provide tensile support and prevent vessel rupture, and confer elasticity to the vessel, providing the ability to recover from pulsatile deformation, respectively [148, 149]. It is the elastic nature of ELAS that dominates the low-strain mechanical response of the vessel to blood flow and prevents pulsatile energy from being dissipated as heat [293, 294].

The capabilities of electrospinning to mimic the microenvironment of a cell are especially important when dealing with vascular grafts. The dynamic situation of a blood vessel creates a complicated sequence of events in which the walls are stretched and the inner lumen is sheared. A microenvironment capable of withstanding these forces with minimal energy loss is essential for proper blood vessel functioning. Electrospinning of polymer fibers into a vascular conduit has been demonstrated to be a potential technique

that not only creates scaffolds simulating the ECM, but also contributes tailorable mechanical properties and minimal energy loss [111].

Currently, the most common vascular materials are Dacron (polyethylene terephthalate) and ePTFE. Dacron is widely known for its use in aortic and iliac grafts. Its success in these areas of the body is due mainly to larger diameters and flow rates, which are not conducive to thrombus formation and the subsequent decrease in luminal diameter. However, for a small diameter graft of 5 mm or less, the following properties must be attained for successful grafting to occur: biocompatibility, lack of chemical reactivity, very low thrombogenicity, porosity, and mechanical strength, including compliance matching that of native artery and resistance to aneurysm formation [222, 225, 295].

Inner luminal wall thickening, hyperplasia, and subsequent occlusion and loss of blood flow in vascular grafts is one of the most critical concerns when designing a vascular prosthetic. Mechanical problems such as compliance mismatch between the natural vessel and prosthetic contribute to this effect, and are a key component to the creation of a successful vascular graft. Recently, our laboratory performed compliance testing of electrospun PDO and ELAS in an effort to match natural arterial compliance. Various ratios of PDO:ELAS were electrospun and tested in a bioreactor with internal pressures changing cyclically from 120mmHg to 80mmHg at 60 Hz, where a blend of 50:50 showed particular promise [248]. This study demonstrated the advantageous aspects of the addition of ELAS proteins to synthetic biodegradable polymers in a physiological setting.

The biomechanics of vascular grafts is one of the most essential components to its success. Previously, we designed a preliminary study to mimic the vascular architecture

through producing a tri-layered vascular analogue [152]. Using a multi-layered technique, grafts can be tailored to exact specifications and optimized thereafter. Aneurysms and graft rupture could be avoided through the use of a "jacketlike" outer layer that would prevent the graft from overextending itself, while the middle layer can be tailored to have the lowest modulus, providing the distension required for proper compliance and blood flow, similar to native artery. Blends of PCL, ELAS, and COL were electrospun in all three layers and mechanically tested through uniaxial tensile, compliance, suture retention, and burst strength. PCL was chosen as a synthetic polymer based on promising results from *in vivo* rat studies that have been conducted by Pektok *et al.*, whereby histological analysis revealed rapid enthothelialization of the inner lumen of the graft and becoming confluent at 12 weeks [93]. Vascular tissue contains between 25-30 % COL and 40-50 % ELAS. Therefore, ratios were chosen for each of the three layers based on native extracellular matrix design while keeping mechanical integrity throughout the graft structure. Results from this tri-layered study revealed that as the modulus of the middle layer was changed, the compliance values increased to within native arterial range, while burst strength remained strong due to the outer layer.

Building off of this blueprint, this study was designed to observe a large range of scaffolds containing high amounts of natural polymer in combinations of ELAS, COL, and SF. Previous research indicated that combinations of ELAS, COL, and SF required fixation in order to retain proteins within the scaffold matrix. Both GEN and EDC were used in a comparison model to determine the proper molarity for each cross-linker. Concentrations of 5 and 50 mM for EDC and 10 and 30 mM for GEN were tested, and it

was concluded that 5 mM EDC and 10 mM GEN had similar cross-linking results to their higher concentrations counterparts. Therefore, in this study, we aimed to evaluate the mechanical properties of tri-layered vascular grafts through uniaxial tensile testing, compliance, and burst strength.

As described earlier, artery is subjected to circumferential, longitudinal, torsional, and shear stress. Although important to the study of coronary arteries, torsion and shear stresses do not ultimately dictate the mechanical behavior of an artery when considering blood pressure supplying a force to the arterial wall *in vivo*. Therefore, mathematical modeling was implemented to help describe CWS of the individual layers and their mechanical effects on surrounding layers using the equations developed by Vorp *et al.* [120, 261]. Combining mathematical modeling with the results of compliance and burst strength would aid in the optimal design of the tri-layered vascular graft, providing valuable information regarding layered behavior.

Materials and Methods

Protein Extraction

SF was extracted from the cocoons of *Bombyx mori* silk worms (The Yarn Tree) through an established protocol [280]. Briefly, cocoons are cut into pieces and boiled in a 0.02 M Na_2CO_3 (Sigma Aldrich) solution for 30 minutes to remove the sericin gum, followed by thorough rinsing in de-ionized water (DI), and drying in a fume hood. The SF is then dissolved in a LiBr (Fisher Scientific) solution at 60°C for 4 hours. This solution is then dialyzed against deionized water for 3 days using 3500 MWCO dialysis tubing

(Fisher Scientific). The SF solution is then frozen and lyophilized to provide a pure SF for electrospinning.

COL type I was extracted from 6 month bovine corium through an acetic acid based process previously described [262]. Briefly, tissue is homogenized, suspended in acetic acid, and subsequently purified via a series of dissolutions, precipitations (using NaCl (Fisher Scientific) and Tris (Fisher Scientific)), and dialyses [263]. Following the final dialysis, COL solutions are frozen and lyophilized.

Electrospinning

The electrospinning setup consisted of a syringe pump (KD Scientific), a high voltage power supply (Spellman CZE1000R, Spellman High Voltage Electronics Corp.), a plastic Becton Dickinson syringe used as the polymer reservoir, attached to an 18-gauge blunt-tip needle. Concentrations of 150 mg/ml of PCL (MW: 125,000, Lakeshore Biomaterials), 200 mg/ml of soluble ELAS from bovine neck ligament (Elastin Products Co. Inc.), 70 mg/ml of COL I (6 month bovine corium), and 80 mg/ml of SF were dissolved in HFP (TCI America). These were then blended in ratios of 50-50 PCL-ELAS, PCL-COL, and PCL-SF. Additionally, ELAS-based scaffold materials were blended in ratios of 45-45-10, 55-35-10, 65-25-10, 45-10-45, 55-10-35, and 65-10-25 PCL-ELAS-COL and PCL-ELAS-SF. To evaluate material properties, blended scaffolds were electrospun onto rectangular mandrels measuring 2.5 cm wide x 10.2 cm long x 0.3 cm thick. The parameters for electrospinning were kept constant with an applied voltage of 25 kV, air gap distance (distance between the needle and rotating drum) of 15 cm, and solution dispensing rate of 4 ml/hr.

To create vascular tubes, each polymer mixture was loaded into a 3 ml plastic Becton Dickinson syringe with an 18 gage blunt tip needle. Insulated Tygon tubing was then run from the needle tip to a 3-1 (input-output) nozzle charged to 25 kV at an air gap distance of 15 cm. The solutions were sequentially electrospun onto a 2 mm diameter cylindrical mandrel rotating at 500 RPM with a translational speed of 6 cm/s over a distance of 12 cm. Flow rates and volumes were as such: the material for the intima was kept constant at 100-0-0 PCL-ELAS-COL and electrospun at a rate of 4 ml/hr and a volume of 0.25 ml followed by a transition combining both intimal and medial syringes for 0.1 ml at 2 ml/hr each for a combined flow rate of 4 ml/hr. The intimal syringe was then shut off and the medial layer was allowed to spin for 0.6 ml at 4 ml/hr followed by a transition between the media and adventitia for 0.1 ml of polymer solution at 2 ml/hr each for a combined flow rate of 4 ml/hr. Finally, the media was stopped and the adventitia was allowed to spin for 0.3 ml at 4 ml/hr.

Medial layers were 45-45-10, 55-35-10, and 65-25-10 PCL-ELAS-COL and PCL-ELAS-SF. Adventitial layers were 45-10-45, 55-10-35, and 65-10-25 PCL-ELAS-COL and PCL-ELAS-SF. Vascular tubes were created using each possible combination and cross-linked using both EDC and GEN to determine layered graft behavior based on differences in protein type and cross-linker type.

Crosslinking

Scaffolds were cross-linked using EDC (FlukaBiochemika), genipin (GEN, Wako Pure Chemical Industries, Ltd.). Using EDC, a 5 mM crosslinking solution was prepared in

90 % ethanol (Fisher Scientific) and allowed to cross-link for 18 hours followed by a 0.1M Na_2HPO_4 rinse for 1 hour and a PBS rinse for 1 hour.

Using GEN, a 10 mM crosslinking solution was prepared in 90 % ethanol (Fisher Scientific) and scaffolds were placed in the cross-linking solution for a period of 72 hours [245], followed by a PBS rinse for 2 hours.

Material Properties of Individual Layers

Uniaxial tensile testing was performed on six samples (n = 6) from one electrospun sheet hydrated in PBS for 24 hours. "Dog-bone" shaped samples were punched from electrospun mats (2.75 mm wide at their narrowest point with a gage length of 7.5 mm) and tested on a MTS Bionix 200 testing system with a 100 N load cell (MTS Systems Corp.) and an extension rate of 10.0 mm/min. Peak stress, modulus, and strain at break were calculated using TestWorks version 4.

Mathematical Modeling

The constitutive equations developed by Vorp *et al.* [120, 261] are based on the principle of the Lamé equations. Following similar assumptions as previously described [261], a three-layered model (Figure 9) was used, describing CWS, at any radius, *r*, of the three layers. Through this we come up with:

$$CWS = \frac{R_I^2 P_I - R_O^2 P_O}{R_O^2 - R_I^2} + \frac{(P_I - P_O) R_I^2 R_O^2}{(R_O^2 - R_I^2) r^2} \text{ for } R_I \leq r \leq R_O$$

Where R_I is the inner radius of a particular layer, R_O is the outer radius of a particular layer, P_I is the inner pressure of a particular layer, and P_O is the outer pressure of a particular layer.

$$P_2 = P_i \frac{2a^2 b}{(b^2 - a^2)E_{INT}} \left[\frac{(c^2 - b^2)^2 E_{MED} k_2}{(c^2 - b^2)^2 E_{MED}^2 k_2 k_1 - 4b^3 c^3} \right]$$

$$P_3 = P_i \frac{2a^2 b}{(b^2 - a^2)E_{INT}} \left[\frac{2(c^2 - b^2)E_{MED} b^2 c}{(c^2 - b^2)^2 E_{MED}^2 k_2 k_1 - 4b^3 c^3} \right]$$

$$k_1 = \frac{b^3(1-\upsilon_{INT}) + a^2 b(1+\upsilon_{INT})}{(b^2 - a^2)E_{INT}} + \frac{b^3(1-\upsilon_{MED}) + b^2 c(1+\upsilon_{MED})}{(c^2 - b^2)E_{MED}}$$

$$k_2 = \frac{c^3(1-\upsilon_{MED}) + b^2 c(1+\upsilon_{MED})}{(c^2 - b^2)E_{MED}} + \frac{c^3(1-\upsilon_{ADV}) + d^2 c(1+\upsilon_{ADV})}{(d^2 - c^2)E_{ADV}}$$

Where k_1 and k_2 are constants, E_{INT}, E_{MED}, and E_{ADV} represent the moduli for the intimal, medial, and adventitial layers, respectively, υ_{INT}, υ_{MED}, and υ_{ADV} represent Poisson's ratio for the intimal, medial, and adventitial layers respectively, and a, b, and c are the inner radii for the intimal, medial, and adventitial layers, respectively, and d is the outer radii of the adventitial layer (equations are adopted from [120, 261]).

Burst Strength

Burst strength testing on six samples (n = 6) from six different electrospun grafts was completed using a device designed in accordance with section 8.3.3.3 of ANSI/AAMI VP20:1994 [29]. Tubes, 2–3 cm in length, were hydrated in PBS, fitted over 1.5 mm diameter nipples attached to the device, and secured with 2-0 silk suture. Air was introduced into the system, increasing the pressure at a rate of 5 mmHg/s until the tubes burst. Results are reported as the pressure in mmHg at which tubes ruptured.

Dynamic Compliance

Dynamic compliance was determined for six 2 mm inner diameter tubular grafts (n = 6) taken from six different electrospun grafts at a length of 3 cm under simulated physiological conditions in accordance with section 8.10 of ANSI/AAMI VP20:1994 [264]. Both individual layers and multi-layered tubular constructs were electrospun and tested under the same conditions. The specimens were tested in an Intelligent Tissue Engineering via Mechanical Stimulation (ITEMS™) Bioreactor developed by Tissue Growth Technologies (Minnetonka, MN) filled with PBS at 37°C. The bioreactor provided a cyclic (1 Hz, representing 60 beats per minute) pressure change to the inside of the graft; three different pressure levels (90/50, 120/80, and 150/110 mmHg systolic/diastolic) were investigated. Briefly, specimens were secured at either end to a nipple with 2-0 silk suture and placed in the bioreactor chamber. PBS then filled the chamber and was run continuously on the outside of the graft to maintain a temperature of 37^{o}C and a pressure of 0 mmHg. Simultaneously, PBS was pumped through the inside of the graft and an actuator in the bioreactor created the difference in pressure. Prior to compliance measurements for each pressure level, all grafts were allowed to stress relax for 30 minutes or 1800 cycles.

Internal pressure was measured with a pressure transducer capable of measuring dynamic pressure up to 200 ± 2 mmHg, while the external diameter was recorded with a laser micrometer system with an accuracy of ±0.001 mm. Prior to insertion into the bioreactor, the grafts were soaked in PBS at 37°C for 24 hours, after which time their average wall thickness was measured. From this, the internal radii of the graft was determined and used in the following equation to calculate compliance for each specimen:

$$\%\ Compliance = \frac{(R_{P2} - R_{P1}) / R_{P1}}{(P_2 - P_1)} \times 10^4$$

Where R is the internal radius, P_1 is the lower internal pressure, and P_2 is the higher internal pressure [296]. Grafts were tested with individual layers electrospun at a wall thickness of 200 μm, and with whole graft samples with an overall wall thickness of 500 μm.

Degradation

Grafts were tested for degradation using a 55mL rotating cell culture system (RCCS, Synthecon, Inc.). First, chosen grafts were electrospun according to the protocols mentioned above. Second, 55 mL of Dulbeco's Modified Eagle Medium F12 (DMEM F12, Invitrogen) supplemented with 10 % fetal bovine serum (Hyclone) and 1 % penicillin/streptomycin (Invitrogen) was placed in each bioreactor. Twelve tri-layered vascular grafts (n = 4) from one polymer blend group were placed in one bioreactor to create three separate timed groups: 1, 2, and 4 weeks. Each bioreactor containing the vascular grafts was then placed in an incubator at 37°C with 5 % CO_2 for 1, 2, and 4 weeks. Media was changed once every 7 days to remove any degradation products and replace enzymatic capabilities. At each time period, grafts were taken out of culture and tested for compliance and burst strength in accordance with the above protocols.

Statistical Analysis

Unless otherwise stated, all statistical analysis was based on a Kruskal-Wallis one way analysis of variance on ranks and a Tukey-Kramer pair-wise multiple comparison

procedure ($\alpha = 0.05$) performed with the JMP®IN 4.0.3 statistical software package (SAS Institute, Inc).

Results

Material Properties

The primary goal of assessing material properties was to analyze how combinations of PCL, ELAS, COL, and SF interact with one another when PCL-ELAS-COL and PCL-ELAS-SF was electrospun at ratios of 45-45-10, 55-35-10, 65-25-10, 45-10-45, 55-10-35, and 65-10-25. The purpose of choosing these volumetric ratios was to incrementally change PCL and ELAS ratios while COL or SF were kept constant. This process was then reversed with COL or SF whereby the ratios of PCL, COL, and SF were incrementally changed and the ELAS protein level was kept constant in solution. Tables 10 and 11 display the data of peak stress, modulus, strain to break, and energy to break. One of the important factors in this portion of the study, as in Chapter 4, was to determine whether or not changes in any of the output values for materials testing occurred between the two different crosslinked scaffolds. Looking at Table 10, peak stress values for EDC crosslinked scaffolds with PCL at volumetric ratios of 65 % were significantly different *($p < 0.05$)* from their GEN counterparts. 65-25-10 EDC had a value of 2.31 MPa and 65-25-10 GEN had a value of 2.02 MPa, while 65-10-25 EDC had a value of 1.49 MPa and 65-10-25 GEN had a value of 1.21 MPa. Both of these groups of scaffolds contained average values where the GEN crosslinked scaffold decreased in peak stress in comparison to the EDC crosslinked scaffold. Although, none of the other crosslinked scaffolds were different from one another, they each possessed a decrease in average peak stress,

excluding the 45-10-45 PCL-ELAS-COL scaffolds. Additionally, as ELAS incrementally increased from 25 to 45% it gradually caused a decrease in peak stress with differences *($p < 0.05$)* between 65-25-10, 55-35-10, and 45-45-10 for both EDC and GEN crosslinked scaffolds. Additionally, 65-10-25 COL based structures differed *($p < 0.05$)* from 45-10-45 strucutres.

Modulus values are especially important to determine a scaffold's stiffness. They can be good determinants or predictors of how well a vascular material will behave under physiological pressures. Crosslinked scaffolds were investigated for differences between EDC and GEN to understand if the crosslinking procedures caused a dramatic change in the overall scaffold properties due to chemical crosslink or crossbridges that would form. As seen in Chapter 4, these values did not differ from one another. Nevertheless, trends still implicated that something could be happening with mechanical properties between the two types of crosslinkers. Examining the values, 65-10-25 PCL-ELAS-COL scaffolds exhibited the highest stiffness, where EDC was the highest and GEN was the lower of the two. Average moduli for GEN scaffolds were also lower than their EDC counterparts for 55-10-35 and 55-35-10. Trends amongst the scaffolds also demonstrated that for both COL and ELAS based scaffolds 65% PCL content was significantly different *($p < 0.05$)* from 45% PCL content. This continues to show that as total protein content increases, stiffness decreases.

Strain to break values for all scaffolds ranged from 1.2 – 0.29 mm/mm. The higher strain values were present in scaffolds with increased PCL content for ELAS based scaffolds. Averages for these scaffolds illustrated how the addition of proteins to a

scaffold significantly decreased *($p < 0.05$)* strain values in upwards of 75%. Differences *($p < 0.05$)* between EDC and GEN occurred for 45-45-10 and 45-10-45 scaffolds. Where GEN crosslinking caused the strain values to decrease for ELAS-based scaffolds and increase for COL based scaffolds. Again, incremental changes in PCL content displayed significant differences *($p < 0.05$)* between 65-25-10 and 45-45-10, and 65-10-25 and 55-10-35.

Energy to failure data is calculated based on the area underneath the stress-strain curve; as a sample increases in strain and in peak force, so does the energy to failure. These values are good determinants of scaffold toughness, or how much energy a material can absorb prior to failure. In the case of a vascular graft it is advantageous for a sample to exhibit an energy to break that will allow the material to withstand the physiological pressures imposed on its walls. Amongst these samples, significant differences *($p < 0.05$)* occurred between 65-25-10 EDC and GEN scaffolds. These scaffolds demonstrated a decrease in energy to break when GEN was used as the crosslinker, decreasing from 10.5 to 9.4 N*mm. For almost every case, the energy to break values decreased when GEN was used as the crosslinker, excluding the 45-10-45 scaffolds. Moreover, as PCL content decreased energy to break values also decreased with significant differences between 65-25-10 and 45-45-10, and 55-10-35 and 45-10-45.

Table 10. Material Property Results PCL-ELAS-COL.* indicates a significant difference between EDC and GEN. # indicates a significant difference between 65 % and 45 % PCL content scaffolds.

	Xlink	Peak Stress (MPa)	Modulus (MPa)	Strain to Break (% Elongation)	Energy to Break (N*mm)
45-45-10	EDC	0.4 ± 0.1	# 2.5 ± 0.55	* 48.0 ± 5.0	0.52 ± 0.17
45-45-10	Genipin	0.3 ± 0.1	2.6 ± 0.33	29.0 ± 3.0	0.23 ± 0.07
55-35-10	EDC	1.0 ± 0.1	9.5 ± 1.61	43.0 ± 7.0	0.98 ± 0.31
55-35-10	Genipin	0.8 ± 0.1	7.2 ± 2.25	42.0 ± 3.0	0.88 ± 0.30
65-25-10	EDC	* 2.3 ± 0.1	10.1 ± 0.63	112.0 ± 11.0	* 10.45 ± 1.39
65-25-10	Genipin	2.0 ± 0.1	10.4 ± 0.60	120.0 ± 13.0	9.35 ± 1.60
45-10-45	EDC	1.0 ± 0.2	# 6.6 ± 0.85	* 33.0 ± 5.0	0.76 ± 0.37
45-10-45	Genipin	1.1 ± 0.2	7.1 ± 0.79	49.0 ± 6.0	1.49 ± 0.41
55-10-35	EDC	1.2 ± 0.3	9.7 ± 2.76	29.0 ± 8.0	0.55 ± 0.33
55-10-35	Genipin	1.1 ± 0.2	8.1 ± 1.94	30.0 ± 4.0	0.49 ± 0.11
65-10-25	EDC	* 1.5 ± 0.2	13.5 ± 3.08	43.0 ± 9.0	1.90 ± 0.61
65-10-25	Genipin	1.2 ± 0.4	11.8 ± 5.51	40.0 ± 8.0	1.38 ± 0.93

According to Table 11, overall average values for peak stress and modulus demonstrated decreases when crosslinked with GEN, while average values for strain to break exhibited decreases for ELAS-based scaffolds, 45-45-10, 55-35-10, and 65-25-10, but had increases for SF-based scaffolds, 55-10-35 and 65-10-25. Specifically looking at the peak stress values, significant differences *($p < 0.05$)* existed between 65-25-10, 45-45-10, and 45-10-45 EDC and GEN scaffolds with marked decreases of 0.2, 0.3, and 0.2 MPa, respectively. In addition to the differences *($p < 0.05$)* between scaffold crosslinkers, there were differences between groups of scaffolds. ELAS and SF-based scaffolds with 65% PCL content were different *($p < 0.05$)* from those containing 45% PCL, each with a decrease in peak stress. 65-25-10 EDC and GEN scaffolds decreased from 1.4 and 1.2 MPa to 1.1 and 0.8 MPa for 45-45-10, respectively. At the same time, 65-10-25 EDC and GEN scaffolds decreased from 1.2 and 1.1 MPa to 0.9 and 0.7 MPa for 45-10-45, respectively.

Moduli displayed average values for all GEN crosslinked ELAS-based scaffolds which were lower than their EDC crosslinked counterparts. For example, 65-25-10 EDC scaffolds decreased from 13.2 to 12.7 MPa, 55-35-10 EDC scaffolds decreased from 11.3 to 9.6 MPa, and 45-45-10 EDC decreased from 4.1 to 3.9 MPa. SF-based scaffolds, however, did not display the same trends with values for 65-10-25 and 45-10-45 increasing from 10.2 to 10.7 MPa and 9.1 to 9.2 MPa, respectively, when crosslinked with GEN. None of the values for either ELAS or SF-based scaffolds were significantly different from one another. Staying consistent with Table 10, differences did exist between the moduli of scaffold groups; 65-25-10 was different from 45-45-10 and 65-10-25 was different from 45-10-45.

Shifting over to strain to break results, the majority of the results are in the range of 0.4-0.7 mm/mm, except for the 65-10-25 and 55-10-35 scaffolds crosslinked with GEN. Significant differences *($p < 0.05$)* between EDC and GEN scaffolds existed only for 65-25-10, 65-10-25, and 55-10-35, where values decreased from 0.7 to 0.5 mm/mm for 65-25-10 and increased from 0.3 to 1.5 mm/mm for 55-10-35 and from 0.5 to 1.5 mm/mm for 65-10-25. These increases, when using GEN as the crosslinking reagent, were particularly interesting. In the previous chapter, 50-50 PCL-SF scaffolds did not demonstrate these increases when using GEN as the crosslinking reagent. In fact, the majority of the results from Chapter 4, pointed to the fact that SF did not have many available binding sites available for crosslinking to occur, containing low absorbance values for untreated TNBS assays and performing the majority of its crosslinking within the first 30 minutes due to the non-aqueous alcohol-based substance, ethanol, used to dissolve the crosslinking reagent.

Therefore, the results seen here could be attributed to the low amount of ELAS present within the scaffold. The ELAS present in the 45-10-45 scaffold may not interact with the PCL and SF in the same specific way that both the 55-10-35 and 65-10-25 scaffolds do, whereby the SF protein dominates the polymer solution.

Energy to break revealed decreases in the amount of energy absorbed by the scaffolds when crosslinked with GEN for all ELAS-based scaffolds, while the SF-based scaffolds of 55-10-35 and 65-10-25 displayed increases in the amount of energy absorbed. This can be attributed to the large strain to break values seen by these scaffolds, increasing the area under the curve as the scaffolds continued to elongate under a constant strain rate. Significant differences *($p < 0.05$)* between EDC and GEN occurred for the 55-10-35, 65-10-25, and 65-25-10 PCL-ELAS-SF scaffolds, clearly demonstrating that a change is occurring when a different crosslinker is used, and that this change is dependent on the ratios of PCL to ELAS and to SF. Additionally, scaffold groups were again different *($p < 0.05$)* from each other with differences between 65-25-10 and 45-45-10 and between 65-10-25 and 45-10-45. This showed that as ELAS or SF were incrementally increased their energy to break decreased with average values decreasing by 3.2 Nmm and 2.6 Nmm for ELAS and SF-based scaffolds, respectively.

Table 11. Material Property Results PCL-ELAS-SF.* indicates a significant difference between EDC and GEN. # indicates a significant difference between 65 % and 45 % PCL content scaffolds.

	Xlink	Peak Stress (MPa)	Modulus (MPa)	Strain to Break (% Elongation)	Energy to Break (N*mm)
45-45-10	EDC	1.1 ± 0.2 *,#	4.1 ± 0.6 #	50.0 ± 12.0	0.9 ± 0.5 #
45-45-10	Genipin	0.8 ± 0.2	3.9 ± 0.6	40.0 ± 6.0	0.7 ± 0.2
55-35-10	EDC	1.4 ± 0.8	11.3 ± 1.1	50.0 ± 10.0	2.1 ± 0.6
55-35-10	Genipin	1.2 ± 0.1	9.6 ± 1.8	50.0 ± 3.0	1.9 ± 0.4
65-25-10	EDC	1.4 ± 0.1	13.2 ± 1.0	* 70.0 ± 4.0	* 4.1± 0.8
65-25-10	Genipin	1.2 ± 0.1	12.7 ± 2.7	50.0 ± 3.0	2.1 ± 0.5
45-10-45	EDC	0.9 ± 0.1 *,#	9.1 ± 2.0 #	50.0 ± 8.0	2.0 ± 0.3 #
45-10-45	Genipin	0.7 ± 0.1	9.2 ± 1.3	50.0 ± 7.0	1.7 ± 0.3
55-10-35	EDC	0.8 ± 0.1	9.3 ± 1.1	* 30.0 ± 3.0	* 1.0 ± 0.1
55-10-35	Genipin	0.7 ± 0.1	8.1 ± 1.6	150.0 ± 5.0	3.1 ± 0.3
65-10-25	EDC	1.2 ± 0.1	10.2 ± 1.9	* 50.0 ± 5.0	* 2.3 ± 0.3
65-10-25	Genipin	1.1 ± 0.1	10.7± 0.8	150.0 ± 33.0	4.3 ± 0.8

Mathematical Modeling

Mathematical modeling was implemented in order to determine where we could effect a change in graft behavior by altering individual layer moduli. Therefore, both Figures 29 and 30 took into account the material properties obtained from uniaxial tensile testing results in Tables 10 and 11 and utilized them in equations 3-8 to predict how individual layers affect one another. Figure 28 depicts how changing the medial layer (a, b, and c) affects the transmural stress distribution when physiological pressures are imposed on the graft material. Each medial layer is then tested for an adventitial layer to predict which type of material combinations will be best suited for future testing and implantation. The medial layers tested in these cases are ELAS-based materials of 45-45-10, 55-35-10, and 65-25-10, while adventitial layer testing was performed with 45-10-45, 55-10-35, and 65-10-25. A few assumptions were made prior to calculating the results. 1.) The wall thickness of the scaffolds was 450 μm where the starting internal radius was 0.95 mm and the external radius was 1.4 mm. 2.) Layer thickness was calculated based on the

percentages of thickness of the individual layers for native muscular arteries. 3.) Materials were homogenous, incompressible, and linearly elastic.

Each of the calculated results were compared to a study done by Holzapfel *et al.* [266], where the individual layers of a human coronary artery were separated and tested for material properties. Observing the trends between Figures 29A-C, we were able to see how the medial layer affects the overall CWS with a gradual decrease in the amount of initial stress exerted onto the intimal layer. In addition to this there is a marked decrease in CWS present in the adventitial layer. These results make sense because as the amount of ELAS is decreased in the electrospun polymer solution, the increase in PCL allowed the scaffold to take on more mechanical load, thereby relieving the intimal and adventitial layers and increasing the load imposed on the medial layer, increasing its CWS. Specifically, Figure 28A displayed an extremely close match with the CWS in the medial layer to the Holzapfel *et al.* results. This could be indicative of a close match between the 45-45-10 moduli and the native artery and could prove beneficial under whole graft analysis with compliance and burst strength. As the adventitial layer is changed, increasing its COL content while its ELAS content stays constant from 65-10-25 to 55-10-35 to 45-10-45, the 55-10-35 and 45-10-45 results appeared to have the best impact on overall transmural stress distribution and consistently possessed the closest adventitial layer properties to that of native artery. One of the interesting facts of Figures 29B and 29C was the way in which the changes in the medial layer affected how the stress imposed on the intimal and adventitial layers changed. As PCL content increased in the adventitial layers, the CWS of the intimal decreased while the adventitial layers increased. This was

especially evident in the 65-25-10 medial layers, where, as the adventitial layer ratios increased in PCL content, the intimal layer decreased the amount of stress imposed on it while the adventitial layer took on more stress. This altered the structure of the stress distribution where the 65-10-25 adventitial layer caused the CWS imposed on the intimal layer to be less than that of the medial layer, a design that was clearly not intended in native artery.

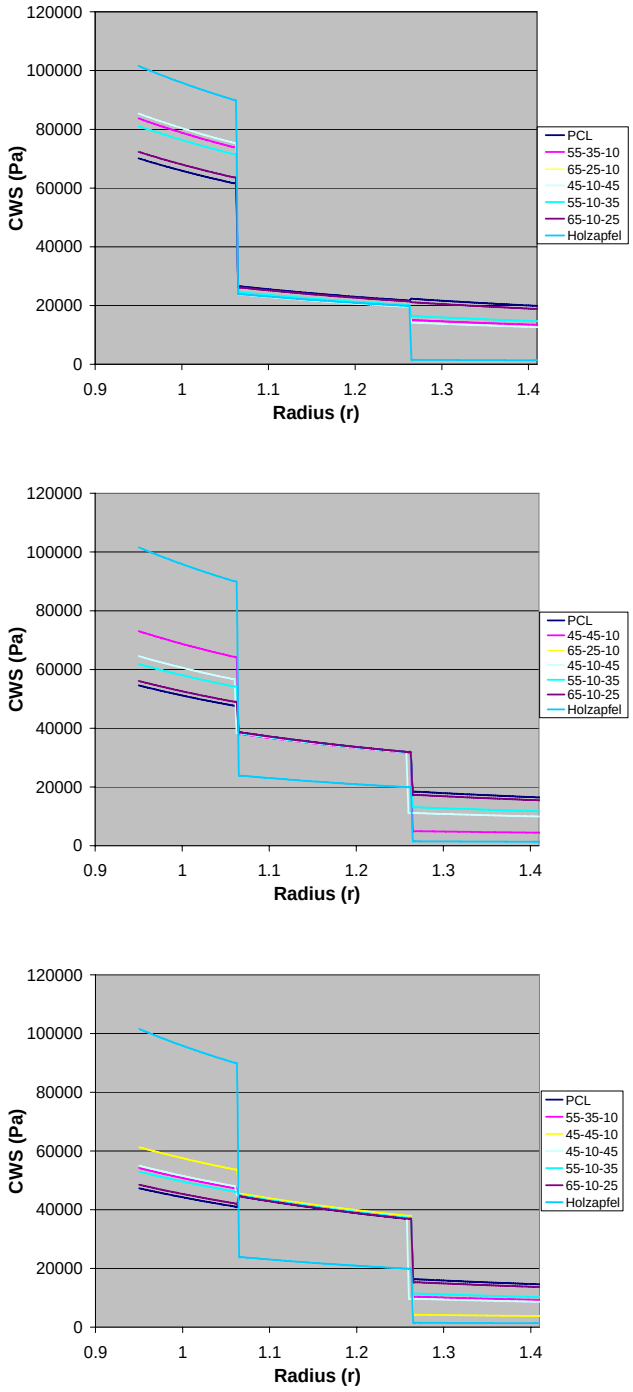

Figure 28. Mathematical modeling using equations 3-8 to determine CWS on increases in adventitial stiffness, while being compared to the moduli found in [32] and [33] for PCL-ELAS-COL samples. (a) Top graph represents the 45-45-10 medial layer, (b) middle graph represents the 55-35-10 medial layer, and (c) bottom graph represents the 65-25-10 medial layer.

Figure 29A-C displayed similar results to that of 28A-C where as the medial layer was changed from a high ELAS content, 45-45-10, to a lower ELAS content, 65-25-10, increased the amount of stress imposed on it. This was clearly evident through the separation that occurred from the comparative CWS medial layer values of the Holzapfel *et al.* study. Again, like Figure 28A the 45-45-10 medial layer seemed to have the best match to the stress distribution of native coronary artery. As PCL content increases from 45-45-10 to 55-35-10, there is a marked increase in the CWS of medial layer and a subsequent decrease in the stress of the intimal and adventitial layers. This is even more pronounced with the 65-25-10 medial layer, where all scaffold combinations have a lower CWS present in the intimal layer, an increase in CWS as it transitions to the medial layer, and another drop in CWS as the stress transitions into the adventitial layer. Like some of the results from Figure 28C, the stress distribution profile determined from the equations did not match that of native artery, indicating that it could be too stiff.

The next step in modeling the stress distribution was to determine the how altering the adventitial layers of the SF-based scaffolds changed the overall stress distribution for each medial layer. Figure 29A showed that as PCL content was decreased there was a slight increase in the CWS of the intimal layer, while there was also a slight decrease in the CWS of the adventitial layer. This decrease in PCL content demonstrates a decrease in modulus values and, therefore, a decrease in the amount of stress that is imposed on the adventitial layer. Instead, this decreased stress is compensated by the intimal layer, which increases in CWS. These results are seen also in Figures 30B and C. Interestingly, the material which takes on the most stress in the intimal layer is 55-10-35 as opposed to 45-

10-45. This indicates that the 55-10-35 adventitial layer should be one of the better candidates for further investigation.

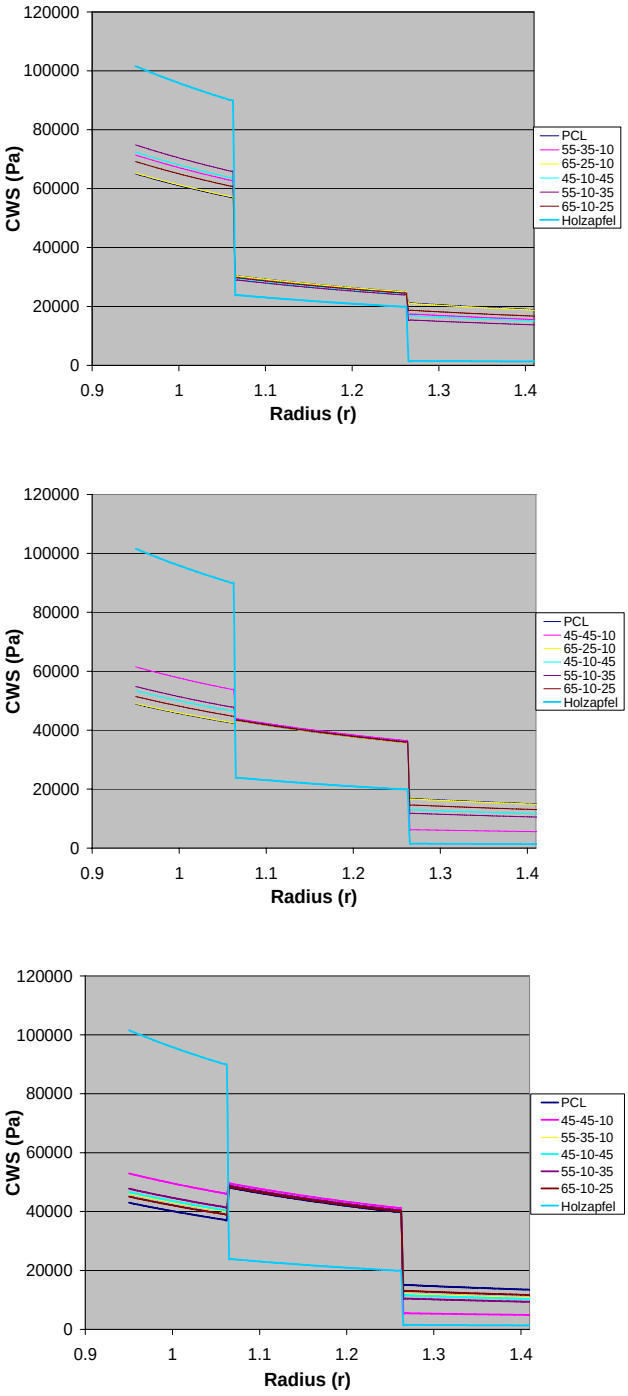

Figure 29. Mathematical modeling using equations 3-8 to determine CWS on increases in adventitial stiffness, while being compared to the moduli found in [32] and [33] for PCL-ELAS-SF samples. (a) Top graph represents the 45-45-10 medial layer, (b) middle graph represents the 55-35-10 medial layer, and (c) bottom graph represents the 65-25-10 medial layer.

Compliance

Mean values for PCL-ELAS-COL vascular grafts, Figure 30, displayed average results in the range of 0.4 - 1.8 %/100mmHg, while individual values went up as high as 2.4 %/100mmHg. While results demonstrated values not within the range of native artery, they did provide some insight into crosslinking dependence. While material property values demonstrated some differences between EDC and GEN crosslinked scaffolds, compliance results displayed differences, which demonstrated that grafts crosslinked with GEN, on average, had higher compliance values than those crosslinked with EDC. This is especially evident for grafts electrospun with a 45-45-10 PCL-ELAS-COL medial layer, where grafts with a 45-10-45 and 55-10-35 GEN crosslinked adventitial layers are significantly higher *($p < 0.05$)* than their EDC counterparts with values of 1.4 and 1.3 %/100mmHg, respectively, compared to 0.6 and 0.4 %/100mmHg for EDC, respectively. In the 55-35-10 medial layer group, both 45-10-45 and 55-10-35 GEN crosslinked adventitial layer grafts are significantly different *($p < 0.05$)* from the same EDC crosslinked grafts, portraying values of 1.2 and 1.4 %/100mmHg compared to 0.7 and 0.6 %/100mmHg. The 65-25-10 medial layer group did not display any significant differences between EDC and GEN crosslinked grafts. Moreover, the GEN crosslinked grafts exhibited significant differences *($p < 0.05$)* as the medial layer changed from 45-45-10 to 65-25-10, where combinations of 45-45-10 medial layer with a 45-10-45 adventitial layer were significantly different *($p < 0.05$)* from combinations of 65-25-10 medial layer with a 45-10-45 adventitial layer. This was the same case for combinations containing the 55-10-35 adventitial layer.

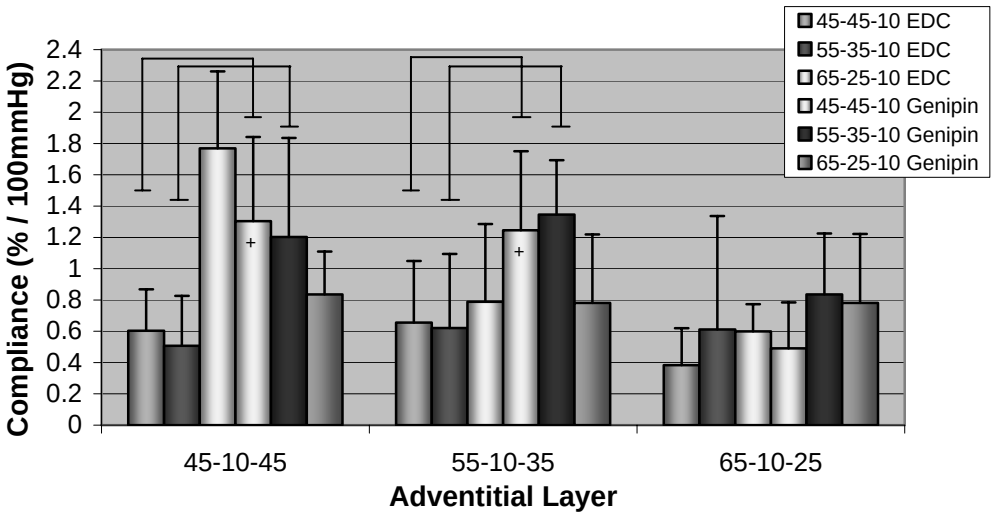

Figure 30. Compliance values determined from external radii at arterial pressures of 120/80 mmHg for PCL-ELAS-COL tri-layered grafts.+ indicates significant difference between 45-45-10 and 65-25-10 medial layer. Bars indicate significant differences between samples.

Looking at Figure 31, grafts with an adventitial layer of 45-10-45 PCL-ELAS-SF tend to increase in compliance as PCL content is increased in the medial layer where average compliance of 45-45-10 medial layers with EDC and GEN crosslinking increase from 0.6 and 0.3 %/100mmHg, respectively, to 0.9 and 1.3 %/100mmHg for EDC and GEN 55-35-10 medial layers. Furthermore, GEN crosslinked 45-45-10 is significantly different *($p < 0.05$)* from 55-35-10. These results are opposite the expected results, and could indicate that the amount of stiffness seen within the compliance results is due to SF. Additionally, in order to overcome the stiffness caused by SF and result in an increased distension of the graft wall, higher amounts of PCL must be added to the solution. In the 55-10-35 adventitial layer group, there were no significant changes for EDC crosslinked scaffolds as PCL content was increased; however, GEN crosslinked scaffolds have significant differences *($p < 0.05$)* between the 45-45-10 medial layers, 1.4 %/100mmHg,

and 65-25-10 medial layers, 0.3 %/100mmHg. Additionally, EDC 45-45-10 medial layers with 55-10-35 adventitial layers are significantly different *($p < 0.05$)* from GEN crosslinked grafts. Finally, in the 65-10-25 adventitial layer group EDC crosslinked 45-45-10 medial layer grafts have the highest compliance of the three medial layers and amongst the whole group with a value of 1.0 %/100mmHg. GEN crosslinked 45-45-10 medial layer grafts have the second highest compliance in the group with a value of 0.9 %/100mmHg. Therefore, there were no significant differences between the EDC and GEN 45-45-10 medial layer grafts when combined with 65-10-25 adventitial layers. Furthermore there were no significant differences between any of the EDC and GEN crosslinked grafts in the 65-10-25 group. However, there was a decrease in average compliance as the medial layer increased in PCL content.

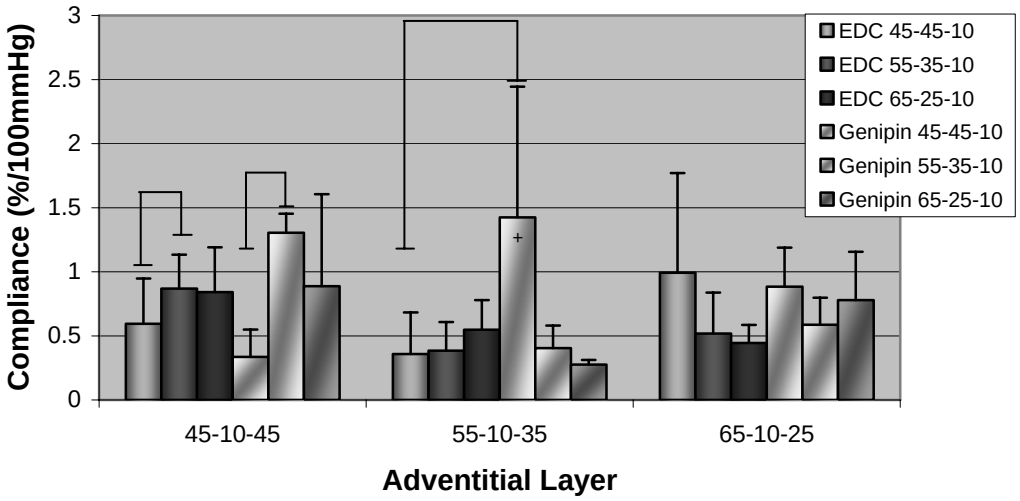

Figure 31. Compliance values determined from external radii at arterial pressures of 120/80 mmHg for PCL-ELAS-SF tri-layered grafts.+ indicates significant difference between 45-45-10 and 65-25-10 medial layer. Bars indicate significant differences between samples.

Burst Strength

The burst strength of all the PCL-ELAS-COL grafts in Figure 32 exceeded the standard 1600 mmHg that is associated with saphenous vein [163]. Notably, the only grafts that possessed values which increased as the PCL content of the medial layer was increased were the grafts in the 45-10-45 adventitial layer group. While EDC crosslinked grafts did not significantly change as the stiffness of the medial layer was increased, GEN crosslinked grafts did change *($p < 0.05$)* increasing from a value of 1614 mmHg, 45-45-10, to a value of 2403 mmHg, 65-25-10. These increases due to an increase in medial layer stiffness were also seen in the 55-10-35 adventitial layer group for both EDC and GEN crosslinking. For this group, 45-45-10 and 65-25-10 EDC crosslinked scaffolds increased from an average value of 2465 to 3059 mmHg and 45-45-10 and 65-25-10 GEN crosslinked scaffolds increased from 2635 to 2946 mmHg, both of which were significantly different *($p < 0.05$)*. Looking at the 65-10-25 adventitial group, the results for EDC crosslinked grafts were all very similar and exhibited no significant differences. However, GEN crosslinked grafts, while retaining very high values, increased in burst strength from values of 3055 to 3464 mmHg for 45-45-10 and 65-25-10 medial layers, respectively. These values were not significantly different. Lastly in Figure 32, there is a gradual trend from the 45-10-45 to the 65-10-25 adventitial group, indicating that as PCL the adventitial layer becomes stiffer the burst pressure increases which reinforced the results from the mathematical modeling.

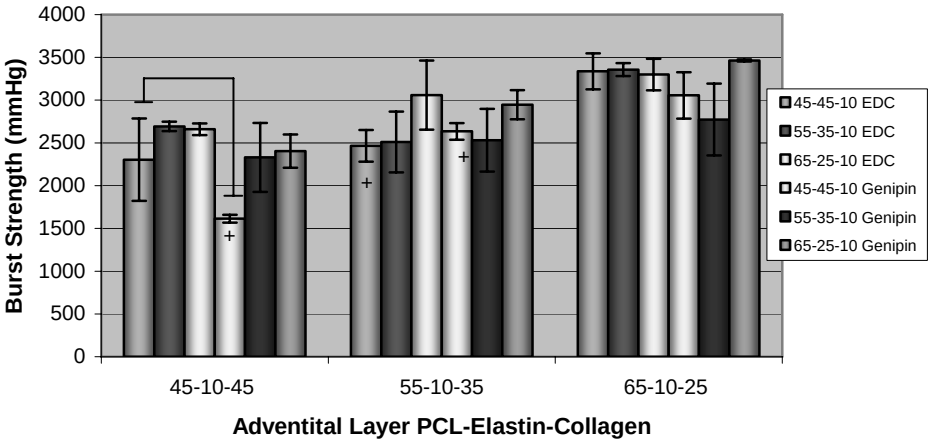

Figure 32. Burst pressure results for tri-layered specimens with changes in the both the medial layers and adventitial layers for PCL-ELAS-COL grafts. + indicates significant difference between 45-45-10 and 65-25-10 medial layer. Bars indicate significant differences between samples.

Examining Figure 33, PCL-ELAS-SF burst strength results revealed very different results from PCL-ELAS-COL. Studying the 45-10-45 adventitial layer group, it was evident that neither EDC nor GEN produced significantly different results from each other or from amongst them. For example, 45-45-10 medial layer combinations are no different from 65-25-10 medial layer combinations for EDC crosslinking, and averages for GEN crosslinked 45-45-10 combinations are only slightly less than 65-25-10 combinations with values of 2146 and 2361 mmHg. The 55-10-35 adventitial layer grafts demonstrated gradual increases in burst strength as the medial layer incrementally increased in PCL content for both EDC and GEN crosslinked grafts. Again for this 55-10-35 group, there were no differences between EDC and GEN crosslinked grafts. However, there were differences as the medial layer increased its stiffness, where 45-45-10 grafts were significantly different from 65-25-10 grafts for both EDC and GEN crosslinking. Examining the 65-10-25 adventitial group, there were again differences *($p < 0.05$)* between

the 45-45-10 and 65-25-10 medial layer combinations for both EDC and GEN crosslinking. Moreover, for both 55-10-35 and 65-10-25 adventitial groupings there were no differences between the 45-45-10 and 55-35-10 medial layer graft combinations.

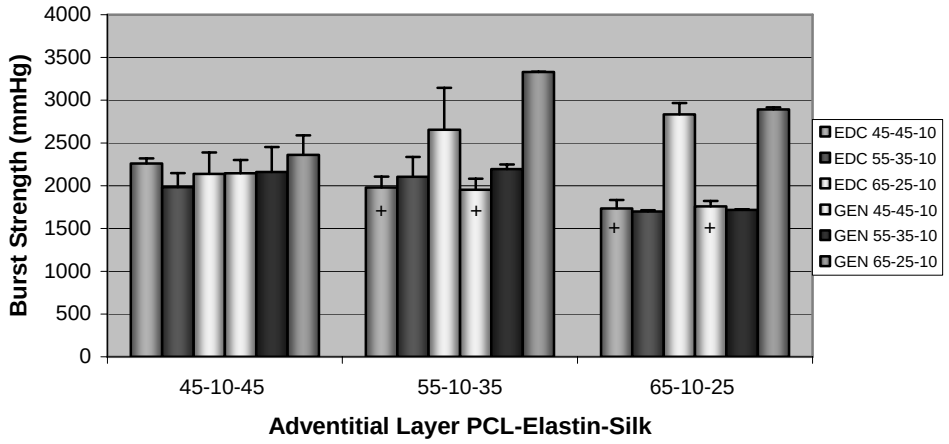

Figure 33. Burst pressure results for tri-layered specimens with changes in the both the medial layers and adventitial layers for PCL-ELAS-SF grafts. + indicates significant difference between 45-45-10 and 65-25-10 medial layer.

Compliance and Burst Degradation

Degradation was carried out over a period of 4 weeks to determine if there were any immediate degradation characteristics which would impact the compliance and burst strength properties of the top tri-layered vascular grafts. Figure 34A and B depict the compliance results for grafts containing COL and SF, respectively. Figure 34A demonstrated a significant increase *($p < 0.05$)* in compliance for 65-10-25 adventitial layer grafts with a 45-45-10 medial between week 0 and week 2 and between week 1 and week 2. Additionally, there was a significant increase *($p < 0.05$)* in compliance from week 1 to week 2 for grafts with a 45-10-45 adventitial layer and 45-45-10 medial layer. However, week 4 compliance results were not different from weeks 0 and 1. Interestingly, the

average values for the 55-10-35 adventitial layers with either a 45-45-10 or a 55-35-10 medial layer incrementally increased from week 0 to week 2, and compliance results for 55-35-10 medial layer displayed a significant difference from week 0. Furthermore, both the compliance of the 65-10-25 adventitia 45-45-10 media and 55-10-35 adventitia 55-35-10 media grafts were within range of native artery.

Figure 34B showed that SF grafts had significant decreases *($p < 0.05$)* in compliance between week 1 and 2 for 55-10-25 adventitial layer grafts with 45-45-10 medial layers. Additionally, the 65-10-25 adventitia with a 45-45-10 media increased in average compliance from week 0 to week 2; however, the difference was not significant. Average compliance values for SF grafts did not reach into the range of native artery. Nonetheless, they did display fairly consistent values amongst the grafts. This would indicate that there was no degradation over the course of two weeks whereas it seems that in Figure 34A COL containing grafts may have experienced slight amounts of degradation.

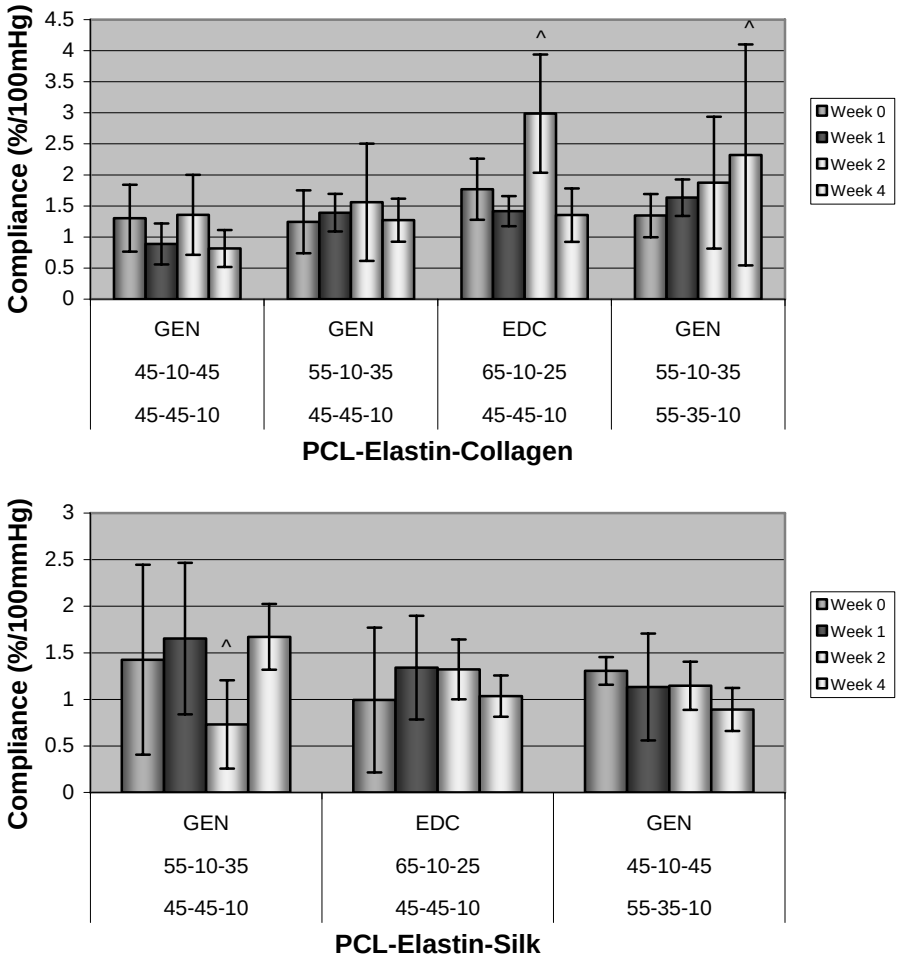

Figure 34. Compliance values for a 4 week degradation study determined from external radii at arterial pressures of 120/80 mmHg. (a) Top graph represents PCL-ELAS-COL tri-layered grafts and (b) bottom graph represents PCL-ELAS-SF tri-layered grafts. ^ indicates a significant difference from weeks 0 and 1.

Figure 35A and B described the burst strength properties of grafts degrading over a 4 week period. It was expected that if any degradation was happening to the grafts, then a decrease in burst strength would have occurred. In the case of the PCL-ELAS-COL grafts in Figure 35A, there was a significant decrease *($p < 0.05$)* between week 0 and 2, week 0 and 1, and week 0 and 4 for 65-10-25 adventitia with 45-45-10 media. Additionally, grafts with a 55-10-35 adventitia and a 55-35-10 media were significantly different *($p < 0.05$)*

between week 1 and week 2. Furthermore, 45-10-45 adventitia 45-45-10 media grafts significantly increased *($p < 0.05$)* in burst strength from week 0 to week 4 but there were no differences amongst weeks 1, 2, and 4.

Figure 35B revealed a significant decrease *($p < 0.05$)* in burst strength for grafts with a 55-10-35 adventitia and a 45-45-10 media between week 0 and week 4, while 45-10-45 adventitia with a 55-35-10 media significantly increased in burst strength from week 0 to week 2. Finally, 65-10-25 adventitia with a 45-45-10 media significantly decreased *($p < 0.05$)* between week 1 and week 2, and the average burst pressure from week 4 was still lower than that of week 1 but similar to week 0.

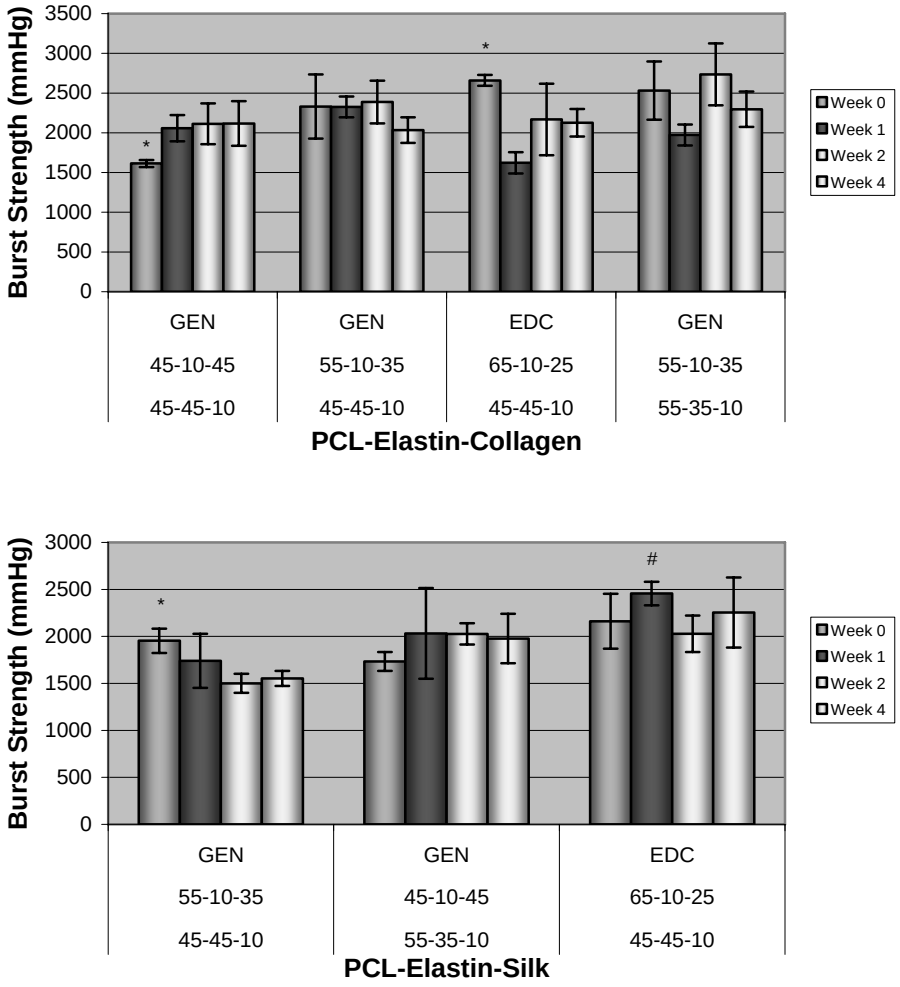

Figure 35. Burst pressure results for tri-layered specimens with changes in the both the medial layers and adventitial layers during a 4 week degradation study. (a) Top graph represents PCL-ELAS-COL tri-layered grafts and (b) bottom graph represents PCL-ELAS-SF tri-layered grafts. * indicates a significant difference from week 4. # represents a significant difference from week 2.

If a correlation is made between the compliance and burst results, then we could determine whether or not degradation was truly occurring or if the differences were mere coincidence. Observing the PCL-ELAS-COL grafts, the only graft to display a possible difference in properties due to degradation was the 55-10-35 adventitia with a 55-35-10 media due to a simultaneous increase in compliance and decrease in burst strength from week 0 to week 4. For PCL-ELAS-SF grafts, there was no correlation to indicate that

degradation had occurred within a group of grafts. Therefore, some degradation may perhaps be occurring with grafts containing COL whereas there is most likely no degradation occurring amongst the SF grafts.

Discussion

Material Properties

The properties of individual layers provide some clues as to how a multi-layered vascular graft should perform under physiological conditions when these results are used in conjunction with a mathematical model. First, peak stress indicates how much stress or pressure can be applied to the structure prior to rupturing. If the desired medial layer is one that is fairly weak with stress values around 1 MPa, its surrounding layers need to be able to take the majority of the imposed stress. Second, modulus indicates how stiff the layer is going to be, which will contribute to the overall compliance of the graft. This is a measure of the slope in the linear region of a material prior to reaching its yield point, where it has undergone only elastic deformation. Third, strain to break indicates how far a material will yield prior to failure. This is also important for vascular grafts because it provides further insight into how a material will fail, brittle failure or ductile failure. Most polymeric materials would be considered to fail under the ductile category; however, these materials could have a more brittle ductile failure where the material does not yield a significant distance. Fourth and finally, energy to failure displays information about how much energy a material can absorb prior to rupture. This is calculated by taking the area under the force v. strain curve. If the energy to failure is high, then a material could have

either had a high peak stress with a short strain to break distance, or it could have had a long strain to break distance with a low peak stress.

For a native artery, material properties are extremely important to be able to decipher the specifics of a tissue. Previous studies which have investigated muscular arteries were not based on experimental data of individual layers such as the intima, media, and adventitia. Instead, these works were based on the biomechaincs of the whole tissue [269, 273]. These early studies considered the vessel wall to consist of homogenous material and the mechanical properties were considered to be uniform throughout the vessel wall [297, 298]. However, native arteries are not completely homogenous materials, containing three different layers, each of which possesses its own biomechical design to support the functionality of the artery. Currently, there have been studies which aimed to analyze the biomechanics of each individual layer either as a two layer model or as a three layer model [265, 266, 271]. Two layer models typically leave the intima and media intact and separate the adventitia, while three layer models carefully separate the intima, media, and adventitia, a tedious process. These studies have demonstrated the specific biomechanics in each layer through the use of uniaxial tensile testing. The results from these tests are then utilized to determine composition, how the tissue behaves, and eventually aid in the development of an equation to predict how a native artery will behave under different circumstances. This same logical approach was used in this study.

Determining the specific mechanical properties of each electrospun material assists in the overall design of a tri-layered vascular graft. According to Table 10, the only significant differences that occurred between EDC and GEN were the 65% PCL groups.

These results showed that when crosslinked with GEN there was a decrease in overall peak stress. This same behavior was shown in a previous study for 50-50 PDO-ELAS scaffolds and pure ELAS scaffolds [110], which helps to support the claim that slight changes exist between the EDC and GEN crosslinked scaffolds. For PCL-ELAS-SF blended scaffolds in Table 11, peak stress also decreased for each scaffold type, and significant differences existed between 65-25-10, 45-45-10, and 45-10-45 EDC and GEN scaffolds. Unlike peak stress, modulus did not display any type of similar trend except for the higher PCL content scaffolds being different from the lower PCL content scaffolds for ELAS-, COL-, and SF-based scaffolds, a trend that is consistent amongst all materials tested in this study. While both peak stress and modulus displayed similar trends for both PCL-ELAS-COL and PCL-ELAS-SF scaffolds, strain to break did not exhibit any similarities despite both sets of failure values occurring mostly between 30.0 and 60.0 % elongation.

GEN is a crosslinker that has not received a great deal of attention and has been used in only a handful of studies. Within these studies, mechanical testing has been performed. One of the hypotheses made in this study was that the long molecular structure of GEN would result in longer strain to breaks and lower elastic moduli and lower peak stress values. In a study by Vieth *et al.*, scaffolds were created through coacervation and subsequent crosslinking of recombinant ELAS-based polypeptide with either pyrroloquinoline quinone (PQQ), another zero-length crosslinker, or GEN [288]. The results from the study demonstrated that PQQ-crosslinked sheets exhibited a lower modulus and peak load, and a higher strain to break than GEN crosslinked sheets. However, they also measured the number of lysines remaining, and PQQ had a

significantly lower number of lysines remaining after crosslinking. Therefore, instead of the molecular length of the crosslinking reagent making a difference in the tensile properties for our particular study, the differences would most likely be due to how well the electrospun materials crosslinked themselves. In another study, COL based constructs were crosslinked using EDC, GEN, and formaldehyde [283]. Here, they found that COL gels crosslinked with GEN had a higher strain to break than EDC constructs, while modulus and peak stress remained similar. Interestingly, the study looked at gelation time and tensile properties, finding that modulus increased as gelation time increased while strain to break decreased, and peak stress remained unchanged.

Both these ELAS and COL gel studies demonstrate that crosslinking time is a clear major issue that should be tailored when considering using crosslinking. The ELAS gel study showed that PQQ contained less lysines which would indicate that it had a lower amount of crosslinking. This increased strain to break and decreased modulus which could be due to the crosslink bond built during the reaction period. If the bond was weaker due to a lower crosslinking percentage, then the molecular structure would retain more mobility to stretch, increasing its strain to break values. The COL gel study reiterated this idea where gelation time increased modulus and decreased strain to break. This demonstrated that as the bonds had more time to form their strength increased significantly, making the structure stiffer and which caused the bonds to become more "brittle".

Turning back towards our hypothesis, these experiments by Vieth and Madhavan do not support the idea that a longer molecular structure would cause the peak stress and

modulus to decrease while strain to break increased. These, however, differ in a lot of ways in comparison to this particular study. Both Vieth and Madhavan tested gelled constructs which have a very different microstructure than electrospun fibers. Additionally, our study utilizes a synthetic polymer as well, which dominates the mechanical environment. The decreases seen in peak stress are most likely due to the combination of PCL, ELAS, and COL. The interaction of these polymers in solution created a different fiber composition for each construct with different chain entanglements and molecular weights. In the ELAS-based constructs we have a decrease in peak stress for 45-45-10 – 65-25-10. However, in the COL-based materials, there is a slight increase in the 45-10-45 scaffolds for GEN crosslinking, but then as the content of COL decreases the ELAS is able to take on more of the mechanical loading. When this ELAS is crosslinked with GEN, it takes on a lower peak stress.

Energy to failure results demonstrated differences between the crosslinkers. For almost every case, the energy to failure values decreased when GEN was used as the crosslinker, excluding the 45-10-45 scaffolds. Differences between EDC and GEN for energy to failure values were found for only the 65-25-10 PCL-ELAS-COL scaffold. Nevertheless, based on the tensile test results, differences between the crosslinking reagents could not be conclusively drawn. Since the moduli were similar for both EDC and GEN structures, EDC crosslinked structures were chosen to be used in the modeling equations so as to simplify the data presented in the models.

Mathematical Modeling

Mathematical modeling is an excellent way to use predictive methods and compares those results to your experimental results. In this experiment, we wanted to be

able to use the uniaxial tensile test results for each polymer of interest and plug those into a set of equations. The intention was to compare those predicted results to the experimental results from compliance and burst strength. This would then validate the model or demonstrate the need to change the predictive model something more complex. Overall, the model used in this experiment is a relatively simple, algebraic one, which was previously developed by Vorp *et al.* to help predict how implanted vascular grafts would behave as they degraded and were subsequently taken over by ECM [261]. Native tissue has been studied relentlessly, using mechanical properties and mathematical modeling of coronary intima, media, and adventitia to gain information that explains how the arterial wall reacts under physiological conditions [120, 265, 266, 269-273]. Many of these models use a strain-energy function in a quasi–linear viscoelastic equation. These equations are typically complicated and require time consuming efforts to derive results. The Vorp *et al.* model used in this experiment, however, displays the necessary information required, such as the CWS, to predict how materials will behave with one another. The results from the compliance and burst strength data were tested and subsequently compared to the model predictions.

Compliance and its Relation to Modeling

It is commonly agreed upon that compliance mismatch between native artery and an implanted graft is one of the fundamental causes of intimal hyperplasia and long-term graft occlusion. At the small diameter level, grafts that retain compliant properties on the order of native artery are highly necessary. The low flow environment exponentially

increases the opportunity for complications to occur. This is the predominant reason why ePTFE grafts possess a very low patency rate for small diameter blood vessels. It is also the reason for the use of saphenous vein as the coronary bypass gold standard. Although native vein contains an altered ECM in comparison to artery, it retains a tri-layered structure, has an endothelial lining, and will adapt itself well to the new physiological pressures imposed on its wall.

An off-the-shelf vascular graft would be ideal for bypass graft cases because it would not involve tissue excision from a vascular site. A tri-layered vascular graft is an ideal vascular replacement because of its tailorability. In this case, we tested how the stiffness of a biodegradable material affects compliance values through changes to the medial and adventitial layer. The results from this study exhibited differences from the trends seen in the preliminary study, where medial layer stiffness was changed while intimal and adventitial layers remained constant. Differences between that study and this are demonstrated through the types of materials used in the adventitial layer. The preliminary study only used a combination of 70-30 PCL-COL which exhibited excellent qualities, but with the side affects of frequent delamination, causing several grafts to be electrospun prior to obtaining one that was free from delamination. One of the main objectives with this study was to find a way to fine tune the adventitial layer so that delamination would no longer be an issue. This was accomplished through the inclusion of a small percentage of ELAS, and allowed us to test adventitial layers containing high amounts of COL protein (45-10-45), a beneficial addition to enhance cellular adhesion, growth, and migration.

In Figure 30, PCL-ELAS-COL blends, EDC crosslinked grafts displayed results opposite what was found in the preliminary study; compliance increased as ELAS content decreased regardless of the adventitial layer. GEN crosslinked grafts, all manufactured in the same manner as EDC grafts, exhibited trends like those seen in the preliminary study, where combinations of 45-45-10 medial layer with a 45-10-45 adventitial layer were significantly different from combinations of 65-25-10 medial layer with a 45-10-45 adventitial layer. This was also the same case for combinations containing the 55-10-35 adventitial layer. There were no changes in the 65-10-25 adventitial layer group. Additionally, as PCL content incrementally increased in the adventitial layer, the compliance decreased incrementally. When a linear regression analysis was performed to quantify these changes, the 45-45-10 medial layers contained an r-squared value of 0.91 while 55-35-10 medial layers contained an r-squared value of 0.59; an indication that both medial layers displayed adequate increases in stiffness as the adventitial layer increased in stiffness. The results of the GEN crosslinked scaffolds matched the predicted data from the mathematical analysis. However, EDC crosslinked scaffolds did not match the predicted model, where a stiffer medial layer would produce a lower compliance. The data did match when the adventitial layer stiffness increased. For example, the 65-25-10 medial layer exhibited an R-squared value of 0.86 in addition to the 45-45-10 medial layer displaying an R-squared value of 0.56. 55-35-10 medial layer displayed an R-squared value of 0.68, but its trend line increased in compliance as the adventitial layer increased in stiffness.

Figure 31 displays the results from the PCL-ELAS-SF vascular grafts. According to the mathematical model, the SF grafts in combination with the 55-10-35 adventitial layer should prove to be beneficial with a high compliance while 45-10-45 and 65-10-25 incrementally increased in stiffness. Unfortunately, all of the EDC crosslinked grafts from this 55-10-35 group failed to produce desirable compliance values. Moreover, the only graft which possessed attractive compliance results out of the 55-10-35 adventitia group was the GEN crosslinked 45-45-10 medial layer. The GEN crosslinked group also produced results that matched that mathematical model where the compliance decreased as the medial layer stiffened. This is demonstrated through a linear regression analysis where the R-squared value is 0.83. 45-10-45 adventitial layer grafts displayed average compliance results between 0.8 and 1.3 %/100mmHg. However, neither the EDC nor the GEN crosslinked grafts matched the model as the PCL content of the medial layer increased. It appeared that 65-10-25 adventitial layer grafts displayed results that matched the modeling data for both EDC and GEN where the compliance decreased as the medial layer gained more PCL. When these results were analyzed further for the 65-10-25 group, EDC grafts displayed regression R-squared values of 0.85 while the GEN crosslinked group had an R-squared value of 0.12. Based on the linear regression analysis GEN grafts did not satisfy the mathematical model despite their decrease in compliance.

Burst Strength and its Relation to Modeling

Burst strength of the all grafts demonstrated ample ability to withstand pressure. The bursting properties also showed how changing the medial or adventitial layers of the graft material influenced its final burst pressure, proving that as the medial stiffness is increased the stresses imposed on both the intimal and adventitial layers are reduced and

allowing the graft to take on more pressure prior to bursting. This is demonstrated in the PCL-ELAS-COL grafts depicted in Figure 32. Grafts within the 45-10-45 adventitial layer group displayed, on average, the lower burst pressures of the three adventitial groups, the lowest belonging to GEN 45-45-10 at 1614 mmHg. On the other side of the spectrum, grafts within the 65-10-25 adventitial layer group showed averages around 3000 mmHg. As the adventitial layers were incrementally increased with PCL, the burst pressure incrementally increased as well. This was shown through linear regression analysis where medial layers of 45-45-10 had an R-squared value of 0.94, 55-35-10 with incrementally increased adventitia had a value of 0.99, and this value was the same for 65-25-10 grafts. Additionally, as the medial layer was increased burst values rose. Linear regression proves this with R-squared values of 0.94, 0.89, and 0.99 for 45-10-45, 55-10-35, and 65-10-25 adventitial groups, respectively. Therefore, PCL-ELAS-COL grafts, under burst pressure, exhibited values which were in agreement with the mathematical model, demonstrating that as PCL content increased and the materials became stiffer there was a subsequent relief of stress from other layers, allowing them to take on more pressure, thereby increasing burst strength.

Observing grafts from Figure 33, PCL-ELAS-SF grafts demonstrate that they do not fit with the mathematical model. Examining each of the adventitial layer groups, both the EDC and GEN 45-45-10 and 55-35-10 medial layers with increasing adventitia stiffness displayed a decrease in burst strength. This was echoed by their linear regression R-squared values of 0.99 and 0.47 for EDC 45-10-45 and 55-10-35, and R-squared values of 0.99 and 0.69 for GEN 45-10-45 and 55-10-35, respectively. Additionally, EDC 65-25-

10 medial layers with increasing adventitia had a positive increase in burst strength with an R-squared value of 0.93. GEN 65-25-10 medial layers displayed a positive increase but the R-squared values were 0.30. This clearly demonstrates that burst pressure in fact went down for adventitial layers of 45-10-45 and 55-10-35, indicating that as less SF was introduced to the scaffold, the overall graft stiffness decreased. However, an encouraging fact was that as the medial layer increased in stiffness, PCL-ELAS-SF grafts increased in burst pressure, indicating that ELAS was still interacting as it should with the graft materials. This was shown through the R-squared values of 0.88 and 0.73 for EDC 55-10-35 and 65-10-25 adventitial layers and values of 0.80 and 0.88 for GEN 45-10-45 and 55-10-35 values, respectively. Both EDC 45-10-45 and GEN 65-10-25 displayed regression lines which were flat so they were not considered to have increased in burst pressure.

Choosing the Best Grafts: Compliance v. Burst Strength

With the large amount of data available through this study, considering two different polymer blends and observing the differences that occur when the ratios of their electrospun materials are changed. Simultaneously, these different structures are crosslinked with two different reagents in incrementally changed combinations. In the end, a total of 36 different graft and crosslinking combinations were used in this experiment. In order to narrow down the data to the top 3 grafts from the COL group and the top 3 from the SF group, burst strength and compliance were plotted together. These results are displayed in the scatter plot below in Figures 35 and 36. One of the key features of Figure 34 demonstrates how the majority of EDC crosslinked scaffolds are clustered together at lower compliance values and higher burst strength. This portrays the idea that

scaffolds with lower burst strength values acquire higher compliance values. This is equally evident in Figure 35. However, there are grafts that have burst strength values around 1600 mmHg, yet they fail attain higher compliance values. This only further demonstrates how PCL-ELAS-SF grafts did not behave as expected. This unexpected behavior can be attributed to the SF. Prior to the beginning of the experimental design, preliminary studies were done to determine if SF would be a good candidate for vascular testing. Under these tests it demonstrated more than desirable results with high compliance values and adequate burst pressures. This has been further shown in several experiments which have researched SF and electrospun SF [277, 299]. For reasons not yet determined, the SF scaffolds exhibited lower average burst strength than the COL scaffolds. Several reasons can be speculated.

1. Chapter 4 displayed the fiber diameter results and SEM images of the different blends. The larger fiber diameters that occurred with higher SF content could have easily created large pores which would have a great deal of permeability. This permeability could account for the low compliance values tested on the ITEMS® bioreactor, failing to provide even pressure on the fibers where the majority of the PBS (the incompressible fluid to cause cyclic distension) would be pushed out of the graft. 2. SF has a significant amount of strength. Naturally, SF displays a great deal of strength. When this is electrospun with a synthetic polymer, it may produce results that impart stronger tensile properties as compared to SF by itself. In a recent study done by our lab, PCL-SF and PDO-SF grafts were electrospun in random and aligned forms. These were then tested for compliance yielding averages near 0.5 %/100mmHg [113]. Although those compliance

values were larger than PCL, it could mean that a limit is reached when SF is added to the system. These speculations can be tested in future studies to determine permeability results using the ITEMS® bioreactor without fluid on the outside of the graft. The inlet flowrate would be set and the amount of time would be measured to reach a specific volume. Additionally, further whole graft testing with SF would be made in specific combinations with ELAS and PCL to examine grafts under compliance, burst, and uniaxial tensile testing.

In any case, GEN crosslinked scaffolds displayed the top results for both Figure 36 and 38. For Figure 36, a cut-off point was made at 1.3 %/100mmHg compliance. In Figure 38, a cut-off point was made at 1.0 %/100mmHg. These cut-off marks provided the top results which were: 1.) GEN 45-45-10 with 45-10-45, 2.) GEN 45-45-10 with 55-10-35, 3.) GEN 55-35-10 with 55-10-35, and 4.) EDC 45-45-10 with 65-10-25 PCL-ELAS-COL. 1.) GEN 45-45-10 with 55-10-35, 2.) GEN 55-35-10 with 45-10-45, and 3.) EDC 45-45-10 with 65-10-25 PCL-ELAS-SF. Each of these grafts was electrospun again and examined for degradation characteristics.

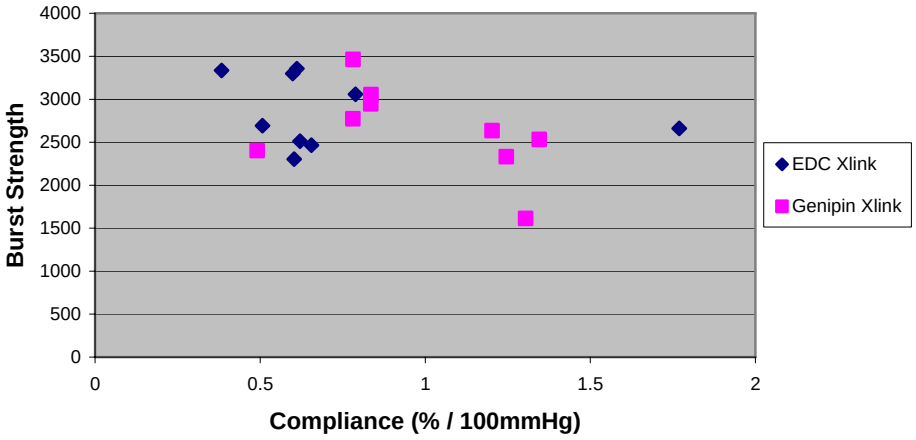

Figure 36. Burst strength v. Compliance to determine best overall PCL-ELAS-Collgaen tri-layered grafts for future testing.

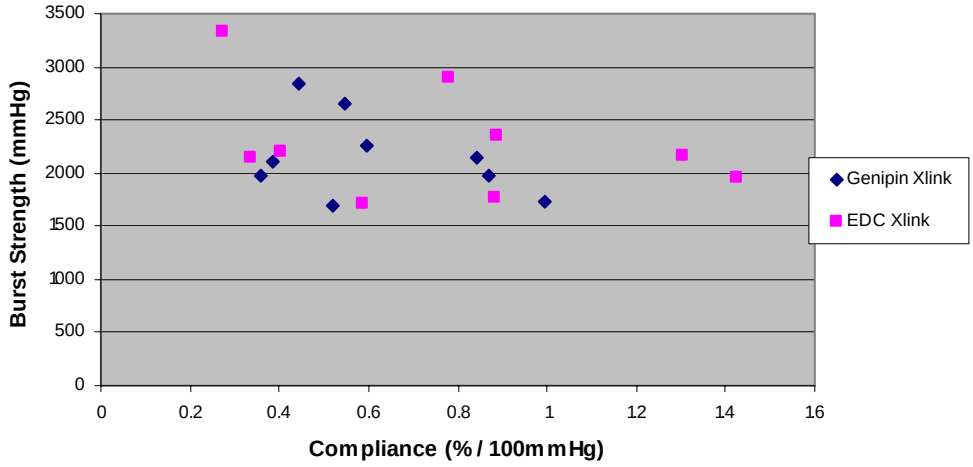

Figure 37. Burst strength v. Compliance to determine best overall PCL-ELAS-SF tri-layered grafts for future testing.

Compliance and Burst Degradation

When biodegradable materials are implanted *in vivo*, they experience both hydrolytic and enzymatic degradation. PCL is a long degrading polymer that has been shown to degrade, *in vitro*, over a period of 12 months. Studies have been performed *in vivo* with electrospun PCL vascular grafts implanted in the descending aorta of rats [93]. This study found that PCL, at both molecular weights of 120 and 80 kDa, began to degrade

after 3 weeks implantation and had degraded by 20% after 24 weeks of implantation. They concluded that the degradation characteristics were most likely due to the cleavage of the ester linkages, but may have also been produced by enzymatic degradation by lipases, although these characteristics had not been shown in humans. Additionally, degradation of biodegradable polymers such as PCL has exhibited faster degradation *in vivo* rather than *in vitro*. This accounted for the dramatic drop in molecular weight seen over 24 weeks. Other studies have, such as Bolgen *et al.* [94] have revealed a molecular weight degradation of 30% after just 3 months.

While PCL degrades mainly due to hydrolytic properties, crosslinked ELAS, COL, and SF would all have to undergo enzymatic degradation. In a study done by Mercuri *et al.*, a comparison was done between glutaraldehyde (GLUT), EDC, and periodate fixations for a glycosaminoglycan (GAG) aortic leaflet [300]. Once fixed, these GAG scaffolds were placed in degrading enzymatic media. Quantification of hexosamines was then performed to determine the amount that the structure had degraded over a period of 24 hours. Results determined that fresh leaflets and GLUT crosslinked were significantly digested. However, EDC crosslinked scaffolds significantly resisted enzymatic digestion. Therefore, crosslinking of scaffolds can significantly alter the amount of time taken to digest the molecular bonds within ELAS and COL proteins. Moreover, SF proteins have also been found to degrade by way of proteolytic digestion [301], which can take in excess of 12 months.

Looking at the degradation characteristics, it appears that a 4 week period did not degrade the polymeric scaffolds. It appears that in some cases there may have been some

batch to batch variations which could have been caused by degradation, non-homgeneity from the electrospinning process, or non-homogeneity in the cross-linking process. For example, there was an increase in compliance and a slight decrease in burst strength for the EDC crosslinked 65-10-25 adventitia with a 45-45-10 media PCL-ELAS-COL after 2 weeks. However, week 4 compliance results revealed similarities to weeks 0 and 1. Meanwhile, 55-10-35 adventitia 55-35-10 media PCL-ELAS-COL grafts showed a gradual increase in compliance and a decrease in burst from week 0 to week 4, which could demonstrate degradation. Nonetheless, week 2 burst strength for these same grafts was the highest of the 4 values. While other PCL-ELAS-COL scaffolds seemed to slightly increase in compliance, yet they did not yield lower burst strength values. PCL-ELAS-SF grafts did not indicate that any degradation had occurred amongst the scaffolds. This is indicative that not only did PCL slightly degrade, but COL and ELAS may have also degraded as well due to the FBS inclusion in the degradation media. FBS has been shown to contain enzymes which would increase degradation rates. Additionally, COL scaffolds demonstrated higher degradation characteristics when compared to SF scaffolds. This could have transpired due to either a low crosslinking molarity, producing weaker crosslinks in both EDC and GEN, or SF's slow degradation process. As future degradation time periods are assessed, it will become clear whether or not degradation of the graft wall is occurring.

Conclusion

In conclusion, we were able to produce nano- to micro-fibrous three-layered small diameter vascular grafts with distinct material properties for each layer. These layers were

then applied to a mathematical model which displayed the transmural stress distribution in the wall of the graft. The results from the compliance and burst strength data proved to change the overall graft properties with incremental changes in scaffold protein. From these experiments, grafts with the best combined compliance and burst properties were chosen to be tested in a 2 week degradation experiment. This experiment displayed signs that some of the grafts were degrading, increasing compliance without a loss of burst strength below 1600 mmHg, and with no signs of delamination between the layers. This is encouraging for future work towards an implantable tri-layered vascular graft, where we will evaluate the cellular characteristics of the graft materials.

Chapter 6: Integrin Binding Analysis of PCL, Collagen, Elastin, and Silk

Abstract

It is well known that a number of integrins (α1β1, α2β1, α3β1) bind to Type I COL in a RGD independent manner and the αvβ3 integrin binds with high affinity to *denatured* COL in a RGD-dependent manner. It has also been suggested, in some cases, that the αvβ3 integrin binds to ELAS through the VAVPG complex. However, debates still circulate about electrospun COL dissolved in hexafluoroisopropanol (HFP) maintaining its ability to bind β1 integrins. Additionally, limited adhesion research has been performed on SF to determine whether any ligand binding sites exist. The hypothesis of this study was that cells would adhere to electrospun COL and ELAS mostly through integrin β1 and β3, respectively. Human umbilical artery smooth muscle cells (hUASMC) were seeded onto crosslinked and uncrosslinked COL, ELAS, and SF blended scaffolds to test for cell adhesion. Cell seeding was done in the presence or absence of anti-integrin β1 and β3 to quantify adhesion to electrospun scaffolds. In addition, an SDS Page was run to compare both extracted COL and electrospun COL to known COL type I sources in addition to soluble ELAS compared to electrospun ELAS. The western blot results demonstrated that extracted and electrospun COL retained its α1(III), α1(II) and α2(I) chains unlike electrospun gelatin (denatured COL). ELAS did not demonstrate any specific molecular weights, appearing as a smear; however, its recovered electrospun form contained no smear possibly showing a change in structure. Cell adhesion data showed that COL dissolved in HFP had excellent adhesion, a significant decrease in cell number with anti-integrin β1, indicating that COL was not denatured by HFP. ELAS dissolved in HFP

demonstrated poor adhesion which was similar to that of bovine serum albumin (negative control), while ELAS dissolved in PBS decreased cell adhesion but did not completely inhibit it. SF blended scaffolds demonstrated a decrease in adhesion when anti-integrin β3 was utilized compared to no treatment. Finally, cross-linking appeared to significantly decrease cellular adhesion to electrospun scaffolds. In conclusion, COL dissolved in PBS or HFP enhanced cell adhesion when uncross-linked, but lost those properties when cross-linked with EDC. ELAS blocked adhesion, while PCL alone proved to be adherent independent from integrins β1 or β3, and SF proved to be adherent independent from integrin β1.

Introduction

The architecture of the vascular wall is highly intricate and requires unique biomechanical properties in order to function properly. Native artery is composed of a mix of COL, ELAS, ECs, SMC, FBs, and proteoglycans arranged into three distinct layers: the intima, media, and adventitia. Throughout artery, COL and ELAS play an important role, providing a mechanical backbone, preventing vessel rupture, and promoting recovery while undergoing pulsatile deformations [2]. The low-strain mechanical response of artery to blood flow is dominated by the elastic behavior of ELAS which prevents pulsatile energy from being dissipated as heat [293]. Previous work has shown the ability to fabricate multi-layered electrospun scaffolds composed of PCL, ELAS, COL, and SF, and their associated mechanical advantages. PCL was chosen, in this case, to provide mechanical integrity and elasticity, while ELAS, SF, and COL would provide further elasticity and bioactivity [104, 253]. However, when the grafts were implanted in the

descending aorta of a rat, cellular results depicted adherence of cells to the outer surface and inner lumen without infiltration. Therefore, further graft optimization was required. The hypothesis of this study was that blended polymers and biopolymers would be conducive for cellular attachment through specific integrin binding sites.

Integrins are a family of the extracellular matrix (ECM) receptors that bind a broad variety of ligands. A functional integrin receptor is a bidirectional signaling complex that is composed of two transmembrane subunits, an alpha (α) and a beta (β) chain [302-304]. Typically, an integrin binding event is mediated by these α and β subunits, anchoring the extracellular environment to the intracellular environment. These binding events allow a cell to detect and respond to specific extracellular constituents, essentially allowing the cells to evaluate the composition of the surrounding microenvironment. Once a cell is bound to a specific ligand, that bound complex can either produce mechanical or biochemical signaling conditions which can influence events that impact the local microenvironment that surrounds the cell. The identity and profile of integrins present on the cell surface may be modulated in response to developmental events in the progression of pathophysiological disease states [302].

The mechanistic events that regulate SMC migration into the arterial intima play an important role in atherosclerosis. While these mechanisms may seem to play a negative role in native tissue, they could prove to be advantageous in the tissue engineering of a blood vessel. During arterial remodeling, both nondividing and proliferating SMCs migrate out of the muscle media and through the internal elastic lamina to increase the intimal SMC number. Factors that affect the cell's ability to adhere to the ECM alter the

balance between cells stability and cell mobility [305]. In terms of tissue engineering, the desired role of a cell is to first enter the mobile state and then progress towards a more stable state as the scaffold material is taken over by cells and remodeled. Two of the major components of the ECM which surround medial SMCs are COL type I and ELAS. COL type I is known to promote cell adhesion and migration in addition to influencing the phenotypic appearance of the SMC [305]. *In vivo*, it has been traditionally thought that ELAS was a protein which did not retain the typical ligands which bind cellular integrins and therefore did not participate in cellular adhesion. However, recent evidence points towards an EBP sequence, Val-Ala-Pro-Gly (VAPG), which has shown to possess adhesive properties when seeded with SMCs. These ELAS sequences have been shown to bind to non-integrin receptors, a galactoside-binding protein, with high affinity [306]. Furthermore, the $\alpha v\beta 3$ integrin has demonstrated an affinity to the VGVAPG sequence which is associated with the EBP sequence [307].

The ligands which bind integrins to COL have been well established. There are four COL-binding integrins, $\alpha 1$, $\alpha 2$, $\alpha 10$, and $\alpha 11$ which each complex with a $\beta 1$ subunit to form a functioning receptor. The $\alpha 1\beta 1$ integrin has been implicated in activation of the Ras-MAPK signaling cascade, which directs cellular functions such as proliferation and survival [308]. The $\alpha 2\beta 1$ integrin on ECs is involved in angiogenesis; however, this integrin also play a role in platelet activation and aggregation [303, 308, 309]. A defining feature of COL is a tightly packed left-handed triple helix made of polypeptide segments with repeating GXY triplets. The small Gly residue fits in the interior of the triple helix, and the X and Y positions are often occupied by proline and hydroxyproline residues

[310]. Several recognition sequences have been identified, GFOGER and GLOGER (where O is hydroxyproline) represent binding sites for α1β1 and α2β1 [308, 311]. Additionally, these same integrins can interact with other amino acid sequences present in COL, which can be more promiscuous, such as Arg-Gly-Asp (RGD). Nevertheless, the binding of the α1β1 and α2β1 integrins to RGD sequences are done in an RGD-*independent* manner, whereas αvβ3 binds very strongly to denatured COL in a RGD-*dependent* manner [312].

In order to display these proteins to SMCs in matrix form via a scaffold, several scaffolding techniques have been employed. One of those, electrospinning, has demonstrated great promise in the field of vascular tissue engineering. Our lab has recently electrospun vascular materials in combination with COL type I, ELAS, and SF [109, 111-113, 152]. Additionally, there have been multiple other studies performed on electrospun COL, ELAS, and SF scaffolds, displaying cell adhesion under normal cell culture conditions [131, 133, 287, 313], which include fetal bovine serum (a liquid containing high concentrations of adhesive proteins). However, none of those studies performed any analysis on their integrin binding characteristics. Therefore, we aimed to study the adhesion of human umbilical artery smooth muscle cells (hUASMC) to blends of PCL, COL, ELAS, and SF through a cell adhesion inhibition experiment using anti-integrin β1 and anti-integrin β3 to further elucidate the cellular properties of these commonly electrospun proteins.

Materials and Methods

Protein Extraction

SF was extracted from the cocoons of *Bombyx mori* silk worms (The Yarn Tree) through an established protocol [280]. Briefly, SF cocoons are cut into pieces and boiled in a 0.02 M Na_2CO_3 (Sigma Aldrich) solution for 30 minutes to remove the sericin gum, followed by thorough rinsing in de-ionized water (DI), and drying in a fume hood. The SF is then dissolved in a LiBr (Fisher Scientific) solution at 60°C for 4 hours. This solution is then dialyzed against deionized water for 3 days using 3500 MWCO dialysis tubing (Fisher Scientific). The SF solution is then frozen and lyophilized to provide a pure SF for electrospinning.

COL type I was extracted from 6 month bovine corium through an acetic acid based process previously described [262]. Briefly, tissue is homogenized, suspended in acetic acid, and subsequently purified via a series of dissolutions, precipitations (using NaCl (Fisher Scientific) and Tris (Fisher Scientific)), and dialyses [263]. Following the final dialysis, COL solutions are frozen and lyophilized.

Electrospinning

The electrospinning setup consisted of a syringe pump (KD Scientific), a high voltage power supply (Spellman CZE1000R, Spellman High Voltage Electronics Corp.), a plastic Becton Dickinson syringe used as the polymer reservoir, attached to an 18-gauge blunt-tip needle. Concentrations of 150 mg/ml of PCL (MW: 125,000, Lakeshore Biomaterials), 200 mg/ml of soluble ELAS from bovine neck ligament (Elastin Products Co. Inc.), 70 mg/ml of COL I (6 month bovine corium), and 80 mg/ml of SF were dissolved in HFP (TCI America). To create scaffolds for cellular adhesion testing,

polymers were blended in volume ratios of 100-0 and 50-50 PCL-COL, PCL-ELAS, and PCL-SF.

Crosslinking

Scaffolds were cross-linked using EDC (FlukaBiochemika). Using EDC, a 50 mM crosslinking solution was prepared in 90 % ethanol (Fisher Scientific). Prior to cellular adhesion scaffolds were placed in the EDC solution, and allowed to cross-link for 18 hours followed by a 0.1M Na_2HPO_4 rinse for 1 hour and a 2 PBS rinses each for 1 hour.

Cell Culture

Human umbilical artery smooth muscle cells (hUASMC, Lonza CC-2579) were cultured in smooth muscle growth media purchased from Lonza (SmGM-2 Bulletkit, CC-3182) and incubated at 37^{o}C in 5% CO_2. hUASMCs were grown to 90% confluency and subsequently trypsinized using 0.05 % Trypsin (Gibco) and suspended in serum-free 1x DMEM (Invitrogen) at a density of 500,000 cells/ml between *passage 3 and 7* (according to Lonza protocols hUASMCs have a maximum passage limit of 15).

Antibodies

For antibody experimentation cell were suspended in serum-free medium at a concentration of 500,000 cells/ml and were incubated with a 1:100 dilution of antibody for a period of 30 minutes at room temperature (RT). For this experiment, anti-integrin beta 1 (β1, Millipore, MAB1987Z) and anti-integrin beta 3 (β3, Millipore, MAB2023Z) were used to inhibit cell adhesion to protein substrates.

TCP Protein Coating Adhesion Assay

Cells were initially tested to determine antibody effectiveness in a 96-well plate. Figure 38a displays the optimal cell seeding density for using the LiCor Odyssey imaging technique. Cells were plated at densities of 0, 2500, 5000, 7500, 12500, and 25000 cells/well to determine the ideal density so that the inhibition assays would not be influenced by cell-cell adhesion. According to Figure 38a, the preferred cell density for hUASMCs were 7500 cells/well. Figure 38b displays an adhesion inhibition assay using integrin antibodies β1 and β3 on COL coated wells with 50 μg/ml of PureCol COL (pCol, Inamed). Here, cells were plated at 7500 cells/well and incubated at 37°C and 5% CO_2 for 20, 30, and 40 minutes. This determined the effectiveness of the antibodies at inhibiting cell adhesion to the protein coated well. According to Figure 38b, antibodies appeared most effective at an incubation period of 30 minutes with a significant difference between β1 and β3.

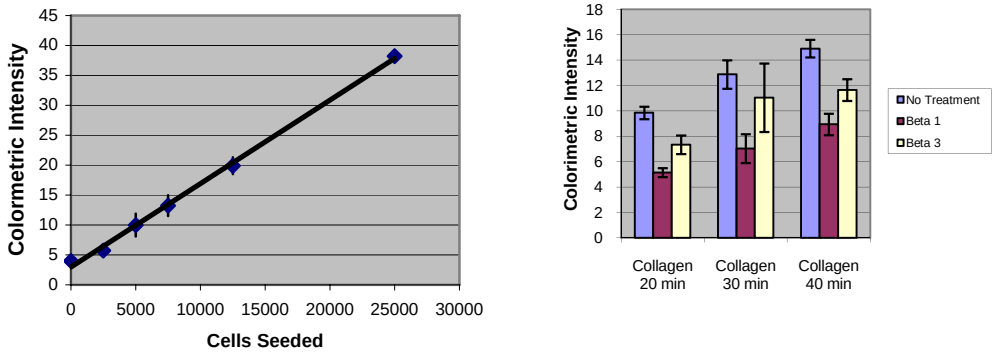

Figure 38. (a) Left figure represents the colormetric intensity as it relates to cell seeding density for a 96-well plate. (b) Right figure represents the colormetric intensity as it relates to the time dependency for cell adhesion with no treatment, anti-integrin β1, and anti-integrin β3.

Once these protocols were established, a protein experiment was carried out using 50 μg/ml pCol, 50 μg/ml fibronectin (FN) dissolved in 1x PBS, 200 mg/ml ELAS (Elastin Products Company, ES12) dissolved in 1x PBS and HFP, 50 μg/ml extracted COL (6 month bovine corium) dissolved in 1x PBS and 70 mg/ml dissolved in HFP, and 1 % bovine serum albumin (BSA) dissolved in 1x PBS. Proteins dissolved in HFP were plated into the 96-well plate and allowed to dry overnight under a fume hood. Proteins dissolved in 1x PBS were plated at 100 μl along with 100 μl of 1x PBS placed into the wells containing HFP dissolved protein. The 96-well plate was then covered and incubated at 4°C for 24 hours. After 24 hours, wells were washed 3 times with 1x PBS, and subsequently seeded with 7500 cells/well and incubated for 30 minutes at 37°C and 5 % CO_2. All samples were done in triplicate.

LiCor Odyssey Imaging

After 30 minutes of incubation, 96-well plates were inverted and shaken twice to remove non-adherent cells. Immediately following, wells were washed once with 100 μl of 1x PBS and fixed using a 10 % buffered formalin solution (Fisher Scientific) for 24 hours at 4°C. Next, fixing solution was removed and cells were permeabilized with five washes using 1x PBS containing 0.1% Triton X-100 for 5 minutes per wash. This was followed with Odyssey Blocking Buffer (LiCor) for 1.5 hours at RT. Next, the primary antibody, glyceraldehyde 3-phosphate dehydrogenase (GAPDH, Sigma, G9545-200UL), was diluted 1:5000 in blocking buffer and incubated with the scaffold at 4°C for 24 hours. The scaffolds were then washed with 0.1 % Tween-20 for 5 minutes at RT for 5 washes. IRDye 800 (LiCor) was then diluted at 1:1000 and incubated with the scaffolds at RT for 1

hour. Finally, the scaffolds were then washed again with 0.1 % Tween-20 for 5 minutes at RT for 5 washes. The scaffolds were then placed on the Odyssey Imager scanning bed for imaging at 800 nm.

Scaffold Cell Adhesion Assay

Scaffolds were either cross-linked as described above or left uncross-linked. All scaffolds were then sterilized in 90% ethanol for 30 minutes and subsequently washed for 10 minutes 3x at RT. Next, scaffolds were secured in a 96-well Bio-Rad® Dot Blot and 150 µl of proteins were added to specific lanes. Lane 1 = no cells, lane 2 = cells no treatment (NT), lane 3 = 1% BSA, lane 4 = 50 µg/ml FN, lane 5 = anti-integrin β1, and lane 6 = anti-integrin β3. All lanes were done in triplicate. Lanes 1, 2, 5, and 6 were filled with 150 µl of 1x PBS since they did not contain proteins in order to maintain scaffold wetness. The blotter/scaffolds were then covered with parafilm and stored at 4°C for 24 hours. All wells were then filled with 100 µl of 1 % BSA for 5 minutes and washed 3x with 200 µl of 1x PBS prior to cell seeding.

hUASMCs were first passaged using 0.05 % Trypsin and suspended in serum-free 1x DMEM at a density of 500,000 cells/ml. Figure 39 determined the proper seeding density for PCL-COL scaffolds to ensure only cell-substrate adhesion. Cells were seeded onto both electrospun PCL and PCL-COL scaffolds at densities of 0, 2500, 5000, 10000, 25000, and 75000 cells/well. Scaffolds were incubated for 30 minutes at 37°C and 5 % CO_2, inverted and shaken twice to remove non-adherent cells. The blotter was then opened and scaffolds were washed twice in 1x PBS and fixed with 10 % buffered formalin. Scaffolds were then imaged using 4',6-diamidino-2-phenylindole (DAPI, Invitrogen)

fluorescent stain and counted. According to the graph, 0, 2500, and 5000 cells/well was too low a number to produce significant differences between PCL and PCL-COL. Therefore, 20,000 cells/well was chosen as a density which would provide significant differences and cell-substrate adhesions.

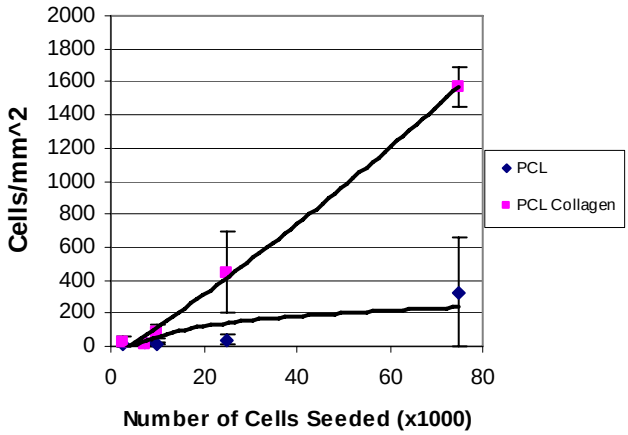

Figure 39. Represents the cells counted per unit of area as it relates the density of cells seeded onto electrospun PCL and PCL-COL scaffolds.

For all scaffolds, 400,000 cells/ml was placed in a separate vial, where a primary antibody for integrin β1 or β3 was added at a 1:100 dilution. Both vials containing anti-integrin β1 and anti-integrin β3 were allowed to sit at RT for 30 minutes. Following this, each well of the blotter was filled with 50 µl of serum-free 1x DMEM, and 50 µl of untreated cell suspensions were added to each well for lanes 1, 2, 3, and 4. 50 µl of anti-integrin β1 and anti-integrin β3 was added to lanes 5 and 6, respectively. The blotter/scaffolds were then placed in the incubator for 30 minutes at 37^{o}C and 5 % CO_2. After time expired, the blotter was inverted and shaken twice. Scaffolds were then

extracted from the blotter and washed twice in 1x PBS followed immediately with fixation in 10% buffered formalin for 24 hours at 4^{o}C.

DAPI Imaging

To image, scaffolds were prepared as mentioned above. After fixation, scaffolds were incubated with a 1:1000 dilution of DAPI for 10 minutes. Each blot was then imaged in 4 separate areas at a magnification of 10x. These images were then used to count the cell nuclei using the Cell Counting plugin for ImageJ version 1.44. The area in which the cells were counted was then measured and cell counts were reported as cells counted per square millimeter and as a percentage of the positive control, FN.

Results

SDS-page gel results in Figure 40 demonstrated that extracted and electrospun COL retained its α1(III), α1(II) and α2(I) chains, indicating a retention of the triple helical structure. Gelatin (denatured COL) has been shown to produce a smear [314]. This indicates that gelatin has undergone a change in its overall structure due to denaturation, losing its triple helical qualities, and, more importantly, its alpha chains. ELAS did not demonstrate any specific molecular weights, appearing also as a smear; however, its recovered electrospun form contained no smear possibly showing a change in structure.

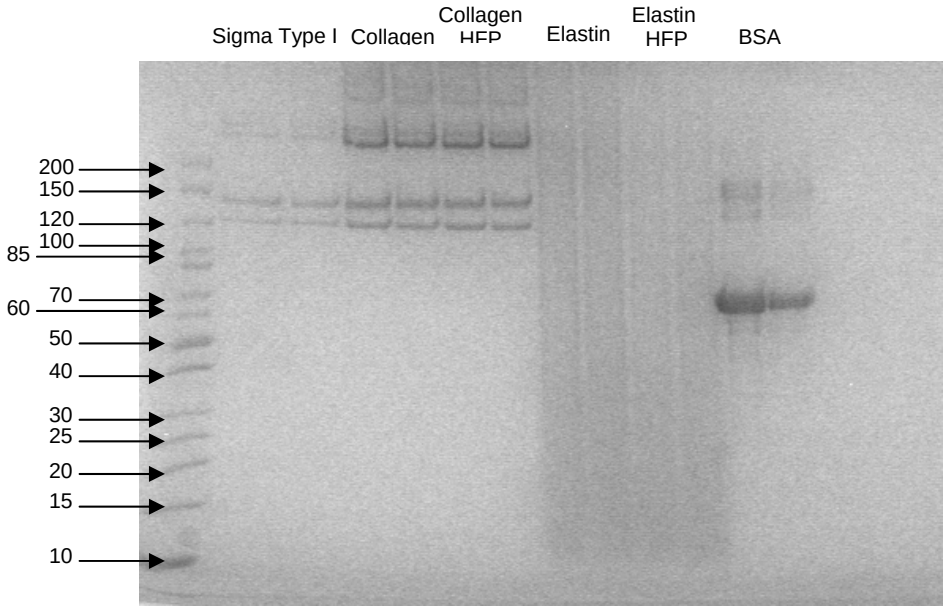

Figure 40. SDS-page gel electrophoresis of Sigma COL, extracted COL dissolved in DI water, extracted COL dissolved in HFP, ELAS dissolved in DI water, ELAS dissolved in HFP, and BSA dissolved in DI water.

A preliminary cell adhesion experiment (Figure 41A and B) using protein coatings in a 96 well plate was performed to determine if differences amongst the proteins existed and if differences in integrin binding affinity occurred. Extracted COL, pureCol COL, and FN (dissolved in deionized (DI) water) were tested with anti-integrin β1 and anti-integrin β3 to determine if the antibodies were decreasing SMC adhesion. All three proteins displayed a decrease in adhesion with both β1 and β3 antibodies. It was expected that COL proteins would display a more significant decrease using the β1 antibody in comparison to using the β3 antibody. However, since COL has been shown to present both RGD peptides and COL specific peptide sequences then it is possible that both of these protein would display a decrease in adhesion but not a knockout. Additionally, the hUASMCs used in this experiment contain integrins with both β1 and β3 specificity. A

major question surrounding the electrospinning of proteins is the possibility of denaturing the proteins using a fluoroalcohol such as HFP. The results from this preliminary adhesion study demonstrated that COL dissolved in HFP had excellent adhesion, a significant decrease *($p < 0.05$)* in cell number with anti-integrin β1, but no difference with anti-integrin β3, indicating that COL was not denatured by HFP especially since the β3 antibody did not display a greater decrease in adhesion when compared to the β1 antibody. ELAS dissolved in HFP demonstrated poor adhesion which was similar to that of BSA (negative control), while ELAS dissolved in PBS decreased cell adhesion but did not completely inhibit it. The results from the ELAS study demonstrated that a conformational change in the soluble ELAS protein occurs when dissolved in HFP, possibly denaturing the VAVPG peptide sequence. This preliminary study thus led to a full electrospun scaffold experiment.

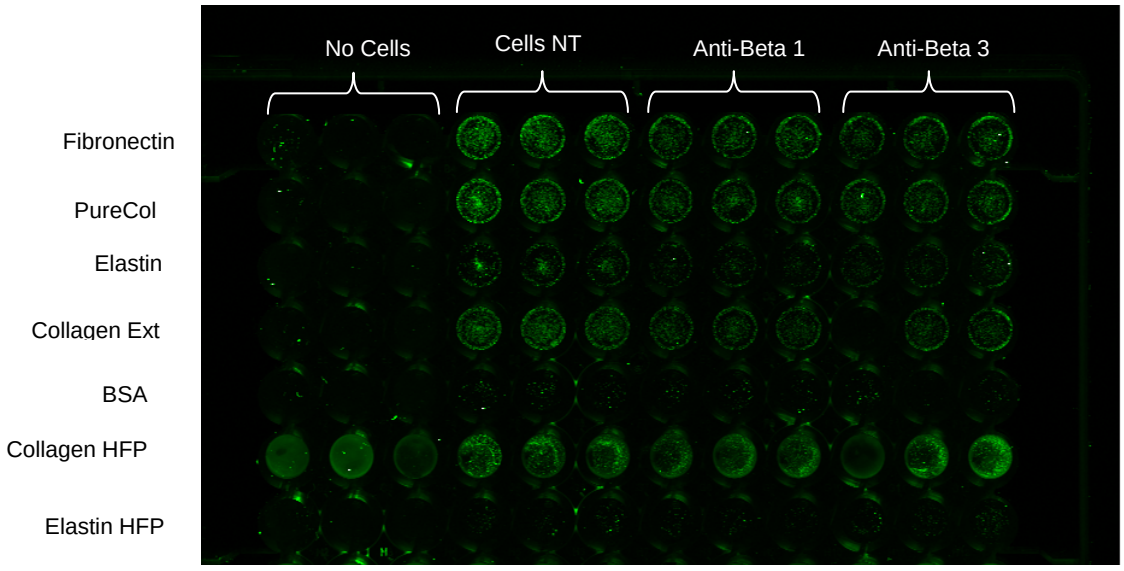

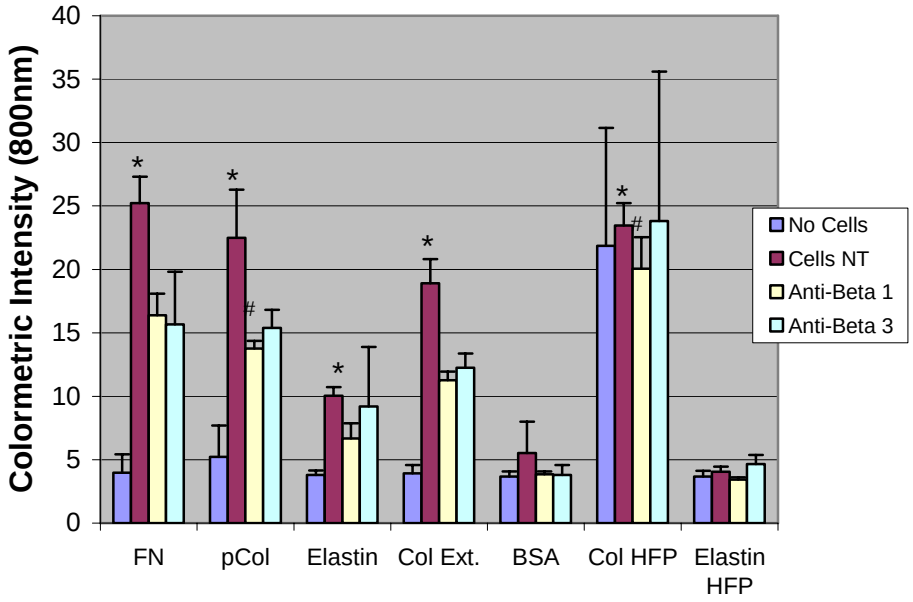

Figure 41. Cell adhesion using in cell Western assay with 96 well plate coated with FN, pureCol (pCol), ELAS, extracted COL (Col Ext), BSA, COL in HFP, and ELAS in HFP. (A) LiCor Odyssey image taken at 800 nm. (B) Graph representation of the data collected from A. * represents a significant difference from β1 and β3. # represents a significant difference from β3.

In view of the fact that the data in Figure 41 displayed formidable characteristics of β1 and β3 antibodies, scaffolds containing a 50-50 blend using PCL-COL, PCL-elasitn, and PCL-SF were electrospun. Figure 42 exhibited similar results to the data in Figure 41, where COL blended scaffolds displayed a significant decrease *($p < 0.05$)* in adhesion using both β1 and β3 antibodies. In this case, β1 exhibited a larger decrease in cellular adhesion compared to β3. Furthermore, NT scaffolds were not different from the positive control, FN. This indicated that peptides to which the integrins were bound were not denatured in the COL scaffolds due to HFP being used as the solvent. BSA, the negative control, also displayed significant differences *($p < 0.05$)* from NT and FN, which could indicate a number of non-specific binding sites were blocked, an unexpected result. The data from the scaffold experiments also demonstrated that the ELAS had no available binding sites for the hUASMCs. Finally, PCL-SF displayed adequate protein adsorption characteristics where FN was significantly different *($p < 0.05$)* from β1, β3, BSA, and NT. There was no β1 integrin binding specificity to the SF blended scaffolds. The NT scaffolds for PCL-SF were significantly different *($p < 0.05$)* from both BSA and β3, a possible suggestion that there is some binding affinity occurring for β3 which may involve a promiscuous RGD peptide. NT PCL-COL demonstrated a significant increase in cell attachment (288 cells/mm^2) when compared to NT PCL (49 cells/mm^2), displaying the advantages of the inclusion of COL.

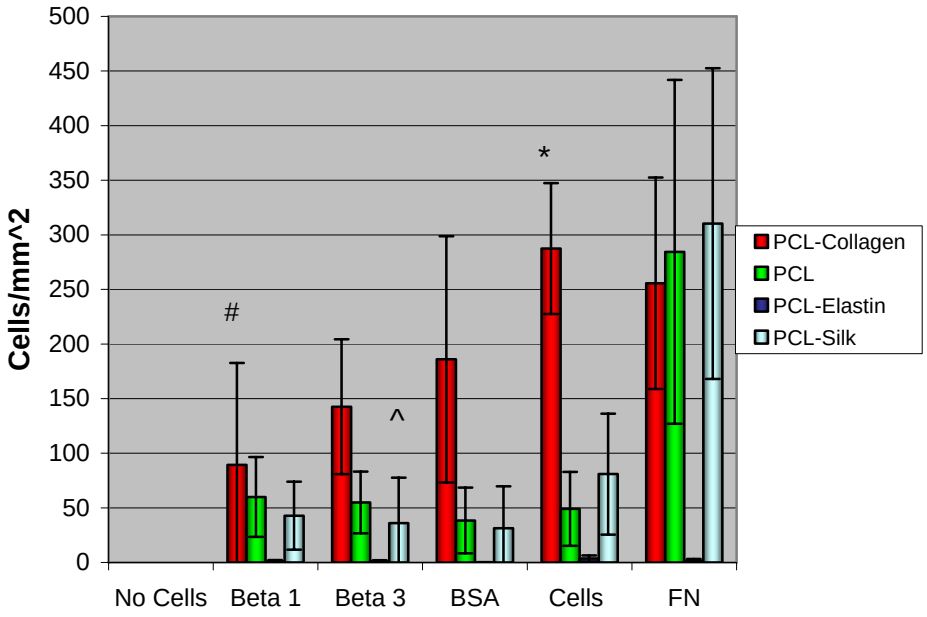

Figure 42. Cell adhesion using DAPI staining with uncross-linked PCL, PCL-COL, PCL-ELAS, and PCL-SF. Results are displayed as cells/mm^2. * represents a significant difference from β1 and β3. # represents a significant difference from β3. ^ represents a significant different from Cells NT.

Figure 43 displayed the data using 50mM EDC cross-linked scaffolds to determine if cross-linking would affect the presentation of the peptide sequences. The data suggested no significant differences between PCL and PCL-COL scaffolds. This is clearly presented in Figure 43, where there are no differences between β1, β3, BSA, NT, and FN for both PCL and PCL-COL scaffolds. PCL-ELAS, similar to Figure 42, exhibited differences from both PCL and PCL-COL where cellular attachment was almost non-existent. According to the data presented here, cross-linking using a high molarity of EDC, 50 mM, significantly affected the adhesion of hUASMCs to the electrospun substrates. Additionally, average cell counts for PCL between Figures 43 and 44 display similarities, indicating that it was the cross-linking of cellular adhesive proteins and not the EDC itself.

Furthermore, average values of cell counts between uncross-linked and cross-linked NT PCL-COL scaffolds decreased by 73% when cross-linked with EDC.

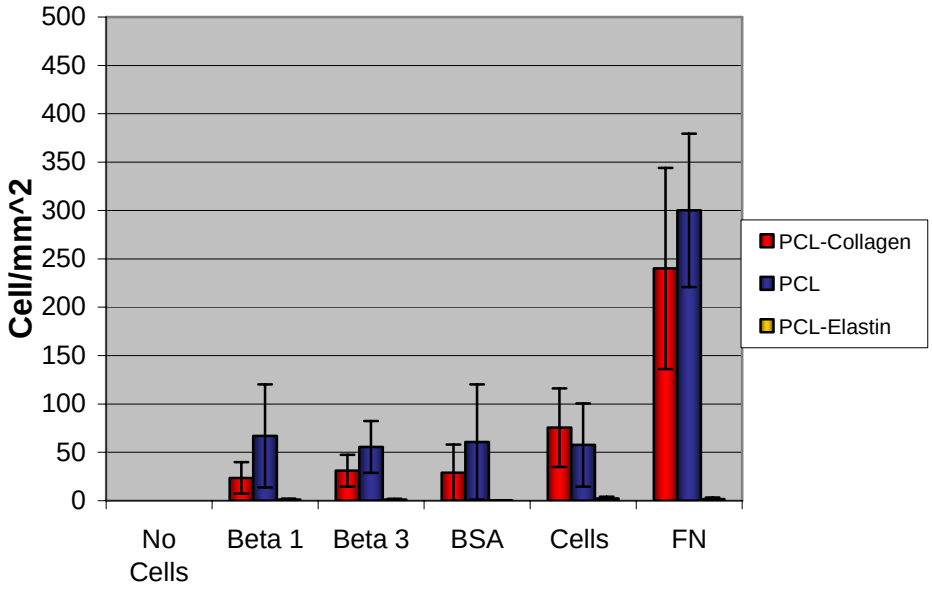

Figure 43. Cell adhesion using DAPI staining with EDC cross-linked PCL, PCL-COL, and PCL-ELAS. Results are displayed as cells/mm^2.

In order to normalize the data presented in Figures 43 and 44, each sample group was calculated as a percentage of FN for both uncross-linked and cross-linked electrospun scaffolds. Results depicted here displayed the same results as found in Figures 43 and 44. This supported those findings through the normalization of the number of cells counted per square millimeter, thereby removing any slight variances in number of cells seeded between each sample run. ELAS blended scaffolds were not displayed in the percentage of FN graphs because of their low and variable cell number, which did not properly demonstrate their low adhesive qualities. The results from Figure 44 reiterate the results found in both Figures 43 and 44, demonstrating that the normalized data still reflected the results from the actual cell counts. The association between these also demonstrated that

cell counting using the DAPI stain technique produced formidable results, verifying its use for future applications.

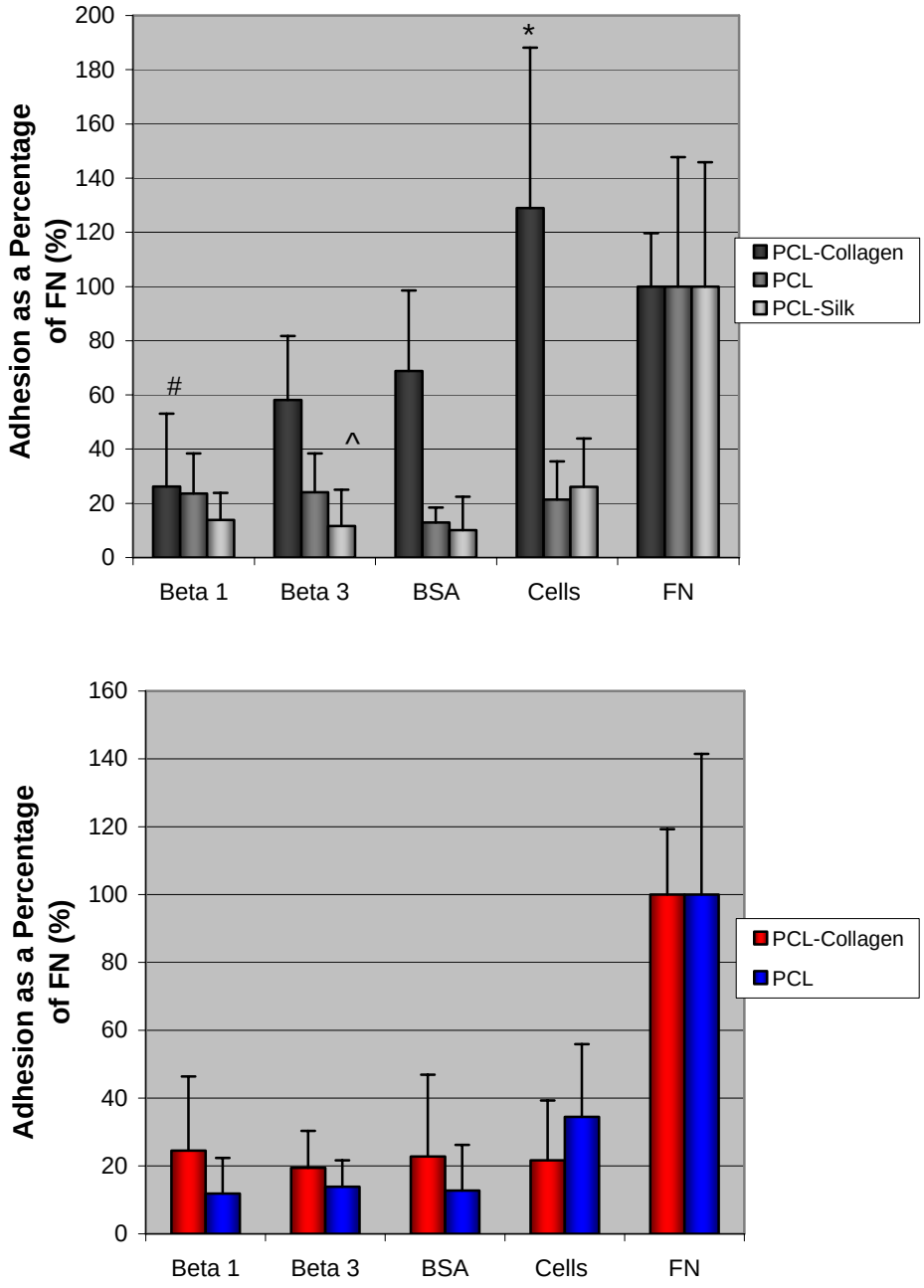

Figure 44. Cell adhesion using DAPI staining with uncrosslinked (A) and EDC cross-linked (B) PCL, PCL-COL, PCL-SF, and PCL-ELAS. Results are normalized and displayed as a percentage of FN.* represents a significant difference from β1 and β3. # represents a significant difference from β3. ^ represents a significant different from Cells NT.

Discussion

Generally, native artery displays characteristics where the media bears the majority of tension under *in vivo* conditions while the adventitia serves to protect the vessel from overstretch. In our tri-layered vascular graft design, the addition of ELAS provided our grafts with a higher compliance, while the addition of COL or SF served as the outer jacket-like layer to protect the graft from overstretch. This design proved to be advantageous through mechanical testing using dynamic compliance and burst strength.

In order to optimize the graft parameters using PCL, COL, ELAS and SF, cell adhesion characterization was performed in order to determine the specifics of integrin binding. It is well known that a number of integrins (α1β1, α2β1, α3β1) bind to COL in a RGD-independent manner and the αvβ3 integrin binds with high affinity to *denatured* COL in a RGD-dependent manner [312, 315]. It has also been suggested, in some cases, that the αvβ3 integrin binds to ELAS through the VAVPG complex [306]. However, debates still circulate about electrospun COL dissolved in HFP maintaining its triple helical structure and ultimately being recognized by cells. Furthermore, experiments using soluble ELAS have shown it to both bind cells and act as a binding inhibitor [316].

In past studies, we have demonstrated that electrospun COL exhibits a 67 nm repeat that resembles the native polymer [130]. To examine whether or not the electrospinning process alters the α chain content and thus the triple helix associated with COL, we performed an SDS-page gel electrophoresis on both COL and ELAS proteins to determine any degrees of denaturation due to HFP. According to the results, the recovered electrospun COL dissolved in HFP resembled that of the same COL dissolved in an aqueous medium. Additionally, COL from Sigma-Aldrich was tested using the same

aqueous medium to confirm the results found with our extracted COL samples. No visible denaturing of the alpha chains was present in the SDS gel. One difference seen between the Sigma COL and our extracted COL was that our extracted COL seemed to contain a few more proteins than anticipated, indicating that it may not be fully purified.

Both Zeugolis *et al.* and Yang *et al.* have found HFP to partially denature COL, however, neither group discussed the amount of time the COL samples were allowed to dissolve in HFP. If these proteins are becoming denatured when subjected to a fluoroalcohols, then there very well may be a time dependency for the protein dissolution prior to electrospinning. Under our conditions, both COL and ELAS are allowed to dissolve in HFP for approximately 10-20 minutes. The solutions are then immediately loaded into the syringe pumps and the electrospinning process is started. This appeared to allow the alpha chains of the COL protein to remain intact. It should be noted though that the SDS-page gel results did not include a pepsin digestion which could ultimately indicate whether or not the triple helix of COL is slightly unfolded or fully intact. Regardless, electrospun COL resembles nothing of gelatin either under SDS-page gels performed by Zeugolis or according to subcutaneous implantations [317], where massive inflammation and encapsulation was encountered with gelatin electrospun samples while COL electrospun samples experienced a low inflammatory response.

Preliminary data in a 96 well plate demonstrated that COL bound cells via integrin β1 and β3. Within this experiment, there did not seem to be a clear affinity for one over the other although the average colorimetric intensity was lower for β1 antibodies for COL coated samples. The fact that β1 antibodies were able to decrease cellular adhesion to the

protein coated TCP indicated that COL ligands were present amongst control groups and HFP dissolved groups. Once HFP dissolved COL had been established as non-denartured through SDS-page gel and preliminary protein coated wells we set out to produce electrospun scaffolds for containing 50-50 blends of PCL-COL compared to 100-0 blends. In this portion of the experiment, the data acquisition method was switched from a LiCor reader to nuclei counting due to the high background noise present on the electrospun samples. Staining cells and subsequently counting them in a fixed field of view is an established procedure which has been used in several publications [315, 318, 319]. Therefore, this technique, although labor intensive, was chosen to count the number of adhered cells to cross-linked or uncross-linked electrospun substrates.

Figures 43 and 45 plainly demonstrate the benefits of electrospun COL, where lanes with NT were similar to lanes treated with FN for both PCL and PCL-COL. Additionally, β1 and β3 antibodies significantly attenuated adhesion of the hUASMCs to the uncross-linked electrospun COL samples, whereas pure PCL samples had no affect. Impressively, percentatges of anti-integrin β1 for PCL-COL shown in Figure 44 were no different from PCL-β1 or BSA, and anti-integrin β3 was different from anti-integrin β1. This demonstrated a dominate presence of COL binding ligands specific to either α1β1 or α2β1, and a remaining percentage binding to RGD peptides through the β3 subunit. Moreover, the affinity of hUASMCs to bind to COL scaffolds through the β1 integrin demonstrated that electrospun COL retained its triple helical structure [308, 320]. Figure 43 and 44B, however, displayed results that implicated a loss of triple helical structure when scaffolds were cross-linked with 50 mM EDC, where NT was not different from

BSA, β1, or β3. Additionally, results from COL scaffolds were no different from PCL scaffolds. This attenuation of cell adhesion to the surface has been shown on cross-linked COL sponges following 7 and 10 days of culture [321], but has yet to be associated with cell adhesion inhibition assays. Therefore, an in-depth study as to the molecular reasons for this decrease in cell adhesion should be investigated in future studies.

ELAS samples were also studied in this experiment. As previously mentioned, extensive research has been performed by our lab with the use of soluble ELAS proteins and their mechanical benefits. However, recent implantation studies (data not shown) displayed little to no cellular infiltration of the vascular graft after 6 months *in vivo*. This was confounding and caused us to investigate the cellular characteristics of this protein further. Preliminary protein coatings (Figure 41B) displayed no integrin binding affinity for the β3 subunit in addition to showing adhesion characteristics similar to that of BSA (negative control). This indicated that the soluble ELAS protein, when dissolved in HFP, did not bind cells. This type of behavior was seen in a study done by Rodgers *et al.* where they looked to identify an integrin binding site on tropoelastin [307]. Nonetheless, the purchased soluble ELAS possesses the VAVPG peptide sequence, also known as the EBP. The ES12 proteins are extracted through an oxalic acid process, producing α, β, and κ ELAS proteins [140]. These proteins can be further purified into mainly α ELAS proteins. It may be these other β and κ proteins, which are masking any integrin binding sites, as α ELAS proteins have been shown to possess good adhesion properties [143]. Electrospun ELAS samples were also tested and similar results to the initial protein coating experiment

using a 96-well plate were found where cell numbers were almost non-existent regardless of whether or not the scaffolds were cross-linked or uncross-linked.

Finally, SF has been implicated in many studies as an excellent biopolymer with good cellular adhesion properties. Consequently, we observed whether or not SF displayed any peptide sequences which would bind hUASMCs. It was determined that SF did not contain integrin binding ligands for β1 subunits, but its NT was significantly different from anti-integrin β3 treated wells. Likewise, SF had a significantly higher NT cell count (81 cells/mm^2) than its negative control, BSA (31 cell/mm^2). This could indicate that SF does possess some peptide sequences for binding hUASMCs, but that these are significantly lower in number compared to either COL or FN. Sofia *et al.* performed a serum-free adhesion study using SF films cast from HFP. These materials were also supplemented with RGD peptides to increase binding affinity for osteoblasts [322]. It was shown that SF films had the lowest cell number in comparison to RGD-SF films. Here, electrospun SF displayed low cell number characteristics in comparison to electrospun COL; however, there were still differences when antibodies were added. Other studies have shown the amino acid composition of SF to contain large amounts of glycine (49.32), alanine (30.08), and serine (7.02) with small amounts of arginine (0.53) and aspartic acid (0.54) [323]. Therefore, it is possible that RGD peptide sequences do exist, but their prevalence may be too low and could thereby require supplementation to create adequate cell adhesion free of serum.

Conclusion

In conclusion we were able provide evidence which would further dispute the denaturation of COL proteins with the use of HFP through SDS-page gel electrophoresis and integrin binding. Additionally, we showed that ELAS scaffolds were not conducive to cellular attachment under serum-free conditions. This could explain the results that were seen in the vascular graft implantation studies, where little to no cell infiltration was observed. SF scaffolds demonstrated the possibility of containing small amounts of RGD peptides which bound the β3 subunits of hUASMCs. Future studies will need to assess the threshold concentrations for ELAS when it is added to PCL-COL or PCL-SF scaffolds. Currently, preliminary adhesion studies have already been performed and have displayed excellent cellular adhesion for 45-10-45 and 50-25-25 PCL-ELAS-COL scaffolds. Nonetheless, there is a slight decrease in cell number as more ELAS is added to the scaffold. More adhesion studies will be performed using 45-45-10 PCL-ELAS-COL blends to determine if ELAS will mask any COL proteins available for cellular attachment.

Conclusion and Future Studies

Overall this study demonstrated the ability to manufacture a tri-layered vascular graft composed of PCL, COL, ELAS, and SF. The percentage of biopolymers to add to the material blends was run through a series of tests to determine the optimal structure, which could be used towards future research *in vitro* and *in vivo*. Tri-layered grafts were found to be within the compliance range and exceeded the burst strength of native vessels. This data points towards a promising future with tri-layered grafts. Ideally, presenting a more tailorable degradation for each layer could bode well for potential graft testing. Through cellular studies it becomes questionable as to whether ELAS should remain a part of the material blends. Cellular testing also brought cross-linking into question as well. If these grafts are to regenerate tissue, the materials should not decrease cell adhesion during the intial periods after implantation. Therefore, several future experiments need to be addressed prior to animal implantation. First, futher cellular adhesion experiments need to be performed to determine the threshold of allowable ELAS in the graft layers. Second, cellular adhesion experiments should be carried out to determine the threshold of cross-linking molarity. These two experiments will help to resolve issues that were previously presented in the initial adhesion experiment. Finally, in order to design a more tailorable degradation rate in each layer of the graft structure, other synthetic biodegradable polymers, such as PDO, should be investigated. Preliminary data has already been performed in a 6 week degradation study where PCL-PDO blends of 70-30, 50-50, and 30-70 were tested for uniaxial tensile strength at time points of 1, 2, 4, and 6 weeks. These results demonstrated that the addition of PDO decreased degradation time. The quest for

the “Holy Grail” is a daunting one, but a multi-layered vascular graft design could potentially provide a new path to the ideal vascular graft.

Literature Cited

1. Rosamond, W., et al., Heart disease and stroke statistics--2008 update: a report from the American Heart Association Statistics Committee and Stroke Statistics Subcommittee. Circulation, 2008. 117(4): p. e25-146.
2. Boland, E.D., J.A. Matthews, K.J. Pawlowski, D.G. Simpson, G.E. Wnek, and G.L. Bowlin, Electrospinning collagen and elastin: Preliminary vascular tissue engineering. Front. Biosci., 2004. 9: p. 1422-1432.
3. Buijtenhuijs, P., et al., Tissue engineering of blood vessels: characterization of smooth-muscle cells for culturing on collagen-and-elastin-based scaffolds. Biotechnol. Appl. Biochem., 2004. 39: p. 141-149.
4. Greenwald, S.E. and C.L. Berry, Improving vascular grafts: the importance of mechanical and haemodynamic properties. The Journal Of Pathology, 2000. 190(3): p. 292-299.
5. Kannan, R.Y., H.J. Salacinski, P.E. Butler, G. Hamilton, and A.M. Seifalian, Current status of prosthetic bypass grafts: a review. J. Biomed. Mater. Res., Part B, 2005. 74B(1): p. 570-581.
6. Tiwari, A., K.S. Cheng, H. Salacinski, G. Hamilton, and A.M. Seifalian, Improving the patency of vascular bypass grafts: the role of suture materials and surgical techniques on reducing anastomotic compliance mismatch. Eur J Vasc Endovasc Surg, 2003. 25(4): p. 287-295.
7. Tiwari, A., H. Salacinski, A.M. Seifalian, and G. Hamilton, New prostheses for use in bypass grafts with special emphasis on polyurethanes. J. Cardiovasc. Surg., 2002. 10(3): p. 191-197.
8. Sarkar, S., T. Schmitz-Rixen, G. Hamilton, and A.M. Seifalian, Achieveing the ideal properties for vascular bypass grafts using a tissue engineered approach: a review. Med Bio Eng Comput, 2007. 45: p. 327-336.
9. Vara, D.S., H.J. Salacinski, R.Y. Kannan, L. Bordenave, G. Hamilton, and A.M. Seifalian, Cardiovascular tissue engineering: state of the art. Pathologic Biologie, 2005. 53: p. 599-612.
10. Thomas, A.C., G.R. Campbell and J.H. Campbell, Advances in vascular tissue engineering. Cardiovascular Pathology, 2003. 12: p. 271-276.
11. Wang, X., P. Lin, Q. Yao, and C. Chen, Development of small-diameter vascular grafts. World Journal of Surgery, 2007. 31: p. 682-689.
12. Xue, L. and H.P. Greisler, Biomaterials in the development and future of vascular grafts. Journal of Vascular Surgery, 2003. 37(2): p. 472-480.
13. Mitchell, S.L. and L.E. Niklason, Requirements for growing tissue-engineered vascular grafts. Cardiovascular Pathology, 2003. 12: p. 59-64.
14. Zarge, J.I., P. Huang and H.P. Greisler, Blood Vessels, in Principles of Tissue Engineering, R. Lanza, R. Langer, and W. Chick, Editors. 1997, R.G. Landes Company: Austin, Texas. p. 349-364.
15. Walpoth, B.H. and G.L. Bowlin, The daunting quest for a small diameter vascular graft. Expert Review of Medical Devices, 2005. 2(6): p. 647-651.

16. Bohr, D.F., A.P. Somlyo and H.V. Sparks, The Cardiovascular System, in Handbook of Physiology, S.R. Greiger, Editor. 1980, American Physiological Society: Bethesda. p. 1-31.
17. Pugsley, M.K. and R. Tabrizchi, The vascular system. An overview of structure and function. J Pharmacol Toxicol Methods, 2000. 44(2): p. 333-40.
18. Wagenseil, J.E. and R.P. Mecham, Vascular extracellular matrix and arterial mechanics. Physiol Rev, 2009. 89(3): p. 957-89.
19. Birukov, K.G., N. Bardy, S. Lehoux, R. Merval, V.P. Shirinsky, and A. Tedgui, Intraluminal pressure is essential for the maintenance of smooth muscle caldesmon and filamin content in aortic organ culture. Arterioscler Thromb Vasc Biol, 1998. 18(6): p. 922-7.
20. Harrison, D.G., The shear stress of keeping arteries clear. Nat Med, 2005. 11(4): p. 375-6.
21. Chatzizisis, Y.S., A.U. Coskun, M. Jonas, E.R. Edelman, C.L. Feldman, and P.H. Stone, Role of endothelial shear stress in the natural history of coronary atherosclerosis and vascular remodeling: molecular, cellular, and vascular behavior. J Am Coll Cardiol, 2007. 49(25): p. 2379-93.
22. Cummins, P.M., N. von Offenberg Sweeney, M.T. Killeen, Y.A. Birney, E.M. Redmond, and P.A. Cahill, Cyclic strain-mediated matrix metalloproteinase regulation within the vascular endothelium: a force to be reckoned with. Am J Physiol Heart Circ Physiol, 2007. 292(1): p. H28-42.
23. Hahn, C. and M.A. Schwartz, Mechanotransduction in vascular physiology and atherogenesis. Nat Rev Mol Cell Biol, 2009. 10(1): p. 53-62.
24. Younis, H.F., et al., Hemodynamics and wall mechanics in human carotid bifurcation and its consequences for atherogenesis: investigation of inter-individual variation. Biomech Model Mechanobiol, 2004. 3(1): p. 17-32.
25. Lehoux, S., Y. Castier and A. Tedgui, Molecular mechanisms of the vascular responses to haemodynamic forces. J Intern Med, 2006. 259(4): p. 381-92.
26. Lip, G.Y., Exacerbation of atherosclerosis by hypertension: potential mechanisms and clinical implications. Arch Intern Med, 1997. 157(11): p. 1265-6.
27. Wu, J.H., J. Hagaman, S. Kim, R.L. Reddick, and N. Maeda, Aortic constriction exacerbates atherosclerosis and induces cardiac dysfunction in mice lacking apolipoprotein E. Arterioscler Thromb Vasc Biol, 2002. 22(3): p. 469-75.
28. Li, C. and Q. Xu, Mechanical stress-initiated signal transduction in vascular smooth muscle cells in vitro and in vivo. Cell Signal, 2007. 19(5): p. 881-91.
29. Sawyer, P.N., Modern Vascular Grafts. 1987, New York: McGraw-Hill.
30. Wright, C.B., Vascular Grafting: Clinical Applications and Techniques. 1983, Boston: J. Wright, PSG Inc.
31. Chlupac, J., E. Filova and L. Bacakova, Blood vessel replacement: 50 years of development and tissue engineering paradigms in vascular surgery. Physiol Res, 2009. 58 Suppl 2: p. S119-39.
32. Herring, M.B., R. Dilley, R.A. Jersild, Jr., L. Boxer, A. Gardner, and J. Glover, Seeding arterial prostheses with vascular endothelium. The nature of the lining. Ann Surg, 1979. 190(1): p. 84-90.

33. Kadletz, M., R. Moser, P. Preiss, M. Deutsch, P. Zilla, and R. Fasol, In vitro lining of fibronectin coated PTFE grafts with cryopreserved saphenous vein endothelial cells. Thorac Cardiovasc Surg, 1987. 35 Spec No 2: p. 143-7.
34. Zilla, P., et al., Use of fibrin glue as a substrate for in vitro endothelialization of PTFE vascular grafts. Surgery, 1989. 105(4): p. 515-22.
35. Pratt, K.J., B.E. Jarrell, S.K. Williams, R.A. Carabasi, M.A. Rupnick, and F.A. Hubbard, Kinetics of endothelial cell-surface attachment forces. J Vasc Surg, 1988. 7(4): p. 591-9.
36. Shindo, S., A. Takagi and A.D. Whittemore, Improved patency of collagen-impregnated grafts after in vitro autogenous endothelial cell seeding. J Vasc Surg, 1987. 6(4): p. 325-32.
37. Prendiville, E.J., J.E. Coleman, A.D. Callow, K.E. Gould, S. Laliberte-Verdon, K. Ramberg, and R.J. Connolly, Increased in-vitro incubation time of endothelial cells on fibronectin-treated ePTFE increases cell retention in blood flow. Eur J Vasc Surg, 1991. 5(3): p. 311-9.
38. Ramalanjaona, G., R.F. Kempczinski, J.E. Rosenman, E.C. Douville, and E.B. Silberstein, The effect of fibronectin coating on endothelial cell kinetics in polytetrafluoroethylene grafts. J Vasc Surg, 1986. 3(2): p. 264-72.
39. van Wachem, P.B., C.M. Vreriks, T. Beugeling, J. Feijen, A. Bantjes, J.P. Detmers, and W.G. van Aken, The influence of protein adsorption on interactions of cultured human endothelial cells with polymers. J Biomed Mater Res, 1987. 21(6): p. 701-18.
40. Schneider, A., R.N. Melmed, H. Schwalb, M. Karck, I. Vlodavsky, and G. Uretzky, An improved method for endothelial cell seeding on polytetrafluoroethylene small caliber vascular grafts. J Vasc Surg, 1992. 15(4): p. 649-56.
41. Lee, Y.S., D.K. Park, Y.B. Kim, J.W. Seo, K.B. Lee, and B.G. Min, Endothelial cell seeding onto the extracellular matrix of fibroblasts for the development of a small diameter polyurethane vessel. Asaio J, 1993. 39(3): p. M740-5.
42. Bellon, J.M., J. Bujan, N.G. Honduvilla, A. Hernando, and J. Navlet, Endothelial cell seeding of polytetrafluoroethylene vascular prostheses coated with a fibroblastic matrix. Ann Vasc Surg, 1993. 7(6): p. 549-55.
43. Williams, S.K., et al., Adult human endothelial cell compatibility with prosthetic graft material. J Surg Res, 1985. 38(6): p. 618-29.
44. Kaehler, J., P. Zilla, R. Fasol, M. Deutsch, and M. Kadletz, Precoating substrate and surface configuration determine adherence and spreading of seeded endothelial cells on polytetrafluoroethylene grafts. J Vasc Surg, 1989. 9(4): p. 535-41.
45. Bowlin, G.L., A. Meyer, C. Fields, A. Cassano, R.G. Makhoul, C. Allen, and S.E. Rittgers, The persistence of electrostatically seeded endothelial cells lining a small diameter expanded polytetrafluoroethylene vascular graft. J Biomater Appl, 2001. 16(2): p. 157-73.
46. Bowlin, G.L., S.E. Rittgers, A. Milsted, and S.P. Schmidt, In vitro evaluation of electrostatic endothelial cell transplantation onto 4 mm interior diameter expanded polytetrafluoroethylene grafts. J Vasc Surg, 1998. 27(3): p. 504-11.

47. Wesolowski, S.A., C.C. Fries, R.T. Domingo, W.J. Liebig, and P.N. Sawyer, The compound prosthetic vascular graft: A pathologic survey. Surgery, 1963. 53(1): p. 19-44.
48. Wesolowski, S.A., C.C. Fries, A. Martinez, and J.D. McMahon, Arterial prosthetic materials. Annals of The New York Academy Of Sciences, 1968. 146(1): p. 325-344.
49. Bowald, S., C. Busch and I. Eriksson, Arterial regeneration following polyglactin 910 suture mesh grafting. Surgery, 1979. 86(5): p. 722-729.
50. Bowald, S., C. Busch and I. Eriksson, Absorbable material in vascular prostheses: A new device. Acta Chir Scand, 1980. 146: p. 391-395.
51. Greisler, H.P., Arterial regeneration over absorbable prostheses. Archives of Surgery, 1982. 117: p. 1425-1431.
52. Greisler, H.P., J.W. Dennis, E.D. Endean, J. Ellinger, K.F. Buttle, and D.U. Kim, Derivation of neointima in vascular grafts. Circulation, 1988. 78(3, Part 2): p. I6-12.
53. Greisler, H.P., J. Ellinger, T.H. Schwarcz, J. Golan, R.M. Raymond, and D.U. Kim, Arterial regeneration over polydioxanone prostheses in the rabbit. Archives Of Surgery, 1987. 122(6): p. 715-721.
54. Campbell, G.R. and J.H. Campbell, Development of tissue engineered vascular grafts. Curr Pharm Biotechnol, 2007. 8(1): p. 43-50.
55. Asahara, T., et al., Isolation of putative progenitor endothelial cells for angiogenesis. Science, 1997. 275(5302): p. 964-7.
56. Asahara, T., et al., Bone marrow origin of endothelial progenitor cells responsible for postnatal vasculogenesis in physiological and pathological neovascularization. Circ Res, 1999. 85(3): p. 221-8.
57. Shin'oka, T., et al., Midterm clinical result of tissue-engineered vascular autografts seeded with autologous bone marrow cells. J Thorac Cardiovasc Surg, 2005. 129(6): p. 1330-8.
58. Campbell, J.H., J.L. Efendy and G.R. Campbell, Novel vascular graft grown within recipient's own peritoneal cavity. Circ Res, 1999. 85(12): p. 1173-8.
59. Chue, W.L., et al., Dog peritoneal and pleural cavities as bioreactors to grow autologous vascular grafts. J Vasc Surg, 2004. 39(4): p. 859-67.
60. Nieponice, A., et al., In vivo assessment of a tissue-engineered vascular graft combining a biodegradable elastomeric scaffold and muscle-derived stem cells in a rat model. Tissue Eng Part A. 16(4): p. 1215-23.
61. Alvarez-Cordero, R., E. Iporre Reyes, M. Guerrero Alcazar, and P. Hernandez-Jauregui, Evaluation of polyglycolic acid sutures in vascular surgery. J Surg Res, 1973. 15(1): p. 35-44.
62. Watts, D.R., S.H. Carr and R.P. Hohf, Poly(glycolic acid) sutures in canine vascular anastomoses. J Biomed Mater Res, 1976. 10(6): p. 867-77.
63. Lauritzen, C., Experimental studies on absorbable vascular grafts for microsurgery. Scand J Plast Reconstr Surg, 1983. 17(2): p. 133-5.
64. Niklason, L.E., J. Gao, W.M. Abbott, K.K. Hirschi, S. Houser, R. Marini, and R. Langer, Functional arteries grown in vitro. Science, 1999. 284(5413): p. 489-93.

65. Prabhakar, V., M.W. Grinstaff, J. Alarcon, C. Knors, A.K. Solan, and L.E. Niklason, Engineering porcine arteries: effects of scaffold modification. J Biomed Mater Res A, 2003. 67(1): p. 303-11.
66. Boland, E.D., T.A. Telemeco, D.G. Simpson, G.E. Wnek, and G.L. Bowlin, Utilizing acid pretreatment and electrospinning to improve biocompatibility of poly(glycolic acid) for tissue engineering. J Biomed Mater Res B Appl Biomater, 2004. 71(1): p. 144-52.
67. Iwasaki, K., K. Kojima, S. Kodama, A.C. Paz, M. Chambers, M. Umezu, and C.A. Vacanti, Bioengineered three-layered robust and elastic artery using hemodynamically-equivalent pulsatile bioreactor. Circulation, 2008. 118(14 Suppl): p. S52-7.
68. Allen, B.T., R.E. Sparks, M.J. Welch, N.S. Mason, C.J. Mathias, and R.E. Clark, Reduction of platelet deposition on vascular grafts using an antiplatelet graft coating technique. J Surg Res, 1984. 36(1): p. 80-8.
69. Lommen, E., S. Gogolewski, A.J. Pennings, C.R. Wildevuur, and P. Nieuwenhuis, Development of a neo-artery induced by a biodegradable polymeric vascular prosthesis. Trans Am Soc Artif Intern Organs, 1983. 29: p. 255-9.
70. van der Lei, B., H.L. Bartels, P. Nieuwenhuis, and C.R. Wildevuur, Microporous, complaint, biodegradable vascular grafts for the regeneration of the arterial wall in rat abdominal aorta. Surgery, 1985. 98(5): p. 955-63.
71. van der Lei, B., C.R. Wildevuur, P. Nieuwenhuis, E.H. Blaauw, F. Dijk, C.E. Hulstaert, and I. Molenaar, Regeneration of the arterial wall in microporous, compliant, biodegradable vascular grafts after implantation into the rat abdominal aorta. Ultrastructural observations. Cell Tissue Res, 1985. 242(3): p. 569-78.
72. van der Lei, B., C.R. Wildevuur, F. Dijk, E.H. Blaauw, I. Molenaar, and P. Nieuwenhuis, Sequential studies of arterial wall regeneration in microporous, compliant, biodegradable small-caliber vascular grafts in rats. J Thorac Cardiovasc Surg, 1987. 93(5): p. 695-707.
73. Stitzel, J.D., K.J. Pawlowski, G.E. Wnek, D.G. Simpson, and G.L. Bowlin, Arterial smooth muscle cell proliferation on a novel biomimicking, biodegradable vascular graft scaffold. J Biomater Appl, 2001. 16(1): p. 22-33.
74. Wang, S., Y. Zhang, H. Wang, G. Yin, and Z. Dong, Fabrication and properties of the electrospun polylactide/silk fibroin-gelatin composite tubular scaffold. Biomacromolecules, 2009. 10(8): p. 2240-4.
75. Zhu, A., F. Zhao and T. Ma, Photo-initiated grafting of gelatin/N-maleic acyl-chitosan to enhance endothelial cell adhesion, proliferation and function on PLA surface. Acta Biomater, 2009. 5(6): p. 2033-44.
76. Hibino, N., E. McGillicuddy, G. Matsumura, Y. Ichihara, Y. Naito, C. Breuer, and T. Shinoka, Late-term results of tissue-engineered vascular grafts in humans. J Thorac Cardiovasc Surg, 2010. 139(2): p. 431-6, 436 e1-2.
77. Mooney, D.J., C.L. Mazzoni, C. Breuer, K. McNamara, D. Hern, J.P. Vacanti, and R. Langer, Stabilized polyglycolic acid fibre-based tubes for tissue engineering. Biomaterials, 1996. 17(2): p. 115-24.

78. Yang, Z., et al., Sustained release of heparin from polymeric particles for inhibition of human vascular smooth muscle cell proliferation. J Control Release, 1999. 60(2-3): p. 269-77.
79. Edelman, E.R., A. Nathan, M. Katada, J. Gates, and M.J. Karnovsky, Perivascular graft heparin delivery using biodegradable polymer wraps. Biomaterials, 2000. 21(22): p. 2279-86.
80. Jay, S.M., B.R. Shepherd, J.P. Bertram, J.S. Pober, and W.M. Saltzman, Engineering of multifunctional gels integrating highly efficient growth factor delivery with endothelial cell transplantation. Faseb J, 2008. 22(8): p. 2949-56.
81. Zhu, W., T. Masaki, Y.H. Bae, R. Rathi, A.K. Cheung, and S.E. Kern, Development of a sustained-release system for perivascular delivery of dipyridamole. J Biomed Mater Res B Appl Biomater, 2006. 77(1): p. 135-43.
82. Qi, X., et al., Sustained delivery of sphingosine-1-phosphate using poly(lactic-co-glycolic acid)-based microparticles stimulates Akt/ERK-eNOS mediated angiogenesis and vascular maturation restoring blood flow in ischemic limbs of mice. Eur J Pharmacol, 2010. 634(1-3): p. 121-31.
83. Wen, S.J., et al., Human vascular smooth muscle cells and endothelial cells cocultured on polyglycolic acid (70/30) scaffold in tissue engineered vascular graft. Chin Med J (Engl), 2007. 120(15): p. 1331-5.
84. Roh, J.D., M.P. Brennan, R.I. Lopez-Soler, P.M. Fong, A. Goyal, A. Dardik, and C.K. Breuer, Construction of an autologous tissue-engineered venous conduit from bone marrow-derived vascular cells: optimization of cell harvest and seeding techniques. J Pediatr Surg, 2007. 42(1): p. 198-202.
85. Izhar, U., et al., Novel synthetic selectively degradable vascular prostheses: a preliminary implantation study. J Surg Res, 2001. 95(2): p. 152-60.
86. Shum-Tim, D., et al., Tissue engineering of autologous aorta using a new biodegradable polymer. Ann Thorac Surg, 1999. 68(6): p. 2298-304; discussion 2305.
87. Xu, C., F. Yang, S. Wang, and S. Ramakrishna, In vitro study of human vascular endothelial cell function on materials with various surface roughness. J Biomed Mater Res A, 2004. 71(1): p. 154-61.
88. Zhu, Y., C. Gao and J. Shen, Surface modification of polycaprolactone with poly(methacrylic acid) and gelatin covalent immobilization for promoting its cytocompatibility. Biomaterials, 2002. 23(24): p. 4889-95.
89. Serrano, M.C., M.T. Portoles, M. Vallet-Regi, I. Izquierdo, L. Galletti, J.V. Comas, and R. Pagani, Vascular endothelial and smooth muscle cell culture on NaOH-treated poly(epsilon-caprolactone) films: a preliminary study for vascular graft development. Macromol Biosci, 2005. 5(5): p. 415-23.
90. Serrano, M.C., R. Pagani, G.A. Ameer, M. Vallet-Regi, and M.T. Portoles, Endothelial cells derived from circulating progenitors as an effective source to functional endothelialization of NaOH-treated poly(epsilon-caprolactone) films. J Biomed Mater Res A, 2008. 87(4): p. 964-71.

91. Ma, Z., W. He, T. Yong, and S. Ramakrishna, Grafting of gelatin on electrospun poly(caprolactone) nanofibers to improve endothelial cell spreading and proliferation and to control cell Orientation. Tissue Eng, 2005. 11(7-8): p. 1149-58.
92. Duling, R.R., R.B. Dupaix, N. Katsube, and J. Lannutti, Mechanical characterization of electrospun polycaprolactone (PCL): a potential scaffold for tissue engineering. J Biomech Eng, 2008. 130(1): p. 011006.
93. Pektok, E., B. Nottelet, J.C. Tille, R. Gurny, A. Kalangos, M. Moeller, and B.H. Walpoth, Degradation and healing characteristics of small-diameter poly(epsilon-caprolactone) vascular grafts in the rat systemic arterial circulation. Circulation, 2008. 118(24): p. 2563-70.
94. Bolgen, N., Y.Z. Menceloglu, K. Acatay, I. Vargel, and E. Piskin, In vitro and in vivo degradation of non-woven materials made of poly(epsilon-caprolactone) nanofibers prepared by electrospinning under different conditions. J Biomater Sci Polym Ed, 2005. 16(12): p. 1537-55.
95. Nottelet, B., E. Pektok, D. Mandracchia, J.C. Tille, B. Walpoth, R. Gurny, and M. Moller, Factorial design optimization and in vivo feasibility of poly(epsilon-caprolactone)-micro- and nanofiber-based small diameter vascular grafts. J Biomed Mater Res A, 2008. 89(4): p. 865-75.
96. Drilling, S., J. Gaumer and J. Lannutti, Fabrication of burst pressure competent vascular grafts via electrospinning: effects of microstructure. J Biomed Mater Res A, 2009. 88(4): p. 923-34.
97. Lee, S.J., S.H. Oh, J. Liu, S. Soker, A. Atala, and J.J. Yoo, The use of thermal treatments to enhance the mechanical properties of electrospun poly(epsilon-caprolactone) scaffolds. Biomaterials, 2008. 29(10): p. 1422-30.
98. Vaz, C.M., S. van Tuijl, C.V. Bouten, and F.P. Baaijens, Design of scaffolds for blood vessel tissue engineering using a multi-layering electrospinning technique. Acta Biomater, 2005. 1(5): p. 575-82.
99. Williamson, M.R., R. Black and C. Kielty, PCL-PU composite vascular scaffold production for vascular tissue engineering: attachment, proliferation and bioactivity of human vascular endothelial cells. Biomaterials, 2006. 27(19): p. 3608-16.
100. Hanson, S.J., K. Jamshidi and R.C. Eberhart, Mechanical evaluation of resorbable copolymers for end use as vascular grafts. ASAIO Trans, 1988. 34(3): p. 789-93.
101. Watanabe, M., et al., Tissue-engineered vascular autograft: inferior vena cava replacement in a dog model. Tissue Eng, 2001. 7(4): p. 429-39.
102. Hibino, N., T. Shin'oka, G. Matsumura, Y. Ikada, and H. Kurosawa, The tissue-engineered vascular graft using bone marrow without culture. J Thorac Cardiovasc Surg, 2005. 129(5): p. 1064-70.
103. Lim, S.H., S.W. Cho, J.C. Park, O. Jeon, J.M. Lim, S.S. Kim, and B.S. Kim, Tissue-engineered blood vessels with endothelial nitric oxide synthase activity. J Biomed Mater Res B Appl Biomater, 2008. 85(2): p. 537-46.
104. Kwon, I.K., S. Kidoaki and T. Matsuda, Electrospun nano- to microfiber fabrics made of biodegradable copolyesters: structural characteristics, mechanical properties and cell adhesion potential. Biomaterials, 2005. 26(18): p. 3929-39.

105. Greisler, H.P., et al., Prostacyclin production by blood-contacting surfaces of endothelialized vascular prostheses. J Cardiovasc Surg (Torino), 1990. 31(5): p. 640-5.
106. Teebken, O.E., A.M. Pichlmaier and A. Haverich, Cell seeded decellularised allogeneic matrix grafts and biodegradable polydioxanone-prostheses compared with arterial autografts in a porcine model. Eur J Vasc Endovasc Surg, 2001. 22(2): p. 139-45.
107. Boland, E.D., B.D. Coleman, C.P. Barnes, D.G. Simpson, G.E. Wnek, and G.L. Bowlin, Electrospinning polydioxanone for biomedical applications. Acta Biomaterialia, 2005. 1: p. 115-123.
108. Smith, M.J., M.J. McClure, S.A. Sell, C.P. Barnes, B.H. Walpoth, D.G. Simpson, and G.L. Bowlin, Suture-reinforced electrospun polydioxanone-elastin small-diameter tubes for use in vascular tissue engineering: a feasibility study. Acta Biomater, 2008. 4(1): p. 58-66.
109. Sell, S.A., M.J. McClure, C.P. Barnes, D.C. Knapp, B.H. Walpoth, D.G. Simpson, and G.L. Bowlin, Electrospun polydioxanone-elastin blends: potential for bioresorbable vascular grafts. Biomedical Materials, 2006. 1(2): p. 72-80.
110. McClure, M.J., S.A. Sell, C.P. Barnes, W.C. Bowen, and G.L. Bowlin, Cross-linking Electrospun Polydioxanone-Soluble Elastin Blends: Material Characterization. Journal of Engineered Fibers and Fabrics, 2008. 3(1): p. 1-10.
111. McClure, M.J., S.A. Sell, D.G. Simpson, and G.L. Bowlin, Electrospun Polydioxanone, Elastin, and Collagen Vascular Scaffolds: Uniaxial Cyclic Distension. Journal Of Engineered Fibers And Fabrics, 2009. 4(2): p. 18-25.
112. Barnes, C.P., S.A. Sell, D.C. Knapp, B.H. Walpoth, D.D. Brand, and G.L. Bowlin, Preliminary investigation of electrospun collagen and polydioxanone for vascular tissue engineering applications. International Journal of Electrospun Nanofibers and Applications, 2007. 1: p. 73-87.
113. McClure, M.J., S.A. Sell, C.E. Ayres, D.G. Simpson, and G.L. Bowlin, Electrospinning-aligned and random polydioxanone-polycaprolactone-silk fibroin-blended scaffolds: geometry for a vascular matrix. Biomed Mater, 2009. 4(5): p. 055010.
114. Garg, K., S.A. Sell, P. Madurantakam, and G.L. Bowlin, Angiogenic Potential of Human Macrophages on Electrospun Bioresorbable Vascular Grafts. Biomed Mater, 2009. In Review.
115. Wolfe, P.S., P. Madurantakam, K. Garg, S.A. Sell, M. Beckman, and G.L. Bowlin, Evaluation of Thrombogenic Potential of Electrospun Bioresorbable Vascular Graft Materials: Acute Monocyte Tissue Factor Expression. J Biomed Mater Res A, 2009. In Review.
116. Guan, J., K.L. Fujimoto, M.S. Sacks, and W.R. Wagner, Preparation and characterization of highly porous, biodegradable polyurethane scaffolds for soft tissue applications. Biomaterials, 2005. 26(18): p. 3961-71.
117. Martz, H., G. Beaudoin, R. Paynter, M. King, D. Marceau, and R. Guidoin, Physicochemical characterization of a hydrophilic microporous polyurethane vascular graft. J Biomed Mater Res, 1987. 21(3): p. 399-412.

118. Martz, H., et al., Hydrophilic microporous polyurethane versus expanded PTFE grafts as substitutes in the carotid arteries of dogs. A limited study. J Biomed Mater Res, 1988. 22(1): p. 63-9.
119. Stankus, J.J., L. Soletti, K. Fujimoto, Y. Hong, D.A. Vorp, and W.R. Wagner, Fabrication of cell microintegrated blood vessel constructs through electrohydrodynamic atomization. Biomaterials, 2007. 28: p. 2738-2746.
120. El-Kurdi, M.S., Y. Hong, J.J. Stankus, L. Soletti, W.R. Wagner, and D.A. Vorp, Transient elastic support for vein grafts using a constricting microfibrillar polymer wrap. Biomaterials, 2008. 29(22): p. 3213-20.
121. Nieponice, A., L. Soletti, J. Guan, B.M. Deasy, J. Huard, W.R. Wagner, and D.A. Vorp, Development of a tissue-engineered vascular graft combining a biodegradable scaffold, muscle-derived stem cells and a rotational vacuum seeding technique. Biomaterials, 2008. 29(7): p. 825-33.
122. Soletti, L., Y. Hong, J. Guan, J.J. Stankus, M.S. El-Kurdi, W.R. Wagner, and D.A. Vorp, A bilayered elastomeric scaffold for tissue engineering of small diameter vascular grafts. Acta Biomater. 6(1): p. 110-22.
123. Hong, Y., S.H. Ye, A. Nieponice, L. Soletti, D.A. Vorp, and W.R. Wagner, A small diameter, fibrous vascular conduit generated from a poly(ester urethane)urea and phospholipid polymer blend. Biomaterials, 2009. 30(13): p. 2457-67.
124. Beckman, M.J., K.J. Shields and R.F. Diegelmann, Collagen. Encyclopedia of Biomaterials and Biomedical Engineering. 2004, New York: Marcel Dekker.
125. Barnes, C.P., S.A. Sell, E.D. Boland, D.G. Simpson, and G.L. Bowlin, Nanofiber technology: Designing the next generation of tissue engineering scaffolds. Advanced Drug Delivery Reviews, 2007. 59: p. 1413-1433.
126. Kolacna, L., et al., Biochemical and biophysical aspects of collagen nanostructure in the extracellular matrix. Physiol Res, 2007. 56 Suppl 1: p. S51-60.
127. Weinberg, C.B. and E. Bell, A blood vessel model constructed from collagen and cultured vascular cells. Science, 1986. 231(4736): p. 397-400.
128. Berglund, J.D., M.M. Mohseni, R.M. Nerem, and A. Sambanis, A biological hybrid model for collagen-based tissue engineered vascular constructs. Biomaterials, 2003. 24(7): p. 1241-54.
129. Cummings, C.L., D. Gawlitta, R.M. Nerem, and J.P. Stegemann, Properties of engineered vascular constructs made from collagen, fibrin, and collagen-fibrin mixtures. Biomaterials, 2004. 25(17): p. 3699-706.
130. Matthews, J.A., G.E. Wnek, D.G. Simpson, and G.L. Bowlin, Electrospinning of collagen nanofibers. Biomacromolecules, 2002. 3(2): p. 232-238.
131. Venugopal, J.R., Y.Z. Zhang and S. Ramakrishna, In vitro culture of human dermal fibroblasts on electrospun polycaprolactone collagen nanofibrous membrane. Artificial Organs, 2006. 30(6): p. 440-446.
132. Tillman, B.W., S.K. Yazdani, S.J. Lee, R.L. Geary, A. Atala, and J.J. Yoo, The in vivo stability of electrospun polycaprolactone-collagen scaffolds in vascular reconstruction. Biomaterials, 2009. 30(4): p. 583-8.
133. Ju, Y.M., J.S. Choi, A. Atala, J.J. Yoo, and S.J. Lee, Bilayered scaffold for engineering cellularized blood vessels. Biomaterials. 31(15): p. 4313-21.

134. He, W., Z. Ma, T. Yong, W.E. Teo, and S. Ramakrishna, Fabrication of collagen-coated biodegradable polymer nanofiber mesh and its potential for endothelial cells growth. Biomaterials, 2005. 26(36): p. 7606-15.
135. Jeong, S.I., et al., Tissue-engineered vascular grafts composed of marine collagen and PLGA fibers using pulsatile perfusion bioreactors. Biomaterials, 2007. 28: p. 1115-1122.
136. Park, I.S., S.H. Kim, Y.H. Kim, I.H. Kim, and S.H. Kim, A collagen/smooth muscle cell-incorporated elastic scaffold for tissue-engineered vascular grafts. J Biomater Sci Polym Ed, 2009. 20(11): p. 1645-60.
137. Rodgers, U.R. and A.S. Weiss, Cellular interactions with elastin. Pathol Biol (Paris), 2005. 53(7): p. 390-8.
138. Debelle, L. and A.M. Tamburro, Elastin: molecular description and function. Int J Biochem Cell Biol, 1999. 31(2): p. 261-72.
139. Vrhovski, B. and A.S. Weiss, Biochemistry of tropoelastin. Eur J Biochem, 1998. 258(1): p. 1-18.
140. Partridge, S.M. and H.F. Davis, The chemistry of connective tissues. 3. composition of the soluble proteins derived from elastin. Biochem. J., 1955. 61: p. 21-30.
141. Duca, L., N. Floquet, A.J. Alix, B. Haye, and L. Debelle, Elastin as a matrikine. Crit Rev Oncol Hematol, 2004. 49(3): p. 235-44.
142. Daamen, W.F., J.H. Veerkamp, J.C. van Hest, and T.H. van Kuppevelt, Elastin as a biomaterial for tissue engineering. Biomaterials, 2007. 28(30): p. 4378-98.
143. Leach, J.B., J.B. Wolinsky, P.J. Stone, and J.Y. Wong, Crosslinked alpha-elastin biomaterials: towards a processable elastin mimetic scaffold. Acta Biomater, 2005. 1(2): p. 155-64.
144. Li, M., M.J. Mondrinos, M.R. Gandhi, F.K. Ko, A.S. Weiss, and P.I. Lelkes, Electrospun protein fibers as matrices for tissue engineering. Biomaterials, 2005. 26(30): p. 5999-6008.
145. Welsh, E.R. and D.A. Tirrell, Engineering the extracellular matrix: a novel approach to polymeric biomaterials. I. Control of the physical properties of artificial protein matrices designed to support adhesion of vascular endothelial cells. Biomacromolecules, 2000. 1(1): p. 23-30.
146. Nicol, A., D.C. Gowda and D.W. Urry, Cell adhesion and growth on synthetic elastomeric matrices containing Arg-Gly-Asp-Ser-3. J Biomed Mater Res, 1992. 26(3): p. 393-413.
147. Wise, S.G., M.J. Byrom, A. Waterhouse, P.G. Bannon, M.K. Ng, and A.S. Weiss, A multilayered synthetic human elastin/polycaprolactone hybrid vascular graft with tailored mechanical properties. Acta Biomater.
148. Berglund, J.D., R.M. Nerem and A. Sambanis, Incorporation of Intact Elastin Scaffolds in Tissue-Engineered Collagen-Based Vascular Grafts. Tissue Eng, 2004. 10: p. 1526-1535.
149. Buttafoco, L., N.G. Kolkman, P. Engbers-Buijtenhuijs, A.A. Poot, P.J. Dijkstra, I. Vermes, and J. Feijen, Electrospinning of collagen and elastin for tissue engineering applications. Biomaterials, 2006. 27(5): p. 724-734.

150. Stitzel, J., et al., Controlled fabrication of a biological vascular substitute. Biomaterials, 2006. 27(7): p. 1088-94.
151. Lee, S.J., J.J. Yoo, G.J. Lim, A. Atala, and J. Stitzel, In vitro evaluation of electrospun nanofiber scaffolds for vascular graft application. J Biomed Mater Res A, 2007. 83(4): p. 999-1008.
152. McClure, M.J., S.A. Sell, D.G. Simpson, B.H. Walpoth, and G.L. Bowlin, A three-layered electrospun matrix to mimic native arterial architecture using polycaprolactone, elastin, and collagen: A preliminary study. Acta Biomater, 2010. 6(7): p. 2422-33.
153. Thomas, V., X. Zhang, S.A. Catledge, and Y.K. Vohra, Functionally graded electrospun scaffolds with tunable mechanical properties for vascular tissue regeneration. Biomed Mater, 2007. 2(4): p. 224-32.
154. Schaner, P.J., et al., Decellularized vein as a potential scaffold for vascular tissue engineering. J Vasc Surg, 2004. 40(1): p. 146-53.
155. Clarke, D.R., R.M. Lust, Y.S. Sun, K.S. Black, and J.D. Ollerenshaw, Transformation of nonvascular acellular tissue matrices into durable vascular conduits. Ann Thorac Surg, 2001. 71(5 Suppl): p. S433-6.
156. Wilson, G.J., D.W. Courtman, P. Klement, J.M. Lee, and H. Yeger, Acellular matrix: a biomaterials approach for coronary artery bypass and heart valve replacement. Ann Thorac Surg, 1995. 60(2 Suppl): p. S353-8.
157. Nemcova, S., A.A. Noel, C.J. Jost, P. Gloviczki, V.M. Miller, and K.G. Brockbank, Evaluation of a xenogeneic acellular collagen matrix as a small-diameter vascular graft in dogs--preliminary observations. J Invest Surg, 2001. 14(6): p. 321-30.
158. Lantz, G.C., S.F. Badylak, A.C. Coffey, L.A. Geddes, and W.E. Blevins, Small intestinal submucosa as a small-diameter arterial graft in the dog. J Invest Surg, 1990. 3(3): p. 217-27.
159. Gui, L., A. Muto, S.A. Chan, C.K. Breuer, and L.E. Niklason, Development of decellularized human umbilical arteries as small-diameter vascular grafts. Tissue Eng Part A, 2009. 15(9): p. 2665-76.
160. Rasmussen, B.L., E. Bruenger and L.B. Sandberg, A new method for purification of mature elastin. Anal Biochem, 1975. 64(1): p. 255-9.
161. Lu, Q., K. Ganesan, D.T. Simionescu, and N.R. Vyavahare, Novel porous aortic elastin and collagen scaffolds for tissue engineering. Biomaterials, 2004. 25(22): p. 5227-37.
162. Starcher, B.C. and M.J. Galione, Purification and comparison of elastins from different animal species. Anal Biochem, 1976. 74(2): p. 441-7.
163. L'Heureux, N., S. Paquet, R. Labbe, L. Germain, and F.A. Auger, A completely biological tissue-engineered human blood vessel. The FASEB Journal, 1998. 12(1): p. 47-56.
164. Konig, G., et al., Mechanical properties of completely autologous human tissue engineered blood vessels compared to human saphenous vein and mammary artery. Biomaterials, 2009. 30(8): p. 1542-50.

165. Stickler, P., et al., Cyclically stretching developing tissue in vivo enhances mechanical strength and organization of vascular grafts. Acta Biomater. 6(7): p. 2448-56.
166. Quaglia, F., Bioinspired tissue engineering: The great promise of protein delivery technologies. International Journal of Pharmaceutics, 2008. 364: p. 281-297.
167. Chen, R.R. and D.J. Mooney, Polymeric Growth Factor Delivery Strategies for Tissue Engineering. Pharmaceutical Research, 2003. 20(8): p. 1103-1112.
168. Tayalia, P. and D.J. Mooney, Controlled Growth Factor Delivery for Tissue Engineering. Advanced Materials, 2009. 21: p. 3269-3285.
169. Zisch, A.H., M.P. Lutolf and J.A. Hubbell, Biopolymeric delivery matrices for angiogenic growth factors. Cardiovascular Pathology, 2003. 12: p. 295-310.
170. Chen, R.R., et al., Integrated approach to designing growth factor delivery systems. FASEB J., 2007. 21: p. 3896-3903.
171. Visscher, G.D., et al., The remodeling of cardiovascular bioprostheses under influence of stem cell homing signal pathways. Biomaterials, 2010. 31: p. 20-28.
172. Zhang, G. and L.J. Suggs, Matrices and scaffolds for drug delivery in vascular tissue engineering. Advanced Drug Delivery Reviews, 2007. 59: p. 360-373.
173. Gu, F., B. Amsden and R. Neufeld, Sustained delivery of vascular endothelial growth factor with alginate beads. Journal of Controlled Release, 2004. 96: p. 463-472.
174. Silva, E.A. and D.J. Mooney, Spatiotemporal control of vascular endothelial growth factor delivery from injectable hydrogels enhances angiogenesis. Journal of Thrombosis and Haemostasis, 2007. 5: p. 590-598.
175. Tilakaratne, H.K., S.K. Hunter, M.E. Andracki, J.A. Benda, and V.G.J. Rodgers, Characterizing short-term release and neovascularization potential of multi-protein growth supplement delivered via alginate hollow fiber devices. Biomaterials, 2007. 28: p. 89-98.
176. Kurane, A. and N. Vyavahare, *In vivo* vascular tissue engineering: influence of cytokine and implant location on tissue specific cellular recruitment. Journal of Tissue Engineering and Regenerative Medicine, 2009. 3: p. 280-289.
177. Obara, K., et al., Photocrosslinkable chitosan hydrogel containing fibroblast growth factor-2 stimulates wound healing in healing-impared *db/db* mice. Biomaterials, 2003. 24: p. 3437-3444.
178. Ishihara, M., et al., Controlled release of fibroblast growth factors and heparin from photocrosslinked chitosan hydrogels and subsequent effect on *in vivo* vascularization. Journal of Biomedical Materials Research, 2003. 64A: p. 551-559.
179. Yamamoto, M., Y. Ikada and Y. Tabata, Controlled release of growth factors based on biodegradation of gelatin hydrogel. Journal of Biomaterials Science, Polymer Edition, 2001. 12(1): p. 77-88.
180. Patel, Z.S., H. Ueda, M. Yamamoto, Y. Tabata, and A.G. Mikos, In Vitro and In Vivo Release of Vascular Endothelial Growth Factor from Gelatin Microparticles and Biodegradable Composite Scaffolds. Pharmaceutical Research, 2008. 25(10): p. 2370-2378.

181. Gosselin, C., D.A. Vorp, V. Warty, D.A. Severyn, E.K. Dick, H.S. Borovetz, and H.P. Greisler, ePTFE Coating with Fibrin Glue, FGF-1, and Heparin: Effect on Retention of Seeded Endothelial Cells. Journal of Surgical Research, 1996. 60(0052): p. 327-332.
182. Nillesen, S.T.M., P.J. Geutjes, R. Wismans, J. Schalkwijk, W.F. Daamen, and T.H. van Kuppevelt, Increased angiogenesis and blood vessel maturation in acellular collagen-heparin scaffolds containing both FGF2 and VEGF. Biomaterials, 2007. 28: p. 1123-1131.
183. Steffens, G.C.M., C. Yao, P. Prevel, M. Markowicz, P. Schenck, E.M. Noah, and N. Pallua, Modulation of Angiogenic Potential of Collagen Matrices by Covalent Incorporation of Heparin and Loading with Vascular Endothelial Growth Factor. Tissue Engineering, 2004. 10(9/10): p. 1502-1510.
184. Kanematsu, A., S. Yamamoto, M. Ozeki, T. Noguchi, I. Kanatani, O. Ogawa, and Y. Tabata, Collagenous matrices as release carriers of exogenous growth factors. Biomaterials, 2004. 25: p. 4513-4520.
185. Nagai, N., N. Kumasaka, T. Kawashima, H. Kaji, M. Nishizawa, and T. Abe, Preparation and characterization of collagen microspheres for sustained release of VEGF. Journal of Material Science: Material Medicine, 2010. 21: p. 1891-1898.
186. Chung, H.J. and T.G. Park, Surface engineered and drug releasing pre-fabricated scaffolds for tissue engineering. Advanced Drug Delivery Reviews, 2007. 59: p. 249-262.
187. Greisler, H., et al., Enhanced endothelialization of expanded polytetrafluoroethylene grafts by fibroblast growth factor type 1 pretreatment. Surgery, 1992. 112(2): p. 244-254.
188. Deutsch, M., J. Meinhart, M. Vesely, T. Fischlein, P. Groscurth, U. von Oppell, and P. Zilla, In vitro endothelialization of expanded polytetrafluoroethylene grafts: A clinical case report after 41 months of implantation. Journal of Vascular Surgery, 1997. 25: p. 757-763.
189. Pang, Y., et al., Local delivery of a collagen-binding FGF-1 chimera to smooth muscle cells in collagen scaffolds for vascular tissue engineering. Biomaterials. 31(5): p. 878-85.
190. Lee, K.Y., M.C. Peters, K.W. Anderson, and D.J. Mooney, Controlled growth factor release from synthetic extracellular matrices. Nature, 2000. 408: p. 998-1000.
191. Tabata, Y., M. Miyae, M. Ozeki, and Y. Ikada, Controlled release of vascular endothelial growth factor by use of collagen hydrogels. Journal of Biomaterials Science, Polymer Edition, 2000. 11(9): p. 915-930.
192. Wissink, M.J.B., R. Beernink, A.A. Poot, G.H.M. Engbers, T. Beugeling, W.G. van Aken, and J. Feijen, Improved endothelialization of vascular grafts by local release of growth factor from heparinized collagen matrices. Journal of Controlled Release, 2000. 64: p. 103-114.
193. Pieper, J.S., T. Hafmans, P.B. van Wachem, M.J.A. van Luyn, L.A. Brouwer, J.H. Veerkamp, and T.H. van Kuppevelt, Loading of collagen-heparan sulfate matrices

with bFGF promotes angiogenesis and tissue generation in rats. Journal of Biomedical Materials Research, 2002. 62: p. 185-194.
194. Mann, B.K., R.H. Schmedlen and J.L. West, Tethered-TGF-β increases extracellular matrix production of vascular smooth muscle cells. Biomaterials, 2001. 22: p. 439-444.
195. Lim, T.Y., C.K. Poh and W. Wang, Poly(lactic-co-glycolic acid) as a controlled release delivery device. Journal of Material Science: Material Medicine, 2009. 20: p. 1669-1675.
196. Cleland, J.L., E.T. Duenas, A. Park, A. Daugherty, J. Kahn, J. Kowalski, and A. Cuthbertson, Development of poly-(D,L-lactice-coglycolide) microsphere formulations containing recombinant human vascular endothelial growth factor to promote local angiogenesis. Journal of Controlled Release, 2001. 72: p. 13-24.
197. Sheridan, M.H., L.D. Shea, M.C. Peters, and D.J. Mooney, Bioabsorbable polymer scaffolds for tissue engineering capable of sustained growth factor delivery. Journal of Controlled Release, 2000. 64: p. 91-102.
198. Kim, T. and D. Burgess, Pharmacokinetic characterization of 14C-vascular endothelial growth factor controlled release microspheres using a rat model. Journal of Pharmacy and Pharmacology, 2002. 54(7): p. 897-905.
199. Golub, J.S., et al., Sustained VEGF delivery via PLGA nanoparticles promotes vascular growth. American Journal of Physiological Heart and Circulation Physiology, 2010. 298: p. H1959-H1965.
200. d'Angelo, I., et al., Nanoparticles Based on PLGA:Poloxamer Blends for the Delivery of Proangiogenic Growth Factors. Molecular Pharmaceutics, 2010. 7(5): p. 1724-1733.
201. Lee, M., T.T. Chen, M.L. Iruela-Arispe, B.M. Wu, and J.C.Y. Dunn, Modulation of protein delivery from modular polymer surfaces. Biomaterials, 2007. 28: p. 1862-1870.
202. Baldwin, S.P. and W.M. Saltzman, Materials for protein delivery in tissue engineering. Advanced Drug Delivery Reviews, 1998. 33: p. 71-86.
203. Thevenot, P.T., A.M. Nair, J. Shen, P. Lotfi, C.-Y. Ko, and L. Tang, The effect of incorporation of SDF-1alpha into PLGA scaffolds on stem cell recruitment and the inflammatory response. Biomaterials, 2010. 31: p. 3997-4008.
204. Richardson, T.P., M.C. Peters, A.B. Ennett, and D.J. Mooney, Polymeric system for dual growth factor delivery. Nature Biotechnology, 2001. 19: p. 1029-1034.
205. Chen, R.R., E.A. Silva, W.W. Yuen, and D.J. Mooney, Spatio-temporal VEGF and PDGF Delivery Patterns Blood Vessel Formation and Maturation. Pharmaceutical Research, 2007. 24(2): p. 258-264.
206. Saif, J., et al., Combination of Injectable Multiple Growth Factor-Releasing Scaffolds and Cell Therapy as an Advanced Modality to Enhance Tissue Neovascularization. Arteriosclerosis, Thrombosis, and Vascular Biology, 2010. 30: p. 1897-1904.
207. Sell, S.A., P.S. Wolfe, J.J. Ericksen, D.G. Simpson, and G.L. Bowlin, Incorporating Platelet-Rich Plasma into Electrospun Scaffolds for Tissue Engineering Applications. Tissue Eng Part A.

208. Shireman, P.K. and H.P. Greisler, Mitogenicity and release of vascular endothelial growth factor with and without heparin from fibrin glue. Journal of Vascular Surgery, 2000. 31: p. 936-943.
209. Ito, Y., G. Chen and Y. Imanishi, Artificial juxtacrine stimulation for tissue engineering. Journal of Biomaterials Science, Polymer Edition, 1998. 9(8): p. 879-890.
210. Masters, K.S., et al., Nitric oxide-generating hydrogels inhibit neointima formation. Journal of Biomaterials Science, Polymer Edition, 2005. 16(5): p. 659-672.
211. Lipke, E.A. and J.L. West, Localized delivery of nitric oxide from hydrogels inhibits neointima formation in a rat carotid balloon injury model. Acta Biomaterialia, 2005. 1(6): p. 597-606.
212. Kanjickal, D., S. Lopina, M.M. Evancho-Chapman, S. Schmidt, and D. Donovan, Sustained local drug delivery from a novel polymeric ring to inhibit intimal hyperplasia. Journal of Biomedical Materials Research, 2010. 93A: p. 656-665.
213. Javerliat, I., O. Goeau-Brissonniere, P. Bruneval, and M. Coggia, Experimental Study of a New Vascular Graft Prebonded with Antibiotic: Healing, Toxicity, and Antibiotic Retention. Annals of Vascular Surgery, 2007. 21(5): p. 603-610.
214. Conte, M.S., The ideal small arterial substitute: a search for the Holy Grail? The FASEB Journal, 1998. 12(1): p. 43-45.
215. Kidoaki, S., I.K. Kwon and T. Matsuda, Mesoscopic spatial designs of nano- and microfiber meshes for tissue-engineering matrix and scaffold based on newly devised multilayering and mixing electrospinning techniques. Biomaterials, 2005. 26(1): p. 37-46.
216. Yang, X., J.D. Shah and H. Wang, Nanofiber Enabled Layer-by-Layer Approach Toward Three-Dimensional Tissue Formation. Tissue Eng Part A, 2009. 15(4): p. 945-56.
217. Telemeco, T.A., Ayres C, Bowlin GL, Wnek GE, Boland ED, Cohen N, Baumgarten CM, Matthews J, Simpson DG, Regulation of cellular infiltration into tissue engineering scaffolds composed of submicron diameter fibrils produced by electrospinning. Acta Biomater, 2005. 1(4): p. 377-385.
218. Altman, G.H., et al., Silk-based biomaterials. Biomaterials, 2003. 24: p. 401-416.
219. Altman, G.H., R.L. Horan, H.H. Lu, J. Moreau, I. Martin, J.C. Richmond, and D.L. Kaplan, Silk matrix for tissue engineered anterior cruciate ligaments. Biomaterials, 2002. 23: p. 4131-4141.
220. Wang, Y., H.-J. Kim, G. Vunjak-Novakovic, and D.L. Kaplan, Stem cell-based tissue engineering with silk biomaterials. Biomaterials, 2006. 27: p. 6064-6082.
221. Thom, T., et al., Heart disease and stroke statistics--2006 update: a report from the American Heart Association Statistics Committee and Stroke Statistics Subcommittee. Circulation, 2006. 113(6): p. e85-151.
222. Boland, E.D., J.A. Matthews, K.J. Pawlowski, D.G. Simpson, G.E. Wnek, and G.L. Bowlin, Electrospinning collagen and elastin: preliminary vascular tissue engineering. Frontiers in Bioscience, 2004. 9: p. 1422-1432.
223. Isenberg, B.C., C. Williams and R.T. Tranquillo, Small-diameter artificial arteries engineered in vitro. Circ Res., 2005. 98: p. 25-35.

224. Teebken, O.E. and A. Haverich, Tissue engineering of small diameter vascular grafts. Eur J Vasc Endovasc Surg, 2002. 23(6): p. 475-485.
225. Kannan, R.Y., H.J. Salacinski, P.E. Butler, G. Hamilton, and A.M. Seifalian, Current status of prosthetic bypass grafts: a review. J Biomed Mater Res B Appl Biomater, 2005. 74(1): p. 570-81.
226. Buttafoco, L., et al., First steps towards tissue engineering of small-diameter blood vessels: preparation of flat scaffolds of collagen and elastin by means of freeze drying. J Biomed Mater Res B Appl Biomater, 2006. 77(2): p. 357-68.
227. Loscalzo, J., M.A. Creager and V.J. Dzau, Vascular medicine: a textbook of vascular biology and diseases. Second ed. 1996, Boston New York Toronto London: Little, Brown and Company. 1312.
228. Lanza, R., R. Langer and J. Vacanti, Principles of tissue engineering. Second ed. 2000, Boston: Academic Press. 427-441.
229. Halliday, A., B.J. Hunt, L. Poston, and M. Schachter, An introduction to vascular biology from physiology to pathophysiology. 1998, New York: Cambridge University Press.
230. Reneker, D.H. and I. Chun, Nanometre diameter fibres of polymer, produced by electrospinning. Nanotechnology, 1996. 7(3): p. 216-223.
231. Venugopal, J. and S. Ramakrishna, Applications of polymer nanofibers in biomedicine and biotechnology. Appl Biochem Biotechnol, 2005. 125(3): p. 147-58.
232. Buttafoco, L., N.G. Kolkman, P. Engbers-Buijtenhuijs, A.A. Poot, P.J. Dijkstra, I. Vermes, and J. Feijen, Electrospinning of collagen and elastin for tissue engineering applications. Biomaterials, 2006. 27(5): p. 724-34.
233. Matthews, J.A., G.E. Wnek, D.G. Simpson, and G.L. Bowlin, Electrospinning of collagen nanofibers. Biomacromolecules, 2002. 3(2): p. 232-8.
234. Huang, L., R.A. McMillan, R.P. Apkarian, B. Pourdeyhimi, V.P. Conticello, and E.L. Chaikof, Generation of synthetic elastin-mimetic small diameter fibers and fiber networks. Macromolecules, 2000. 33: p. 2989-2997.
235. Boland, E.D., B.D. Coleman, C.P. Barnes, D.G. Simpson, G.E. Wnek, and G.L. Bowlin, Electrospinning polydioxanone for biomedical applications. Acta Biomater, 2005. 1(1): p. 115-23.
236. Hench, L.L. and J.M. Polak, Third-generation biomedical materials. Science, 2002. 295(5557): p. 1014-7.
237. Zhong, S., W.E. Teo, X. Zhu, R. Beuerman, S. Ramakrishna, and L.Y. Yung, Formation of collagen-glycosaminoglycan blended nanofibrous scaffolds and their biological properties. Biomacromolecules, 2005. 6(6): p. 2998-3004.
238. Zhong, S., W.E. Teo, X. Zhu, R.W. Beuerman, S. Ramakrishna, and L.Y. Yung, An aligned nanofibrous collagen scaffold by electrospinning and its effects on in vitro fibroblast culture. J Biomed Mater Res A, 2006. 79(3): p. 456-63.
239. Zhao, P., H. Jiang, H. Pan, K. Zhu, and W. Chen, Biodegradable fibrous scaffolds composed of gelatin coated poly(epsilon-caprolactone) prepared by coaxial electrospinning. J Biomed Mater Res A, 2007.

240. McManus, M.C., E.D. Boland, D.G. Simpson, C.P. Barnes, and G.L. Bowlin, Electrospun fibrinogen: feasibility as a tissue engineering scaffold in a rat cell culture model. J Biomed Mater Res A, 2007. 81(2): p. 299-309.
241. Tsai, C.C., R.N. Huang, H.W. Sung, and H.C. Liang, In vitro evaluation of the genotoxicity of a naturally occurring crosslinking agent (genipin) for biologic tissue fixation. J Biomed Mater Res, 2000. 52(1): p. 58-65.
242. Park, S.N., J.C. Park, H.O. Kim, M.J. Song, and H. Suh, Characterization of porous collagen/hyaluronic acid scaffold modified by 1-ethyl-3-(3-dimethylaminopropyl)carbodiimide cross-linking. Biomaterials, 2002. 23(4): p. 1205-12.
243. Huang, L.L., H.W. Sung, C.C. Tsai, and D.M. Huang, Biocompatibility study of a biological tissue fixed with a naturally occurring crosslinking reagent. J Biomed Mater Res, 1998. 42(4): p. 568-76.
244. Barnes, C.P., C.W. Pemble, D.D. Brand, D.G. Simpson, and G.L. Bowlin, Cross-linking electrospun type II collagen tissue engineering scaffolds with carbodiimide in ethanol. Tissue Eng, 2007. 13(7): p. 1593-605.
245. Sung, H.W., W.H. Chang, C.Y. Ma, and M.H. Lee, Crosslinking of biological tissues using genipin and/or carbodiimide. J Biomed Mater Res A, 2003. 64(3): p. 427-38.
246. Fung, Y.C., Biodynamics: circulation. blood flow in arteries. 1984, New York: Springer-Verlag.
247. Hiroshi, Y., Strength of biological materials. 1970, New York: Robert E. Krieger Publishing Company.
248. Sell, S.A., M.J. McClure, C.P. Barnes, D.C. Knapp, B.H. Walpoth, D.G. Simpson, and G.L. Bowlin, Electrospun polydioxanone-elastin blends: potential for bioresorbable vascular grafts. Biomedical Materials, 2006. 1: p. 72-80.
249. Pullens, R.A., M. Stekelenburg, F.P. Baaijens, and M.J. Post, The influence of endothelial cells on the ECM composition of 3D engineered cardiovascular constructs. J Tissue Eng Regen Med, 2009. 3(1): p. 11-8.
250. Yokota, T., et al., In situ tissue regeneration using a novel tissue-engineered, small-caliber vascular graft without cell seeding. J Thorac Cardiovasc Surg, 2008. 136(4): p. 900-7.
251. Roh, J.D., et al., Small-diameter biodegradable scaffolds for functional vascular tissue engineering in the mouse model. Biomaterials, 2008. 29(10): p. 1454-63.
252. Ryu, W., S.W. Min, K.E. Hammerick, M. Vyakarnam, R.S. Greco, F.B. Prinz, and R.J. Fasching, The construction of three-dimensional micro-fluidic scaffolds of biodegradable polymers by solvent vapor based bonding of micro-molded layers. Biomaterials, 2007. 28(6): p. 1174-84.
253. Venugopal, J., L.L. Ma, T. Yong, and S. Ramakrishna, In vitro study of smooth muscle cells on polycaprolactone and collagen nanofibrous matrices. Cell Biol Int, 2005. 29(10): p. 861-7.
254. Nottelet, B., E. Pektok, D. Mandracchia, J.C. Tille, B. Walpoth, R. Gurny, and M. Moller, Factorial design optimization and in vivo feasibility of poly(epsilon-

caprolactone)-micro- and nanofiber-based small diameter vascular grafts. J Biomed Mater Res A, 2008.
255. Dong, Y., T. Yong, S. Liao, C.K. Chan, and S. Ramakrishna, Long-term viability of coronary artery smooth muscle cells on poly(L-lactide-co-epsilon-caprolactone) nanofibrous scaffold indicates its potential for blood vessel tissue engineering. J R Soc Interface, 2008. 5(26): p. 1109-18.
256. Del Gaudio, C., A. Bianco, M. Folin, S. Baiguera, and M. Grigioni, Structural characterization and cell response evaluation of electrospun PCL membranes: micrometric versus submicrometric fibers. J Biomed Mater Res A, 2009. 89(4): p. 1028-39.
257. Lee, S.J., J. Liu, S.H. Oh, S. Soker, A. Atala, and J.J. Yoo, Development of a composite vascular scaffolding system that withstands physiological vascular conditions. Biomaterials, 2008. 29(19): p. 2891-8.
258. Martins-Green, M., The Dynamics of Cell-ECM Interactions with Implications for Tissue Engineering. Principles of Tissue Engineering, ed. R. Lanza, R. Langer, and W. Chick. 1997: R.G. Landes Company. 23-46.
259. Heydarkhan-Hagvall, S., et al., Three-dimensional electrospun ECM-based hybrid scaffolds for cardiovascular tissue engineering. Biomaterials, 2008. 29(19): p. 2907-14.
260. Ma, Z.W., W. He, T. Yong, and S. Ramakrishna, Grafting of gelatin on electrospun poly(caprolactone) nanofibers to improve endothelial cell spreading and proliferation and to control cell orientation. Tissue Engineering, 2005. 11(7-8): p. 1149-1158.
261. Vorp, D.A., M.L. Raghavan, H.S. Borovetz, H.P. Greisler, and M.W. Webster, Modeling the transmural stress distribution during healing of bioresorbable vascular prostheses. Ann Biomed Eng, 1995. 23(2): p. 178-88.
262. Barnes, C.P., C.W. Pemble, D.D. Brand, D.G. Simpson, and G.L. Bowlin, Cross-linking electrospun type II collagen tissue engineering scaffolds with carbodiimide in ethanol. Tissue Eng, 2007.
263. Brand, D.D., Protocols: acid extraction of fetal bovine skin collagen. 2005, University of Tennessee: Memphis, TN. p. RDRCC Collagen Core Center.
264. Institute, A.N.S., ANSI 2000 Cardiovascular implants - Vascular graft prostheses, A.f.t.A.o.M. Instrumentation, Editor. 1994.
265. Lu, X., A. Pandit and G.S. Kassab, Biaxial incremental homeostatic elastic moduli of coronary artery: two-layer model. Am J Physiol Heart Circ Physiol, 2004. 287(4): p. H1663-9.
266. Holzapfel, G.A., G. Sommer, C.T. Gasser, and P. Regitnig, Determination of layer-specific mechanical properties of human coronary arteries with nonatherosclerotic intimal thickening and related constitutive modeling. Am J Physiol Heart Circ Physiol, 2005. 289(5): p. H2048-58.
267. McClure, M.J., S.A. Sell, D. Simpson, and G.L. Bowlin, Electrospun Polydioxanone, Elastin, and Collagen Vascular Scaffolds: Uniaxial Cyclic Distension. Journal of Engineered Fibers and Fabrics, 2009. In Press.

268. Donovan, D.L., S.P. Schmidt, S.P. Townshend, G.O. Njus, and W.V. Sharp, Material and structural characterization of human saphenous vein. J Vasc Surg, 1990. 12(5): p. 531-7.
269. Wang, C., M. Garcia, X. Lu, Y. Lanir, and G.S. Kassab, Three-dimensional mechanical properties of porcine coronary arteries: a validated two-layer model. Am J Physiol Heart Circ Physiol, 2006. 291(3): p. H1200-9.
270. Roy, S., P. Silacci and N. Stergiopulos, Biomechanical properties of decellularized porcine common carotid arteries. Am J Physiol Heart Circ Physiol, 2005. 289(4): p. H1567-76.
271. Holzapfel, G.A., T.C. Gasser and R.W. Ogden, Comparison of a multi-layer structural model for arterial walls with a fung-type model, and issues of material stability. J Biomech Eng, 2004. 126(2): p. 264-75.
272. Pandit, A., X. Lu, C. Wang, and G.S. Kassab, Biaxial elastic material properties of porcine coronary media and adventitia. Am J Physiol Heart Circ Physiol, 2005. 288(6): p. H2581-7.
273. Fung, Y.C. and S.Q. Liu, Determination of the mechanical properties of the different layers of blood vessels in vivo. Proc Natl Acad Sci U S A, 1995. 92(6): p. 2169-73.
274. Newton, D., R. Mahajan, C. Ayres, J.R. Bowman, G.L. Bowlin, and D.G. Simpson, Regulation of material properties in electrospun scaffolds: Role of cross-linking and fiber tertiary structure. Acta Biomater, 2009. 5(1): p. 518-29.
275. Barnes, C.P., C.W. Pemble, D.D. Brand, D.G. Simpson, and G.L. Bowlin, Cross-Linking Electrospun Type II Collagen Tissue Engineering Scaffolds with Carbodiimide in Ethanol. Tissue Engineering, 2007. 13(7): p. 1593-1605.
276. Bruel, A., G. Ortoft and H. Oxlund, Inhibition of cross-links in collagen is associated with reduced stiffness of the aorta in young rats. Atherosclerosis, 1998. 140(1): p. 135-45.
277. Zhang, X., C.B. Baughman and D.L. Kaplan, In vitro evaluation of silk fibroin scaffolds for vascular cell growth. Biomaterials, 2008. 29: p. 2217-2227.
278. Buttafoco, L., N.G. Kolkman, A.A. Poot, P.J. Dijkstra, I. Vermes, and J. Feijen, Electrospinning collagen and elastin for tissue engineering small diameter blood vessels. J Control Release, 2005. 101(1-3): p. 322-4.
279. Altman, G.H., et al., Silk-based biomaterials. Biomaterials, 2003. 24(3): p. 401-416.
280. Jin, H.J., J. Chen, V. Karageorgiou, G.H. Altman, and D.L. Kaplan, Human bone marrow stromal cell responses on electrospun silk fibroin mats. Biomaterials, 2004. 25(6): p. 1039-47.
281. Powell, H.M. and S.T. Boyce, Engineered human skin fabricated using electrospun collagen-PCL blends: morphogenesis and mechanical properties. Tissue Eng Part A, 2009. 15(8): p. 2177-87.
282. Olde Damink, L.H., P.J. Dijkstra, M.J. van Luyn, P.B. van Wachem, P. Nieuwenhuis, and J. Feijen, Cross-linking of dermal sheep collagen using a water-soluble carbodiimide. Biomaterials, 1996. 17(8): p. 765-73.

283. Madhavan, K., D. Belchenko, A. Motta, and W. Tan, Evaluation of composition and crosslinking effects on collagen-based composite constructs. Acta Biomater. 6(4): p. 1413-22.
284. Chiono, V., E. Pulieri, G. Vozzi, G. Ciardelli, A. Ahluwalia, and P. Giusti, Genipin-crosslinked chitosan/gelatin blends for biomedical applications. J Mater Sci Mater Med, 2007.
285. Shenoy, S.L., W.D. Bates and G. Wnek, Correlations between electrospinnability and physical gelation. Polymer, 2005. 46(21): p. 8990-9004.
286. Canetti, M., A. Seves, F. Secundo, and G. Vecchio, CD and small-angle x-ray scattering of silk fibroin in solution. Biopolymers, 1989. 28(9): p. 1613-24.
287. Alessandrino, A., B. Marelli, C. Arosio, S. Fare, M.C. Tanzi, and G. Freddi, Electrospun Silk Fibroin Mats for Tissue Engineering. Engineering in Life Sciences, 2008. 8(3): p. 219-225.
288. Vieth, S., C.M. Bellingham, F.W. Keeley, S.M. Hodge, and D. Rousseau, Microstructural and tensile properties of elastin-based polypeptides crosslinked with genipin and pyrroloquinoline quinone. Biopolymers, 2007. 85(3): p. 199-206.
289. Chiono, V., E. Pulieri, G. Vozzi, G. Ciardelli, A. Ahluwalia, and P. Giusti, Genipin-crosslinked chitosan/gelatin blends for biomedical applications. Journal of Materials Science, 2008. 19(2): p. 889-898.
290. Hafemann, B., K. Ghofrani, H.G. Gattner, H. Stieve, and N. Pallua, Cross-linking by 1-ethyl-3- (3-dimethylaminopropyl)-carbodiimide (EDC) of a collagen/elastin membrane meant to be used as a dermal substitute: effects on physical, biochemical and biological features in vitro. J Mater Sci Mater Med, 2001. 12(5): p. 437-46.
291. Niklason, L.E., Replacement Arteries Made to Order. Science, 1999. 286(5444): p. 1493.
292. Rhodin, J.A.G., Architecture of the vessel wall, in Handbook of Physiology, S. Geiger, Editor. 1980, American Physiological Society: Bethesda, MD. p. 1-31.
293. Huang, L., R.A. McMillan, R.P. Apkarian, B. Pourdeyhimi, V.P. Conticello, and E.L. Chaikof, Generation of synthetic elastin-mimetic small diameter fibers and fiber networks. Macromolecules, 2000. 33(8): p. 2989-2997.
294. Strandness, D.E. and D.S. Sumner, Hemodynamics for Surgeons. 1975, New York: Grune & Stratton, Inc. 698.
295. Conte, M.S., The ideal small arterial substitute: a search for the Holy Grail? Faseb J, 1998. 12(1): p. 43-5.
296. ANSI, ANSI 2000 Cardiovascular implants - Vascular graft prostheses, A.f.t.A.o.M. Instrumentation, Editor. 1994.
297. Takamizawa, K. and K. Hayashi, Strain energy density function and uniform strain hypothesis for arterial mechanics. J Biomech, 1987. 20(1): p. 7-17.
298. Fung, Y.C., K. Fronek and P. Patitucci, Pseudoelasticity of arteries and the choice of its mathematical expression. Am J Physiol, 1979. 237(5): p. H620-31.
299. Soffer, L., X. Wang, X. Zhang, J. Kluge, L. Dorfmann, D.L. Kaplan, and G. Leisk, Silk-based electrospun tubular scaffolds for tissue-engineered vascular grafts. J. Biomater. Sci. Polymer Edn., 2008. 19(5): p. 653-664.

300. Mercuri, J.J., J.J. Lovekamp, D.T. Simionescu, and N.R. Vyavahare, Glycosaminoglycan-targeted fixation for improved bioprosthetic heart valve stabilization. Biomaterials, 2007. 28(3): p. 496-503.
301. Lu, Q., B. Zhang, M. Li, B. Zuo, D.L. Kaplan, Y. Huang, and H. Zhu, Degradation mechanism and control of silk fibroin. Biomacromolecules. 12(4): p. 1080-6.
302. Simpson, D.G., Integrins, in Encyclopedia of Biomaterials and Biomedical Engineering, T. Francis, Editor. 2006. p. 1-16.
303. Yamamoto, M., M. Yamato, M. Aoyagi, and K. Yamamoto, Identification of integrins involved in cell adhesion to native and denatured type I collagens and the phenotypic transition of rabbit arterial smooth muscle cells. Exp Cell Res, 1995. 219(1): p. 249-56.
304. Lee, J.W., W.N. Qi and S.P. Scully, The involvement of beta1 integrin in the modulation by collagen of chondrocyte-response to transforming growth factor-beta1. J Orthop Res, 2002. 20(1): p. 66-75.
305. Clyman, R.I., K.A. McDonald and R.H. Kramer, Integrin receptors on aortic smooth muscle cells mediate adhesion to fibronectin, laminin, and collagen. Circ Res, 1990. 67(1): p. 175-86.
306. Gobin, A.S. and J.L. West, Val-ala-pro-gly, an elastin-derived non-integrin ligand: smooth muscle cell adhesion and specificity. J Biomed Mater Res A, 2003. 67(1): p. 255-9.
307. Rodgers, U.R. and A.S. Weiss, Integrin alpha v beta 3 binds a unique non-RGD site near the C-terminus of human tropoelastin. Biochimie, 2004. 86(3): p. 173-8.
308. Seo, N., B.H. Russell, J.J. Rivera, X. Liang, X. Xu, V. Afshar-Kharghan, and M. Hook, An engineered alpha1 integrin-binding collagenous sequence. J Biol Chem. 285(40): p. 31046-54.
309. Heino, J., The collagen receptor integrins have distinct ligand recognition and signaling functions. Matrix Biol, 2000. 19(4): p. 319-23.
310. Kim, J.K., et al., A novel binding site in collagen type III for integrins alpha1beta1 and alpha2beta1. J Biol Chem, 2005. 280(37): p. 32512-20.
311. Xu, Y., et al., Multiple binding sites in collagen type I for the integrins alpha1beta1 and alpha2beta1. J Biol Chem, 2000. 275(50): p. 38981-9.
312. Davis, G.E., Affinity of integrins for damaged extracellular matrix: alpha v beta 3 binds to denatured collagen type I through RGD sites. Biochem Biophys Res Commun, 1992. 182(3): p. 1025-31.
313. Nettles, D.L., A. Chilkoti and L.A. Setton, Applications of elastin-like polypeptides in tissue engineering. Adv Drug Deliv Rev. 62(15): p. 1479-85.
314. Zeugolis, D.I., et al., Electro-spinning of pure collagen nano-fibres - Just an expensive way to make gelatin? Biomaterials, 2008. 29(15): p. 2293.
315. Grzesiak, J.J. and M. Bouvet, Determination of the ligand-binding specificities of the alpha2beta1 and alpha1beta1 integrins in a novel 3-dimensional in vitro model of pancreatic cancer. Pancreas, 2007. 34(2): p. 220-8.
316. Bax, D.V., U.R. Rodgers, M.M. Bilek, and A.S. Weiss, Cell adhesion to tropoelastin is mediated via the C-terminal GRKRK motif and integrin alphaVbeta3. J Biol Chem, 2009. 284(42): p. 28616-23.

317. Simpson, D.G., Dermal templates and the wound-healing paradigm: the promise of tissue regeneration. Expert Review Of Medical Devices, 2006. 3(4): p. 471-484.
318. Lebourg, M., J.S. Anton and J.L.G. Ribelles, Characterization of calcium phosphate layers grown on polycaprolactone for tissue engineering purposes. Composites Science And Technology. 70(13): p. 1796-1804.
319. Thacker, S.G., C.C. Berthier, D. Mattinzoli, M.P. Rastaldi, M. Kretzler, and M.J. Kaplan, The Detrimental Effects of IFN-alpha on Vasculogenesis in Lupus Are Mediated by Repression of IL-1 Pathways: Potential Role in Atherogenesis and Renal Vascular Rarefaction. Journal Of Immunology. 185(7): p. 4457-4469.
320. Knight, C.G., L.F. Morton, A.R. Peachey, D.S. Tuckwell, R.W. Farndale, and M.J. Barnes, The collagen-binding A-domains of integrins alpha(1)beta(1) and alpha(2)beta(1) recognize the same specific amino acid sequence, GFOGER, in native (triple-helical) collagens. Journal Of Biological Chemistry, 2000. 275(1): p. 35-40.
321. McKegney, M., I. Taggart and M.H. Grant, The influence of crosslinking agents and diamines on the pore size, morphology and the biological stability of collagen sponges and their effect on cell penetration through the sponge matrix. J Mater Sci Mater Med, 2001. 12(9): p. 833-44.
322. Sofia, S., M.B. McCarthy, G. Gronowicz, and D.L. Kaplan, Functionalized silk-based biomaterials for bone formation. J Biomed Mater Res, 2001. 54(1): p. 139-48.
323. Motta, A., D. Maniglio, C. Migliaresi, H.J. Kim, X. Wan, X. Hu, and D.L. Kaplan, Silk fibroin processing and thrombogenic responses. J Biomater Sci Polym Ed, 2009. 20(13): p. 1875-97.

APPENDIX A

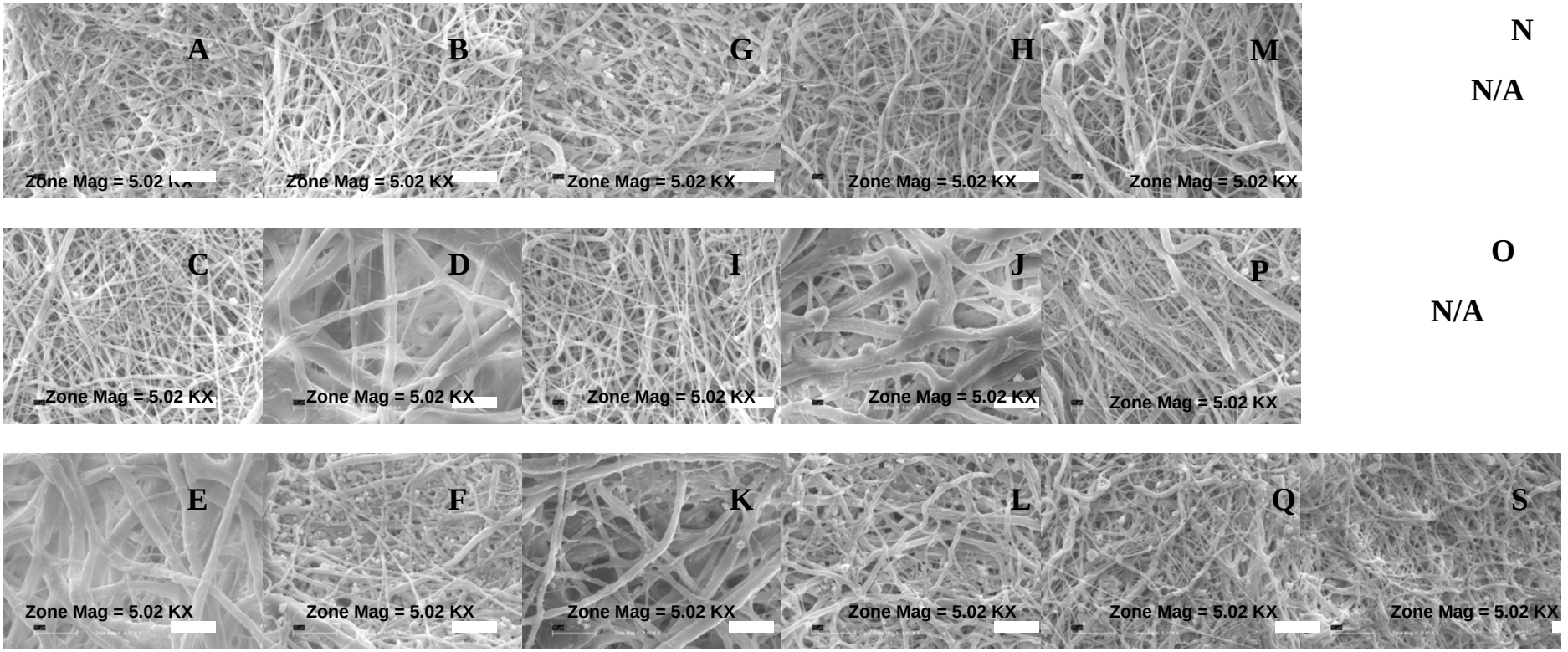

Scanning electron microscopy images taken at 5000x for the intimal, medial, and adventitial layers of the 45-45-10 (A-F), 55-35-10 (G-L), and 65-25-10 (M-S) PCL-Elastin-Collagen graft after cross-linking with 50 mM EDC, hydrated in PBS for 24 hours, frozen at -70^{o}C, and lyophilized dry to demonstrate differences in fiber morphology. (A,G,M) Inside Intima, (B,H,N-image missing due to inability to separate layers without scaffold destruction) Outside Intima, (C,I,O-image missing due to inability to separate layers without scaffold destruction) Inside Media, (D,J,P) Outside Media, (E,K,Q) Inside Adventitia, (F,L,S) Outside Adventitia. Scale bars = 10 μm.

APPENDIX B

Scanning electron micrographs of 45-45-10, 55-35-10, 65-25-10, 45-10-45, 55-10-35, 65-10-25 PCL-Elastin-Silk uncrosslinked (top right), cross-linked with EDC (bottom left), and cross-linked with GEN (bottom right). Micrographs were taken at 2500x.

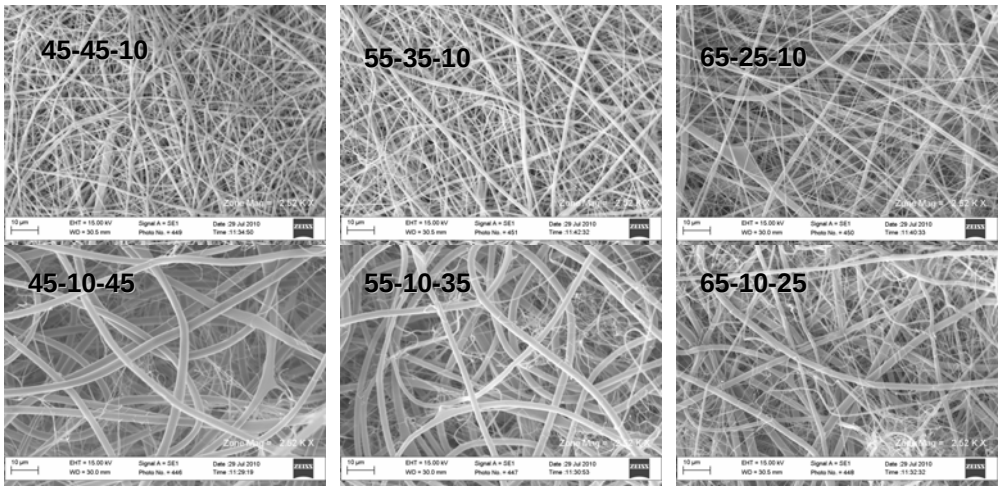

EDC Xlink

GEN Xlink

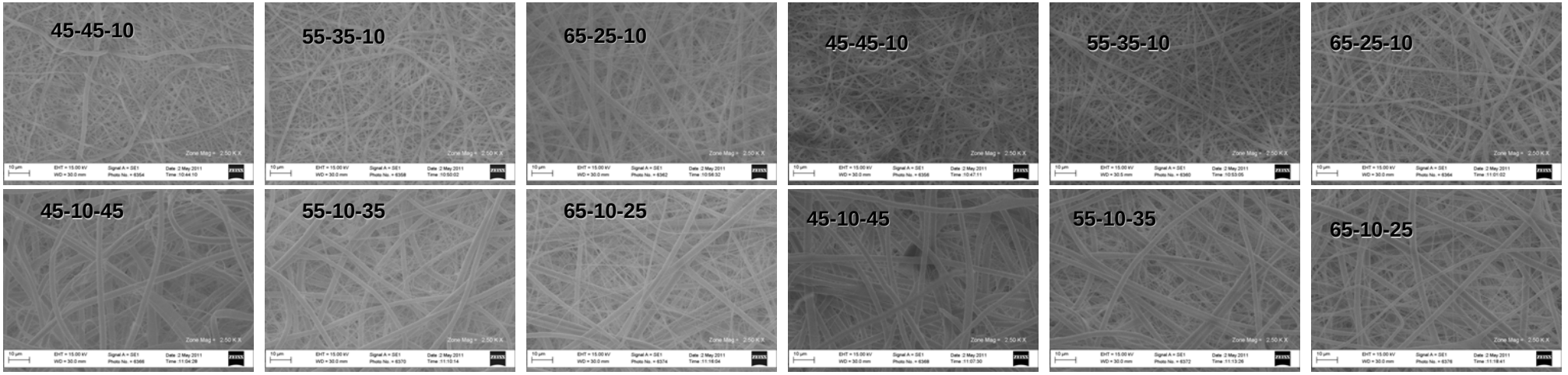

APPENDIX C

Scanning electron micrographs of 45-45-10, 55-35-10, 65-25-10, 45-10-45, 55-10-35, 65-10-25 PCL-Elastin-COL uncrosslinked (top right), cross-linked with EDC (bottom left), and cross-linked with GEN (bottom right). Micrographs were taken at 1000x.

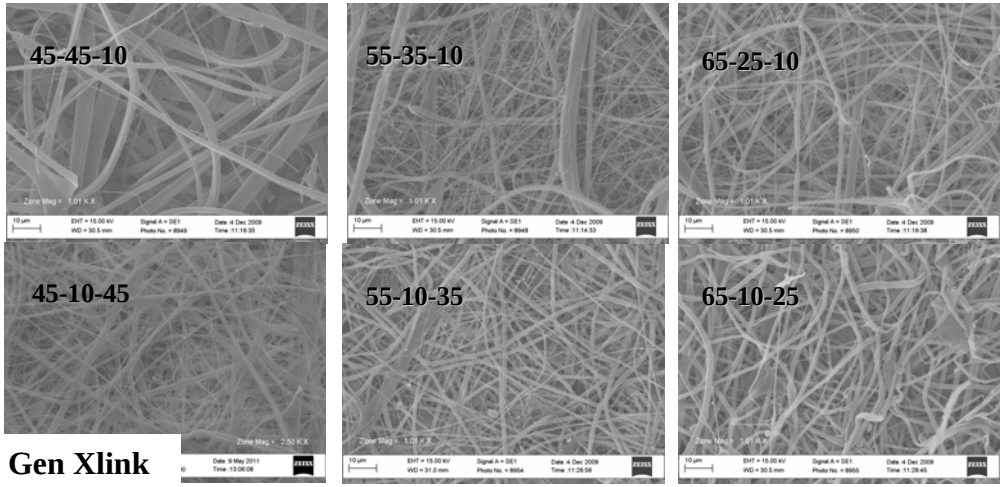

EDC Xlink

Gen Xlink

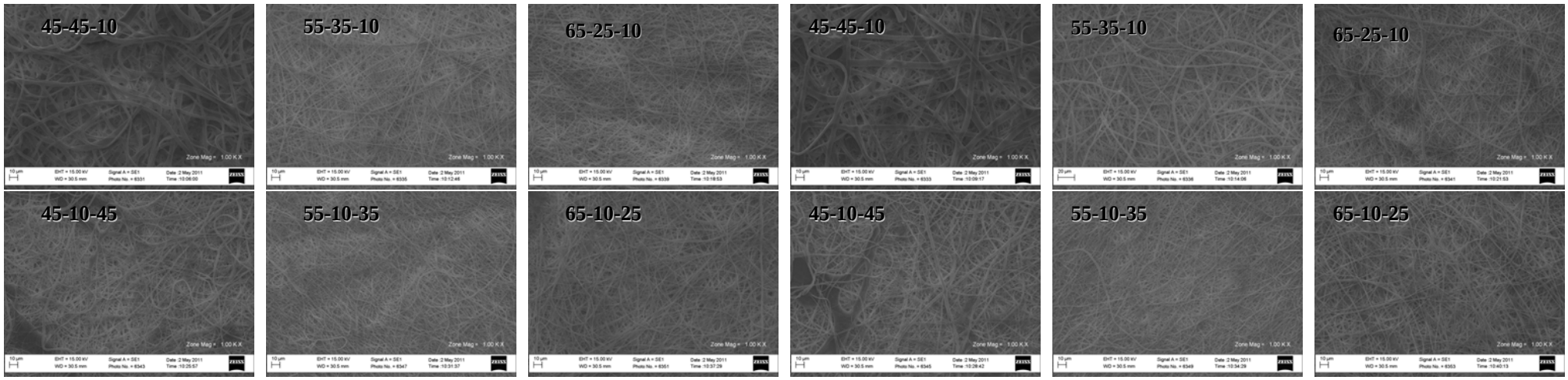

APPENDIX D

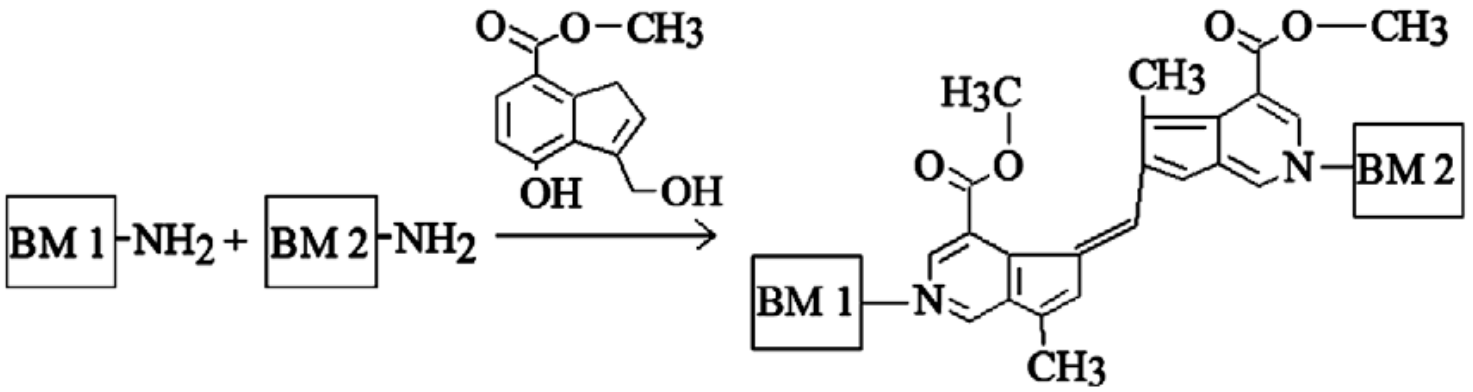

Biopolymer crosslinking mechanism using genipin (GEN) [283].

APPENDIX E

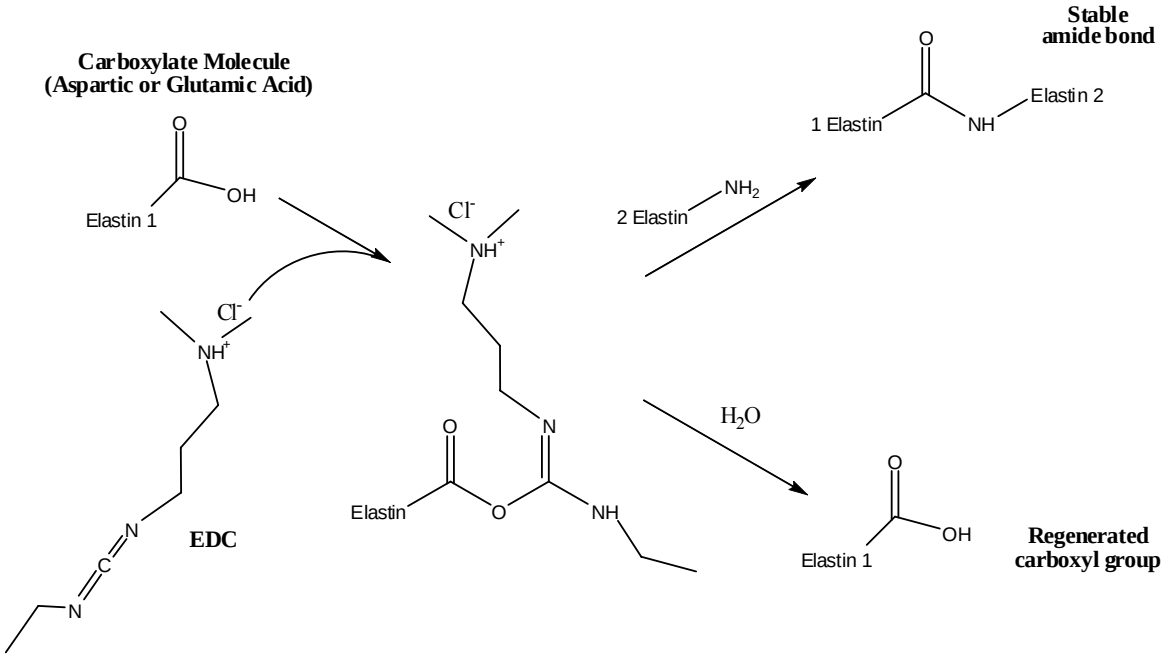

The cross-linking reaction using EDC.Adapted from Pierce Biotechnology; Thermo Fisher Scientific, Inc. EDC.

VITA

Michael James McClure, M.S.

506 ½ North 26th St.
Richmond, VA 23223
Cell Phone: 504-616-5293
Email: mccluremj2@vcu.edu

EXPERIENCE

Virginia Commonwealth University, August 2005-Present, *Research Assistant*
Design and conduct experiments involving biodegradable vascular grafts using a polymer processing technique, electrospinning.

Life Recovery Systems, Inc., September 2006 – July 2008, *Consultant*
Trained doctors and nurses on the use of an external, hypothermic suit for cardiac arrest and stroke patients.

Vanderbilt University, May 2004 - May 2005, *Research Assistant*
Designed and constructed, using fluid dynamics, a large scaledevice which would create topological chaos in laminar flow environments.

EDUCATION

Doctor of Philosophy in Biomedical Engineering
Virginia Commonwealth University, 2007-expected August 2011

Master of Science in Biomedical Engineering
Virginia Commonwealth University, 2005-2007

Bachelor of Engineering in Mechanical Engineering
Vanderbilt University, 2001-2005

AWARDS AND AFFILIATIONS

Virginia Commonwealth University Dissertation Assistantship Award, 2010
American Society for Artificial Internal Organs, 2009-Present
Biomedical Engineering Society, 2009-Present
Tissue Engineering and Regenerative Medicine International Society, 2009-2010

MENTORED STUDENTS

Patrick Barrenger, Undergraduate Researcher from Washington University

PUBLICATIONS

1. Sell S A, McClure M J, Barnes C P, Knapp D C, Walpoth B H, Simpson D G, and Bowlin G L, Electrospun polydioxanone-elastin blends: potential for bioresorbable vascular grafts.Biomedical Materials, 2006.**1**(2): p. 72-80.

2. Sell S A, Barnes C P, Smith M J, McClure M J, Madurantakam P, Grant J, McManus M, and Bowlin G L. Extracellular matrix regenerated: tissue engineering via electrospun biomimetic nanofibers. Polymer International 56, 1349-1360 (2007).

3. Smith M J, McClure M J, Sell S A, Barnes C P, Walpoth B H, Simpson D G, and Bowlin G L, Suture-reinforced electrospun polydioxanone-elastin small-diameter tubes for use in vascular tissue engineering: a feasibility study.Acta Biomaterialia, 2008.**4**(1): p. 58-66.

4. McClure M J, Sell S A, Barnes C P, Bowen W C, and Bowlin G L, Cross-linking Electrospun Polydioxanone-Soluble Elastin Blends: Material Characterization.Journal of Engineered Fibers and Fabrics, 2008.**3**(1): p. 1-10.

5. Sell S A, Francis M P, Garg K, McClure M .J, Simpson D G, and Bowlin G L. Cross-linking methods of electrospun fibrinogen scaffolds for tissue engineering applications. Biomedical Materials **3**(4), Epub 2008.

6. McClure M J, Sell S A, Simpson D G, and Bowlin G L, Electrospun Polydioxanone, Elastin, and Collagen Vascular Scaffolds: Uniaxial Cyclic Distension. Journal of Engineered Fibers and Fabrics, 2009, **4**(2) p. 18-25.

7. Sell S A, McClure M J, Garg, K, Wolfe PS, and Bowlin G L. Electrospinning of Collagen / Biopolymers for Regenerative Medicine and Cardiovascular Tissue Engineering. Advanced Drug Delivery Reviews.2009, **61**(12) p. 1007-19.

8. McClure M J, Sell S A, Ayres C E, Simpson D G, and Bowlin G L. Electrospinning-Aligned and Random Polydioxanone-Polycaprolactone-Silk Fibroin Scaffolds: Geometry for a Vascular Matrix. Biomedical Materials. 2009, **4**(5) 055010.

9. McClure M J, Sell S A, Simpson D G, Walpoth B H, andBowlin, G L. A three-layered electrospun matrix to mimic native arterial architecture using polycaprolactone, elastin, and collagen: A preliminary study. Acta Biomaterialia.2010, **6**(7) p. 2422-33.

10.Sell S A, McClure M J, Ayres C E, Simpson D G, and Bowlin G L. Preliminary Investigation of Airgap Electrospun Silk-Fibroin-Based Structures for Ligament Analogue Engineering. Journal of Biomaterials Science: Polymer Edition. 2010

11. McClure M J, Wolfe P S, Rodriguez I A, and Bowlin G L. Bioengineering of Vascular Grafts: Improving Vascular Tissue Engineering Through Scaffold Design. Journal of Drug Delivery Science and Technology. 2011, 21(3) p. 211-227.

12 McClure M J, Garg K, McCool J M, Rodriguez I A, and Bowlin G L. ECM Analogues Fabricated by Electrospinning. Electrospinning for Applications and Advanced Therapies. August 2011.

13. McClure M J, Simpson D G, and Bowlin G L. Mechanical characterization of tri-layered electrospun vascular grafts using polycaprolactone, elastin, collagen, and silk fibroin. Biomedical Materials. In Preparation.

14. McClure M J, Simpson D G, and Bowlin G L. Preliminary investigation of air flow impedance for controlled porosity. Biomaterials. In Preparation.

ABSTRACTS

Poster Presentations:

1. McClure MJ, Sell SA, Simpson DG, Walpoth BH, Bowlin GL. 2007. Cross-linking Electrospun Polydioxanone-Soluble Elastin Blends: Material Characterization. Regenerative Medicine Conf., Hilton Head, SC.

2. McClure M J, Sell S A, Barnes C P, Walpoth B H, and Bowlin G L. 2007. Long-term cyclic loading to determine energy loss in electrospun polydioxanone and elastin vascular scaffolds. Second International Conference on Mechanics of Biomaterials & Tissues. Kauai, HI.

3. McClure MJ, Sell SA, Simpson DG, Walpoth BH, Bowlin GL. 2008. Multilayer Vascular Graft: Cross-linked Electrospun Polycaprolactone and Collagen. Regenerative Medicine Conf., Hilton Head, SC.

4. McClure MJ, Sell SA, Simpson DG, Walpoth BH, Bowlin GL. 2008. Tri-Layered Electrospun Polycaprolactone – Elastin – Collagen Small Diameter Grafts: Compliant Tubes for Reproducing Native Vessel Mechanics. ISACB Conf., Bordeaux, France.

5. McClure MJ, Sell SA, Walpoth BH, Bowlin GL. 2008. Reproducing Native Vessel Architecture: Multilayered Electrospun Small Diameter Vascular Grafts. TERMIS Conf., La Jolla, CA.

6. McClure MJ, Sell SA, Simpson DG, Bowlin GL. 2009. Electrospun Aligned and Random Matrices with Silk Fibroin for Vascular Tissue Engineering. Regenerative Medicine Conf., Hilton Head, SC.

7. McClure MJ, Sell SA, Walpoth BH, Bowlin GL. 2008. Multi-Layered Compliant Scaffolds for Reproducing Native Vessel Mechanics: Dynamic Mechanical Characterization. ESAO Conf., Geneva, Swizterland.

8. McClure MJ, Sell SA, Walpoth BH, Bowlin GL.2009. Multilayered Electrospun Small Diameter Vascular Grafts for Tissue Engineering. BMES Conf., Pittsburgh, PA.

9. McClure MJ, Sell SA, Ayres, CE, Simpson DG, Bowlin GL 2010. Electrospinning aligned and random polydioxanone-polycaprolactone-silk fibroin blended scaffolds: geometry for a vascular matrix. Regenerative Medicine Conf., Hilton Head, SC.

10. McClure MJ, Sell SA, and Bowlin GL 2010. Tri-layered electrospun vascular grafts: *in vitro* characterization. ISACB Conf., Boston, MA.

11. McClure MJ, Sell SA, Simpson DG, and Bowlin GL 2011. Tri-layered vascular grafts: mechanical and cellular analysis. ESAO Conf., Semmering, Austria.

12. McClure MJ, Sell SA, Simpson DG, and Bowlin GL 2011. Integrin binding analysis of electrospun polycaprolactone, collagen, and elastin.Regenerative Medicine Conf., Hilton Head, SC.

Podium Presentations:

1. McClure MJ, Sell SA, Bowlin GL . 2008. Multi-layered Polycaprolactone – Elastin – Collagen Small Diameter Conduits for Vascular Tissue Engineering. Summer Bioengineering Conf., Marco Island, FL

2. McClure, M. J., Sell, S. A., Simpson, D. G., Walpoth, B. H. & Bowlin, G. L. 2010. A three-layered electrospun matrix to mimic native arterial architecture using polycaprolactone, elastin, and collagen: A preliminary study. Summer Bioengineering Conf., Naples, FL